STRUCTURE-FUNCTION STUDIES OF TRANSLOCATED EFFECTORS FROM THE LATE BLIGHT PATHOGEN

STUART R. F. KING

A thesis submitted to the University of East Anglia

for the degree of Doctor of Philosophy

Department of Biological Chemistry, John Innes Centre

and The Sainsbury Laboratory, Norwich, UK

June 2013

Abstract

An almost universal feature of successful pathogens is the secretion of effector proteins, many of which translocate inside host cells. These effectors manipulate host processes for the pathogen's benefit. However, in response to this manipulation, plants have evolved to monitor for effectors and trigger defence responses.

Amongst plant pathogens, oomycetes of the genus *Phytophthora* have arguably caused almost unrivalled levels of human suffering and represent significant threats to global food security. The late blight pathogen, *Phytophthora infestans*, is the most devastating pathogen of potato – the fourth most important food crop worldwide. Effective and durable resistance against late blight is desperately needed; and will depend on an improved understanding of the mechanistic basis of disease. Determining the adaptive functions of effectors might reveal previously unexploited management strategies.

This work details structure-function studies of two translocated effectors from the late blight pathogen; PexRD2, a representative RXLR effector, and CRN8, an effector with kinase activity. Efforts to heterologously express CRN8 were hampered by protein insolubility and low yields. However, the crystal structure of PexRD2 revealed that it homodimerises, and was crucial to the discovery of a conserved oomycete effector protein fold, the WY-domain fold.

Yeast two-hybrid screening identified four PexRD2-interacting host proteins, including MAPKKKε, a known positive regulator of plant immunity. MAP-kinase cascades transduce the perception of invading pathogens into effective defence responses, and MAPKKKε is involved in resistance against *P. infestans*. PexRD2 specifically suppresses cell deaths that are either MAPKKKε-dependent or triggered by MAPKKKε overexpression. PexRD2 also inhibits MAPKKKε-triggered MAPK activation. Further, structure-led mutagenesis of PexRD2 suggests that this effector benefits the pathogen by interacting with MAPKKKε to inhibit the kinase's signalling. Discovering the PexRD2-MAPKKKε interaction, and its implications for plant immunity, has suggested unexploited management strategies that could enhance crop resistance to this devastating pathogen.

Acknowledgements

Undertaking a PhD is a challenge; but the people around you can definitely make the whole process easier. As such, there are many people to thank from the past four years.

First and foremost, I want to thank my supervisor Dr. Mark Banfield, along with my secondary supervisor Prof. Sophien Kamoun, for allowing me the freedom to pursue different avenues of my project, whilst sharing their knowledge and providing guidance to help me stay focused on what is important.

I'd also like to thank the entire Banfield lab: Richard, Lennart, John, Marina, Mim, Ben, and Abbas; it's been a joy to work with such a great group of people. Special thanks must go to Richard, and former lab members, Laurence and Ally, for 'showing me the ropes'; this project wouldn't be where it is today without your input. Thanks also to Ben and Abbas for accepting the challenge of pursuing the PexRD2 story, good luck guys!

My thanks also go to the 'Kamounity', past and present, in particular, Joe, Diane, Angela, Lili, Tolga, Seb, and Mireille, for always being ready with advice and assistance.

My gratitude also goes to our collaborators, Prof. Paul Birch, and Miles, Hazel, and Petra from the Birch lab. This collaboration was yielded great results, and I won't forget the warm welcome I received when I visited (*No literally, before I'd thought it was medically and meteorologically impossible to get sunburnt in Scotland!*).

I also want to thank the other residents of the student office: Fuzz, John (*again!*), Jo, Kat and Inga, for somehow providing just the right level of distraction to keep me sane during writing-up. Special thanks go to previous residents, Marcus, James and Tracey, and to honorary resident Dan (*the kettle's been lonely without you*) for proving that writing a thesis isn't the impossible task it first seems.

My thanks go to the rest of Lab 116, especially Clare and Karl for passing on their years of wisdom during tea breaks, and to the rest of the department too. Thanks to all my friends here in Norwich for adventures outside of the lab, my time here wouldn't have been the same without you guys. Thanks also to my close friends back in Essex for keeping me grounded. Special thanks to Wally, for being my *longest-serving* friend and visiting me in the depths of Norfolk (*and although this isn't quite a namedrop in a Nobel Prize acceptance speech, I guess it'll do for now*).

Finally, I am truly grateful for my family, who have always loved, supported and encouraged me. Thanks to Mum, Dad and Amy (and Chris too)!

Abbreviations

3AT	3-amino-1,2,4-triazole
Å	Ångström
A_{280}	absorbance at 280 nm
AD	activation domain
AIM	auto-induction media
AP	alkaline phosphatase
ARM	Armadillo
At	*Arabidopsis thaliana*
ATP	adenosine triphosphate
ATR	*Arabidopsis thaliana* recognised
AVR	avirulence
BCIP/NBT	5-bromo-4-chloro-3-indolyl-phosphate/nitro blue tetrazolium
bp	base pair
BTI	Boyce Thompson Institute for Plant Research, Ithaca, New York
BT-PCD	BAX-triggered PCD
CC	coiled coil
cDNA	complementary DNA
CDPK	calcium-dependent protein kinase
CF	culture filtrate
CF-ICD	culture filtrate-induced cell death
CHES	*N*-cyclohexyl-2-aminoethanesulfonic acid
CRN	crinkling and necrosis
cv.	Cultivar
Da	Dalton
DAMP	damage-associated molecular pattern
dATP	deoxyadenosine triphosphate
DBD	DNA-binding domain
DTT	dithiothreitol
DMSO	dimethyl sulfoxide
DNA	deoxyribonucleic acid
dNTP	deoxyribonucleotide triphosphate
dpi	days post infiltration
dpt	days post treatment
dpz	days post zoospore infection
EDTA	ethylenediaminetetraacetic acid
EGTA	ethylene glycol tetraacetic acid
EHM	extrahaustorial membrane
eLRR	extracellular leucine-rich repeats
ETI	effector-triggered immunity
ETS	effector-triggered susceptibility

FT	flow through
$GAL4_{AD}$	GAL4 activation domain
$GAL4_{DBD}$	GAL4 DNA-binding domain
GC-content	guanine-cytosine content
GCK	germinal centre kinase
gDNA	genomic DNA
GFP	green fluorescent protein
GST	glutathione S-transferase
HA	haemagglutinin
HCl	hydrochloric acid
HEPES	4-(2hydroxyethyl)-1-piperazineethanesulfonic acid
HG	heptaglucan
His_6	hexa-histidine
Hpa	*Hyaloperonospora arabidopsidis*
hpi	hours post infiltration
hpt	hours post treatment
HR	hypersensitive response
HRP	horseradish peroxidase
HSD	(Tukey) honestly significantly different
HSP	heat-shock protein
IB	inclusion body
ICD	INF1-induced cell death
I_{hkl}	intensity scattered by a reciprocal lattice point (hkl)
IMAC	imobilised metal ion affinity chromatography
IP	immunoprecipitation
IPTG	isopropyl β-D-1-thiogalactopyranoside
JHI	James Hutton Institute, Invergowrie, Scotland
JIC	John Innes Centre, Norwich Research Park
kb	kilobases
KD	kinase domain
kDa	kilodalton
LRR	leucine-rich repeats
MAMP	microbe-associated molecular pattern
MAPK	mitogen-activated protein kinase
MAPKK (or MAP2K)	mitogen-activated protein kinase kinase
MAPKKK (or MAP3K)	mitogen-activated protein kinase kinase kinase
MBP	maltose-binding protein
MDa	megadalton (1000 kDa)
MES	2-(N-morpholino)ethanesulfonic acid
min	minute
MOPS	3-(N-morpholino)propanesulfonic acid
MQ	Milli-Q
mRNA	messenger RNA

NBS	nucleotide binding site
NLS	nuclear localisation signal
NMR	nuclear magnetic resonance
nt	nucleotide
OD_{600}	optical density at 600 nm
OE	over-expression
oe-PCR	overlap extension PCR
PAGE	polyarcylamide gel electrophoresis
PAK	p21-activated kinase
PAMP	pathogen associated molecular pattern
Pc	*Phytophthora capsici*
PCD	programmed cell death
PCR	polymerase chain reaction
PEG	polyethylene glycol
PexRD2PI	PexRD2-interacting protein
PDB	Protein Data Bank
Pi	*Phytophthora infestans*
PIP	phosphatidylinositol phosphate
Pm	*Phytophthora mirabilis*
PMSF	phenylmethanesulfonyl fluoride
PR	pathogenesis-related
PRR	pattern recognition receptors
psi	pounds per square inch
PTI	PAMP-triggered immunity
PUB	plant U-box
pv.	pathovar
PVDF	polyvinylidene fluoride
PVPP	polyvinylpolypyrrolidone
PVX	potato virus X
qRT-PCR	real-time qualitative reverse-transcriptase PCR
R	(disease) resistance
r.m.s.d.	root-mean-square deviation
RFP	red fluorescent protein
RLK	receptor-like kinase
RLP	receptor-like protein
RNA	ribonucleic acid
ROS	reactive oxygen species
rpm	revolutions per minute
RT	room temperature
RuBisCO	ribulose-1,5-bisphosphate carboxylase oxygenase
SA	salicylic acid
SAD	single-wavelength anomalous dispersion
SC	synthetic complement

SDS	sodium dodecyl sulfate
SEC	size exclusion chromatography
siRNA	short interferring RNA
Sl	*Solanum lysopersicum*
St	*Solanum tuberosom*
T3SS	type III secretion system
TBS	Tris-buffered saline
TBS-T	Tris-buffered saline with Tween®-20
T-DNA	transfer DNA
TFB	transformation buffer
Ti	tumor inducing
TMV	tobacco mosaic virus
Tris	tris(hydroxymethyl)aminomethane
TRV	tobacco rattle virus
TSL	The Sainsbury Laboratory, Norwich Research Park
U	unit
UAS	upstream activating sequence
UTR	untranslated region
UV	ultraviolet
v/v	volume to volume
var.	variant
VIGS	virus-induced gene silencing
w/v	weight to volume
x *g*	times gravity
X-gal	5-bromo-4-chloro-3-indolyl-β-D-galactopyranoside
Y2H	yeast two-hybrid
λ	wavelength

Table of Contents

Table of Figures

Table of Tables

Chapter 1:

General Introduction

1 General Introduction

1.1 Effectors and plant immunity

An almost universal feature of successful plant pathogens is the secretion of proteins that manipulate host processes for the pathogen's benefit (Collinge *et al.*, 2010). These proteins, now called *effectors*, have long been described by plant pathologists under a number of other terms, including avirulence and virulence factors, elictors and toxins. However, unlike these terms, effector is considered neutral as it does not imply either a positive or negative impact on the outcome of the disease interaction. Effectors have been defined as 'pathogen produced molecules that alter host cell structure and function, thereby facilitating infection and/or triggering defence responses' (Kamoun, 2007). Thus, although their genes reside in the genomes of the pathogens, effectors function at the interface with or even within host cells, and as such provide perhaps some of the most vivid examples of genes with '*extended phenotypes*' (Dawkins, 1982, Kamoun, 2007). This neutral definition of effectors has represented a crucial conceptual development in the field of plant pathology (Kamoun, 2006, Hogenhout *et al.*, 2009), as it is less restrictive than the alternative terms. Using this definition, 'effector' can easily be applied to molecules that have dual and conflicting functions in the outcomes of disease interactions. For example, an effector that induces cell death or defence responses in host plants would be considered an elicitor if expressed by some pathogens, and a toxin if expressed by others, dependent on ultimate outcome for the invading pathogen. Furthermore, a single effector from the same pathogen can have contrary effects on the outcome of infection, dependent on the genotype of the host plant infected. Examples of effectors with these conflicting functions have now been reported in a number of plant-microbial pathosystems (Kjemtrup *et al.*, 2000, Alfano and Collmer, 2004, Oliva *et al.*, 2010).

Although some effectors may serve structural roles, or aid nutrient acquisition or pathogen dispersal; most effectors of phytopathogenic microbes are thought to have evolved to enhance microbial fitness by manipulating the immune systems of their hosts (Jones and Dangl, 2006). In general, plants have both preformed and inducible

defences against infection. Preformed physical barriers include the waxy cuticle on the plant epidermis and plant cell walls; whereas pre-emptive chemical barriers include the low pH of the apoplastic space, antimicrobial secondary metabolites called *phytoanticipins*, and antimicrobial peptides called *plant defensins* (Guest and Brown, 1997). Plants respond to pathogens that breach these preformed barriers using a multilayered immune response. These defences rely on responses at the level of each individual cell, alongside the use of systemic signals that emanate from infection sites (McDowell and Dangl, 2000, Jones and Dangl, 2006). The first layer of the plant immune system recognises and responds to molecules common to many classes of microbe, called microbe- or pathogen-associated molecular patterns (MAMPs or PAMPs) (Ingle *et al.*, 2006), and endogenous molecular patterns, which are present only when the tissue is infected or damaged (damage-associated molecular patterns or DAMPs) (Schilmiller and Howe, 2005, Huffaker and Ryan, 2007, De Lorenzo *et al.*, 2011). The second layer recognises specific pathogen effectors, either directly or indirectly through their effects on host proteins or processes (Jones and Takemoto, 2004, Jones and Dangl, 2006).

Unifying features of PAMPs are that they comprise conserved molecular patterns, common to many classes of microbe, with functions essential to general microbial fitness, but are otherwise absent in potential hosts (Nürnberger and Brunner, 2002). Recognition of PAMPs typically occurs via surface-localised pattern recognition receptors (PRRs) and results in the triggering of defence responses known as PAMP-triggered immunity (PTI) (Figure 1.1). In some cases these responses are capable of halting any further colonisation. However, most successful pathogens suppress or otherwise manipulate this resistance by deploying effectors that interfere with PTI. This counter-defensive targeting of components involved in PAMP perception signalling or executors of defence responses can restore the pathogen's virulence and result in effector-triggered susceptibility (ETS) (Figure 1.1) (Jones and Dangl, 2006).

In reply to this manipulation by effectors, plants have evolved an additional layer of defence surveillance that monitors for the presence or activities of these counter-defensive effectors. This second layer of the innate immune system recognises specific effectors using the gene products of host disease resistance genes, or *R* genes. These typically encode cytoplasmic NBS-LRR proteins, which are named

after their characteristic nucleotide binding site (NBS) and leucine-rich repeat (LRR) domains (van der Biezen and Jones, 1998, Dangl and Jones, 2001). Less frequently *R* genes encode extracellular LRR (eLRR) proteins that possess a single transmembrane domain and either a short intracellular C-terminus or kinase domain (Hammond-Kosack and Parker, 2003). An effector that is specifically recognised by one of the host's R proteins is often termed an *avirulence* factor (Avr), and triggers the development of effector-triggered immunity (ETI) (Figure 1.1) (Jones and Dangl, 2006). ETI resembles an amplified PTI response, and is typically associated with the hypersensitive response (HR), a form of programmed cell death (PCD). This response, localised at the infection site, is an effective response against pathogens that need to interact with living host tissue to survive (Glazebrook, 2005).

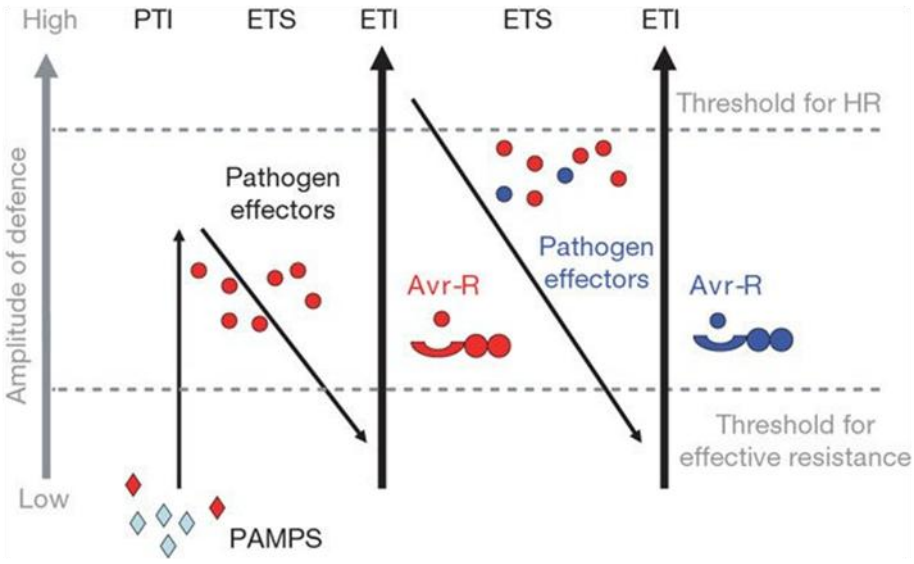

Figure 1.1 The zig-zag model illustrating the quantitative output of the plant immune system

Plants detect pathogen-associated molecular patterns (PAMPs) via PRRs to trigger PAMP-triggered immunity (PTI). Successful pathogens deliver effectors that interfere with PTI, resulting in effector-triggered susceptibility (ETS). Specific effectors (indicated as red circles) are recognized by an NBS-LRR protein, activating effector-triggered immunity (ETI), which resembles an amplified version of PTI that often passes a threshold for induction of hypersensitive cell death (HR). Pathogen isolates are selected that have lost the red effector, and perhaps gained new effectors (in blue) – these can help pathogens to suppress ETI. Selection favours new plant NBS-LRR alleles that can recognize one of the newly acquired effectors, resulting again in ETI. *Figure taken from Jones and Dangl, (2006)*

Perhaps the simplest explanation of how the interplay between *Avr* and *R* genes affects the outcome of a disease interaction is provided by the *gene-for-gene* concept (Flor, 1971). This states that: for genes conferring *avirulence* to a pathogen, there are juxtaposed *R* genes conferring *resistance* in the host. In incompatible host-pathogen interactions, R proteins recognise their cognate avirulence ligands, either directly or indirectly by its effect on other host proteins (van der Biezen and Jones, 1998, van der Hoorn and Kamoun, 2008), and trigger ETI. Alternatively, if the host lacks the corresponding *R* gene, ETI is not triggered and disease may result. In these compatible interactions, the Avr effector might actually function as a *virulence* factor, and subvert host cellular function by acting upon host-encoded targets (van der Biezen and Jones, 1998).

The antagonistic interplay between defensive and counter-defensive molecules of pathogens and hosts has resulted in a continuous co-evolutionary arms race between the two (Dodds and Rathjen, 2010). Natural selection favours pathogens that lose effectors to evade recognition or evolve new effectors to maintain ETS; whereas hosts are selected to circumvent manipulation by virulent pathogens, continue to recognise their effectors, and thus maintain disease resistance. Consistent with this view of an ensuing co-evolutionary arms race, effector genes have been demonstrated to undergo rapid sequence divergence and effector proteins typically show higher than average levels of amino acid polymorphisms (Schornack *et al.*, 2009). Furthermore, many *NBS-LRR* genes also show evidence for positive selection. The impact of this selection is heterogeneous between different domains, with the LRR region, predicted to be involved in protein recognition, showing the strongest evidence for diversifying selection (Mondragón-Palomino *et al.*, 2002, McHale *et al.*, 2006).

The events that occur downstream of PAMP and effector perception overlap significantly. Amongst the earliest responses following perception of PAMPs in plants are ion fluxes, in particular an increase in cytosolic calcium ions (Ca^{2+}) (Boller and Felix, 2009). This responses have also been implicated in R protein-mediated resistance (Martin *et al.*, 2003). The accumulation of apoplastic reactive oxygen species (ROS) in response to pathogen perception, the *oxidative burst*, is also a signature of the early plant immune response (Zipfel, 2009). ROS can act as toxins

against invading pathogens, as well as mediate structural reinforcement of the plant cell wall (Mehdy, 1994, Bolwell, 1999, Passardi *et al.*, 2004). The synergistic interplay between ROS and the phytohormone salicylic acid- (SA)-signalling pathway (Blee *et al.*, 2004), which plays important regulatory roles in both PTI and ETI, is also believed to activate a signal amplification loop that drives hypersensitive cell death and establishment of systemic defences (Doehlemann and Hemetsberger, 2013).

Both calcium-dependent protein kinases (CDPKs) and mitogen-activated protein (MAP) kinase cascades participate in signalling events that regulate both PTI and ETI (Martin *et al.*, 2003, Boller and Felix, 2009, Segonzac *et al.*, 2011). MAPK cascades appear to exert their control of plant defenses via a network of transcription factors, especially those of the WRKY superfamily (Mao *et al.*, 2011). Plant responses to pathogen attack require large-scale transcriptional reprogramming, mediated, in part, by WRKY transcription factors. Changes in gene expression include the induction of genes involved in cell wall re-inforcement and *phytoalexin* biosynthesis, and as well as *pathogenesis-related* (*PR*) genes (Pandey and Somssich, 2009). Phytoalexins are antimicrobial secondary metabolites that are synthesized *de novo* by plants and accumulate rapidly at areas of pathogen infection (Dixon, 1986). *PR* genes encode a variety of proteins that accumulate in infected and surrounding tissue, as well as remote uninfected tissue and are induced by SA (Ebrahim *et al.*, 2011). PR proteins may constitute up to 10% of the total soluble protein of an infected leaf (Heil and Bostock, 2002, Bolton, 2009), and include proteins with potent antimicrobial activities, including hydrolytic enzymes such as chitinases and β-glucanases; and peroxidises that have been implicated in plant cell wall reinforcement (Ebrahim *et al.*, 2011).

The similar responses induced following perception of PAMPs and effectors, by PRR or R proteins respectively, has lead to the suggestion that the PTI-ETI dichotomy is an oversimplification, and in fact there is a continuum between PTI and ETI in plants (Thomma *et al.*, 2011).

1.2 The late blight pathogen

Amongst the most notorious and economically important pathogens of crop species are the plant pathogenic oomycetes. Together with the fungi, these two taxa cover the majority of eukaryotic plant pathogens (Agrios, 2005). Although oomycetes exhibit similar lifestyles and, to some extent, morphology with fungi, these two groups of microorganisms actually represent some of the most divergent eukaryotic pathogens (Baldauf *et al.*, 2000). Their pathogenic lifestyles are therefore examples of convergent evolution and have evolved independently. The oomycetes are actually *stramenopiles* (Sogin and Silberman, 1998, Baldauf *et al.*, 2000, Margulis and Schwartz, 2000), and are hence more closely related to the photosynthetic golden brown algae and diatoms, and distantly related to the apicomplexan parasites of animals, such as *Plasmodium* spp. (Schlegel, 2003, Adl *et al.*, 2005, Harper *et al.*, 2005). Within the oomycetes, species of the genus *Phytophthora* are the best known. This genus was named after the Greek for '*plant destroyer*' and its members are amongst the most serious threats to both agricultural food production and natural ecosystems worldwide (Latijnhouwers *et al.*, 2003, Lamour *et al.*, 2007). For example, *Phytophthora infestans* and *Phytophthora sojae*, the causative agents of late blight of potato and tomato, and stem and root rot of soybean, respectively, have both had longstanding histories of causing devastating disease in these economically important crops (Wrather and Koenning, 2006, Torto-Alalibo *et al.*, 2007, Fry, 2008). Other phytopathogenic oomycetes, such as the sudden oak death pathogen, *Phytophthora ramorum*, caused extensive damage to oak populations across North America and Europe (Rizzo *et al.*, 2005).

Phytophthora infestans is the most destructive pathogen of potato and also represents a model organism within the oomycetes (Haas *et al.*, 2009). As the causative agent of potato and tomato late blight, it is infamous for attacking European potato crops in the mid-nineteenth century. This outbreak led to the Irish potato famine of 1845–1849 and almost unrivalled levels of starvation, human mortality and mass emigration (Judelson and Blanco, 2005, Turner, 2005, Yoshida *et al.*, 2013). In addition to its historical importance, a re-emergence of late blight during the late twentieth century has ensured that this disease remains a critical threat to current global food security (Fry and Goodwin, 1997, Fisher *et al.*, 2012). Today, in terms of

total production, potato represents the fourth largest food crop, after maize, wheat and rice (Source: FAOSTAT). The benefits of this staple crop as an alternative to the major cereals in providing food security for an increasing world population are becoming progressively more apparent (Haas *et al.*, 2009, Reader, 2009). Unlike cereal crops, potato is not a globally traded commodity (Source FAOSTAT) and as such, potato crops are less susceptible to price inflation driven by global market competition. Instead, the price of potatoes is heavily determined by local supply and demand, meaning that investing in potatoes is highly recommended as a food security safeguard for low-income countries.

Late blight has the potential to destroy an entire field of potato within days. The frequent emergence of 'resistance-breaking strains' that overcome the resistance conferred to cultivars carrying specific *R* genes, necessitates growers to rely on potentially environmentally hazardous agrochemicals to protect their crops (Fry, 2008). The cost of control and crop losses associated with late blight are conservatively estimated at $6.7 billion per year (Haverkort *et al.*, 2008). As such, the development of novel management strategies that are durable and effective against this devastating pathogen continues to represent a major challenge (Fry, 2008). Tackling this problem will arguably be dependent on an improved understanding of the mechanistic basis of disease interactions.

Like most other *Phytophthora* species, *P. infestans* has both asexual and sexual lifecycles and produces a range of spore types that are involved in the disease cycle (Figure 1.2) (Judelson and Blanco, 2005). These spores include the asexual sporangia and zoospores, and the characteristic sexual spore or oospore, which play crucial roles in dispersal and overwintering survival, respectively (Drenth *et al.*, 1995, Flier *et al.*, 2002b). The efficient production and dispersal of these spores represents an important prerequisite for successful infection, and many sporulation and infection cycles can occur within a single potato growing season (Flier *et al.*, 2002a). Sporangia are multinucleate, egg-shaped spores that develop on the termini of specialised aerial hyphae, called sporangiophores. In *P. infestans*, these sporangia are easily detached and can act directly in the dispersal of the pathogen. These sporangia can then, depending on the environmental conditions, either germinate directly or undergo indirect germination, also known as zoosporogenesis (Tani *et al.*,

2004). The latter of the two predominates under cooler environmental temperatures and involves cytoplasmic cleavage of the sporangium resulting in the formation of multiple, wall-less, uninucleate zoospores. These spores are motile and possess two flagella that function in their dispersal through water drops and films on plant surfaces or in waterlogged soil. The zoospores of *P. infestans* can then locate new hosts, possibly via chemotaxis, electrotaxis and autoaggregation (Tyler, 2002). Upon contacting the host, zoospores discard their flagella and affix themselves to the host surface, becoming immobile walled cysts. These cysts are short-lived and germinate within hours of encystment. These germinated cysts, or germinated sporangia in the case of direct germination, then initiate infection via the production of germ tubes. These then form appressorium-like structures under which the host's surface is penetrated, facilitated by the secretion of cell wall degrading enzymes (Hardham and Blackman, 2009).

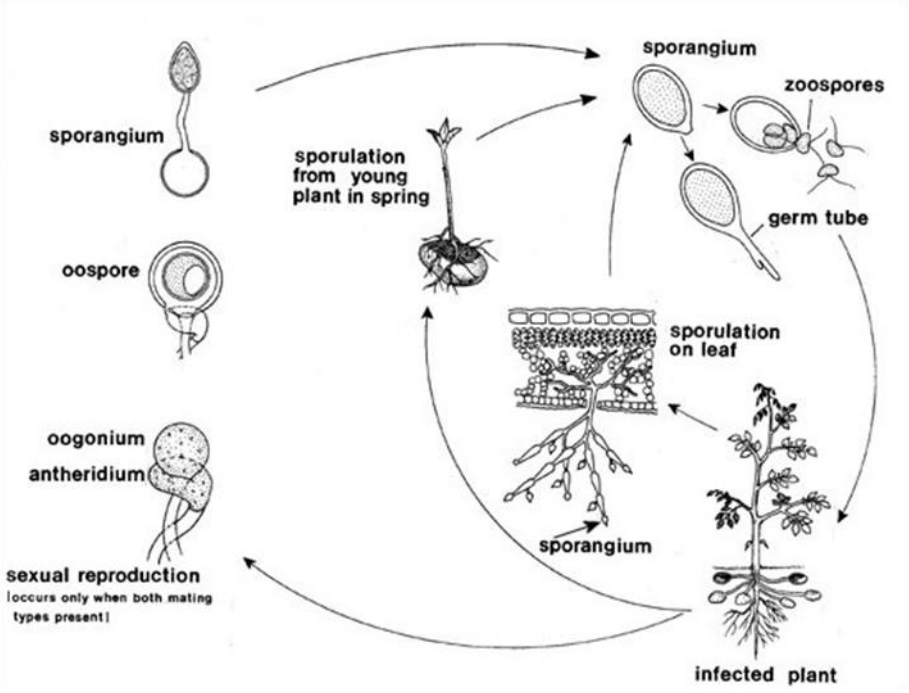

Figure 1.2 Disease cycle of *Phytophthora infestans*

Figure taken from Schumann, G.L. and C. J. D'Arcy. 2000. Late blight of potato and tomato. The Plant Health Instructor. DOI: 10.1094/PHI-I-2000-0724-01

P. infestans is a hemibiotrophic pathogen and the subsequent infection of host plants occurs as two distinct phases: an early biotrophic phase and a later necrotrophic phase (Latijnhouwers *et al.*, 2003). In the initial biotrophic phase of infection, the pathogen requires living plant tissue to survive. Hyphal growth is predominantly intercellular within the apoplastic space, and specialised infection and feeding structures called haustoria are established. Haustoria are formed by both biotrophic and hemibiotrophic fungi and oomycetes, and essentially involve the penetration of the plant cell wall and subsequent invagination of the host cell membrane around the cell wall of an intercellular hyphae (Hardham and Blackman, 2009). The formation of the host-derived extrahaustorial membrane involves the *de novo* production of host membrane components, as well as the selective exclusion of certain host cell proteins including: aquaporin, calcium transporters and specific PRRs (Lu *et al.*, 2012). *P. infestans*, like other hemibiotrophic oomycetes, establishes small finger- or digit-like haustoria (Latijnhouwers *et al.*, 2003). Haustoria represent an intimate contact between the pathogen and living host protoplasm; and the dependence on these associations with living host cells means that successful early colonisation of the host is dependent on the pathogen evading the plant's innate immune defences. However, as the infection progresses into the necrotrophic phase, the infected host tissue subsequently dies, forming necrotic lesions, and nutrients are obtained from these dead or dying host cells (Kamoun, 2007, Whisson *et al.*, 2007).

1.3 Oomycete PAMPs

A range of oomycete specific molecules that display properties of PAMPs have been identified. Elicitins are 10 kDa secreted proteins, that are almost ubiquitous in *Phytophthora* spp. (Kamoun *et al.*, 1994). These proteins are capable of binding sterols, and are proposed to shuttle host-derived sterols to the pathogen (Mikes *et al.*, 1998, Osman *et al.*, 2001a, Blein *et al.*, 2002). Oomycetes lack several of the enzymes that are required for the conversion of sterol precursors to mature sterols, which are required for their growth and sporulation (Gaulin *et al.*, 2010). Elicitins also trigger a suite of PTI responses, such as ROS production, phytoalexin biosynthesis, MAPK activation, and non-specific systemic acquired resistance

(Bonnet *et al.*, 1996, Keller *et al.*, 1996, Rustérucci *et al.*, 1996, Zhang *et al.*, 1998, Asai *et al.*, 2008), as well as HR-like cell death in most *Nicotiana* species (Kamoun *et al.*, 1993, Takemoto *et al.*, 2005). Sterol-loading of elicitins has been suggested to be a prerequisite for their recognition (Osman *et al.*, 2001b). INF1 is the major elicitin from *P. infestans* (Kamoun *et al.*, 1997). Recognition of INF1 is mediated by the membrane localised receptor-like protein ELR1 (Du *et al.*, 2012) and LRR-RLK (leucine-rich repeat-receptor-like kinase) SERK3/BAK1[*] (Chaparro-Garcia *et al.*, 2011), although the exact composition of the receptor complex remains unknown and other INF1-interacting plant membrane proteins have also been identified (Kanzaki *et al.*, 2008). The signalling cascade following INF1 recognition and leading to HR-like cell death has been shown to require a respiratory burst oxidase homolog Nbrboh (Yoshioka *et al.*, 2003), the heat-shock proteins HSP70 and HSP90 (Kanzaki *et al.*, 2003), and a ubiquitin ligased associated protein SGT1[†] (Peart *et al.*, 2002).

GP42 is a 42 kDa glycoprotein that is abundantly expressed in the cell wall of *P. sojae*, and conserved in other *Phytophthora* species including *P. infestans*, that also displays PAMP-like properties. This protein is a calcium-dependent transglutaminase (TGase) (Brunner *et al.*, 2002); a class of enzymes that display protein cross-linking activity, with the resultant isopeptide bonds conferring increased resistance to proteolysis (Greenberg *et al.*, 1991). GP42 is recognised via a 13-amino-acid surface exposed fragment, Pep-13 (Nürnberger *et al.*, 2004, Reiss *et al.*, 2011). This peptide potently induces several PTI responses, including ROS production and phytoalexin biosynthesis, in both host and non-host plant species (Nürnberger *et al.*, 1994, Brunner *et al.*, 2002). Within this peptide, mutations that reduced its ability to induce defence responses also abolished the protein's TGase activity. This is indicative of plants having evolved to recognise a conserved motif of the protein that is indispensable to its function.

Cellulose-binding elicitor lectin (CBEL) is another oomycete cell wall associated glycoprotein that was initially isolated from *Phytophthora parasitica* var. *nicotianae*,

[*] SERK3 = SOMATIC EMBRYOGENESIS RECEPTOR KINASE 3, BAK1 = brassinosteroid-associated kinase 1

[†] SGT1 = suppressor of G2 allele of skp1

the causal agent of tobacco Black Shank disease (Mateos *et al.*, 1997). CBEL-like domain containing proteins have been identified in multiple *Phytophthora* spp. including *P. infestans* (Sierra *et al.*, 2010). CBEL induces HR-like lesions and defense responses associated with PTI in both tobacco (*Nicotiana tabacum*) and non-host plants including *Arabidopsis thaliana* (Khatib *et al.*, 2004, Gaulin *et al.*, 2006). Suppression of *CBEL* expression in *P. parasitica* var. *nicotianae* caused developmental abnormalities, suggesting a role in cell wall polysaccharide deposition and adhesion to cellulose, although knockdown transformants did not display significantly reduced virulence when plants were inoculated using mycelia explants.

Branched heptaglucoside (HG) oligosaccharides derived from oomycete cell walls may also represent oomycete PAMPs. Their recognition is mediated by binding to apoplastic β-glucan-binding proteins (GBPs), and can trigger the production of phytoalexins (Cosio *et al.*, 1992). However, since GBP-like proteins are found in many plant species, yet the ability to respond to HG appears to be restricted to the legumes, additional signalling components must be required (Fliegmann *et al.*, 2004).

In spite of oomycete PAMPs being recognised by plant species and triggering a wide array of defence responses, phytopathogenic oomycetes are still able to successfully colonise plants. Similarly to many bacterial and fungal plant pathogens, this colonisation is believed to be accomplished by the suppression of host cell defences by pathogen-derived effectors (Birch *et al.*, 2006, Kamoun, 2006).

1.4 Oomycete effectors

The genomes of sequenced *Phytophthora* species reveal that the effector secretomes of these pathogens are highly complex; with several hundred predicted proteins in families, typically significantly expanded with relation to those in non-pathogenic relatives (Haas *et al.*, 2009). Comparative genetics has also revealed that *Phytophthora* species carry distinct repertoires of effectors genes, with only a limited number of examples belonging to a core set of shared orthologs (Haas *et al.*, 2009,

Schornack *et al.*, 2009). In general, however, oomycete effectors can be divided into two classes that target distinct sites in host tissues: apoplastic effectors that are secreted into the plant extracellular space, where they interact with extracellular targets and surface receptors; and translocated effectors that act inside the plant cell, where they may target different subcellular compartments (Schornack *et al.*, 2009).

1.4.1 Apoplastic effectors

As many plant pathogenesis-related (PR) proteins that accumulate in the apoplast are hydrolytic enzymes, it is unsurprising that many apoplastic effectors that have been identified to date represent enzymatic inhibitors (Kamoun, 2006). Such effectors would include the glucanase inhibitors, GIP1 and GIP2 (Rose *et al.*, 2002), which are secreted into the apoplastic space by *P. sojae*. These effectors exhibit significant structural similarity to the trypsin class of serine proteases, although are proteolytically inactive because of mutated catalytic residues. These are thought to function as counter-defensive molecules by inhibiting the degradation of components of the pathogen cell wall and possible release of defence-eliciting oligosaccharides by host β1-3-glucanases. At least four effector genes with similarity to GIPs have also been identified in *P. infestans* (Damasceno *et al.*, 2008).

In addition, apoplastic effectors from *P. infestans* also include serine protease inhibitors, such as EPI[‡]1 and EPI10, and cystatin-like cysteine protease inhibitors, such as EPIC1 and EPIC2 (Kamoun, 2006). These are also thought to function in counter-defence, by inhibiting defence-related host proteases. EPI1 and EPI10 are multi-domain modular proteins containing N-terminal signal peptides followed by several Kazal-like domains. Signal peptides are short amino-acid sequences that target proteins for export through the general secretory pathway, also known as the type II secretion system (von Heijne, 1990), whereas the Kazal-like domains mediate protease inhibition (Laskowski Jr and Kato, 1980). These secreted proteins' roles in counter-defence are thought to be achieved by the inhibition of the tomato PR protein P69B, a subtilisin-like serine protease (Tian *et al.*, 2004, Tian *et al.*, 2005). The cysteine protease inhibitors EPIC1 and EPIC2 possess all the signature

[‡] EXTRACELLULAR PROTEASE INHIBITOR

sequences of cystatin-like protease inhibitors, and have been shown to inhibit PIP1 and C14, apoplastic PR proteins of tomato and *Nicotiana benthamiana* with significant similarity to papain-like cysteine proteases (Tian *et al.*, 2007, Kaschani *et al.*, 2010).

1.4.2 Translocated effectors

Other oomycete effectors function within host cells and are translocated into the host cytoplasm. (Kamoun, 2006, Birch *et al.*, 2009). The translocated oomycete effectors discovered so far belong to two effector families, the RXLR effectors and the CRN effectors (crinkling and necrosis or 'Crinklers'). Both *CRN* and *RXLR* effector genes have been shown to occur predominantly in repeat rich, gene-sparse genomic regions; and represent gene families that have undergone significant expansion, apparently driven by non-allelic homologous recombination (Haas *et al.*, 2009). Similar to oomycete apoplastic effectors, and the secreted effectors of bacterial phytopathogens such as *Pseudomonas syringae* (Alfano and Collmer, 2004), these translocated effectors are modular proteins; and consist of N-terminal regions, involved in secretion and translocation into host cells, followed by diverse C-terminal domains, which are not required for translocation but instead confer the biochemical effector functions (Morgan and Kamoun, 2007). The two cytoplasmic effector families of *Phytophthora* spp. have been characterised by conserved peptide motifs within their N-terminal targeting domains.

1.4.2.1 RXLR effectors

Proteins in the RXLR family are widely considered the archetypical oomycete translocated effectors and have received the most attention (Kamoun, 2006, Morgan and Kamoun, 2007, Haas *et al.*, 2009). RXLR effectors are secreted proteins, which average between 100 and 200 amino acids in length, and are defined by the N-terminal amino acid motif arginine-x-leucine-arginine (where x signifies any residue). This motif is often followed by an acidic region including a 'dEER' motif (aspartate-glutamate-glutamate-arginine), although the second motif is frequently

less well conserved (Birch *et al.*, 2006). These peptide motifs have been shown to be necessary for the translocation of RXLR effectors into host cells; most notably AVR3a from *P. infestans* (Whisson *et al.*, 2007) and Avr1b from *P. sojae* (Dou *et al.*, 2008b). However, it is important to emphasize that these motifs are not on their own sufficient to promote translocation and require additional flanking sequences (Whisson *et al.*, 2007, Birch *et al.*, 2008).

The precise mechanism by which oomycete, or indeed fungal, effectors are delivered into plant cells is not well understood, and continues to be a very active area of research (Panstruga and Dodds, 2009). In general two basic mechanisms for translocation of oomycete effectors inside host cells have been proposed based on observations of other pathosystems. These include entry mechanisms that are dependent on pathogen-derived translocation machinery, as well as the environmental conditions established by the specialised infection structures, the haustoria (Morgan and Kamoun, 2007, Birch *et al.*, 2008). This would suggest that entry occurs in a manner analogous to the Gram-negative bacterial type III secretion system (T3SS). Alternatively, it is possible that entry into host cells may utilise an entirely host-derived mechanism, following secretion via the general secretory pathway. It has been reported that RXLR-mediated entry of Avr1b can occur in the absence of the pathogen and therefore independently of any possibly pathogen-encoded translocation machinery or specialised infection structures (Dou *et al.*, 2008b). This pathogen-independent translocation has been suggested to be dependent on RXLR-mediated binding of phosphatidylinositol phosphates (PIPs) (Kale *et al.*, 2010). This interaction with PIP head groups exposed on the external surface of the plant's plasma membrane was postulated to stimulate endocytosis of the effectors into plant cells. However, several subsequent studies have failed to reproduce many of these results (Wawra *et al.*, 2012, Yaeno and Shirasu, 2013), and the debate over the exact mechanism of translocation looks set to continue (Ellis and Dodds, 2011, Tyler *et al.*, 2013).

All oomycete avirulence effectors discovered so far have been RXLR effectors; and although they were originally identified on the basis of their avirulence activity in resistant plant cultivars or species, several RXLR effectors have now been attributed

additional virulence activities that would confer a selective advantage when infecting a susceptible host (Morgan and Kamoun, 2007).

The *P. infestans* effector AVR3a provides perhaps the best example of a translocated effector with an immunity suppressing virulence function. The *AVR3a* gene encodes at least two polymorphic secreted proteins that differ at only three residues, the last two of which are present in the mature protein. The avirulence allele, $AVR3a^{C19,K80,I103}$, typically referred to as $AVR3a^{KI}$, is carried by isolates that are avirulent on potato cultivars expressing the NBS-LRR resistance protein R3a, whereas virulent isolates carry only the virulence allele, $avr3a^{S19,E80,M103}$, the gene product of which, $AVR3a^{EM}$, is not recognised by R3a (Armstrong *et al.*, 2005, Kamoun, 2006). The avirulent isoform, $AVR3a^{KI}$, has also been demonstrated to be a potent suppressor of the cell death response triggered by INF1 (Bos *et al.*, 2006*).* Other avirulence RXLR effectors such as Avr1b, and ATR13[§] from *Hyaloperonospora arabidopsidis* (*Hpa*) have also been demonstrated to enhance virulence in infections of susceptible plants and suppress defence responses induced by pathogenic attack (Sohn *et al.*, 2007, Dou *et al.*, 2008a, Schornack *et al.*, 2009). The demonstration of virulence functions for numerous RXLR effectors, in addition to the previously described avirulence functions, has confirmed these pathogen-derived proteins as a critical area for further study to understand the determinants of the outcome of infection.

The hundreds of candidate RXLR effector genes revealed in the genomes of phytopathogenic oomycetes (Haas *et al.*, 2009) is in stark contrast to the comparatively small complement of T3SS effectors required for infection by phytopathogenic bacteria (approximately 15 – 35 per *Pseudomonas syringae* pathovar) (Lindeberg *et al.*, 2008, Kvitko *et al.*, 2009). Furthermore many RXLR effectors fall into gene families with numerous paralogs. These two observations have highlighted the great potential for functional redundancy in oomycete effector families (Birch *et al.*, 2008). When considered within the context of a pathogen–host co-evolutionary arms race, this redundancy may be advantageous for the pathogen. For example, if an effector is inactivated, by mutation or loss of expression to

[§] *A*rabidopsis *t*haliana recognised 13

prevent recognition by host R proteins, it need not necessarily reduce the pathogen's fitness; since, other related effectors may continue to provide the same virulence function in susceptible cultivars.

1.4.2.2 CRN effectors

CRN effectors form a distinct, yet complex, family of secreted proteins that are also thought to play an important role in disease progression. The *P. infestans* genome contains a large family of 196 CRN genes, which is heavily expanded in *P. infestans* relative to *P. sojae* (100 CRNs) and *P. ramorum* (19 CRNs) (Haas *et al.*, 2009). The CRNs are relatively large proteins, on average 400 – 850 amino acids, and like the RXLR effectors, they possess a modular structure. The hallmark feature of the CRNs is a highly conserved N-terminal domain structure. This comprises a conserved LFLAK domain which is approximately 50 amino acids and includes the conserved LXLFLAK peptide motif (Win *et al.*, 2006), adjacent to a diversified DWL domain which ends with a HVLVXXP sequence motif (Haas *et al.*, 2009). In the majority of CRNs, these domains are located downstream of a predicted signal peptide and followed by diverse C-terminal effector domains (Haas *et al.*, 2009).

Analogous to the RXLR region, the LFLAK domain has been demonstrated to be a functional translocation motif, and mediate the delivery of C-terminal effector domains inside plant cells, when expressed from transgenic *Phytophthora capsici*[**] (Schornack *et al.*, 2010). Although the mechanism of LFLAK mediated transfer is also unknown, this motif overlaps with an RXLR motif in the N-termini region of some *Hpa* effectors, and results in a combined RXLRLFLAK motif (Win *et al.*, 2007).

The CRN effectors were originally discovered following an *in planta* function expression screen of candidate secreted proteins from *P. infestans* (Torto *et al.*, 2003). CRN1 and CRN2, identified in this screen, were shown to be constitutively expressed during colonization of the host plant tomato; and elicited a leaf-crinkling and cell death phenotype when expressed in both tomato and *Nicotiana* spp. (Torto *et al.*, 2003). Expression of CRN2 was accompanied by an induction of defence and *PR* genes, reminiscent of known general defence elicitors from *Phytophthora* spp.,

[**] *Phytophthora capsici* is a hemibiotrophic pathogen of pepper and curbits.

but with delayed timing and a slightly different appearance of the necrotic response. The adaptive significance of the necrotic response has yet to be determined. However, it has been proposed the CRNs may function to aid *Phytophthora* spp. colonization of plant tissues during the late necrotrophic phase of infection (Qutob *et al.*, 2002). Although their exact function remains unknown, it appears that the roles fulfilled by the CRN family of effectors may be significantly differently from those of the RXLRs.

Genome analyses have revealed that, unlike the RXLR effectors, which appear restricted to the haustoria-forming phytopathogenic oomycetes, the CRN family is ubiquitous in plant pathogenic oomycetes (Schornack *et al.*, 2010). CRNs have been identified in the more distantly related oomycetes such as *Aphanomyces euteiches*, which infects a variety of legumes but does not form haustoria (Schornack *et al.*, 2010). These findings suggest that the CRNs form a more ancient effector family that arose early in oomycete evolution.

The CRN C-terminal regions are highly divergent, exhibiting a wide variety of domain structures. Thirty-six different conserved domains have been identified among the C-terminal regions of the 315 *Phytophthora* CRN proteins (Haas *et al.*, 2009). There is strong evidence that this diversity of effector domains has been driven by recombination events between different clades, occuring predominantly after the conserved HVLVXXP motif in the N-terminal domain. This suggests an evolutionary mechanism similar to the C-terminal re-assortment reported for T3SS effectors of phytopathogenic bacteria (Stavrinides *et al.*, 2006, Schornack *et al.*, 2009). Although, like the RXLR effectors, most CRNs have no similarity to known sequences, the C-terminal domain of some CRN-like proteins show homology to protein kinases and phosphotransferases, suggesting possible mechanisms for these effectors to manipulate host physiology (Haas *et al.*, 2009).

1.5 Potential of *'structural effectoromics'*

In spite of the substantial progress that has been made in recent years, there is still a lot that as yet remains unclear about oomycete effectors. To date, genome sequence

analyses and comparative genomics have been extremely successful in identifying a plethora of putative effectors, of previously unexpected complexity and diversity (Haas *et al.*, 2009). However, extensive effort is required to link these identified sequences to specific phenotypes. Within the field of plant pathology, there is now an increasing shift in emphasis of effector research towards improving our biochemical understanding of effector protein function. Although inferring gene function on the basis of sequence homology is one potential method to annotate unknown proteins, most oomycete effectors fail to demonstrate any significant homology to sequences present in public databases. Structural biology methods have the potential to overcome this limitation, and will hopefully play an important role in improving our understanding through the determination of the three-dimensional structure of effector proteins.

Plant pathogenic bacteria, such as *P. syringae*, manipulate host cellular functions by employing structural mimicry of eukaryotic host proteins. Nearly all effector proteins from phytopathogenic bacteria eluded functional annotation on the basis of primary amino-acid sequence. However, solving their three-dimensional structures revealed important clues about their virulence mechanisms (Desveaux *et al.*, 2006). The crystal structure of AvrB revealed that it shares features with protein kinases, that were not obvious from its primary sequence (Lee *et al.*, 2004, Desveaux *et al.*, 2007), whilst the NMR structure of a recognised fragment of AvrPto demonstrated that it transitioned between unfolded and folded states, and adopted a helical-fold implicated in mediating protein recognition (Wulf *et al.*, 2004).

Structural characterisation of fungal effectors has also shed light on the determinants of virulence and avirulence activity. The structures of two proteins from the AvrL567 family of translocated effectors from the flax rust fungus, *Melampsora lini*, have been solved (Wang *et al.*, 2007). This family of effectors are recognized by the flax R proteins L5, L6 and L7 via direct protein interaction (Dodds *et al.*, 2006). Knowledge the three-dimensional structures allowed the contribution to molecular recognition events of specific polymorphic residues to be assessed within a structural context, as well as suggesting testable hypotheses to investigate the virulence activities of these effectors further (Oliva *et al.*, 2010).

At the time of starting this PhD, no structural information was available for translocated effectors from oomycete species, although other oomycete protein structures have been published (Figure 1.3). The protein structures of a number of PAMP-like elicitins have revealed their capacity to bind sterols enclosed within a large hydrophobic cavity (Boissy *et al.*, 1999, Rodrigues *et al.*, 2006, Lascombe *et al.*, 2007). Nep1[††]-like protein (NLP) from *Pythium aphanidermatum,* a soil-borne phytopathogenic oomycete, stimulates leaf necrosis and immune response in dicots (Pemberton and Salmond, 2004). The crystal structure revealed structural homology to fungal lectins and actinoporins, suggesting a possibly shared cytolitic membrane-disintergrating mode of action (Ottmann *et al.*, 2009). The NMR structure of phytotoxic protein PcF from *Phytophthora cactorum*[‡‡], identified a novel fold among protein effectors, but showed structural homology to a plant protein suggesting a possible biological activity based on molecular mimicry (Nicastro *et al.*, 2009).

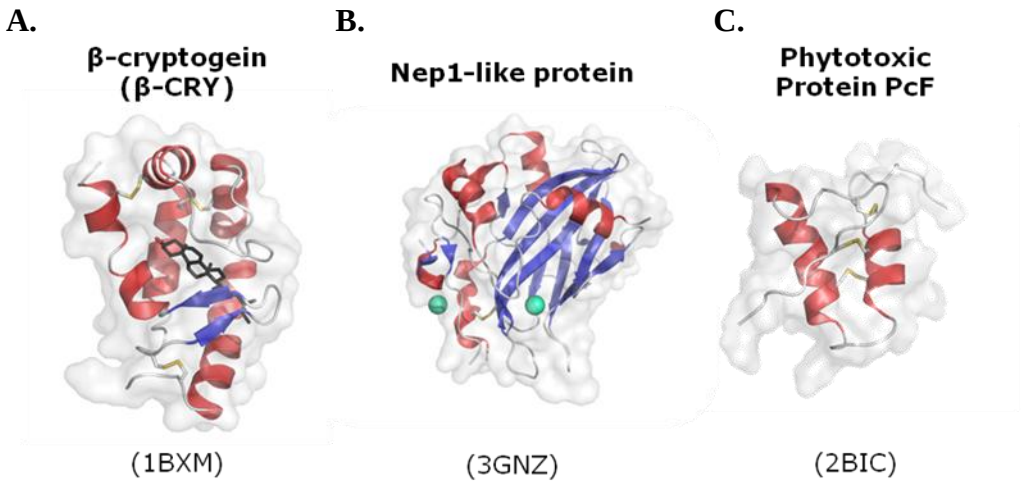

Figure 1.3 Published three-dimensional structures of oomycete proteins involved in plant-pathogen interactions

(A.) Crystal structure of elicitin from *Phytophthora cryptogea* in complex with ergosterol (black). **(B.)** Crystal structure of NLP from *Pythium aphanidermatum* showing position of bound Mg^{2+} ions (cyan) **(C.)** NMR structure of phytotoxic protein PcF from *Phytophthora cactorum*. α-helices are coloured in red, β-strands in blue, and disulfide bridges in yellow. PDB IDs are indicated below each structure.

[††] NECROSIS- AND ETHYLENE-INDUCING PEPTIDE1

[‡‡] *P. cactorum* can cause root, collar, and crown rots, as well as foliar and fruit infections in an extremely large number of hosts (Jeffers and Aldwinkle, 1987).

The ultimate aim of effector biology is to improve our understanding of the molecular basis of oomycete pathogenesis and resistance. A prerequisite for achieving this will be developing a comprehensive knowledge of both oomycete effector structure and function. It is widely hoped that with this improved understanding, the much needed novel strategies for manipulating plants towards resistance to devastating phytopathogenic oomycetes, such as the late blight pathogen, will become apparent.

1.6 Project aims and objectives

This project's objectives were to conduct structure-function analyses on translocated effectors from the late blight pathogen, with the aim of providing insights into the adaptive function of these proteins. A representative of both the RXLR and CRN effectors were included in this project. Structural data obtained was used to direct future studies aimed at assigning virulence functions to the effector in question. This approach was supported by a combination of protein-protein interaction techniques, and *in planta* assays.

Chapter 2:

Materials and Methods

2 Materials and Methods

2.1 Bacterial strains and plasmids

The *Escherichia coli* strains used in this worked are described in Table 2.1. Routine DNA work was conducted with DH5α and TOP10. BL21(DE3) was used for protein expression, and *ccd*B Survival™ 2 cells were used for amplification of pDONR™201 or destination vectors containing the *ccd*B lethal gene.

Table 2.1 ***Escherichia coli*** **strains**

Strain	Genotype	Source/Reference
DH5α	F– Φ80*lac*ZΔM15 Δ(*lac*ZYA-*arg*F) U169 *rec*A1 *end*A1 *hsd*R17 (rK–, mK+) *pho*A *sup*E44 λ– *thi*-1*gyr*A96 *rel*A1	(Hanahan, 1983)
TOP10	F– *mcr*A Δ(*mrr-hsd*RMS-*mcr*BC) Φ80*lac*ZΔM15 Δ*lac*X74 *rec*A1 *ara*D139 Δ(*ara leu*) 7697 *gal*U *gal*K *rps*L (Str^R) *end*A1 *nup*G	Invitrogen
BL21(DE3)	F– *omp*T *gal dcm* lon *hsd*SB(rB- mB-) λ(DE3)	Stratagene. Amsterdam, Europe
ccdB Survival™ 2	F- *mcr*A Δ(*mrr-hsd*RMS-*mcr*BC) Φ80*lac*ZΔM15 Δ*lac*X74 *rec*A1 *ara*Δ139 Δ(*ara-leu*)7697 *gal*U *gal*K*rps*L (StrR) *end*A1 *nup*G *fhuA::IS2*	Invitrogen

Agrobacterium tumefaciens strain GV3101 (Van Larebeke *et al.*, 1974), harbouring the disarmed Ti (tumour inducing) helper plasmid pMP90 (Koncz and Schell, 1986), was used for routine agroinfiltration, unless specified otherwise. This strain was selected on L agar plates supplemented with rifampicin (chromosomal marker) and gentamycin (Ti plasmid marker) at the concentrations described below.

The plasmid vectors, together with all DNA constructs generated and/or used in this work, are described in Appendix Tables A – E.

2.2 General chemicals

All chemicals were purchased from Sigma-Aldrich Company Ltd. (Poole, Dorset UK), Fisher Scientific UK Ltd (Loughborough, UK) or VWR International (West Chester, Pennslyvania USA), unless specified otherwise.

2.3 Media and culture conditions

All media were made using de-ionised water and sterilised by autoclaving at 121 ºC, 15 psi for 30 min. Sterilised molten agar was allowed to cool to ~50 ºC prior to addition of heat sensitive supplements.

E. coli strains were cultured on Lysogeny broth (LB) media [1.0% (w/v) tryptone, 0.5% (w/v) yeast extract, 1.0% (w/v) sodium chloride, pH 7.0] (Bertani, 1951). When using salt-sensitive antibiotics bacteria were grown using L media [1.0% (w/v) tryptone, 0.5% (w/v) yeast extract, 0.5% (w/v) sodium chloride, 1.0% (w/v) glucose, pH 7.0]. LB and L agar were made as above, although supplemented with 1% (w/v) microbiology grade agar.

When appropriate, media were supplemented with antibiotics at final concentrations as follows; carbenicillin (100 $\mu g.mL^{-1}$), kanamycin (50 $\mu g.mL^{-1}$), gentamicin (25 – 30 $\mu g.mL^{-1}$), rifampicin (50 $\mu g.mL^{-1}$), spectinomycin* (100 $\mu g.mL^{-1}$), streptomycin* (100 $\mu g.mL^{-1}$), hygromycin B* (100 $\mu g.mL^{-1}$), and chloramphenicol (34 $\mu g.mL^{-1}$).

2.4 General DNA procedures

2.4.1 Isolation of plasmid DNA from bacteria

A single, isolated *E. coli* colony harbouring the desired plasmid was inoculated into 4 – 10 mL of LB broth supplemented with the appropriate antibiotics. After incubation at 37 ºC for 16 h with shaking between 200 – 230 rpm, the cells were harvested by centrifugation at 3,600 x *g* for 10 min at 4 ºC. The plasmid DNA was

* salt-sensitive antibiotics

isolated from the pelleted *E. coli* using either a QIAprep Spin Miniprep Kit (Qiagen) or ISOLATE Plasmid Mini Kit (BIOLINE) and as described in the accompanying manuals. These kits follow a modified alkaline lysis method originally developed by Birnboim and Doly (Birnboim and Doly, 1979), followed by neutralisation of the cell lysate, centrifugation to pellet cellular debris, and adsorption of the plasmid DNA on to a silica gel membrane in the presence of high concentrations of chaotropic salts. The DNA is then washed with the provided buffers containing ethanol to remove contaminating material, prior to elution of the DNA in 30 – 50 μL of water, and storage at -20 ºC.

Isolation of plasmid DNA from *Agrobacterium* was conducted using very similar methods to those described above, with the exception that 100 μL of a freshly prepared stock of 10 $mg.mL^{-1}$ lysozyme was added to the resuspension buffer and incubated at room temperature for at least 5 min to increase cell lysis, and DNA was eluted from silica membrane using water preheated to 60 ºC.

2.4.2 Transformation of chemically competent *E. coli*

Transformation of *E. coli* was conducted using a slightly modified version of the procedure developed by Hanahan (Hanahan, 1983). Competent cells were prepared by inoculating a single well isolated colony from a freshly streaked LB agar plate into 5 mL of LB broth, and incubating at 37 ºC for 16 h with shaking between 200 – 230 rpm. The following day, this was used to inoculate 200 mL of fresh LB broth. The culture was incubated as before until a cultural density of OD_{600} = 0.3 was achieved. At which point, the culture was chilled on ice for 10 min, and the cells harvested by centrifugation at 1,500 x *g* for 10 min at 4 ºC. The supernatant was discarded and the pelleted cells resuspended in 80 mL of filter sterilised TFB1 [30 mM potassium acetate, 10 mM calcium chloride, 100 mM rubidium chloride, 50 mM manganese chloride, 15% (v/v) glycerol, pH 5.8]. The cells were harvested as above, and resuspended in 8 mL of filter sterilised TFB2 [10 mM MOPS, 75 mM calcium chloride, 10 mM rubidium chloride, 15% (v/v) glycerol, pH 6.5]. Aliquots of 50 – 100 μL were made in prechilled microcentrifuge tubes and rapidly frozen in liquid nitrogen. The frozen competent cells, were stored at < -70 ºC prior to use.

For transformation, competent cells were thawed on ice and incubated with plasmid DNA immediately upon thawing, for 30 min. Cells were then subjected to a heat shock, at 42 ºC for 30 sec, and returned to cool on ice for 3 min. At this point, 500 µL of SOC broth [2.0% (w/v) tryptone, 0.5% (w/v) yeast extract, 10 mM sodium chloride, 2.5 mM potassium chloride, 21.3 mM magnesium chloride, 10 mM magnesium sulphate, 20 mM glucose] was added to the transformation mixture, and the cells recovered by incubation at 37 ºC with shaking for 1 h. Cells were then spread on LB agar plates supplemented with the appropriate antibiotics and incubated at 37 ºC for 16 h in a static incubator to allow growth of single colonies.

2.4.3 Transformation of electrocompetent *Agrobacterium*

Preparation of electrocompetent *A. tumefacians* GV3101 was conducted as follows. A single well isolated colony was inoculated into 50 mL of LB broth, and cultured for 24 h at 28°C, with shaking between 200 – 230 rpm. This culture was then diluted (1:200) in to 1 L of LB broth in a 2 L flask and grown for a further 16 h at 28°C and shaking, as before. The 1 L culture was allowed to grow until an OD_{600} of 1.5 was achieved. At this point the culture was transferred into four 1000-mL Nalgene® Centrifuge bottles. The bottles were then immediately placed into a prechilled Fibrelite® F9S-4x1000y rotor (Thermo Scientific) and centrifuged at 5,650 x *g* for 15 min at 4 ºC using an RC 6+ Centrifuge (Thermo Scientific®/Sorvall®). The supernatant was discarded and the pelleted cells resuspended in a total volume of 2 L of prechilled sterile water. The cells were pelleted as before, and resuspended again in a total volume of 1 L of prechilled sterile water. The cells were pelleted as before, before being resuspended in a total volume of 40 mL of prechilled sterile 10% (v/v) glycerol. The resuspended cells were then divided between two 50-mL Oak Ridge Centrifuge Tubes (Nalgene®), and centrifuged at 5,650 x *g* for 15 min at 4 ºC using an RC 6+ Centrifuge (Thermo Scientific/Sorvall) using a prechilled SS34 rotor (Sorvall). Each pellet was then resuspended in 1 mL of prechilled 10% (v/v) glycerol. Aliquots of 50 – 100 µL were made in prechilled microcentrifuge tubes and rapidly frozen in liquid nitrogen. The frozen electrocompetent cells, were stored at < -70 ºC prior to use.

For transformation, aliquots of electrocompetent cells were thawed on ice. The plasmid DNA was added immediately upon thawing, and the transformation mix transfer to a prechilled 0.1 cm electroporation cuvette. The cuvette was then 'pulsed' using a MicroPulser Electroporator (Bio-Rad Laboratories Ltd., Bio-Rad House, Maxted Road, Hemel Hempstead, Hertfordshire, UK) using the pre-programmed 'Agr' setting to deliver a single pulse of 2.20 kV. Next, 500 μL of SOC broth was added to transformation mixture and transferred to a microcentrifuge tube. The cells were recovered by incubation at 28 ºC with shaking for 1 h; before being spread on to L agar plates supplemented with the appropriate antibiotics and incubated at 28 ºC for 36 – 48 h in a static incubator to allow growth of single colonies.

2.4.4 Polymerase chain reaction (PCR)

Standard end-point PCR was performed as described by Mullis (Mullis, 1990), using PfuTurbo® DNA polymerase (Stratagene) or VELOCITY DNA polymerase (BIOLINE) using the buffers provided by the manufacturers. Reaction mixes consisted of 1x buffer, 0.2 mM of each dNTP, 0.1 – 0.5 μM of each primer and either 1.25 U of PfuTurbo® DNA polymerase, 1.0 U of VELOCITY DNA polymerase or 1 μL of Phire® Hot Start DNA polymerase, plus template DNA and made up to 50 μL with sterile water. The amount of template DNA added was varied depending on its source (Table 2.2). For PCRs that proved problematic, primer annealing temperature was varied and/or PCR enhancers, such as 5% (v/v) DMSO or 1 M betaine, were also added. Thermal cycling was performed using a Biometra T3000 Thermocycler (Biometra, Goettingen, Germany), and amplification of products was typically achieved using the conditions described in Table 2.2.

2.4.4.1 Synthesis of oligonucleotide primers

Oligonucleotide primers were synthesised to order by Integrated DNA Technologies, Inc. (Belguim). Primers were supplied in a lyophilised form and resuspended in sterile water to a final concentration of 100 μM, prior to dilution to a working concentration 5 – 10 μM, and stored at -20 ºC. The oligonucleotide primers used in this study are described in Appendix Table F.

Table 2.2 General PCR conditions

	PfuTurbo® DNA polymerase			VELOCITY DNA polymerase			Phire® Hot Start DNA polymerase		
Amount of template DNA per 50 µL reaction									
genomic DNA / cDNA	50 – 100 ng			5 - 200 ng			25 - 250 ng		
plasmid DNA				50 pg- 50 ng			2.5 pg- 25 ng		
PCR reaction conditions									
Activation	95 ºC	2 min	1 x	98 ºC	4 min	1 x	98 ºC	30 s	1 x
Denaturation	95 ºC	60 s	30 x	98 ºC	30 s	40 x	98 ºC	5 s	35 x
Primer annealing*	45 - 69 ºC	60 s		50 - 68 ºC	30 s		60 ºC	5 s	
Primer extension	72 ºC	60 s per kb		72 º	15 – 30 s per kb		72 ºC	15 s	
Final extension	72 ºC	10 min	1 x	72 ºC	4 min	1 x	72 ºC	1 min	1 x
Holding step	4 ºC	∞	1 x	10 ºC	∞	1 x	4 ºC	∞	1 x

* Primer annealing temperature was typical 2 – 5 ºC below the predicted melting temperature (Tm) for the primer in the pair with the lowest value. Tm values were calculated using the OligoAnalyzer 3.1 tool on the IDT) website (http://eu.idtdna.com/analyzer/applications/oligoanalyzer/).

2.4.4.2 Colony PCR

Colony PCR was conducted to confirm that transformed cells contained the construct of interest, prior to DNA isolation and sequencing. In brief, single colonies were picked from plates and small amount transferred to a PCR tube, with the remainder of the colony inoculated into 4 – 10 mL of LB broth supplemented with the appropriate antibiotics. To each PCR tube was added 2.0 µL of 5 x Crimson *Taq* Reaction Buffer, 0.2 µL of 10 mM dNTPs, 0.2 µL of both the forward and reverse

primers (5 – 10 μM), 7.3 μL of water, and 0.1 μL of Crimson *Taq* DNA Polymerase (New England Biolabs). Thermal cycling was performed using the conditions described in Table 2.3. Five-μL of PCR reactions were loaded directly onto agarose gels, and gel electrophoresis performed (Section 2.4.5) to confirm amplification of a product of the expected size.

Table 2.3 Colony PCR conditions

Activation/ Cell lysis	95 ºC	10 min	1 x
Denaturation	95 ºC	30 s	35 x
Primer annealing*	45 - 55 ºC	60 s	
Primer extension	60 ºC	2 min	
Final extension	68 ºC	5 min	1 x
Holding step	8 ºC	∞	1 x

2.4.5 Agarose gel electrophoresis

Gels of between 0.7 – 4.0 % (w/v) agarose were cast in TAE buffer [40 mM Tris-acetate, 1.0 mM EDTA, pH 8.0] containing 0.5 $\mu g.mL^{-1}$ ethidium bromide. Gels were submerged horizontally in TAE buffer. Prior to loading, DNA samples were mixed with 4 x DNA loading buffer [12% (w/v) Ficoll 400 and 0.25% (w/v) Orange G]. Samples were loaded alongside molecular weight markers [1 kb Plus DNA ladder (Invitrogen), or Low Molecular Weight DNA Ladder (New England Biolabs)]. Once loaded, gels were run at a constant voltage of ~ 100 V, until the tracker dye had run sufficiently through the gel. DNA was visualised using exposure to ultraviolet (UV) (λ = 365 nm) light from a transilluminator.

2.4.5.1 Purification of DNA fragments by spin column

PCR products and DNA fragments were purified using the QIAquick PCR Purification Kit (Qiagen) or NucleoSpin® Extract II Kit (MACHEREY-NAGEL) as per the manufacturers' protocol. Essentially this method utilises a silica-gel membrane that adsorbs DNA, only in high concentrations of chaotropic salts. After washing to remove contaminants, DNA was eluted for the membrane in 30 – 50 μL in sterile water and stored at -20 ºC.

2.4.5.2 Purification of DNA fragments by gel extraction

DNA fragments were subject to agarose gel electrophoresis as described above (Section 2.4.5) until sufficient separation was achieved, to allow excision of bands from the gel using a sterile razor blade. Purification of DNA was carried out using the QIAquick Gel Extraction Kit and QIAEX II Gel Extraction Kit (Qiagen), or NuceloSpin® Extract II Kit (MACHEREY-NAGEL) as per the manufacturer's protocol.

2.4.6 Site-directed mutagenesis

The majority of mutants used in this study were supplied to order by Genscript (USA), either by mutagenesis of a template DNA or synthesis of mutant sequence flanked by the *att*B recombination sites and supplied in a pUC57 vector. However, two mutants were generated using the two different methods outlined below. In all cases, the mutations were confirmed by DNA sequencing (Section 2.4.7).

2.4.6.1 Whole plasmid mutagenesis by Quikchange method

Whole plasmid mutagenesis was employed to introduce a site-directed point mutation into the PexRD2$^{vloop-8}$ DNA sequence (see Section 5.2.10) using a modification of the Quikchange PCR protocol (Stratagene). Pairs of primers containing the desired E90A mutation were designed using the QuikChange Primer Design online tool (Agilent Technologies). Reaction mixes consisted of 1x x HI-Fi Buffer, 0.2 mM of each dNTP, 0.1 μM of each primer, 3% (v/v) DMSO and 1.0 U of

VELOCITY DNA polymerase, plus 10 ng of purified plasmid DNA (pDONR™201:vloop-8) and made up to 50 µL with sterile water. Amplification was carried out using the conditions as described in Table 2.4.

Digestion of original template DNA was achieved by addition of 1 µL of DpnI to the reaction mix followed by incubation at 37 ºC for 1 h, prior to transformation into chemically competent *E. coli* as described in Section 2.4.2. The mutated pDONR™201:vloop-7 was obtained by isolation of plasmid DNA followed by DNA sequencing to confirm presences of the desired mutation.

Table 2.4 Quikchange PCR conditions

Activation	98 ºC	5 min	1 x
Denaturation	96 ºC	50 s	18 x
Primer annealing*	65 ºC	50 s	
Primer extension	72 ºC	3 min 20 s	
Final extension	72 ºC	10 min	1 x
Holding step	8 ºC	∞	1 x

2.4.6.2 Overlap extension PCR (oe-PCR)

Overlap extension allows the introduction of specific mutations, by using PCR to generate two DNA fragments that have overlapping ends containing the desired mutation, before reconstitution of the full length (Ho *et al.*, 1989). This method was used when whole plasmid mutagenesis proved problematic for generation of the CRN8-D2$^{R469A/D470A}$ mutations (Section 6.2.1), presumably as a result of the large size of the vector backbone. A set of complementary primers were designed so that they differed from the template sequence only by the substitutions required to cause the desired mutation. Two PCR reactions were set up as described above (Section 2.4.4), but each using one flanking primer and one of these internal 'mis-matched' primers (see Figure 2.1). The PCR products of these two reactions were subjected to DpnI digestion to remove template DNA, and purified as described above. One-µL aliquots of each of the purified products were then mixed and diluted 250-fold in

water. This template mix was then used in an overlap extension PCR reaction mix as follows: 1x PfuTurbo® buffer, 0.2 mM of each dNTP, 0.5 µL of template mix and 1.25 U of PfuTurbo® DNA polymerase and made up to 47.5 µL with sterile water. This mix was subjected to seven cycles of PCR to cause extension from the overlapping region and regenerate the full length product. At this point 1 µL of each of the flanking primers (5 mM), plus an additional 0.5 µL of 10 mM dNTPs was added (total volume = 50 µL). The reaction was mixed by gentle pipetting, and subjected to PCR as described above (Section 2.4.4). The resultant full length PCR product containing the desired mutations was then purified from the reaction mix by gel purification (Section 2.4.5), and used for subsequent In-Fusion PCR cloning (Section 2.4.8.1).

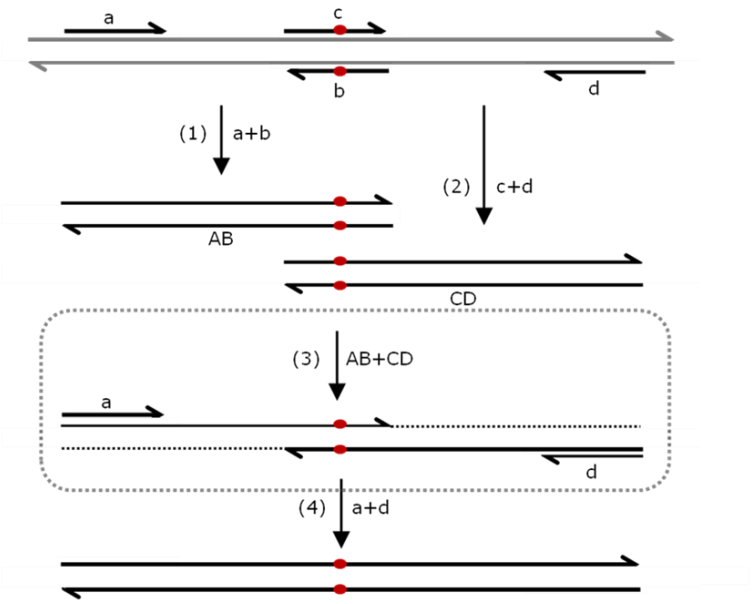

Figure 2.1 Site-directed mutagenesis by overlap-extension PCR

Template DNA (grey arrows) was mixed with one flaking primer and one internal primer containing the desired mutation (red circle) (a + b or c + d). Two separate PCRs were conducted (1 and 2). The purified products of these reactions, AB and CD were then mixed and subjected to further rounds of PCR (3). Extension from the overlap region recreated the full length product (dotted lines). The flanking primers (a + d) were then added to the same reaction mix (within the dotted rectangle) and further rounds of PCR conducted to amplify the full length product containing the desired mutation.
Figure based original from Ho et al., (1989).

2.4.7 DNA Sequencing

DNA sequencing was performed to order by GATC Biotech AG (European Custom Sequencing Centre, Köln, Germany). Between 0.6 – 2 μg of purified plasmid was sent, together when required with custom sequencing primers at a final concentration of 10 pmol.μL^{-1}. Sequencing was performed using the dideoxy chain termination/cycle sequencing technique on an ABI 3730xl (Applied Biosciences, California, USA). Alternatively, ~100 ng of plasmid DNA, was mixed with 2 μL of 5 x sequencing buffer [350 mM Tris-HCl pH 8.8 and 2.5 mM magnesium chloride], 1 μL ABI Big Dye Terminator Ready Reaction Mix Ver 3.1 (Invitrogen), 1 μL of 30% (v/v) DMSO, and 1 μL of sequencing primer (5 – 10 μM) in a total volume of 10 μL. Reactions were mixed and incubated in a Thermocycler using the conditions described in Table 2.5, Reactions were then submitted to Genome Enterprise Ltd (Norwich Research Park) and analysed on an ABI 3730xl sequencer.

Table 2.5 DNA sequencing conditions

Denaturation	96 ºC	10 s	
Primer annealing	45 or 50 ºC	5 s	25 x
Primer extension	60 ºC	4 min	
Holding step	8 ºC	-	1 x

2.4.8 Cloning methods

2.4.8.1 In-Fusion® PCR cloning

The In-Fusion® PCR cloning system is based on a proprietary enzyme with proof-reading exonuclease activity, which catalyses the joining of DNA duplexes via exposure of complementary single-stranded sequences. Consequently, linearised vectors and inserts can be precisely joined in an entirely sequence-independent manner, as long as there are sufficient regions of homology in their ends. This

homology can be engineered into the PCR-generated insert by designing primers that include homology to the linearised vector sequence (Berrow *et al.*, 2007). During incubation of the amplified PCR products and the linearised vector with the In-Fusion™ enzyme, the 3'→5' proofreading activity causes the exposure of complementary single-stranded sequences. These intermediates anneal to form a population of joint molecules that are relatively resistant to exonuclease activity and hence accumulate in the reaction (Hamilton *et al.*, 2007).

In-Fusion® cloning reactions with pOPIN vectors were conducted as described in the user manual. Vectors were linearised by treatment with KpnI and HindIII, before being purified by gel extraction (Section 2.4.5.2, Figure 2.2 A). PCR, using primers designed to add 15-bp of sequence homologous to the ends of the linearised vector, was conducted to amplify the fragment (Figure 2.2 B). Since the proofreading exonuclease activity of the In-Fusion® enzyme occurs in a 3'→5' direction, the 3'-overhang in the 5'-In-Fusion site, caused by KpnI, is lost. On the other hand, the 5'-overhang in the 3'-In-Fusion site, caused by HindIII, is maintained, and the adapter sequences added to the respective primers are designed taking this into consideration. Purified PCR insert (10 – 100 ng) was then mixed with 100 ng of linearised vector, in 10 μL of water and added to one well of In-Fusion™ Dry-Down (Clontech) and mixed to resuspend the pellet. Alternatively, the PCR insert and linearised vector were combined with 2 μL of 5X In-Fusion™ HD enzyme premix (Clontech) and diluted to a total volume of 10 μL with water. These reaction mixes were incubated at 42 ºC for 30 min (Figure 2.2 C). Next, either 3 – 5 uL of this reaction volume were transformed into chemically competent *E. coli* DH5α as described above (Section 2.4.2), or the reaction was frozen until ready to proceed. Transformed cells were subjected to blue/white screening using LB agar selection plates supplemented with 100 $\mu g.mL^{-1}$ carbenicillin, 1 mM IPTG, and 0.02% (w/v) X-gal. White colonies were selected for downstream processing, and all constructs were confirmed by sequencing.

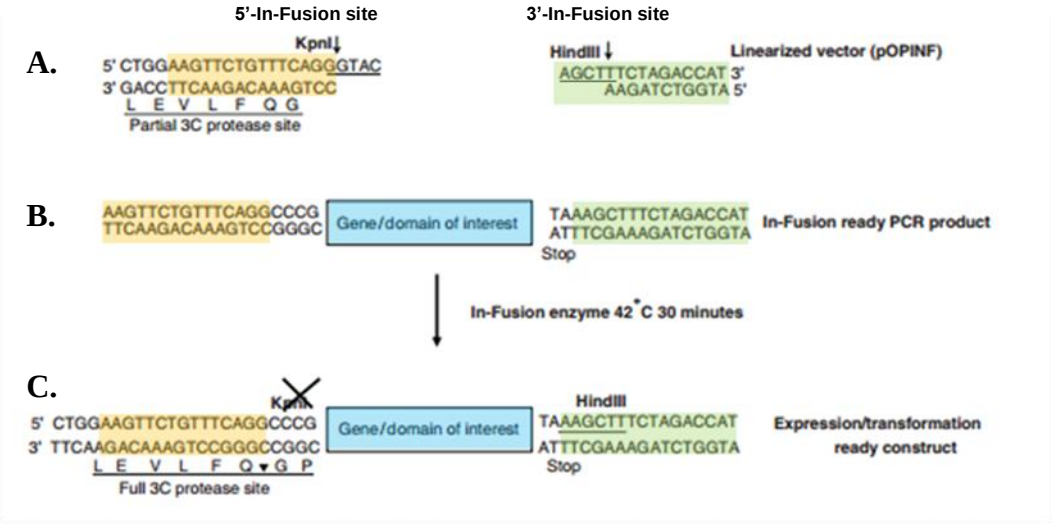

Figure 2.2 In-Fusion® PCR cloning using pOPIN vectors

(A.) pOPINF following digestion with KpnI and HindIII exposes 5'- (orange) and 3'- (green) In-Fusion sites. **(B.)** Amplification of gene of interest (blue), flanked by sequences homologous to infusion sites (coloured as in A.) **(C.)** In-Fusion® reaction ligates the PCR product into the linearised vector, removing the KpnI site and creating the full 3C protease site. *Figure adapted from Berrow* et al.*, (2009)*

2.4.8.2 Endonuclease restriction and ligation cloning

Restriction endonucleases and T4 ligase together with appropriate buffers were purchased from standard commercial sources (New England Biolabs (UK) Ltd, Hertfordshire, UK or Fermentas International Inc.), and reactions carried out according to the manufacturers' instructions, using the appropriate supplied reaction buffers for the enzyme/s being used. Where buffer requirements were compatible, double digests involving two restriction endonucleases in a single reaction were used. Restriction endonuclease digests were typically performed in 30-µL reaction volumes at 37 ºC for 2 – 16 h. If possible, resulting digests were heat inactivated and digested products were analysed by gel electrophoresis, prior to purification by gene extraction (Section 2.4.5.2) or spin column procedure (Section 2.4.5.1). To prevent re-ligation, up to 1 µg of linearised vectors were treated with rAPid Alkaline Phosphatase (Roche) to dephosphorylate 5' ends, according to the "Standard Dephosphorylation Procedure" in the product instructions. Reaction volumes of 10 – 20 µL were used for DNA ligations. Samples were incubated at 4 ºC for 16 h, prior to transformation into chemically competent *E. coli* (Section 2.4.2).

2.4.8.3 TOPO® cloning

Gel purified PCR products (Section 2.4.5.2) were cloned into pENTR™/D-TOPO® vector (Invitrogen) as described in the manufacturer's manual with the following minor modifications. Reaction mixes were incubated at RT for 15 – 30 min, and the entire reaction volumes were transformed into aliquots of chemically competent *E. coli* as described in Section 2.4.2.

2.4.8.4 T-vector cloning

PCR products were cloned into pGEM®-T Easy Vector (Promega) as outlined below. To add 3' adenosines to the ends of DNA fragments, purified PCR products amplified using a proof-reading polymerase were incubated with 1.0 µl of 10x *Taq* reaction buffer, 0.3 µl of 50 mM MgCl2, 0.2 µl of 10 mM dATP, 1.0 µl of Taq DNA polymerase in a total volume of 10 µL, at 70 ºC for 20 min. Three-µL of these A-tailing reactions were then incubated with 5 µL of 5X Rapid Ligation Buffer, 1 µL of pGEM®-T Easy Vector (50 ng.µl^{-1}) and 1 µL of T4 DNA Ligase (3 Weiss units.µl^{-1}) in a total volume of 10 µL. Samples were incubated at 4 ºC for 16 h, prior to transformation into chemically competent *E. coli* (Section 2.4.2). Transformed cells were subjected to blue/white screening using LB agar selection plates supplemented with 100 µg.mL^{-1} carbenicillin, 1 mM IPTG, and 0.02% (w/v) X-gal. Typically, white colonies were selected for downstream processing.

2.4.8.5 Gateway® cloning

Gateway® cloning was conducted using Gateway® BP Clonase™ II Enzyme Mix and Gateway® LR Clonase™ II Enzyme Mix (Invitrogen) as described in the manufacturer's manuals with the following minor modifications. Reaction mixes were incubated at RT for 1 – 16 h, prior to Proteinase K treatment. Up to 6 µL of the final reaction volume was used for transformation into an aliquot of chemically competent *E. coli* as described in Section 2.4.2.

In some instances, entry clones and destination vectors contained the same antibiotic selection gene, typically conferring kanamycin resistance. To overcome this entry clones were linearised by digestion (Section 2.4.8.2) with NruI which cuts within the

KanR gene or the entire *KanR* gene was removed by digestion with BspHI, which cuts at sites flanking the gene in the pENTR-D/TOPO vector, followed by gel purification (Section 2.4.5.2). These Kan^R disabled entry clones were then included in LR reactions as described above.

2.4.8.6 Construction of pERCH vector

A double haemagglutination-epitope tag was amplified by PCR, using Phire® Hot Start DNA polymerase, from the pBTEX:Pto-2xHA binary vector (provided by Professor Gregory Martin, (Boyce Thompson Institute for Plant Research, Ithica, NY)) (Section 2.4.4). This sequence was flanked by 5' PacI and 3' SpeI restriction sites, encoded in the primers used for amplification. This fragment was cloned into pGEM®-T Easy Vector to yield pGEM:H1 by T-vector cloning (Section 2.4.8.4). This plasmid was digested by double digest with PacI and SpeI and the epitope encoding fragment purified by gel extraction. This purified fragment was then ligated into linearised, dephosphorlyated pER8 vector that had been sequentially digested with PacI, and then SpeI (Section 2.4.8.2). Sequential digestion was employed, as opposed to double digestion, since the two restriction sites overlapped in the vector sequence. The sequence of the multiple cloning site and epitope tag of the resultant pERCH (pER8 with C-terminal HA-tag) was confirmed by DNA sequencing (Section 2.4.7).

2.5 Protein procedures

2.5.1 Separation of proteins by discontinuous sodium dodecyl sulphate polyacrylamide gel electrophoresis (SDS-PAGE)

SDS-PAGE gels were run as previously described by Laemmli (Laemmli, 1970) with minor modifications. Resolving gels of either 12% or 17% (w/v) polyacrylamide were prepared by diluting the appropriate volume of a 30% (w/v) stock solution of acylamide/bis-acrylamide (37.5:1) in 375 mM Tris-HCl pH 8.8 and 0.1% (w/v) SDS, supplemented with 0.1% (w/v) ammonium persulfate, and 0.04% (v/v) N,N,N',N'-tetramethylethylenediamine added immediately prior to

pouring. The resolving gel was poured between two Mini PROTEAN® system (Bio-Rad) glass plates separated by 1 mm until the meniscus reached approximately 2 cm from the top of the shorter plate. Water-saturated butanol was then overlaid on top of the resolving gel until it had set, to ensure a level surface. The butanol was subsequently removed by extensive washing with Milli-Q (ultrapure) water. A 5% (w/v) polyacrylamide stacking gel was prepared by diluting the appropriate volume of a 30% (w/v) stock solution of acylamide/bis-acrylamide in 63 mM Tris-HCl pH 6.8 and 0.1% (w/v) SDS, supplemented with 0.1% (w/v) ammonium persulfate, and 0.1% (v/v) N,N,N',N'-tetramethylethylenediamine added immediately prior to pouring on top of the resolving gel. A plastic comb was then inserted into the liquid stacking gel to provide wells for sample loading. After the gel was set they were individually wrapped in cling film and stored, until required, at 4 ºC in a humid atmosphere - a sealed plastic box lined with wet paper towels.

To run a gel, the gel was placed into a Mini PROTEAN® Tetra Cell system (Bio-Rad) and the plastic comb removed. The gel was completely covered and both chambers were filled with SDS-running buffer [25 mM Tris-HCl, 250 mM glycine, and 0.1% (w/v) SDS]. Protein samples were typically prepared by adding a 4x SDS gel-loading buffer [0.2 M Tris-HCl pH 6.8, 0.4 M DDT, 8 % (w/v) SDS, 0.4% (w/v) bromophenol blue, 40% glycerol] to a protein extract or solution and incubating them at 95 ºC for 5 min, before loading into the wells in the stacking gel. Samples were loaded alongside molecular weight markers [SeeBlue® Plus2 Pre-Stained Standard (Novex), PageRuler™ Prestained Protein Ladder (Fermentas) or BenchMark™ His-tagged Protein Standard (Novex)]. Electrophoresis was performed at a constant voltage of typically 150 V for 45 – 60 min.

2.5.2 Staining of SDS-PAGE gel

Protein gels were stained with InstantBlue (Novexin, Babraham Hall, Babraham, Cambridge, UK) following manufacturer's procedures. InVision™ His-Tag In-Gel Stain (Novex) was used to detect hexa-histidine tagged proteins in accordance with the manufacturer's procedures.

2.5.3 Expression of recombinant proteins in *E. coli*

Typical small scale expression tests of recombinant proteins were conducted as follows. A single colony from plates of BL21(DE3), freshly transformed with the desired plasmid, was inoculated into 10 mL of LB media containing appropriate antibiotics. This culture was then grown for 16 h at 37 ºC with shaking and used to inoculate 10 mL (1/20) of either LB media or auto-induction media (AIM - LB Broth Base including Trace elements (ForMedium™)), supplemented with appropriate antibiotics. These cultures were grown further at 37 ºC with shaking until a cultural density of OD_{600} = 0.4 – 0.6 was achieved. At this point the cultures grown in LB media were induced with 1 mM IPTG, and 4 mL of each culture was transferred into two 24 deep well plates (STARLAB group). One plate was incubated at 37 ºC as before for a further 3 – 4 h, whilst the other was incubated at 18 ºC for approximately 16 h. After these incubations were complete, the cells were harvested by centrifugation at 3,600 x *g* for 5 min at 4 ºC using a Legend® RT centrifuge (Sorvall) and stored at < -70 ºC for at least 1 h before proceeding to protein extraction.

Protein extraction was conducted by allowing the pellets to thaw before resuspension in 1 mL of Lysis Buffer [50 mM Tris-HCl pH8.0, 300 mM sodium chloride, 20 mM imidazole, 5% (v/v) glycerol, supplemented with 0.1% polyethylenimine (PEI), EDTA free protease inhibitor tablets and 0.5 $mg.mL^{-1}$ lysozyme]. Cells were then lysed, in the 24 deep well plates, by sonication using a Vibra-Cell™ 750 Watt ultrasonic processor, VC 750, (Sonics & Materials, Inc., Newtown, CT , USA) and a 24-element probe. Cells were sonicated using a maximum amplitude of 40%, and repeated cycles of a 1-second pulse followed by a 2-second pause for a total of 3 min, to minimise heat generation. The 24 deep well plates were kept on ice throughout to further counteract heat generation.

A volume of 30 µL of cell lysate was mixed with 10 µL of 4x SDS gel-loading buffer and this total protein sample prepared and analysed by SDS-PAGE (Section 2.5.1). The remainder of the cell lysate was clarified by centrifugation at 3,600 x *g* for 40 min at 4 ºC using a Legend® RT centrifuge (Sorvall). A 30 µL sample of clarified cell lysate was mixed with 10 µL of 4x SDS gel-loading buffer as before to give a soluble fraction sample for SDS-PAGE analysis.

Once optimal expression conditions for each recombinant protein had been determined using small scale expression trials, these conditions were scaled up to 1 L culture volumes grown in 2 L flasks to ensure good aeration. Typically, these cultures were inoculated with 50 mL (1/20) of an overnight starter culture, grown at 37 ºC with shaking until a cultural density of OD_{600} = 0.4 – 0.6 was achieved. At this point a 4-mL sample of uninduced cells was harvested and prepared for SDS-PAGE analysis as described for small scale expression trials above. The cultures were induced with 1 mM IPTG and incubated as determined in the small scale expression trials. Following this a further 4-mL sample of induced cells was harvested and prepared for SDS-PAGE analysis. The remaining culture was transferred into two 1000-mL Nalgene® Centrifuge bottles per original litre of culture. The bottles were then immediately placed into a prechilled Fibrelite® F9S-4x1000y rotor (Thermo Scientific) and centrifuged at 5,670 x *g* for 7 min at 4 ºC using an RC 6+ Centrifuge (Thermo Scientific/Sorvall). Pelleted cells were resuspended in <50 mL of LB media, transferred to 50 mL centrifuge tubes (CORNING) and centrifuged again at 3,600 x g for 10 min at 4 ºC using a Legend® RT centrifuge (Sorvall), prior to storage at < -70 ºC.

2.5.4 Purification of recombinant proteins from soluble fraction

Cell pellets from large scale expressions were typically resuspended in 25 mL per original litre of culture of chilled A1 buffer [50 mM Tris-HCl pH 8.0, 50 mM glycine, 5% (v/v) glycerol, 500 mM sodium chloride, 20 mM imidazole] supplemented prior to use with EDTA free protease inhibitor tablets. Cells were then lysed: either by sonication as described above (Section 2.5.3), but for a total time of 6 – 9 min; or by using a cell disrupter (Constant Systems Limited, Low March, Daventry, Northamptonshire, UK) in ONE-SHOT mode and at a pressure of 25 kpsi. Resuspended cell pellets and lysates were kept chilled on ice throughout. The whole cell lysate was then clarified by centrifugation in 50-mL Oak Ridge Centrifuge Tubes (Nalgene), and centrifuged at 40,000 x *g* for 20 min at 4 ºC using an RC 6+ Centrifuge (Thermo Scientific/Sorvall) using a prechilled SS34 rotor (Sorvall). Following this first centrifugation, the supernatant was transferred to a fresh

centrifuge tube and centrifuged for a further 20 min as before to yield a clarified cell lysate.

2.5.4.1 Purification of proteins by immobilised metal ion affinity chromatography (IMAC)

The clarified cell lysate was applied to a 5 mL nickel (II) (Ni^{2+}) charged HisTrap FF column (GE Healthcare) that had been pre-equilibriated in A1 buffer (Section 2.5.4) using an ÄKTAxpress (GE Healthcare) at 4 ºC. The column was then washed with ~10 column volumes of A1 buffer, before the protein of interest was step-eluted with B1 buffer [50 mM Tris-HCl pH 8.0, 50 mM glycine, 5% (v/v) glycerol, 500 mM sodium chloride, 500 mM imidazole]. Eluted fractions spanning the peak on the elution profile, as measured by absorbance at 280 nm, were prepared and analysed by SDS-PAGE.

2.5.4.2 Purification of proteins by size exclusion chromatography

Size exclusion chromatography separates macromolecules based on their size and shape. Pooled fractions containing the protein of interest were concentrated using an appropriate molecular weight cut off centrifuge cell (Sartorius) to a volume of <10 mL. Concentrated protein was centrifuged at 15,000 x *g* at 4 ºC for 30 min to pellet any insoluble material. Protein solution was then injected on to a Hi-Load 26/60 Superdex 75 prep grade gel filtration column (GE Healthcare) pre-equlibrated and run in A4 buffer [50 mM HEPES, 150 mM sodium chloride, pH 7.5]. Columns were run using an AKTA Xpress at 4 ºC. A flow-rate of 3 $mL.min^{-1}$ was used, with a total flow volume of two column volumes. Absorption at 280 nm was monitored continuously throughout and peak fractions collected.

2.5.5 Cleavage of the affinity tag using 3C protease

The affinity tags of recombinant proteins, expressed using the pOPIN suite of vectors, were removed by proteolytic cleavage by recombinant human rhinovirus (HRV) 3C protease owing to the presence of 3C protease site (LEVLFQ▼GP) in the

linker region. Following cleavage, only the short glycine-proline dipeptide remains at the N-terminus of the cleaved protein. The protease itself has a hexa-histidine tag to allow its own purification, and separation from the cleaved fusion protein.

Proteolytic cleavage was conducted in A4 buffer (Section 2.5.4.2) supplemented with 2 mM β-mercaptoethanol and 12 μg of recombinant protease per mg of fusion protein, using a concentration of fusion protein of 1 – 2 $mg.mL^{-1}$. This reaction solution was then typically incubated at 4 ºC for approximately 16 h. Next, the reaction solution was applied directly to a 5 mL Ni^{2+} charged HisTrap HP column that had been pre-equilibriated in A1 buffer (Section 2.5.4). The column was then washed with five column volumes of A1 buffer using a peristaltic pump and the flow-through, which should contain the cleaved protein of interest, was collected. Any proteins bound to the nickel column, i.e. the cleaved hexa-histidine tags, the recombinant HRV 3C protease and any uncleaved fusion protein, were subsequently eluted in five column volumes of B1 buffer (Section 2.5.4) using a peristaltic pump.

Samples of the fusion protein before and after incubation with protease, alongside samples of the HisTrap column flowthrough and eluted proteins were analysed by SDS-PAGE to assess efficiency of cleavage. The flowthrough containing the cleaved fusion protein was concentrated to a volume of <10 mL before injecting onto a Hi-Load 26/60 Superdex 75 gel filtration column (GE Healthcare) as described above (Section 2.5.4.2).

2.5.6 Purification of recombinant proteins from inclusion bodies

Inclusion bodies (IB) were purified as described below. The insoluble cell pellets formed after the clarification of cell lysates (Section 2.5.4) were washed five times in IB Wash buffer [50 mM Tris-HCl pH 8.0, 150 mM sodium chloride, 500 mM urea, 0.5% (v/v) Triton X-100, supplemented with EDTA free protease inhibitor tablets]. Each wash consisted of resuspending the cell pellets in a volume of 10 mL of buffer per litre of culture volume, before centrifugation at 2,200 x *g*, for 10 min at 4 ºC. The purpose of the detergent in the washing buffer is to remove contaminating lipids and membranes from the insoluble cellular debris. However, detergent can interfere with downstream characterisation of the protein (Prince and Jia, 2012). As such the

washed inclusion bodies were washed three more times in the IB Rinse buffer, which contains no detergent [50 mM Tris-HCl pH 8.0, 150 mM sodium chloride, 500 mM urea, supplemented with EDTA free protease inhibitor tablets]. The cleaned inclusion body pellet was then solubilised by resuspension in IB Solubilisation buffer [50 mM Tris-HCl pH 8.0, 150 mM sodium chloride, 8.0 M urea, 5 mM β-mercaptoethanol, supplemented with EDTA free protease inhibitor tablets], using 12.5 mL of buffer per litre of culture volume. The solubilisation solution was left at RT for 16 – 20 h with stirring.

Any remaining insoluble material was then removed by two centrifugation steps at 17,000 x *g* for 45 min and 15 ºC. The solubilised material was applied to a 5 mL nickel (II) (Ni^{2+}) charged HisTrap HP column (GE Healthcare) that had been pre-equilibrated in A1-denaturing buffer [50 mM Tris-HCl pH8.0, 150 mM sodium chloride, 8.0 M urea, 5 mM β-mecraptoethanol, 20 mM imidazole] using an ÄKTApurifier (GE Healthcare) at RT. The column was then washed with 10 column volumes of A1-denaturing buffer, and fractions corresponding to this flow-through (FT) were collected. The protein of interest was step-eluted with B1-denaturing buffer [50 mM Tris-HCl pH 8.0, 150 mM sodium chloride, 8.0 M urea, 5 mM β-mecraptoethanol, 500 mM imidazole]. Eluted fractions spanning the peak on the elution profile as measured by absorbance at 280 nm were prepared and analysed by SDS-PAGE, alongside the FT fraction samples.

The fractions containing the denatured protein were then pooled and the protein refolded by rapid dilution. Initially a small scale refolding condition screen was conducted to determine conditions that minimised protein aggregation upon removal of the denaturant. The pH of the refolding buffer was assessed using four different buffers (sodium citrate-HCl pH 4.0; MES-NaOH pH 6.0; Tris-HCl pH 8.0; and CHES-NaOH pH 10.0). Two salt concentrations were also tested in a fully factorial design. As such, the eight refolding buffers tested contained 50 mM of the appropriate pH buffer, either 150 mM or 500 mM sodium chloride, 10% (v/v) glycerol, 20 mM imidazole, and 5 mM β-mercaptoethanol. 100-µL aliquots of pooled denatured protein (concentration ~3.0 $mg.mL^{-1}$) were then added dropwise to 5 mL (1/50 dilution) of each refolding buffer, kept ice cold and with stirring. Each refolding solution was then incubated at 4 ºC for 1 h, after which the turbidity of each refolded protein solution was assessed visually. A 2-mL sample of each

solution was centrifuged at 17,000 x *g*, for 40 min at 4 ºC, and a sample of the supernatant collected for SDS-PAGE analysis. Precipitant pellet formation following centrifugation was also scored visually. Optimal refolding conditions were determined as those that minimised buffer turbidity and pellet formation and maintained the protein in solution following centrifugation.

Large-scale protein refolding was then conducted using optimised refolding conditions by rapid dilution as described above. Following refolding the solution was clarified by centrifugation at 17,000 x *g*, for 40 min at 4 ºC and the supernatant purified using IMAC and SEC (Section 2.5.4.1 – 2.5.4.2).

2.6 Crystallographic methods

Protein crystals are required for X-ray crystallography since the diffraction from a single molecule would be too weak to be measurable. Using a crystal, where multiple protein molecules are arranged in an ordered three-dimensional lattice, magnifies the signal. The aim of protein crystallisation is to bring a protein solution to a supersaturated state whereby nucleation and subsequent crystal growth can occur. All crystallisation in this study was conducted using the vapour diffusion method (Figure 2.3). This involves the diffusion of water vapour from a small drop of protein solution containing precipitant and a larger reservoir with a much higher concentration of precipitant in a closed system. This leads to an increase in the concentration of protein and precipitant in the drop. In ideal cases the concentration of precipitant increases to a level that results in the formation of crystallisation nuclei. As the protein crystal forms, the concentration of protein remaining in solution decreases and falls into the 'metastable zone' where no more nuclei are formed but existing protein crystal continue to grow.

2.6.1 Initial crystallisation trials

Initial crystallisation trials were set up using protein with the affinity tag cleaved and concentrated in A4 buffer, following purification by size exclusion chromatography (Section 2.5.4.2). Pooled fractions containing the protein of interest were

concentrated using an appropriate molecular weight cut off centrifuge cell (Sartorius) and centrifuged in a microcentrifuge at 17,000 x *g* for 30 min at 4 ºC to pellet any insoluble material. The protein concentration of a diluted sample of the concentrated protein was determined by measuring the absorbance at 280 nm using a NanoDrop 1000 spectrophotometer (Thermo Scientific). The computed percent solution extinction coefficient for the protein, as estimated by the ProtParam program (Gasteiger *et al.*, 2005) located on the Expert Protein Analysis System (ExPASy) proteomics server, was used to establish the protein's concentration (Equation 2.1). The solution was then diluted accordingly in A4 buffer to adjust the protein concentration to 12 $mg.mL^{-1}$.

Initial crystallisation trials were conducted in 96-well format with sitting drops in MRC 2-well crystallisation plates (Molecular Dimensions) using the vapour diffusion method (Figure 2.3). Screens used in this study are listed in Table 2.6. The reservoir of each well in the plate was filled with 100 µL of precipitant solution from each sparse-matrix screen, using a Freedom EVO (Tecan). Aliquots of 0.3 µL of this concentrated protein solution were then mixed with equal volumes of the precipitant solution from each reservoir and placed into the sub-well using an OryxNano crystallisation robot (Douglas Instruments). The wells were then sealed with adhesive tape and left to equilibrate at 18 ºC. The plates were examined with a microscope after 24 h, and then at regular intervals for several weeks.

Equation 2.1

Calculating the concentration of a given protein in solution using the absorbance at 280 nm

$$\frac{\mathbf{A}_{280\ \mathrm{nm}}\ \text{of diluted sample}}{\begin{array}{c}\textbf{percent solution extinction coefficent}\\ (\textbf{for } \mathbf{0.1\%}\ \textbf{aquaeous solution})\end{array}} \times \frac{\mathbf{1}}{\textbf{dilution factor}}$$

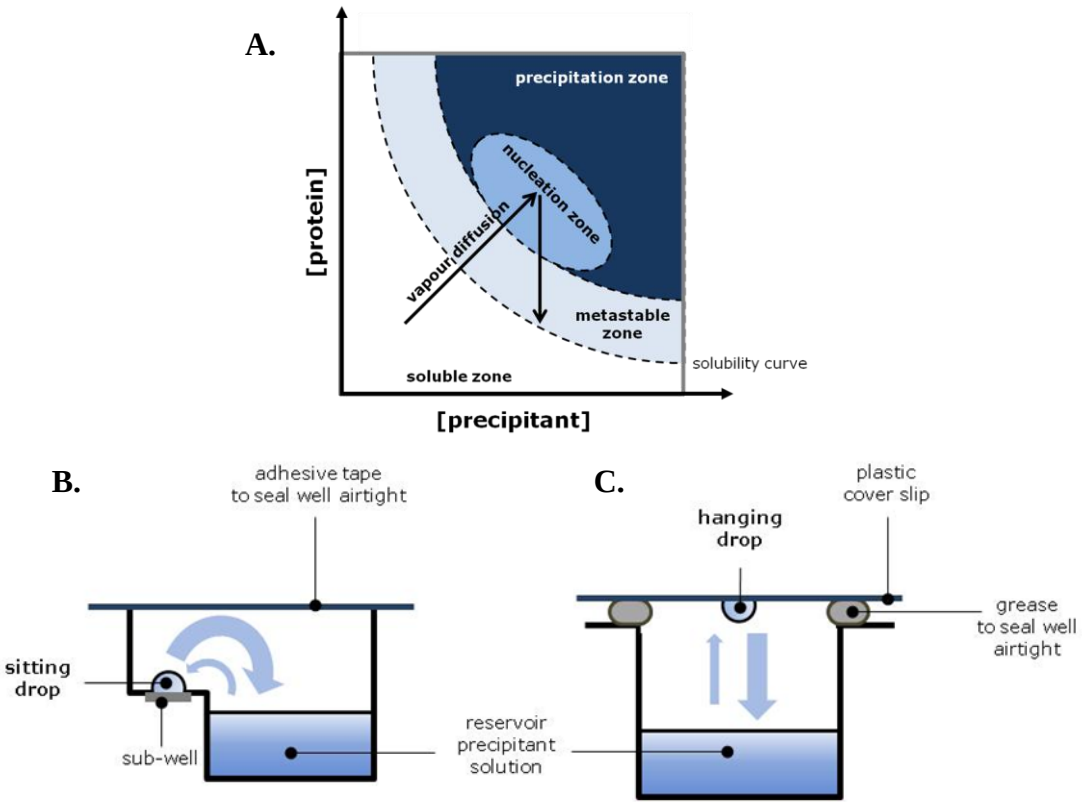

Figure 2.3 Crystallisation by vapour diffusion

(A.) Protein solubility phase diagram showing crystallisation by vapour diffusion. Schematic representations of **(B.)** sitting drop and **(C.)** hanging drop methods. Arrows represent the diffusion of water molecules.

Table 2.6 Crystallisation screens used in this study

Screen	Supplier
The PEGs suite	Qiagen
The $AmSO_4$ Suite	Qiagen
JCSG-plus™	Molecular Dimensions (MD1-37)
PACT premier™	Molecular Dimensions (MD1-29)
Structure Screen 1 and 2	Molecular Dimensions (MD1-01, MD1-02)

2.6.2 Optimisation of crystallisation conditions

Any promising conditions observed in initial crystallisation screens were optimised with the aim of producing more, diffraction quality, protein crystals. All optimisations were conducted using hanging drop vapour diffusion method (Figure 2.3) using 24-well plates (Molecular Dimensions). A range of reservoir solutions, based on the promising conditions, were prepared by slightly varying the concentration of precipitants, buffer, and pH and by the addition of potential cryoprotectants. Each well of the plate contained 1 mL of a variant reservoir solution, and 2 μL of each reservoir solution was mixed with 2 μL of concentrated protein solution (Section 2.6.1) in A4 buffer (Section 2.5.4.2) on a plastic cover slip. The cover slip was then placed over the corresponding well sealed in place using vacuum grease (Figure 2.3). These plates were then left to equilibrate at 18 ºC, and examined with a microscope at regular intervals until crystals developed.

2.6.3 Cryoprotection of protein crystals for data collection

A cryoprotectant is necessary so that the crystals can be cooled to cryogenic temperatures without the formation of ordered crystalline ice. Formation of crystalline ice should be avoided as it disrupts the internal order of the crystal, owing to its expansion in solvent channels upon freezing, and causes characteristic 'ice rings' on diffraction patterns, that can obscure the protein crystal's diffraction. Cryoprotectants act to decrease the rate at which this cooling process must occur to vitrify the water contained in the crystal by 5 – 6 orders of magnitude (Garman and Owen, 2005).

Commonly used cryoprotectant agents can be divided into two main types: those such as glycerol which penetrate into solvent channels; and oils which are used to coat the crystal, displacing the excess solvent that typically surrounds the protein crystal, and often contributes significantly to the 'ice rings' seen in the diffraction patterns of flash cooled protein crystals (Riboldi-Tunnicliffe and Hilgenfeld, 1999). Following removal from optimisation drops using loops, protein crystals were cryoprotected with N-paratone oil (Hampton Research) before being cryo-cooled either by plunging into liquid nitrogen or placing in a cryostream.

Equation 2.2 Bragg's law : constructive interference and hence diffraction spots occur where n is an integer, λ is the wavelength of incident wave, dhkl is the spacing between the planes hkl in the atomic lattice, and θ is the angle between the incident ray and the scattering planes

$$2\boldsymbol{d}\text{hkl}\,\sin\boldsymbol{\theta} = \boldsymbol{n\lambda}$$

2.6.4 Data collection

All X-ray data were collected from cryo-cooled crystals at the I02 tuneable diffraction beamline of the Diamond Light Source synchrotron facility (DLS, Oxfordshire, UK).

2.6.5 Data processing and reduction

X-ray diffraction images for each dataset were processed using iMOSFLM (Leslie and Powell, 2007). This program attempts to automatically determine crystal parameters such as unit cell dimensions, crystal orientation, point group and can estimate a value for the mosaicity. This process predicts where in reciprocal space conditions satisfying Bragg's Law (Equation 2.2) and hence where a diffraction spot [Miller index (hkl)] is expected. These estimates are then refined to elucidate more accurate parameters enabling the images to be integrated, with further refinement of the crystal parameters to best predict *hkl* positions. An experimental measurement of each diffraction spot intensity is obtained (I_{hkl}), along with their standard deviations.

Following integration, the data reduction was performed using POINTLESS and SCALA (Evans, 2011) as supplied within the CCP4 suite (Collaborative Computational Project, Number 4, 1994) (Navaza, 1994, Winn *et al.*, 2011). POINTLESS was used to determine the space group of the crystal, and re-index (or change the space group) of datasets where appropriate. Datasets were scaled using SCALA, which attempts to make symmetry-related and duplicate measurements of a

reflection equal and puts all observations on a common scale; hence making all data internally consistent. SCALA was also used to set the high resolution limit.

2.6.6 Obtaining phase information

In essence two things are required to produce an interpretable electron density map and in the end solve a crystal structure; the amplitudes and phases of the diffracted X-rays. The amplitudes are provided by the measured intensities of the reflections, as described by the following relationship $|F_{hkl}| = I_{hkl}^{½}$, but the phase relations between the reflections are lost. Obtaining the missing phase information, or solving the so-called phase problem, is a fundamental issue in protein crystallography and is typically achieved by one of two major methods: molecular replacement and experimental phasing. Molecular replacement can be use if a previously determined, structurally similar model is available (Rossmann, 1990). This model can be used to calculate initial phases, by positioning the known model correctly within the new unit cell. These initial phases are then applied in the initial reconstruction of the electron density.

In the absence of a suitable known structure model, as for the protein structure solved in this project, phases must be determined *de novo* by experimental phasing methods. These most generally applicable experimental phasing methods rely on the determination of the location of a few atoms, or even a single atom, within the asymmetric unit of one of the crystals from which data have been collected. These atoms, referred to as the marker atom substructure, are identified based on intensity difference data.

In general, experimental phasing methods work on the basis of determining the locations of a smaller number of identifiable atoms within the unit cell, and calculating the structure factors for this known substructure. This calculation provides both amplitudes and, importantly, phases that can then be ‘bootstrapped’ onto all atoms in the unit cell to produce an initial electron density map.

When using the isomorphic replacement method, this substructure typically consists of one or more heavy atoms present in one, or more, derivative crystals but absent in the native crystals. The location of this small number of atoms within the unit cell

can be determined using the difference in the intensity of reflections from the derivative data set compared to a native data set, so long as the crystal lattices are isomorphic, meaning that they are otherwise identical with the exception of the heavy atoms.

The second means of experimentally obtaining phase information takes advantage of heavy atom's abilities to absorb x-rays of specified wavelength, and reemit it with an altered phase. This absorption violates Friedl's Law and the intensity of symmetry related reflections is no longer equal ($I_{hkl} \neq I_{-k-h-l}$). This inequality is referred to as anomalous scattering or anomalous dispersion. These anomalous differences between Friedl's pairs can be used to locate the anomalous scatterers within the unit cell and obtain the phase information.

2.6.6.1 Phase determination using single-wavelength anomalous dispersion (SAD) and initial model building

Single-wavelength anomalous dispersion (SAD) involved collecting highly redundant data at the high energy side of the absorptive edge (labelled peak in Figure 2.4), where absorptive values (f'') is maximum. This dataset was then used to locate the anomalous scatterers present in the unit cell using SHELXC/D (Sheldrick, 2010), which finds the heavy atom sites using a Patterson function. These sites were then used for experimental phasing by PHASER-EP (McCoy *et al.*, 2007), as implemented in the CCP4 suite. These initial phases derived from both enantiomeric arrangements of the heavy atoms, were then independently subjected to automated density modification and phase improvement using PARROT (Cowtan, 2010). An initial model was the generated, using the initial phases from one of enantiomeric arrangements using two rounds of autobuilding with BUCCANEER (Cowtan, 2006) with refinement using REFMAC5 (Murshudov *et al.*, 1997). As expected, attempts to autobuild an initial model using the heavy atom positions of the other, incorrect, hand were unsuccessful.

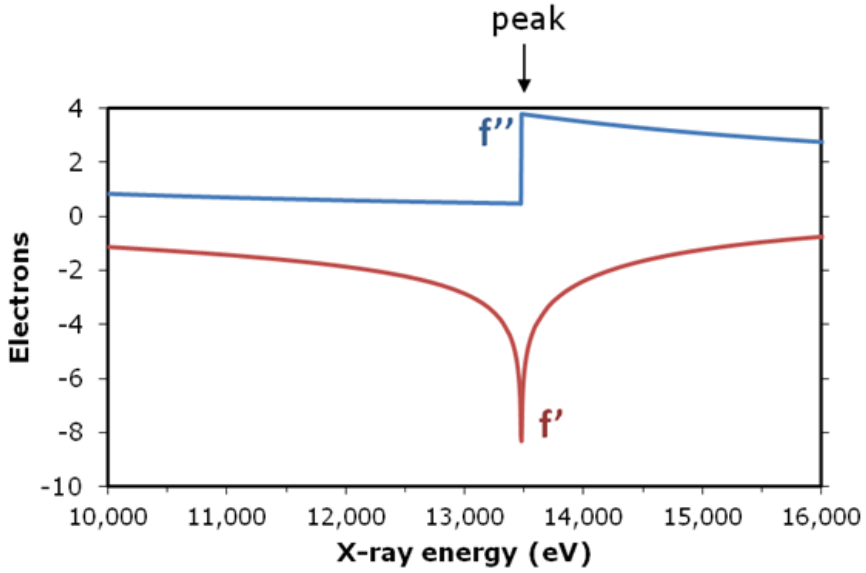

Figure 2.4 Theoretical excitation spectrum at the K edge of bromine

Peak absorption spectrum (f'') shown alongside the dispersive spectrum (f') for the element bromine, plotted as a function of incident X-ray energy. Values presented are theoretical approximations calculated as described previously (Brennan and Cowan, 1992) and obtain from http://skuld.bmsc.washington.edu/scatter/AS_periodic.html

2.6.7 Refinement, model building and validation

Initial models created by automatic building programs will likely obtain a correct fold but will also contain many incorrect features, since the experimentally derived structure factors will be in poor agreement with the calculated structure factors used in the initial model. Crystallographic refinement aims to improve the fit between the model and the data, by finding a set of atomic positions for the protein model that give calculated values for the amplitude of structure factors, $|F_{calc}|$, that are as close as possible to the observed values $|F_{obs}|$. This can be assessed using the crystallographic *R* factor; but this is susceptible to manipulation and so a more demanding and revealing criterion of model accuracy, the free *R*-factor or R_{free} was also used (Tickle *et al.*, 1998). This is computed in the same way as the *R* factor, but uses only a small 'test-set' of randomly chosen intensities that are not used during refinement, but reserved for cross validation. *R* and R_{free} values range from zero, for perfect agreement to about 0.6, if observed amplitudes were compared with a random set of amplitudes. In this project, this initial model was then refined against the high resolution data. REFMAC5 (Murshudov *et al.*, 1997) uses the amplitude

based maximum likelihood method of refinement, and was used for rigid body, restrained and TLS refinement of the protein structure. Fitting and refinement of the water molecules was conducted using ARP/wARP (Langer *et al.*, 2008). Electron density and anomalous difference maps, as well as the protein model were visualised using COOT (Emsley and Cowtan, 2004), and used for manual rebuilding of the protein model to improve the fit with the electron density. The final models were produced through iterative rounds of refinement using REFMAC5, and rebuilding with COOT, until the calculated and observed data were in close agreement as assessed by monitoring the R and R_{free} values. Structures were validated using the validation tools in COOT, and finally using the MOLPROBITY server (Davis *et al.*, 2007, Chen *et al.*, 2009). All crystallography images displayed in this thesis were produced using PyMOL (The PyMOL Molecular Graphics System, Version 1.5.0.4 Schrödinger, LLC).

2.7 Blotting Procedures

2.7.1 Wet blotting

Transfer by wet blotting was conducted using a Mini Trans-Blot® Electrophoretic Transfer Cell (Bio-Rad) as follows. Two foam pads and two pieces of 3 mm filter paper (Whatman™), cut to size of the gel, were soaked in Bjerrum transfer buffer [48 mM Tris, 39 mM glycine, pH 9.3, 20% methanol] supplemented with 0.0125% (w/v) SDS (Bjerrum and Schafer-Nielsen, 1986). A piece of Immobilon-P PVDF membrane (Merck Millipore) also cut to the size of the gel was activated by incubating briefly in methanol prior to equilibration in transfer buffer for at least 10 min with agitation. Following equilibration of the membrane, the transfer sandwich was assembled within a gel holder cassette as follows from bottom to top: a foam pad, one piece of filter paper, the gel, the equilibrated PVDF membrane, the second filter paper and the second foam pad. A blot roller was used to remove any air from between the assembled layers, and the holder cassette was secured via the locking-mechanism. The assembled cassette was inserted into the Mini Trans-Blot® cell, placed inside a Mini PROTEAN® Tetra Cell system tank along with the provided blue cooling unit and a magnetic stir bar. The tank was filled with ice cold Bjerrum

transfer buffer, and the transfer conducted, with the tank positioned on a magnetic stirrer, using either a constant current of 250 mA for 1 – 2 h, or a constant voltage of 30 V, at 4 ºC, for 16 h.

2.7.2 Semi-dry blotting

Transfer by semi-dry blotting was conducted using a Trans-Blot® Turbo™ Blotting System (Bio-Rad) and traditional semi-dry consumables as outlined in the instruction manual, but with minor modifications. Four pieces of 3 mm filter paper (Whatman™) were cut to size of the gel and soaked in Bjerrum transfer buffer [48 mM Tris, 39 mM glycine, pH 9.3, 20% methanol] supplemented with 0.0125% (w/v) SDS (Bjerrum and Schafer-Nielsen, 1986). A piece of Immobilon-P PVDF membrane (Merck Millipore) also cut to the size of the gel was activated by incubating briefly in methanol prior to equilibration in transfer buffer for at least 10 min with agitation. Following equilibration of the membrane, the transfer sandwich was assembled on the base of the transfer cassette (anode). Two pieces of wet filter paper were laid on the bottom; the equilibrated membrane was then added, followed by the gel, and finally the two remaining pieces of wet filter paper. A blot roller was used to remove any air from between the assembled layers. The cassette lid (cathode) was placed onto the base and secured in place via the locking-mechanism. The assembled cassette was inserted into the bay unit, and the transfer was conducted using the pre-programmed protocol "STANDARD SD": a constant voltage of 25 V, a current of up to 1.0 A, for 30 min.

2.7.3 Ponceau S staining of membranes

Equal loading and efficient transfer of proteins onto the PVDF membrane was confirmed by Ponceau S staining as follows. Immediately after blotting, the membrane was activated by immersion in methanol for 30 sec. The membrane was then incubated in Ponceau S stain [0.1% (w/v) Ponceau S in 5% (v/v) acetic acid] for 5 min with agitation and rinsed with MQ water until distinct bands were observed and background staining was low. Staining of the membrane was completely

reversed by incubating in 0.1 M sodium hydroxide, followed by repeated rinsing with MQ water.

2.7.4 Immunodetection

PVDF membranes containing immobilised proteins following transfer were blocked in 5% (w/v) dried skimmed milk powder in 0.1% TBS-T buffer [50 mM Tris-HCl, 200 mM sodium chloride, pH 7.4, supplemented with 0.1% (v/v) Tween®-20] with incubation at 8 ºC for 16 h with shaking of 100 rpm, unless stated otherwise.

For typical two-step detections, following blocking, the membranes were briefly washed three times in 0.1% TBS-T buffer, prior to probing with the appropriate primary antibody (Table 2.7). Membranes were then washed again, three times in 0.1% TBS-T, and probed with the appropriate secondary antibody (Table 2.7). After incubation with the secondary antibody, membranes were washed as before, prior to the addition of appropriate detection reagents. The procedure for one-step detection was similar, with the exception that the detection reagents were added immediately after the wash steps following probing with the primary antibody.

Peroxidase signal of the horseradish peroxidise (HRP)-conjugated antibodies was detected by treating the membranes with SuperSignal West Pico Chemiluminescent Substrate (Thermo Scientific), occasionally supplemented with 10% (v/v) SuperSignal West Femto Chemiluminescent Substrate (Thermo Scientific) to increase sensitivity, as described in the provided manuals. Signal was detected by exposing the treated membranes to Fuji Medical X-ray Film (Fuji) with exposure times ranging from 2 sec to over 8 h.

Detection of alkaline phosphatase (AP) signal after probing with the α-FLAG-AP antibody was conducted by first washing the membrane three times in 0.05% TBS-T [TBS supplemented with 0.05% (v/v) Tween®-20], before treating the membranes with BCIP/NBT Color Development Substrate (Promega) as described in the provided manuals.

Table 2.7 Antibodies used in this study

Antibody	Supplier	Origin	Working dilution	Buffer	Incubation conditions	Detection reagents
Primary antibodies						
α-GFP	(A11122) Invitrogen	rabbit polyclonal	1:4,000	0.1% TBS-T	RT for 1 h	n/a
α-HA	(3F10) Roche	rat monoclonal	1:6,000	0.1% TBS-T	RT for 1 h	n/a
α-HIS	(70796) Novagen	mouse monoclonal	1:1,000	0.1% TBS-T	RT for 1 h	n/a
α-pTEpY	(#91015) Cell Signaling Technology	rabbit monoclonal	1:1,000	0.1% TBS-T +5% (w/v) BSA	8ºC for 16 h	n/a
α-FLAG-AP*	(A9469) Sigma	mouse monoclonal	1:1,000	0.05% TBS-T	RT for 1 h	AP
α-$GAL4_{DBD}$-HRP*	(RK5C1) Santa Cruz Biotechnology	mouse monoclonal	1:1,000	0.1% TBS-T	RT for 2 h	Pico
Secondary antibodies						
α-mouse-HRP	(A4416) Sigma	goat	1:20,000	0.1% TBS-T	RT for 1 h	Pico
α-rat-HRP	(A9037) Sigma	goat	1:20,000	0.1% TBS-T	RT for 1 h	Pico or Pico/Femto
α-rabbit-HRP	(A0545) Sigma	goat	1:20,000	0.1% TBS-T (+/- 5% (w/v) milk powder	RT for 1 h	Pico/Femto

Antibodies marked with * were suitable for one-step detection procedure, 'AP' indicates detection using BCIP/NBT Color Development Substrate, whilst 'Pico' or 'Pico/Femto' indicates detection with SuperSignal West Pico Chemiluminescent Substrate, without or supplemented with SuperSignal West Femto Chemiluminescent Substrate (Thermo Scientific) as described above.

2.8 Yeast two-hybrid procedures

2.8.1 Yeast strains and culture media

Yeast two-hybrid screening and analyses were conducted with *Saccharomyces cerevisiae* strain MaV203. This strain contains deletions in the endogenous *GAL4* and *GAL80* transcription factor genes, allowing use with *GAL4*-based two-hybrid systems. The strain is also auxotrophic for leucine, tryptophan and uracil, but contains three GAL4-inducible reporter genes, *HIS3*, *LacZ* and *URA3*[†], to identify protein-protein interactions.

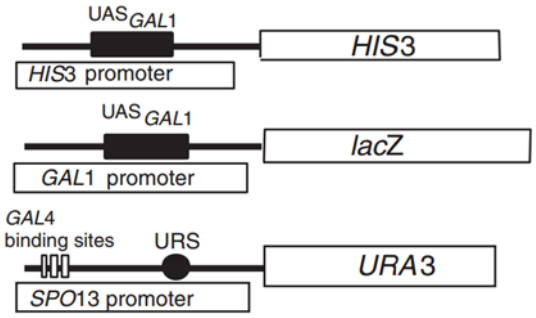

Figure 2.5 The three GAL4-inducible reporter genes in MaV203

Schematic of the reporter genes in MaV203, including promoter regions. UAS = upstream activation sequence. URS = Upstream regulator / repressor sequence. *Figure taken from ProQuest™ Two-Hybrid System User Manual (Invitrogen™).*

Untransformed MaV203 was cultured on YPAD agar [YPAD broth = 1% (w/v) yeast extract, 2% (w/v) bactopeptone, 2% (w/v) glucose, 0.003% (w/v) adenine hemisulphate, pH 6.0; supplemented with 2% (w/v) microbiology grade agar]. Colonies were streaked onto fresh plates, incubated at 28 ºC for 4 days, prior to storage at 4 ºC for up to 2 months. For longer term storage, aliquots of cultures, grown in YPAD broth at 28 ºC for 16 h, were supplemented with 20% (v/v) filtered sterile glycerol before freezing in liquid nitrogen and storage at < -70 ºC.

[†] *HIS3* encodes imidazoleglycerol-phosphate dehydratase which catalyses the sixth step in histidine biosynthesis, *URA3* encodes orotidine 5-phosphate decarboxylase which catalyzes one reaction involved in pyrimidine ribonucleotide biosynthesis, and *lacZ* encodes β-galactosidase, an enzyme that cleaves the disaccharide lactose.

The ProQuest™ system uses low-copy number ARS/CEN[‡]-based vectors. Low-copy vectors are claimed to improve the reproducibility of results, through reduced toxicity and consistent expression levels. The bait vector, pDEST™32, utilises the *LEU2* selection marker, complementing the leucine auxotrophy; whereas the prey vector pDEST™22, utilises the *TRP1* selection marker, complementing the tryptophan auxotrophy. By utilizing three reporter genes and low copy number vectors, the ProQuest™ System is reported to benefit from fewer false positives than other systems

The ProQuest™ Two-Hybrid System includes four two-hybrid control plasmids based on the interaction of Krev1 with the ras association domain of RalGDS (Herrmann *et al.*, 1996, Serebriiskii and Kotova, 2004). Three yeast co-transformants expressing a $GAL4_{DBD}$-fusion of Krev1, together with $GAL4_{AD}$-fusions of either wildtype RalGDS, mutant $RalGDS^{I77T}$ or $RalGDS^{L65P}$ were obtained from Dr. Miles Armstrong (JHI). The interaction between the two wild-type proteins represents a strong protein-protein interaction, whereas the two mutations in RalGDS either weaken or abolish, respectively, the detectable interaction between the two proteins. These three co-transformants were used as standard controls in all Y2H analyses.

Co-transformants were selected and maintained on double-dropout synthetic complement (SC) medium (SC-LW) agar plates [0.67% (w/v) Yeast Nitrogen Base without Amino Acids (Y0626), 0.16% (w/v) Yeast Synthetic Drop-out Medium Supplements (Y2001), 0.0075% histidine, 0.0075% uracil, 2% (w/v) glucose, pH 5.6; supplemented with 2% (w/v) microbiology grade agar]. Triple-dropout SC medium plates used in reporter gene assays, were made as described above, although with the histidine (SC-LWH, or -HIS), or uracil (SC-LWU or -URA) omitted. Between 10 – 50 mM 3-amino-1,2,4-triazole (3AT) was added to molten SC-LTH agar just prior to pouring plates, to repress growth caused by unspecific auto-activation of the *HIS3* reporter gene.

[‡] ARS = autonomously replicating sequence, CEN = a yeast centromere

2.8.2 Small scale transformation of yeast by lithium acetate/single-stranded carrier DNA/polyethylene glycol method

Small scale transformation of *S. cerevisiae* was conducted using a slightly modified version of the procedure outlined in the ProQuest™ Two-Hybrid System User Manual (Invitrogen™). Fresh batches of competent cells were prepared, prior to each transformation, by inoculating a single well isolated colony of MaV203 from an YPAD agar plate into 10 mL of YPAD broth using a flamed wire loop under a laminar flow hood. This culture was then vortex mixed to resuspend the colony and incubated for 20 h at 28 ºC with shaking between 200 – 230 rpm. Next day, this culture was diluted to a culture density of OD_{600} = 0.4 in 40 mL of YPAD broth, before being incubated, as before, for a further 3 h. The cells were then harvested by centrifugation at 1,600 x *g* for 5 min at room temperature using a Legend® RT centrifuge (Sorvall®). Pelleted cells were washed by resuspending in 40 mL of sterile water. The cells were harvested as above and resuspended in 0.5 mL of filter-sterilised yeast resuspension buffer [100 mM lithium acetate and 5 mM Tris-HCl, 0.5 mM EDTA, pH 7.5]. This was then incubated at room temperature for 10 min, before proceeding immediately to transformation of the competent MaV203 cells.

For each transformation, approximately 150 ng of both bait and prey construct plasmid DNA were mixed with 10 µg of salmon sperm DNA, previously sheared by

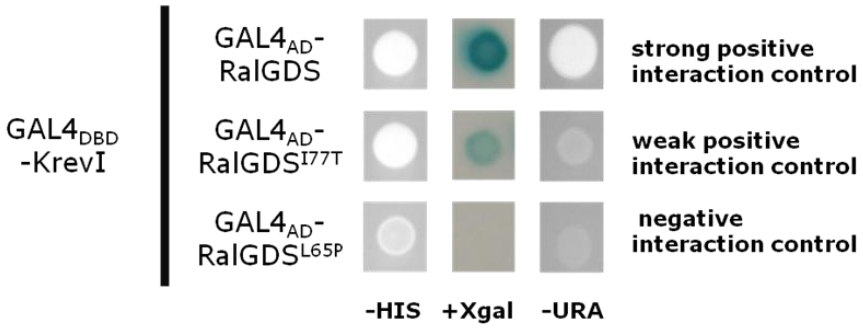

Figure 2.6 The standard controls included in Y2H analyses

Co-transformants carrying control bait and prey constructs as indicated. –HIS indicates plates lacking histidine, +Xgal indicates LacZ reporter assay, whereas –URA indicates plates lacking uracil. See Section 2.8.3.

sonication, and denatured and rendered single-stranded just prior to use, by boiling and subsequent rapid cooling on ice respectively. To this DNA mix was added 10 µL of the competent MaV203 cell suspension, followed by 70 µL of yeast transformation buffer [40% PEG 3350, 100 mM lithium acetate and 10 mM Tris-HCl, 1 mM EDTA, pH 7.5] and mixed well. The transformation mix was then incubated at 28 ºC for 30 min, at which point 8.8 µL of DMSO was added, and mixed well, and heat shocked at 42 ºC for 7 min. The cells were pelleted by centrifugation at 1,000 x *g* for 1 min at room temperature using a Legend® RT centrifuge (Sorvall) and the supernatant removed. The cell pellets were then resuspended in 100 µL of sterile MQ water and plated onto selective double-dropout SC medium (SC-LW) agar plates, and incubated for 3 – 4 days at 28 ºC in a static incubator to allow growth of single colonies.

2.8.3 Yeast two-hybrid reporter assays

To test specific protein-protein interactions, the proteins were transferred using GATEWAY® cloning (Section 2.4.8.5) into either the bait (pDEST™32) or prey (pDEST™22) destination vectors as described in the ProQuest™ Two-Hybrid System. The resultant expression clones (see Appendix Table B) were then co-transformed into chemically competent yeast cells as described above (Section 2.8.2). Each bait or prey expression clone to be tested was also co-transformed with either the empty pDEST22 or pDEST32 plasmid respectively to serve as a negative interaction control. The three standard controls (Section 2.8.1) were also included in all analyses. Colonies that grew following co-transformations were then replica plated onto selective Y2H assay plates as follows. Using a sterile pipette tip, between 1 – 2 mm^3 of yeast cells from a single colony was resuspended in 100 µL of sterile MQ water. At least three independent colonies were picked per protein-protein or protein-control interaction to be tested. Aliquots of 2.5 µL of re-suspended yeast cells were then spotted onto large (14 cm diameter) selective Y2H assay plates. The positioning of the colonies on the different plates was replicated on all plates and carefully noted. Double-dropout SC medium plates (SC-LW) were used to confirm that colonies selected retained both plasmids. Triple-dropout SC medium plates lacking histidine but containing between 10 – 50 mM 3AT, (SC-LWH, or -HIS),

were used to test for activation of the *HIS3* reporter gene, whilst activation of the *URA3* reporter genes was tested by replica spotting onto Triple-dropout SC medium plates lacking uracil (SC-LWU or -URA). Plates were incubated for at least 24 h at 28 ºC in a static incubator, and the growth of co-transformants on the selective plates was scored. If any negative interaction controls showed growth on plates lacking histidine, suggesting auto-activation of reporter genes, the colonies were rescreened on SC-LWH plates and the concentration of 3AT was increased to either 25 mM or 50 mM.

Activation of the *LacZ* reporter gene was tested using the colourimetric assay described in the ProQuest™ Two-Hybrid System User Manual (Invitrogen). Re-suspended yeast colonies were replica spotted onto a nylon membrane on the surface of an YPAD agar plate. This plate was incubated for 24 h at 28 ºC in a static incubator to allow colony growth. At this point, the nylon membrane was removed from the plate and immersed in liquid nitrogen for 30 s to lyse the yeast cells. The nylon membrane was then carefully placed in a plastic box, upon two layers of filter paper that had been pre-soaked in an X-gal solution. The X-gal solution was prepared by dissolving 20 mg of X-gal in 100 µL of N,N-dimethyl formamide (DMF), before adding 60 µL of β-mercaptoethanol and 10 mL of Z-buffer [60 mM disodium hydrogen phosphate (Na_2HPO_4), 40 mM sodium dihydrogen phosphate (NaH_2PO_4), 10 mM potassium chloride, 1 mM magnesium sulfate, pH 7.0]. The box and membrane was incubated at 37 ºC for 24 h at a slight angle to ensure excess X-gal solution collected away from the membrane. After incubation the membranes were assessed for the development of a blue colouration.

2.8.4 Preparation of yeast protein extracts for western blot analysis

Yeast protein extracts were prepared as described in Clontech Yeast Protocols Handbook (p.12). For each transformed yeast strain to be assayed, a single isolated colony (aged between 3 – 4 days) was inoculated into 5 mL of double-dropout SC medium broth (as described in Section 2.8.1, although omitting microbiology grade agar) using a flamed wire loop under a laminar flow hood. A colony of untransformed MaV203 was inoculated into 10 mL of YPAD broth as a negative control. These cultures were then vortex mixed to resuspend the colony and

incubated for 16 – 20 h at 28 ºC with shaking between 200 – 230 rpm. Next day, these cultures were vortex mixed, to disperse cell clumps, and separately inoculated into 50 mL aliquots of YPAD broth. These cultures were then incubated, as before, until the cultural density reached between OD_{600} = 0.4 – 0.6 (approximately 4 h), at which point the OD_{600} of a 1 mL sample was recorded and multiplied by the culture volume to obtain the total number of OD_{600} units. At this point, the cultures were quickly chilled by pouring it into prechilled 250-mL Nalgene® Centrifuge bottles halfway filled with ice. The bottles were then immediately placed into a prechilled Fibrelite® F14S-6x250y rotor (Thermo Scientific) and centrifuged at 1,000 x *g* for 5 min at 4 ºC using a Legend® RT centrifuge (Sorvall). The supernatant and unmelted ice was discarded. The cell pellet was then washed, by resuspending in 50 mL of ice-cold sterile MQ water and centrifugation at 1,000 x *g* for 5 min at 4 ºC using a Legend® RT centrifuge (Sorvall). Again the supernatant was discarded and the cell pellet was immediately frozen in liquid nitrogen and stored at < -70 ºC before proceeding to protein extraction.

Yeast proteins were extracted using a urea/SDS protein extraction method as follows. The cell pellets, obtained as described above, were quickly thawed by separately resuspending each one in cracking buffer [8 M urea, 5% (w/v) SDS, 40 mM Tris-HCl pH 6.8, 0.1 mM EDTA, 0.4 $mg.mL^{-1}$ bromophenol blue] prewarmed to 60 ºC and supplemented with 125.7 mM β-mercaptoethanol, 6.2 $\mu g.mL^{-1}$ Pepstatin A, 1.9 µM Leupeptin, 9.0 mM Benzamidine, 22.9 $\mu g.mL^{-1}$ Aprotinin, and 4.4 mM phenylmethanesulfonyl fluoride (PMSF). For every 7.5 OD_{600} units of cells, 100 µL of supplemented cracking buffer was used. Each cell suspension was then transferred to a 2-mL screw-cap microcentrifuge tube containing 80 uL of glass beads (425 – 600 µm; Sigma Cat No. G-8772) per 7.5 OD_{600} units of cells. The samples were then incubated at 70 ºC for 10 min, and vortexed vigorously for 1 min. Cellular debris and unbroken cells were pelleted using a microcentrifuge at 17,000 x *g* for 5 min at 4 ºC. The supernatants, hence termed first supernatants, were each transferred to fresh 1.5 mL tubes and placed on ice. The pellets were boiled at 100 ºC for 5 min, prior to vigorous vortexing and centrifugation as before. The resulting supernatant (second supernatant) was then combined with the corresponding first supernatant, before the samples being briefly boiled at 100 ºC for 3 – 5 min. These samples were either

immediately loaded on a 17% SDS-PAGE gel for, or stored at < -70 ºC before proceeding to, western blot analysis.

2.8.5 Detection of yeast $GAL4_{DBD}$ fusion proteins by western blot

Protein extracts, prepared as outlined above (Section 2.8.4), were separated by SDS-PAGE (Section 2.5.1), and transferred to PVDF membrane via semi-dry blotting (Section 2.7.2). Following Ponceau S staining, to confirm protein loading and efficient transfer (Section 2.7.3), immunoblotting and detection, using the α-$GAL4_{DBD}$ HRP-conjugated antibody and ECL reagents respectively, was conducted as previously outlined (Section 2.7.4, Table 2.7).

2.9 *In planta* procedures

2.9.1 Growth conditions

Nicotiana benthamiana and *Nicotiana tabacum* cv. Petite Gerard plants were grown in controlled environment rooms at 22 ºC with 55% humidity and a 16-h/8-h light/dark photoperiod, or in controlled glasshouses under similar conditions.

2.9.2 Transient gene expression *in planta* via agroinfiltration

Transient gene expression *in planta* was conducted via agroinfiltration (Kapila *et al.*, 1997, van der Hoorn *et al.*, 2000). In brief, recombinant *Agrobacterium* strains harbouring appropriate binary plasmids (see Appendix Table C) were grown in LB or L broth supplemented with appropriate antibiotics for 16 – 36 h at 28 ºC with shaking. The cells were then harvested by centrifugation at 1,500 x *g* for 10 min at room temperature, and resuspended in MMA buffer [10 mM magnesium chloride, 10 mM MES pH 5.6, 150 – 200 μM acetosyringone] to the desired OD_{600} (typically between 0.1 and 2.0). For co-agroinfiltrations, where the parallel expression of multiple transgenes on separate T-DNAs within the same tissue was desired, resuspended cells harbouring the appropriate binary vectors, were then mixed at the

appropriate ratios to achieve the desired final OD_{600} for each recombinant *Agrobacterium* (typically between 0.1 and 0.6). Unless specified otherwise, the cells were then incubated at room temperature for 1 – 2 h prior to infiltration into 4-week old *Nicotiana benthamiana* plants using a blunt syringe applied to the abaxial surface of the leaf. Superficial wounding of the leaf using a needle was used to aid infiltration when necessary.

For binary vectors with transgenes expressed under the control of an estradiol-responsive promoter, such as pER8, or its derivative pERCH (see Section 2.4.8.6), the expression was triggered by the application of 10 μM β-estradiol to both the axial and abaxial sides of the leaf using a trigger-spray bottle at 48 h after agroinfiltration; with additional spray treatments at 48 h intervals when necessary.

2.9.3 Protein extraction from *Nicotiana benthamiana*

Total protein extracts were obtained from *Nicotiana benthamiana* leaf tissue, either 3 – 4 days post agroinfiltration or 24 h post estradiol induction, as follows. For small scale extractions, for example to confirm protein expression, four leaf disks of 8 mm in diameter were harvested per sample and collected in a single tube. These tissue samples were rapidly frozen in liquid nitrogen, and kept at -70 ºC until ready for protein extraction. Tissue samples were placed on dry ice, and ground to a fine powder using a metal micropestle that had been prechilled in liquid nitrogen. To each sample was added 150 μL of GTEN buffer [10% (v/v) glycerol, 150 mM Tris-HCl pH 7.5, 1 mM EDTA, 150 mM sodium chloride] supplemented with 10 mM DTT, 2% (w/v) polyvinyl polypyrrolidone (PVPP), 1% (v/v) Protease Inhibitor Cocktail (P 9599, Sigma), 0.1% (v/v) Tween®-20. The samples were homogenised by vortexing for 30 sec, prior to centrifugation at 17,000 x *g* for 10 min at 4 ºC.

For larger scale extractions, for example for co-immunoprecipitation experiments, the mid-veins from entire infiltrated leaves were removes using a razor blade and discarded, the remaining leaf tissue was wrapped in foil and rapidly frozen in liquid nitrogen, and kept at -70 ºC until ready for protein extraction. Tissue was ground to a fine powder using a pestle and mortar that had been prechilled in liquid nitrogen. Ground tissue was transferred to a prechilled 15 mL-centrifuge tube (CORNING)

and weighed. Two millilitres of GTEN buffer, supplemented as described above, was added per gram of ground tissue. The samples were homogenised by vortexing for 30 sec, prior to centrifugation at 11,500 x *g* for 10 min at 4 ºC. The supernatant was then transferred to a new, chilled, 15 mL-centrifuge tube and centrifuged again as before.

These clarified total protein extracts were then prepared for analysis by SDS-PAGE as described in Section 2.5.1, or used in co-immunoprecipitation experiments (Section 2.9.4).

2.9.4 Co-immunoprecipitation from plant extracts

Co-immunoprecipitation (co-IP) experiments were performed using total soluble protein extracts (Section 2.9.3). FLAG-IPs were performed using M2 anti-FLAG agarose (Sigma). Fifty-µL of resuspended affinity matrix per sample was washed in three times in a 5x volume of IP buffer [GTEN buffer + 0.1% (v/v) Tween®-20]. Washed affinity matrix was resuspended in the original volume of IP buffer, and 50 µL was added to 250 µL of protein extract and 1750 µL of IP buffer in a 2-mL microcentrifuge tube. The extracts were then mixed on a rotary mixer at 4 ºC for 1 – 2 h. Affinity matrix was collected at the bottom of the centrifuge tube by centrifugation at 800 x *g* for 1 min at 4 ºC. The majority of the supernatant was discarded and the matrix washed by adding 1 mL of fresh chilled IP buffer and resuspended resin by inversion, centrifuged as before, before discarding the supernatant again. The wash step was repeated as the above a further four times. After the last wash, the tubes were centrifuged again to collect any excess liquid. Elution of the bound protein was achieved by adding 100 µl IP buffer containing 150 $ng.\mu l^{-1}$ 3x FLAG peptide, and incubating with gentle shaking at 4°C for 30 min. Following centrifugation as before, the supernatant containing the eluted proteins was transferred to a fresh microcentrifuge tube, and prepared and analysed by SDS-PAGE (Section 2.5.1), and western blotting (Section 2.7).

HA-IPs were conducted as above, although 75 µL of anti-HA Affinity Matrix (Roche) was added to 1 mL of undiluted protein extract in a 2 mL microcentrifuge tube, prior to mixing on a rotary mixer. After mixing, samples were transferred to

SigmaPrep™ Spin Columns (Sigma) and washed five times with 0.6 mL of IP buffer in accordance with the manufacturer's protocol. Elution of the bound protein was achieved as before, but by adding 75 – 100 µL of IP buffer containing 1 $mg.mL^{-1}$ HA-peptide (Roche).

GFP-IPs were conducted using GFP-Trap® coupled to agarose beads (GFP-Trap®-A), or coupled to coupled to magnetic particles (GFP-Trap®-M). For both, 25 µL of affinity matrix was added to 1.5 – 2 mL of undiluted protein extract in a 2 mL microcentrifuge tube, prior to mixing on a rotary mixer. GFP-Trap®-A affinity matrix was washed as described above, either with or without the use of a SigmaPrep™ Spin Column (Sigma). GFP-Trap®-M affinity matrix was washed in 5x 1 mL of IP buffer, using a magnetic rack to separate the beads until the supernatant was clear. Elution of the bound protein was achieved by incubating the affinity matrix in 50 µL of 1 x SDS-loading buffer at 95 ºC for 10 min.

2.9.5 Purification of protein expressed in *N. benthamiana* by immobilised metal ion affinity chromatography (IMAC)

Extraction of proteins from *N. benthamiana* for subsequent purification by IMAC was conducted as follows. Infiltrated leaves with the mid-veins removed, were wrapped in foil and rapidly frozen in liquid nitrogen. Tissue was ground to a fine powder using a pestle and mortar that had been prechilled in liquid nitrogen. Ground tissue was transferred to a prechilled 50 mL-centrifuge tube and weighed. Two millilitres of GTEN+I buffer [10% (v/v) glycerol, 150 mM Tris-HCl pH 7.5, 1 mM EDTA, 300 mM sodium chloride, 20 mM imidazole] supplemented with 2% (w/v) PVPP, 1% (v/v) Protease Inhibitor Cocktail (P 9599, Sigma), 0.1% (v/v) Tween20, 2 mM β-mercaptoethanol and 20 mM sodium fluoride, was added per gram of ground tissue. The samples were homogenised by vortexing for 30 s, prior to centrifugation at 11,500 x *g* for 15 min at 4 ºC. The supernatant was then transferred to a new, chilled, 50 mL-centrifuge tube and centrifuged again as before.

The EDTA within the clarified plant extract was chelated, by the addition of 10 mM magnesium chloride, and the solution filtered using a 0.45 µm filter, prior to loading on to a 1 mL nickel (II) (Ni^{2+}) charged HisTrap crude column (GE Healthcare) that had been pre-equilibriated in chilled A1 buffer (Section 2.5.4) using an ÄKTAprime

(GE Healthcare). The column was then washed with ~10 column volumes of A1 buffer, before the protein of interest was eluted with chilled B1 buffer using a gradient elution (Section 2.5.4.1). Eluted fractions spanning the peak on the elution profile, as measured by absorbance at 280 nm, were prepared and analysed by SDS-PAGE (Section 2.5.1), and western blot (Section 2.7).

2.9.6 Virus induced gene silencing

Recombinant *Agrobacterium* strains harbouring pTRV1 and pTRV2 binary plasmids were grown in L media supplemented with appropriate antibiotics and 6 mM magnesium sulphate, harvested and resuspended to an OD_{600} of 1.0 as described in Section 2.8.2. Immediately prior to agroinfiltration *Agrobacterium* harbouring pTRV1 was mixed with equal volumes of *Agrobacterium* harbouring and each of TRV2 construct used (final OD_{600} = 0.5), and infiltrated into the two largest leaves of *N. benthamiana* plants at the four leaf stage (typically 2 – 3 weeks old).

2.9.6.1 Bioinformatic analysis of putative off-target silencing

Bioinformatic analysis of the DNA sequences cloned into the pTRV2 vector was performed using PERL scripts, written by Dr. Joe Win (TSL). These were used to identify all 21-nt sequences that displayed the following characteristics, previously identified as predicting high silencing efficiency in mammalian cells and chicken embryos (Ui-Tei *et al.*, 2004). Putative efficient siRNAs had the 5' end of the antisense strand as an adenine (A) or uracil (U); the first seven bases of the antisense strand including at least five A or U bases; the 5' end of the sense strand as a guanine (G) or cytosine (C), and a GC-content between 30 – 70%.

These putative siRNAs were then used to find homologous transcripts (targets) in the recently released *Nicotiana benthamiana* draft genome (Bombarely *et al.*, 2012). Since assessments of siRNA specificity suggest that mRNAs with only partial complementarity to a siRNA can also be targeted for destruction (Jackson *et al.*, 2003, Haley and Zamore, 2004), the level of mismatch allowed was varied from zero, perfect complementarity, up to a maximum of five mismatches. In all cases, no more than a single mismatch was permitted within the so called 'seed region'

(positions 2 – 12 from the 5' end) and purine:purine mismatches at position 16 were also excluded, as these had been previously shown to drastically reduce silencing efficiency (Jackson *et al.*, 2006, Schwarz *et al.*, 2006)

2.9.7 *In planta* infection with *Phytophthora infestans*

P. infestans strains were grown on as previously described by Kamoun *et al.*, (1998) at 18°C in the dark on rye sucrose agar (RSA) plates. Zoospores were harvested from 12- to 14-day old plates by flooding the plate with 4 – 5 mL of chilled sterile water and incubating at 4 ºC for 3 h. Zoospore suspensions were diluted to 100 spores per µL and stored on ice until inoculation. Infection of TRV-silenced *N. benthamiana* plants was conducted 14 – 16 days after agroinfiltration of TRV constructs, whilst infection of leaf tissue transiently expressing effectors, or vector control, was conducted 24 hpi. Droplets of 10 µl of zoospore suspension were applied onto the abaxial sides of detached leaves and incubated for several days on wet paper towels in 100% relative humidity.

Mycelial growth of *P. infestans* 88069td was visualised using a Leica Stereomicroscope (Leica Microsystems CMS GmbH) mounted with a CCD camera under UV LED illumination and filter settings for DsRed. White light images of infected leaves were taken using a Nikon COOLPIX L24 digital camera. Lesion areas were determined with GIMP (v2.8) software[§].

2.9.8 *In planta* cell death/cell death suppression assays

Recombinant *Agrobacterium* strains harbouring appropriate binary plasmids were grown, harvested and resuspended in MMA buffer as described in Section 2.9.2. To test for MAPKKKε-dependency of cell death events, *Agrobacterium* strains harbouring R protein constructs (Cf4, Pto, or R3a) were then mixed with *Agrobacterium* strains harbouring effector protein constructs (Avr4, AvrPto, or AVR3a^{KI}), to achieve final OD_{600} values of 1.0 and 0.5, respectively. *Agrobacterium* strains harbouring 35S:INF1, CRN8-D2 or, pTRBO:PexRD2 constructs were diluted

[§] http://www.gimp.org/

to achieve final OD_{600} values of 0.5, 0.3 and 0.3, respectively. *Agrobacterium* mixtures were infiltrated into leaves of 4- to 6-week old TRV-treated *N. benthamiana* plants (Section 2.9.6) at 14 - 28 days post-VIGS agroinfiltration. Each agroinfiltration site corresponded to a disk-shape approximately 2 cm in diameter. At least three (mid-level) leaves were used per plant, with typically 3 – 4 plants serving as biological replicates per independent experiment. Progression of hypersensitive response (HR)/programmed cell death (PCD) was monitored daily typically up to 7 days post agroinfiltration (dpi). An agroinfiltration site was scored positive for HR/PCD following the development of clear necrosis occupying greater than 50% of the agroinfiltrated area.

Effector-mediated cell death suppression was assessed as above, with minor modifications. *Agrobacterium* strains harbouring R protein/effector protein combinations were diluted with *Agrobacterium* harbouring wild-type or mutant *PexRD2* or an empty vector control (pK7WGF2) to achieve final OD_{600} values of 0.6, 0.3 and 0.3, respectively. *Agrobacterium* strains harbouring 35S:INF1, or CRN8-D2 were diluted to achieve final OD_{600} values as above, with wild-type or mutant *PexRD2*, or an empty vector control (pK7WGF2) at a 1:1 ratio. *Agrobacterium* mixtures were infiltrated into leaves of 4-week old *N. benthamiana* plants and progression of HR/PCD was monitored daily, and scored as described above.

Effector-mediated suppression of kinase-triggered cell death was assessed by mixing *Agrobacterium* strains harbouring pER8/pERCH contructs, the P19 suppressor of silencing and wild-type or mutant *PexRD2* or an empty vector control (pK7WGF2) to achieve final OD_{600} values of 0.25, 0.1 and 0.3, respectively. These *Agrobacterium* mixtures were infiltrated into leaves of 4-week old *N. benthamiana* plants, and expression of kinase induced as described in Section 2.9.2. Development of cell death was monitored daily up to 7 days post estradiol treatment (dpt), and sites scored positive as described above.

2.9.9 Ion leakage assay

Ion leakage associated with tissue necrosis was measured as described by Melech-Bonfil and Sessa (2010), with minor modifications. Three 8-mm diameter leaf disks were floated on 15 mL of MQ-water in 50-mL centrifuge tubes (CORNING) with

gentle shaking for > 2 h. Conductivity measurements, in microsiemens per cm ($\mu S.cm^{-1}$), were taken using a B-173 Compact Twin Conductivity Meter (HORIBA).

2.9.10 MAPK activation assay

The activation of endogenous MAP kinases in *Nicotiana benthamiana* following either agroinfiltration (Section 2.9.2) or PAMP treatment; was assessed by adapting a previously published methodology (Heese *et al.*, 2007, Segonzac *et al.*, 2011). In brief, eight leaf disks of 8 mm in diameter were harvested per condition and combined in one microcentrifuge tube. These tissue samples were rapidly frozen in liquid nitrogen, and kept at -70 ºC until ready for protein extraction.

For total protein extraction, tissue samples were placed on dry ice, and ground to a fine powder using a metal micropestle that had been prechilled in liquid nitrogen. To each sample was added 200 µL of activated Lacus buffer [50 mM Tris-HCl pH 7.5, 10 mM magnesium chloride, 15 mM EGTA, 100 mM sodium chloride, 1 mM sodium fluoride, 1 mM sodium molybdate, 0.5 mM activated sodium orthovanadate, 30 mM glycerol 2-phosphate, 0.1% (v/v) Igepal CA-630 (Sigma), supplemented just prior to use with 0.5 mM PMSF, 1 % (v/v) Protease Inhibitor Cocktail (P 9599, Sigma), 100 nM calyculin A and 2 mM DTT]. The samples were homogenised by vortexing for 30 s, prior to centrifugation at 17,000 x *g* for 10 min at 4 ºC. The total protein concentrations of the resulting supernatants were assessed by Bradford assay (Hammond and Kruger, 1994) and the samples standardised by dilution in activated Lacus buffer. The standardised samples were then boiled and separated by SDS-PAGE on a 12% (w/v) polyacrylamide gel (Section 2.5.1), and transferred to PVDF membrane by semi-dry blotting (Section 2.7.2). Ponceau S staining was used to confirm protein loading and efficient transfer (Section 2.7.3). Immunoblotting was conducted as described in Section 2.7.4, but with minor modifications. The PVDF membrane containing immobilised proteins was blocked in 5% (w/v) dried skimmed milk powder in 0.1% TBS-T buffer and incubated for 1 h at RT with shaking at 100 rpm. The membrane was then probed using a primary antibody that cross-reacts with the dually phosphorylated active form of the MAPK ERK1 (α-pTEpY, Table 2.1) at 8 ºC for 16 h, followed by an α-rabbit secondary antibody diluted in 5% (w/v) dried

skimmed milk powder in 0.1% TBS-T buffer (Table 2.1). The signal was detected using SuperSignal West Femto Chemiluminescent Substrate (Thermo Scientific).

For PAMP treatment, eight leaf disks of 5 mm in diameter were harvested from 4-week old *N. benthamiana* plants and added to wells of a 96-well microtitre plate, containing 100 µL of either MQ-water, 100 nM flg22 peptide (provided by Simon Lloyd (JIC)) or 100-fold diluted *P. infestans* culture filtrate (provided by Angela Chaparro-Garcia (TSL)). These leaf disks were then collected in a single microcentrifuge per treatments, and the samples rapidly frozen in liquid nitrogen. Total protein extraction using Lacus buffer was conducted as described above.

2.9.11 Leaf and epidermis cell area measurement

The third and fourth leaves from five independent TRV-treated plants were collected and digitally photographed. Leaf area was determined with GIMP (v2.8) software. To measure the total cell area, the third leaf from five independent plants were removed, and observed on a Leica Stereomicroscope (Leica Microsystems CMS GmbH). The area of abaxial epidermal cells (n = 50–150) was calculated using GIMP (v2.8) software. Average leaf and cell areas were used to calculate cell numbers.

Chapter 3:

Structural Characterisation of PexRD2

3 Structural Characterisation of PexRD2

3.1 Introduction

This introduction refers to the state of the knowledge at the start of this project in November 2009. Subsequent publications relevant to this chapter of this thesis are referenced throughout, and discussed at the end of, this chapter.

3.1.1 PexRD2, a candidate RXLR effector

PexRD2, *Phytophthora* extracellular (Pex) effector containing an RXLR-dEER (RD) motif 2, was first cloned from genomic DNA from *Phytophthora infestans* isolate 88069 using an allele mining strategy (Oh *et al.*, 2009). This, and other, candidate effectors were selected from a collection of >80,000 ESTs (expressed sequence tags) on the basis of a typical modular domain organisation (Figure 3.1) (Win *et al.*, 2007, Chen *et al.*, 2009). In PexRD2, the first twenty amino acids at the N-terminus were bioinformatically predicted to represent a functioning signal peptide, that would mediate its secretion from the pathogen, and be cleaved in the mature protein (Nielsen *et al.*, 1997). The N-terminal region of this effector also contained the conserved peptide motifs that define this class of effectors, an RXLR motif, (RLLR,

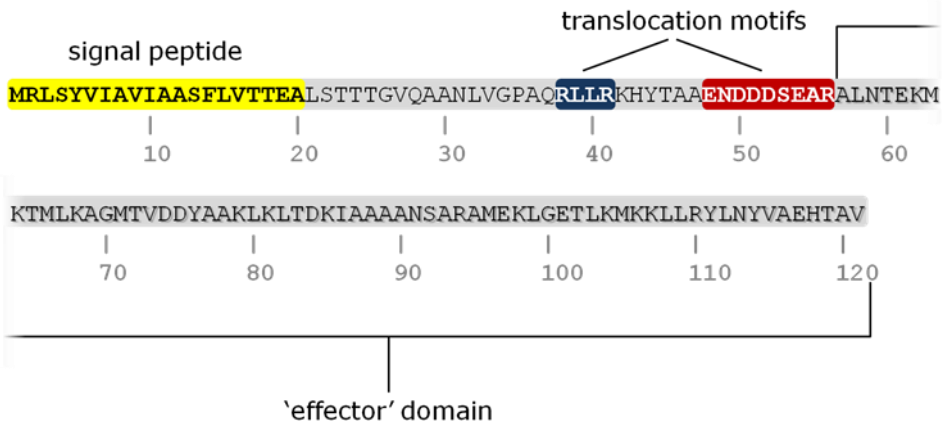

Figure 3.1 PexRD2 displays a typical modular domain organisation.

Protein sequence of PexRD2 from *Phytophthora infestans* isolate 88069 highlighting the signal peptide (yellow), RXLR (blue) and 'dEER' (red) translocation motifs, as well as the C-terminal 'effector' domain.

residues 38 – 41), and a putative variant of the more degenerate 'dEER' motif, (ENDDDSEAR, residues 48 – 56). These peptide motifs had been implicated as required for the translocation of effectors across the host cell plasma membrane and into the host cytosol (Whisson *et al.*, 2007, Dou *et al.*, 2008b, Schornack *et al.*, 2010), although the exact mechanism by which this occurs was unknown and still remains highly contentious within the field (Panstruga and Dodds, 2009, Ellis and Dodds, 2011). As such, the N-terminal region of this protein contained peptide motifs required for the delivery of this protein from the pathogen to the inside of host cells, but was predicted to likely be dispensible for any subsequent biological activity of the effector, which had been shown to be the case for other RXLR-family effectors (Schornack *et al.*, 2009). The remainder of this protein, from Ala57 to the C-terminal Val121, henceforth referred to as the 'effector' domain, showed no significant sequence homology to any known non-redundant protein sequences, outside of the oomycetes, as determined using BLASTP (Altschul *et al.*, 1990). This lack of similarity to characterised proteins made assignment of biochemical function from primary sequence impossible, although it is not unexpected as RXLR effectors frequently lack any sequence homology to other proteins within their effector domains (Kamoun, 2007, Oliva *et al.*, 2010).

There are five paralogs of PexRD2 present in the *P. infestans* reference genome, isolate T30-4 (Haas *et al.*, 2009) (Figure 3.2 A). The amino acid sequence of all paralogs is identical within their effector domains, but they do display a number of non-synonymous polymorphisms in their signal peptides and the region preeceding the RXLR motifs (Figure 3.2 B).

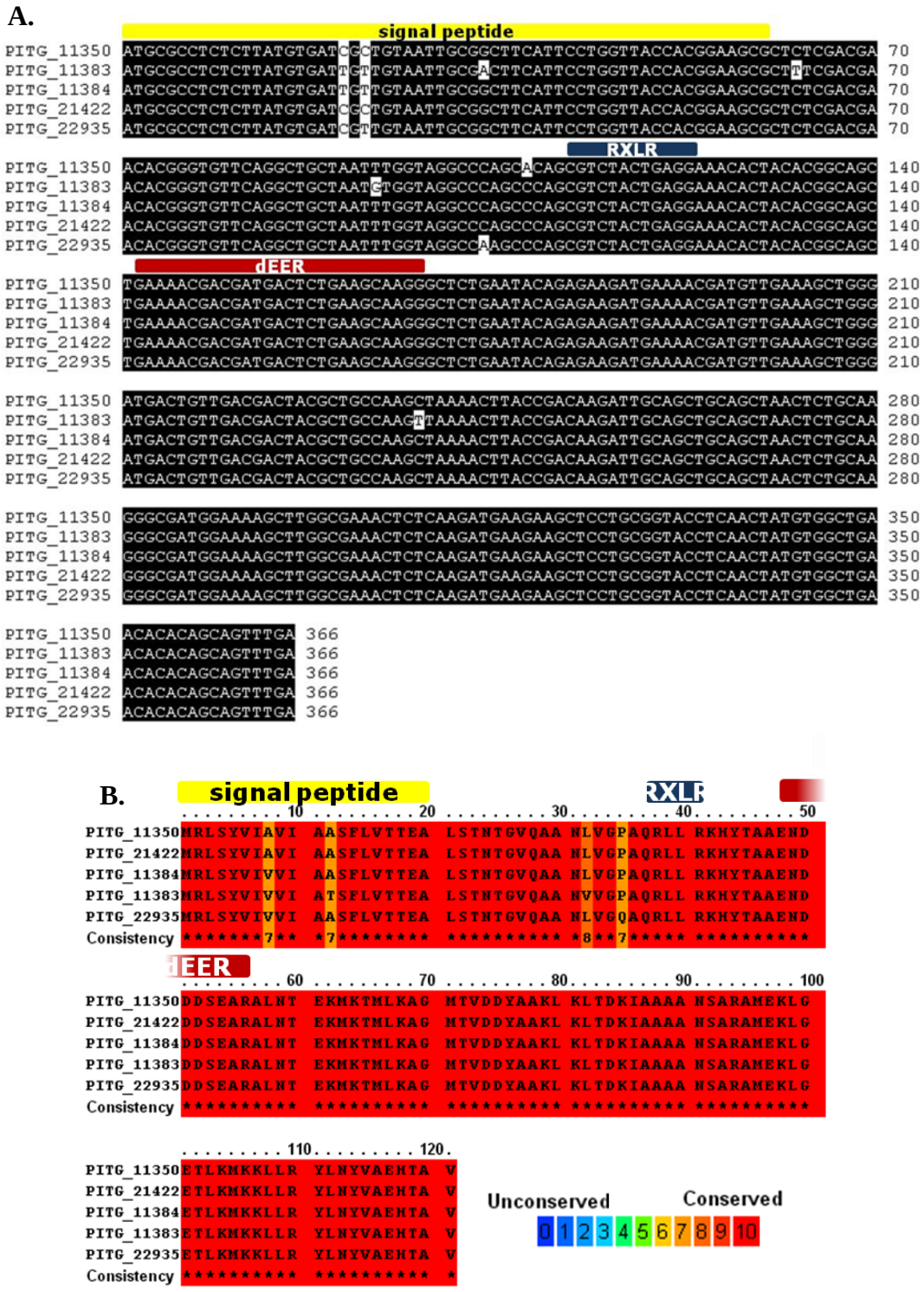

Figure 3.2 PexRD2 paralogs show high sequence identity

(A.) Sequence alignment of full-length coding sequences (CDS) for the five PexRD2 paralogs from *P. infestans* reference genome (T30-4). Conserved nucleotide bases are shaded in black. **(B.)** Sequence alignment for full length protein sequences for PexRD2 paralogs with conservation status coloured using the PRALINE server. Signal peptide and RXLR and 'dEER' translocation motifs are coloured as in Figure 3.1.

3.1.2 PexRD2 induces a weak cell death response *in planta*

Similar to other plant pathogen effectors, where transient expression of effector proteins within plant tissues leads to macroscopic symptoms (Kjemtrup *et al.*, 2000, Torto *et al.*, 2003, Cunnac *et al.*, 2009, Gürlebeck *et al.*, 2009), ectopic expression of the mature PexRD2 (residues 21 – 121, i.e. excluding the signal peptide) from a Potato Virus X (PVX) based vector triggers a weak cell death in the model plant *Nicotiana benthamiana* (Oh *et al.*, 2009) and in several susceptible and resistant *Solanum* spp (Vleeshouwers *et al.*, 2008). This response was observed using both PVX agroinfection via toothpick wounding (Kanneganti *et al.*, 2007) and agroinfiltration (Figure 3.3 A and B, respectively).

The cell death observed was concluded to be dose-dependent, since co-agroinfiltration of a binary vector expressing P19, a suppressor of post-transcriptional gene silencing (PTGS) from the Tomato bushy stunt virus, accelerated and enhanced the cell death response triggered by PexRD2 (Oh *et al.*, 2009) (Figure 3.3 B). Co-infiltration with P19 had previously been shown to increase expression of a number of transgenes *in planta* (Voinnet *et al.*, 2003)

The cell death was also shown to be dependent on the host ubiquitin ligase associated protein SGT1. This SGT1-dependency had previously been observed for a variety of cell death responses in plants (Peart *et al.*, 2002). Virus induced gene silencing (VIGS) of SGT1 in *N. benthamiana* suppressed the cell death triggered by PexRD2, even in the presence of P19 (Figure 3.3 C).

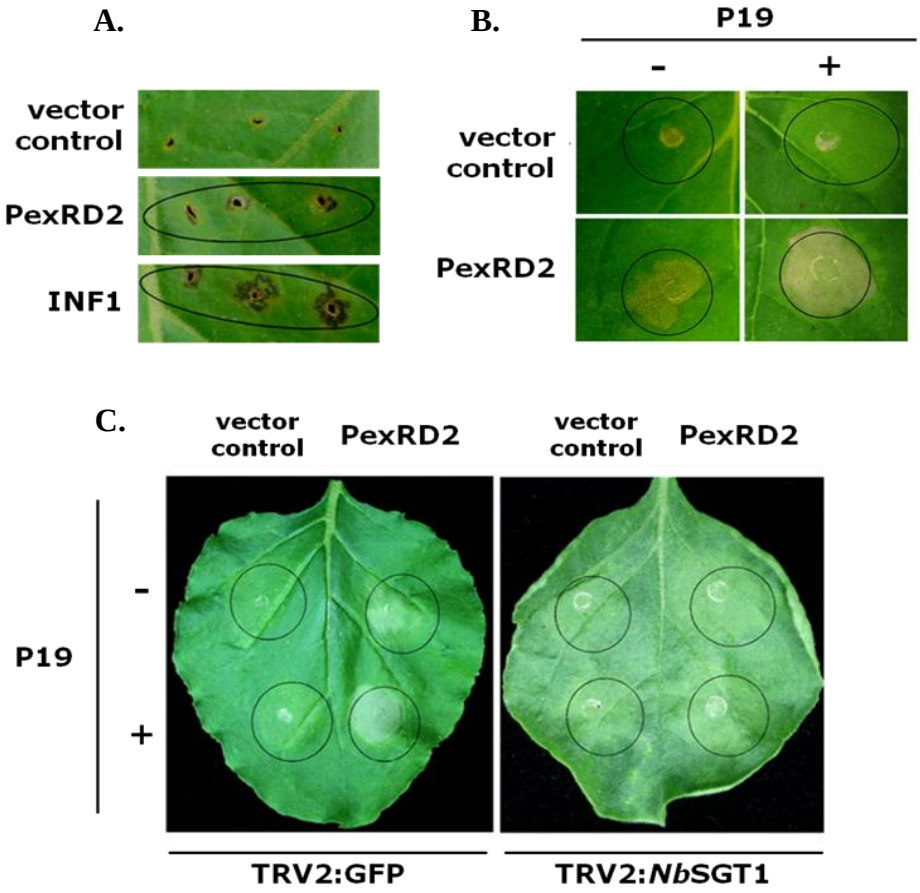

Figure 3.3 PexRD2 induces a weak cell death response *in planta*

(A.) Cell death response triggered by PexRD2 via PVX agroinfection. Image taken after 12 days. Response is weaker than that triggered by the *P. infestans* elicitin INF1, expressed via the same system. (**B.)** Cell death response triggered by PexRD2 via agroinfiltration, with or without the suppressor of gene silencing P19. Image taken after 6 days. **(C.)** SGT1 is required for the cell death response induced by PexRD2. *SGT1*-silenced (TRV2:*Nb*SGT1) plants challenged by agroinfiltration with PexRD2 do not develop PexRD2-associated cell death, whereas control-silenced plants (TRV2:GFP) showed cell death that was enhanced in the presence of P19. *Figure adapted from Oh* et al., *(2009).*

3.2 Results and Discussion

3.2.1 Expression and purification of PexRD2 effector domain

Note: At the beginning of the work described in this chapter Dr Laurence Boutemy (JIC) had constructed the recombinant plasmid (pOPINF:PexRD2) for the expression in E. coli *of recombinant PexRD2 effector domain and identified expression conditions that yielded soluble protein in small scale expression tests.*

The recombinant plasmid pOPINF:PexRD2 comprises a DNA sequence encoding the effector domain of PexRD2, sub-cloned into the expression vector pOPINF, using ligation-independent cloning (Berrow *et al.*, 2007). The sequence was amplified from a synthetic construct previously codon optimised for *E. coli* expression (Figure 3.4). This plasmid was designed to express recombinant PexRD2 effector domain and lack the N-terminal putative signal peptide and translocation motifs. These regions were omitted either because they were likely to be absent from the mature secreted protein (Nielsen *et al.*, 1997) or predicted to be largely disordered (Yang *et al.*, 2005; Figure 3.5). As stated previously, the published literature had also suggested that these regions were often dispensable for RXLR effector function. The effector domain of PexRD2 was expressed with an N-terminal hexa-histidine tag that was cleavable using 3C protease (Figure 3.6).

```
PITG_21422 CDS  ATGCGCCTCTCTTATGTGATCGCTGTAATTGCGGCTTCATTCCTGGTTACCACGGAAGCGCTCTCGACGA 70
CODON OPTIMISED ------------------------------------------------------------------- 0

PITG_21422 CDS  ACACGGGTGTTCAGGCTGCTAATTTGGTAGGCCCAGCCCAGCGTCTACTGAGGAAACACTACACGGCAGC 140
CODON OPTIMISED ------------------------------------------------------------------- 0

PITG_21422 CDS  TGAAAACGACGATGACTCTGAAGCAAGGGCTCTGAATACAGAGAAGATGAAAACGATGTTGAAAGCTGGG 210
CODON OPTIMISED ----------------------------GCGCTGAACACGAAAAAATGAAAACCATGCTGAAAGCGGGC 42

PITG_21422 CDS  ATGACTGTTGACGACTACGCTGCAAGCTAAAACTTACCGACAAGATTGCAGCTGCAGCTAACTCTGCAA 280
CODON OPTIMISED ATGACCGTGGATGATTATGCGGCGAAACTGAAACTGACCGATAAAATTGCGGCGCGGCGAACAGCGCGC 112

PITG_21422 CDS  GGGCGATGGAAAAGCTTGGCGAAACTCTCAAGATGAAGAAGCTCCTGCGGTACCTCAACTATGTGGCTGA 350
CODON OPTIMISED GTGCGATGGAAAAACTGGGCGAAACCCTGAAAATGAAAAAACTGCTGCGTTATCTGAACTATGTGGCGGA 182

PITG_21422 CDS  ACACACAGCAGTTTGA 366
CODON OPTIMISED ACATACCGCGGTGTAA 198
```

Figure 3.4 Wild-type vs. codon optimised PexRD2 DNA sequences

A sequence alignment of full-length coding sequence (CDS) for PexRD2 (paralog PITG_21422) from *P. infestans* reference genome (T30-4) against the synthesised codon optimised DNA sequence encoding the effector domain, as cloned into pOPINF. Conserved nucleotide bases are shaded in black.

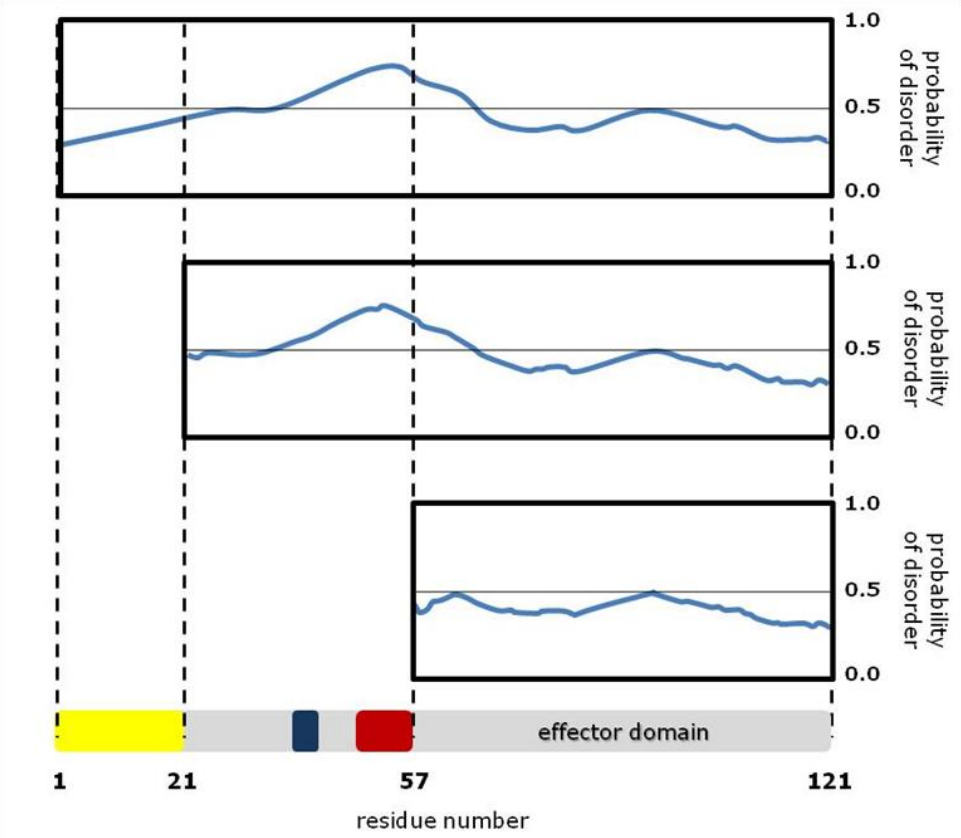

Figure 3.5 Disorder predictions for PexRD2 protein sequences

Protein disorder predictions conducted using the RONN protein disorder prediction tool (http://www.strubi.ox.ac.uk/RONN) aligned to the polypeptide sequence of different regions of PexRD2. Peptide motifs are coloured as in Figure 3.1

Small scale expression tests had determined that using *E. coli* BL21(DE3) grown in LB media yielded soluble protein. Protein expression was induced at an OD_{600} of 0.6 with 1 mM IPTG, before further incubation for 3 – 4 hours at 37ºC. These growth conditions were applied to large scale inductions. Cells were harvested and lysed by sonication. Cell lysates, clarified by centrifugation were applied to a pre-equilibriated nickel affinity column as described in Section 2.5.4.1. Fractions containing eluted proteins were pooled and concentrated prior to further purification by size exclusion chromatography (SEC) (Section 2.5.4.2). The protein eluted as a single broad peak, as measured using A_{280}, and appeared to be very pure, as determined by SDS-PAGE analysis (Figure 3.7).

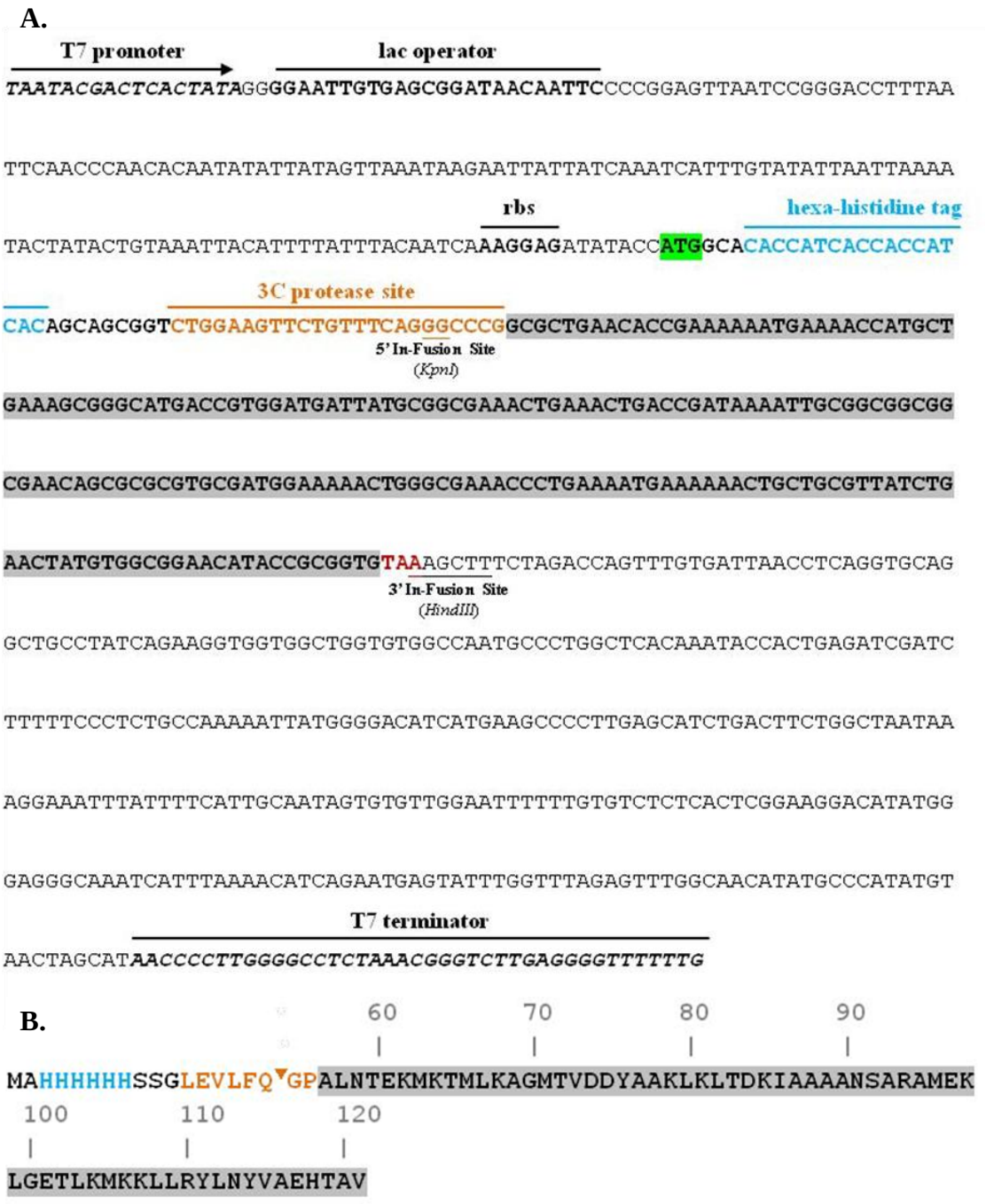

Figure 3.6 pOPINF:PexRD2

(A.) The codon optimised PexRD2 DNA sequence (shaded) as cloned into the In-Fusion site of pOPINF expression vector. Important vector features have been highlighted in bold type and labelled above. *PexRD2* was cloned in-frame with the vector encoded N-terminal hexa-histidine tag (shown in light blue) and the 3C protease site (orange). **(B.)** The amino acid sequence of the PexRD2 fusion protein as expressed from pOPINF:PexRD2, the hexa-histidine tag and 3C cleavage site are coloured as in (A.), with the point of protein cleavage marked with ▼.

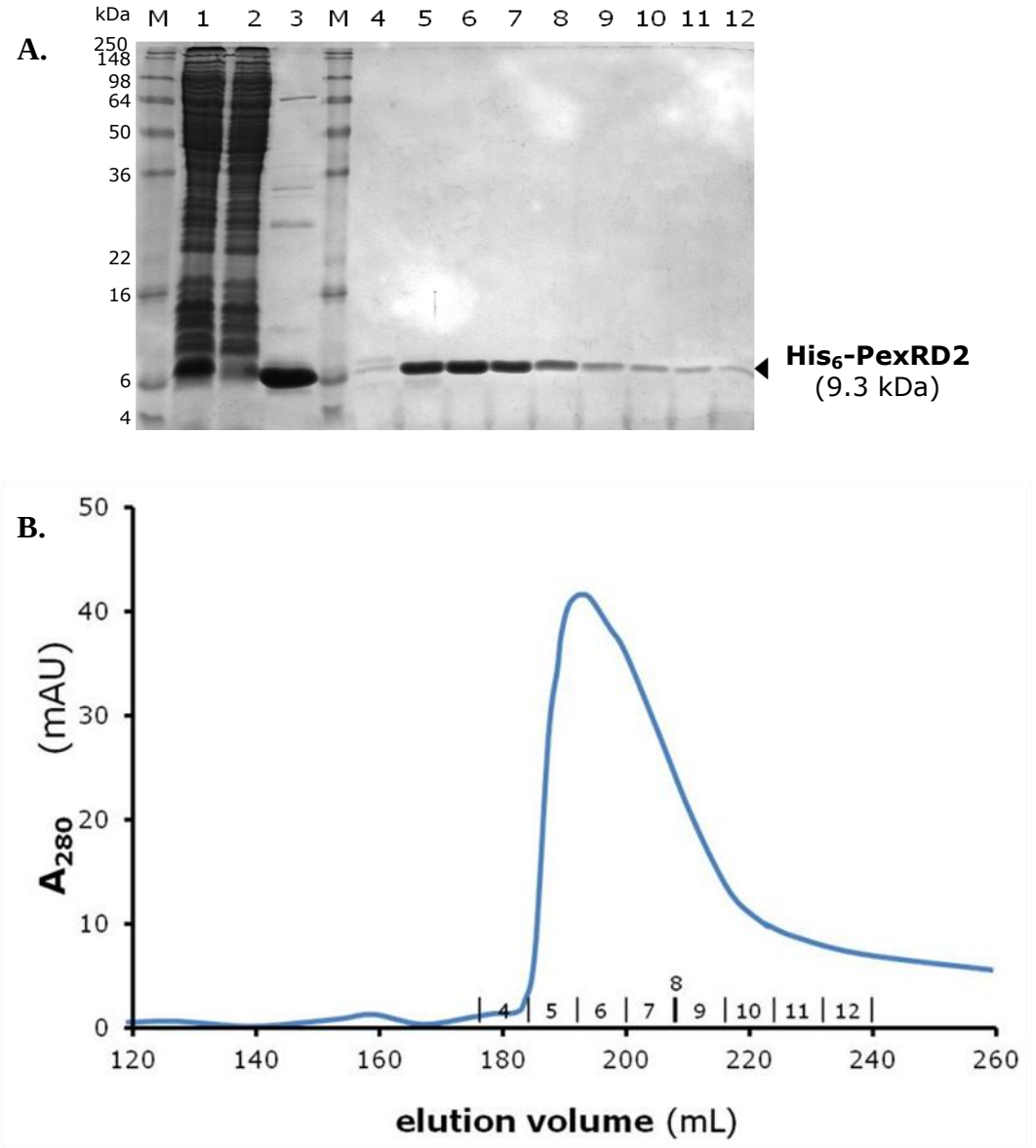

Figure 3.7 Purification of hexa-histidine-tagged PexRD2

(A.) 17% SDS-PAGE analysis at different stages of the purification of the effector domain of PexRD2 expressed from pOPINF. Lane 1: soluble fraction of cell lysate. Lane 2: unbound flow-through (FT) after passing through nickel affinity column (IMAC). Lane 3: pooled elution from IMAC. Lane 4-12: size exclusion chromatography (SEC) fractions corresponding to A_{280} peak. M indicate lanes containing SeeBlue® Plus2 molecular weight markers. **(B.)** Representation of $A_{280\ nm}$ elution profile for SEC of His_6-PexRD2. Fractions analysed by SDS-PAGE are numbered as in (**A)** (lanes 4 – 12).

Fractions containing purified protein of the correct size, as determined by comparison with the molecular marker, were pooled and concentrated to approximately 1 mg.mL^{-1} prior to a trial 3C protease digestion to determine optimum conditions for the cleavage of the tag. Two 100-µL reaction solutions were prepared as described in Section 2.5.5 and incubated at either room temperature (RT) or 4ºC. Ten-µL aliquots were taken immediately prior to adding the protease, and at regular intervals from 30 min to 22 h. Samples taken were immediately prepared for SDS-PAGE analysis. Overnight incubation at 4ºC was sufficient to achieve complete digestion, without the development of the possible degradation products that were observed following prolonged incubation at RT (Figure 3.8).

Proteolytic cleavage of the remainder of the concentrated fusion protein was then conducted using these optimised conditions with protein concentrated to approximately 2 mg.mL^{-1}. The cleaved protein was purified from the reaction solution, as described in Section 2.5.5, using a pre-equilibrated nickel affinity column, followed by further purification using size exclusion chromatography (Section 2.5.4.2). Again the protein eluted as a single broad peak, although at a larger elution volume than the affinity tagged protein (~200 mL vs ~190 mL respectively), as would be expected owing to the reduced molecular weight of the cleaved protein (Figure 3.9). SDS-PAGE analysis of eluted fractions showed little evidence of contamination indicating the solution was of high purity (Figure 3.9. A). These fractions were pooled and concentrated to 12 mg.mL^{-1}. The identity of the purified protein was confirmed by intact mass spectrometry which gave a value of 7337.92 Da, perfectly matching the predicted theoretical mass (7337.92 Da).

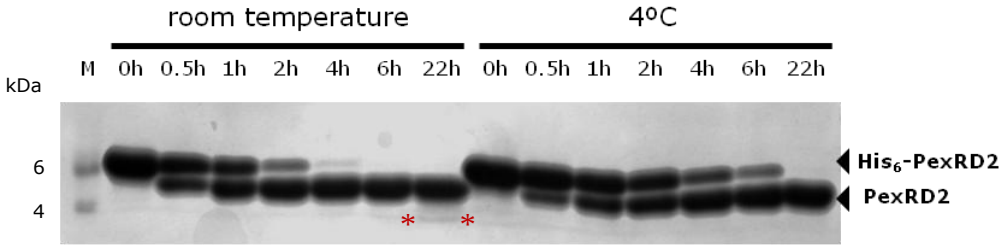

Figure 3.8 Trial digestion of His_6-PexRD2 by 3C protease

17% SDS-PAGE analysis of time course of hexa-histidine-tagged PexRD2 effector domain (His_6-PexRD2) incubated with 3C protease at room temperature or 4ºC. M indicates lane containing SeeBlue® Plus2 molecular weight markers. Asterisks indicate potential degradation products.

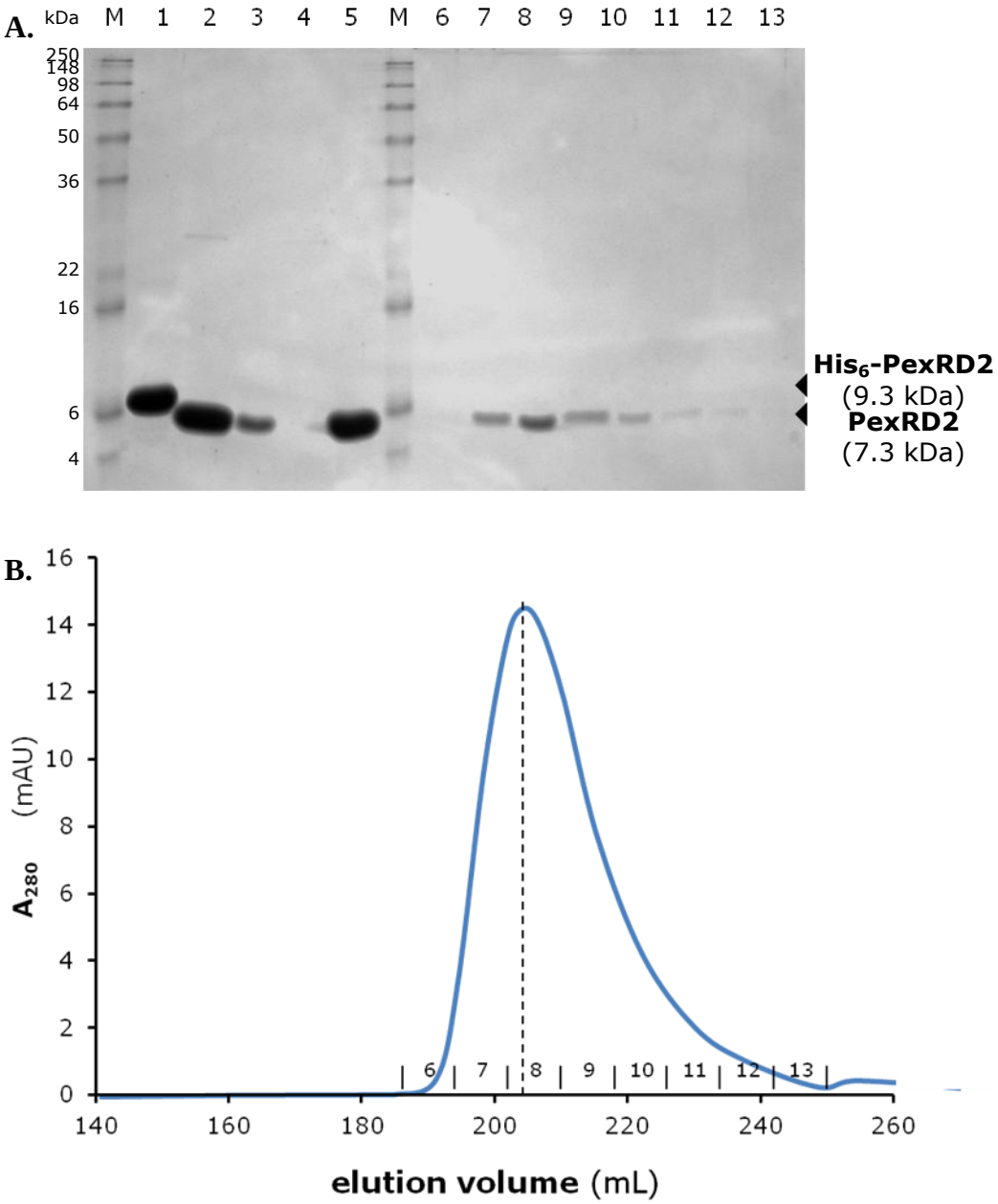

Figure 3.9 Purification of untagged PexRD2 effector domain

(A.) 17% SDS-PAGE analysis at different stages of the removal of the affinity tag and subsequent purification of the effector domain of PexRD2. Lane 1. His_6-PexRD2 concentrated to 2 $mg.mL^{-1}$. Lane 2: post-incubation with His_6-tagged 3C protease, at 4°C for ~20 h. Lane 3: unbound flow-through (FT) after passing through nickel affinity column (IMAC). Lane 4: elution from IMAC. Lane 5: re-concentrated unbound FT. Lanes 6–13: size exclusion chromatography (SEC) fractions corresponding to A_{280} peak. M indicate lanes containing SeeBlue® Plus2 molecular weight markers. **(B.)** Representation of $A_{280\ nm}$ elution profile for SEC of untagged PexRD2. Fractions analysed by SDS-PAGE are numbered as in **(A)** (lanes 6 – 13). The dashed line indicates the peak elution volume of 203.9 mL.

3.2.2 Crystallisation of PexRD2 effector domain

Crystallisation trials were performed with PexRD2 effector domain purified with the affinity tag cleaved as outlined in Section 3.2.1. Initial trials were set up as described in Section 2.6.1 using protein concentrated to 12 $mg.mL^{-1}$ and the vapour diffusion sitting drop method. Of the 480 conditions screened, a single crystal was obtained in only one condition: 2.2 M ammonium sulfate, 0.2 M ammonium bromide ($AmmSO_4$ screen, condition H2). This crystal formed within two days, and after the formation of a small amount of light granular precipitate (Figure 3.10 A). This condition was then optimised using the hanging-drop method in a 24-well plate, as described in Section 2.6.2. The concentrations of protein and ammonium bromide used were the same as those as in the initial trials. The concentration of ammonium sulfate was varied from 1.6 to 2.6 M; and conditions with or without the addition of 100 mM Tris-HCl pH 7.0 – 8.0 were also screened using a fully factorial design. Multiple crystals were obtained from a range of these optimised conditions and formed between 2 days and 4 weeks (Figure 3.10 B – C). As before, crystals formed after the appearance of a small amount of light granular precipitate, however, in optimisation trials a visible skin precipitate over the surface of drops was also observed.

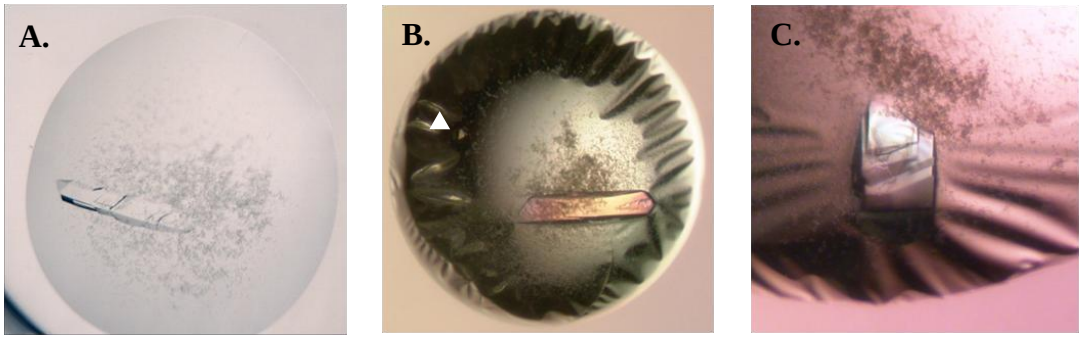

Figure 3.10 Crystals of PexRD2 effector domain

(A.) A single crystal formed in the initial trial (2.2 M ammonium sulfate, 0.2 M ammonium bromide). Crystals formed in a range of optimised conditions: **(B.)** 2.6 M ammonium sulfate, 0.2 M ammonium bromide, 100mM Tris-HCl pH 7.0 (a second cuboid crystal is highlighted by the white arrow); **(C)** 2.6 M ammonium sulfate, 0.2 M ammonium bromide, 100mM Tris-HCl pH 7.5; and 2.2 M ammonium sulfate, 0.2 M ammonium bromide, 100mM Tris-HCl pH 7.0 (not shown).

3.2.3 Data collection

Note: All datasets from protein crystals of PexRD2 effector domain were collected by Dr. Allister Crow (JIC).

For data collection, crystals from optimised conditions were harvested and cryo-protected using paratone-N, and subsequently cryo-cooled, as described in Section 2.6.3. Two diffraction datasets were collected (Figure 3.11) from an optimised crystal at the I02 tuneable diffraction beamline of the Diamond Light Source synchrotron facility (DLS, Oxfordshire, UK). One dataset was collected at a wavelength of 0.8984 Å corresponding to the peak side of the theoretical value for the K-edge of bromine (13.4737 keV, or 0.9202 Å, Figure 2.2). A second, higher resolution, dataset was collected at a wavelength of 0.9700 Å.

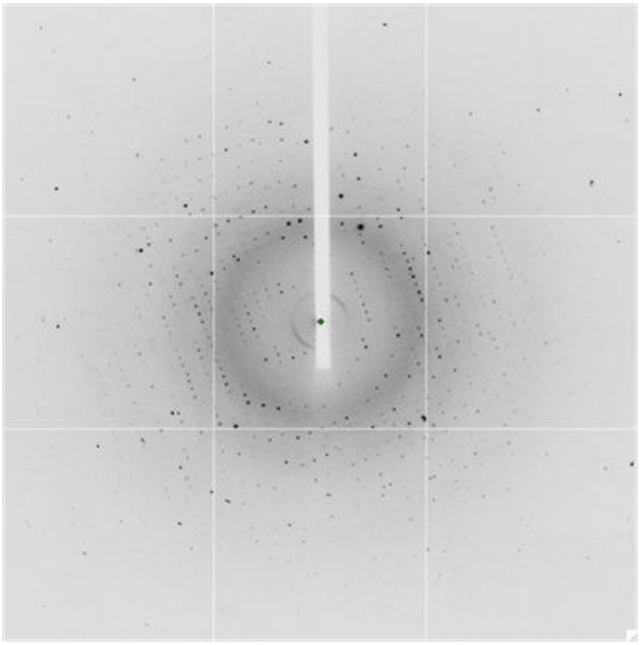

Figure 3.11

Example of a diffraction image collected from PexRD2 crystals

A representative diffraction image taken from a dataset collected from a PexRD2 effector domain crystal.

3.2.4 Data processing and structure solution

The 'bromide peak' dataset consisted of 360 images and diffracted to a maximum resolution of 1.9 Å. The data were processed using iMOSFLM (Leslie and Powell, 2007), then scaled and reduced with SCALA (Evans, 2011) as described in Section 2.5.5. The data collection statistics are shown in Table 3.1. The crystal could be satisfactorily processed in the orthorhombic space group $P2_12_12_1$ with an overall R_{merge} of 6.5%. Unit cell dimensions were established as **a** = 44.80 Å, **b** = 52.36 Å,

c = 53.32 Å; and **α** = **β** = **γ** = 90º. Unit cell calculations predicted two molecules within the asymmetric unit giving a solvent content of 42.4%. This dataset was used for initial phase calculations. The phase problem was solved using a single-wavelength anomalous dispersion (SAD) approach utilising the anomalous signal of bromide ions present in the crystal lattice, as described in Section 2.6.6.1. SHELX C/D (Sheldrick, 2010) predicted 11 heavy atom sites that were used by PHASER-EP (McCoy *et al.*, 2007) for experimental phasing. These initial phases were subjected to phase improvement by PARROT (Cowtan, 2010), and an initial model, comprising at least the backbone of 127 residues docked within the density, was generated using BUCCANEER (Cowtan, 2006).

3.2.5 Refinement, rebuilding and validation

The 'high resolution' dataset consisted of 360 images and diffracted to a maximum resolution of 1.75 Å. These data were processed using iMOSFLM, then scaled and reduced with SCALA, as described in Section 2.6.5. The data collection statistics are shown in Table 3.1. The crystal belonged to the orthorhombic space group $P2_12_12_1$, with an overall R_{merge} of 7.9% and unit cell dimensions of **a** = 44.45 Å, **b** = 52.92 Å, **c** = 53.73 Å; and **α** = **β** = **γ** = 90º. The initial model solved using bromine SAD on the bromine peak data set was then refined against the high resolution dataset using REFMAC5 (Murshudov *et al.*, 1997) extending the maximum resolution to 1.75 Å. The model was improved via iterative cycles of refining with REFMAC5 and rebuilding in COOT. Water molecules were fitted and refined using ARP/wARP (Langer *et al.*, 2008), followed by manual inspection in COOT. The occupancy of bromide ions in the predicted sites was also modified manually in COOT. During the final stages of refinement, translation, libration, and screw-rotation (TLS) restraints were used grouping the fitted residues of chain-a and chain-b into two TLS groups. The final model comprised the N-terminal residue of the expressed construct, Gly55, through to the penultimate residue Ala120 in chain-a, and from Gly55 to Thr119 in chain-b. The C-terminal Val121 in chain-a, and residues Ala120 – Val121 in chain-b, were excluded owing to a lack of well defined electron density to determine

Table 3.1 Data Collection and Refinement Statistics for PexRD2

	PexRD2 bromide peak	PexRD2 high resolution
Data Collection		
Instrumentation	DLS-I02	DLS-I02
Wavelength (Å)	0.8984	0.9700
Resolution range (Å)[a]	44.80–1.90 (2.00–1.90)	37.70–1.75 (1.84–1.75)
Space Group	$P\ 2_12_12_1$	$P\ 2_12_12_1$
Unit cell parameters (Å)	a = 44.80, b = 52.36, c = 53.32, $\alpha = \beta = \gamma = 90.00^o$	a = 44.45, b = 52.92, c = 53.73, $\alpha = \beta = \gamma = 90.00^o$
Completeness (%)[b]	99.0 (98.7), 99.3 (99.1)	99.9 (100.0), 100.0 (100.0)
Unique Reflections[a]	10229 (1451)	13313 (1907)
Redundancy[b]	12.9 (13.3), 7.0 (7.0)	15.8 (16.3), 8.4 (8.5)
R_{merge} (%)[a, c]	6.5 (43.0)	7.9 (42.5)
$I/\sigma(I)$[a]	25.4 (6.7)	26.3 (9.9)
Number of SAD sites	11	
FOM	0.34	
Refinement		
Resolution range (Å)		37.70 – 1.75
R_{work} (%)[a]		18.9 (23.8)
R_{free} (%)[a]		24.4 (27.3)
No. of non-hydrogen atoms (protein/waters)		1154 (1027/127)
RmsBond (Å)		0.015
RmsAngles (°)		1.446
ESU (based on ML) (Å)		0.08
Mean *B* factors (Å^2)		14.145
Ramachandran plot favoured/allowed/disallowed (%)[d]		99.3 / 100 / 0

[a] Values in parentheses are those for the highest resolution shell.

[b] Completeness and Redundancy. First value given is for merged data, second represents separated anomalous pairs (values in parentheses for highest resolution shell).

[c] Reflection statistics are as reported in SCALA. R_{merge} is calculated as described by Evans (2005).

[d] As calculated by MOLPROBITY (Davis *et al.*, 2007, Chen *et al.*, 2009).

their positions. The side chain atoms of a number of lysine, glutamine and arginine residues were also excluded for the same reasons. Another 11 residues with flexible side chains were modelled with alternate conformations where clear electron density indicated their positions. Seven bromide ions were retained within the final model although the occupancy of these sites varied from 0.5 – 1. Final refinement statistics for the PexRD2 effector domain crystal structure are given in Table 3.1.

The final structure was checked for geometric and structural validity using COOT tools during refinement and MOLPROBITY (Figure 3.12) (Davis *et al.*, 2007, Chen *et al.*, 2009) to generate Ramachandran plots. These plots are a way of visualising the Φ against Ψ dihedral angles of each of the residues present in the structure. The Ramachandran plot for PexRD2 effector domain revealed that all residues are within the allowed regions and there are no outliers (Figure 3.13). MOLPROBITY also analyses the other aspects of protein geometry. It compares the conformations of each amino acid in protein structures deposited in the Protein Data Bank (PDB) to the residues present in the structure being analysed, and determines whether they are in acceptable conformations. The MOLPROBITY score of 1.6 is excellent, putting the structure in the 89th percentile of structures of a comparable resolution, 1.75 Å ± 0.25 Å, already deposited in the PDB (Figure 3.12). Only two residues with unacceptable conformations, or 'poor rotamers', were identified; however, the positioning of the side chains was supported by the observed electron density in both cases.

All-Atom Contacts	Clashscore, all atoms:	6.12		92nd percentile* (N=932, 1.75Å ± 0.25Å)
	Clashscore is the number of serious steric overlaps (> 0.4 Å) per 1000 atoms.			
Protein Geometry	Poor rotamers	2	2.22%	Goal: <1%
	Ramachandran outliers	0	0.00%	Goal: <0.05%
	Ramachandran favored	126	98.44%	Goal: >98%
	MolProbity score^^	1.60		89th percentile* (N=11713, 1.75Å ± 0.25Å)
	Cβ deviations >0.25Å	0	0.00%	Goal: 0
	Bad backbone bonds:	0 / 522	0.00%	Goal: 0%
	Bad backbone angles:	0 / 649	0.00%	Goal: <0.1%

Figure 3.12 Validation of final structure of PexRD2 effector domain

Analysis conducted by MOLPROBITY. * 100th percentile is the best amongst structures of comparable resolution; 0th percentile is the worst.

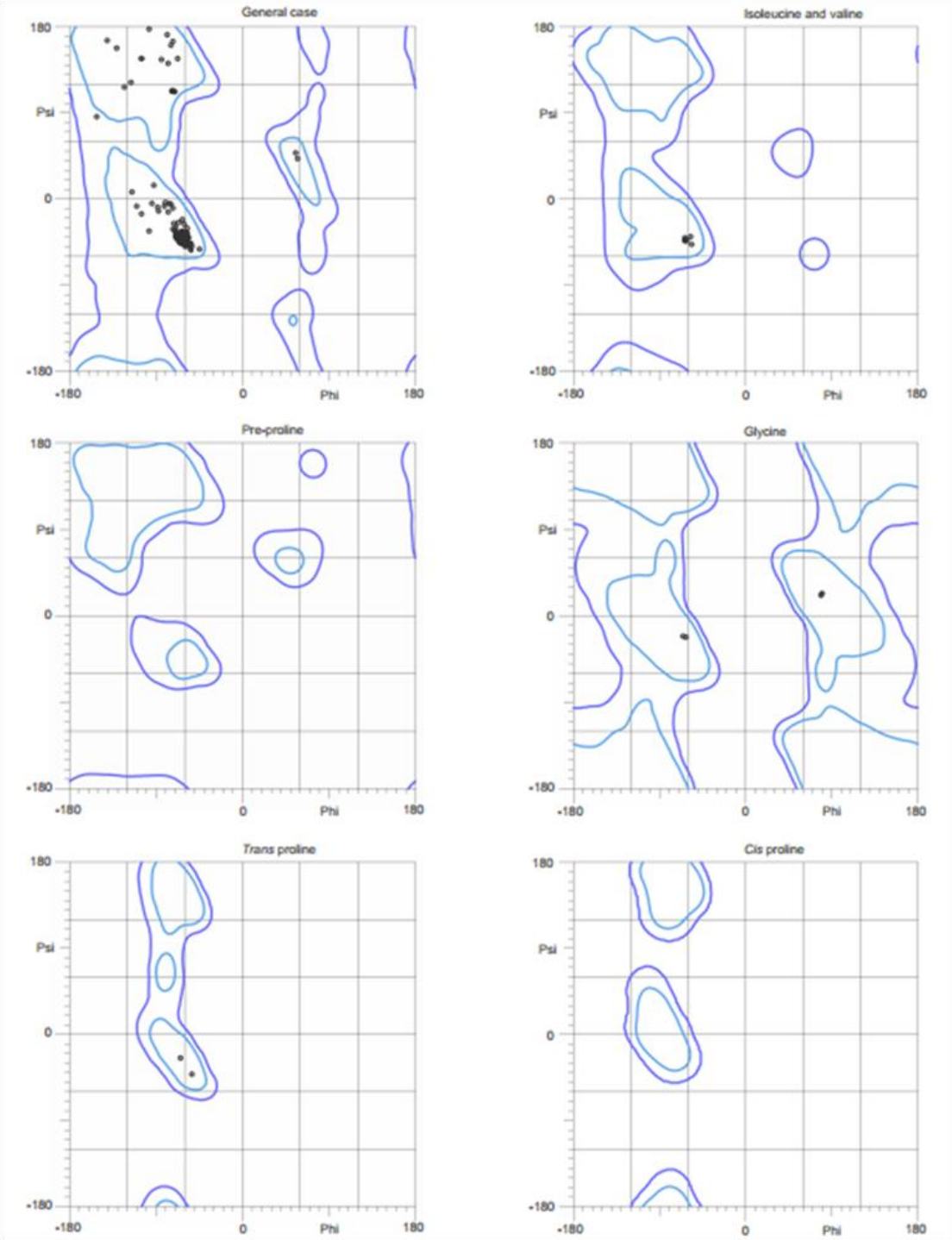

Figure 3.13 Ramachandran plot for refined PexRD2 structure

99.3% (137/138) of all residues were in favoured (98%) regions, 100.0% (138/138) of all residues were in allowed (>99.8%) regions. There were no outliers. Produced by MOLPROBITY.

3.2.6 Structure of PexRD2 effector domain

The structure of the effector domain of PexRD2 is composed of five α-helices and crystallises as a dimer (Figure 3.14). The buried surface area between the two chains is equal to 1830 $Å^2$, the equivalent to 20% of the surface area of each monomer as measured using the 'Protein interfaces, surfaces and assemblies' service PISA (Krissinel and Henrick, 2007). This interface was given a high Complex Significance Score (CSS) of 0.89 (values range from 0 – 1).

Within the dimer, the two protein chains show the same overall fold. Superposition of one chain onto the other gives a root mean square deviation (r.m.s.d.) for all atoms of 0.484 Å. Helices α1, α2 and α5 show almost identical orientations, as do the residues comprising the loop between α1 and α2. Slight differences, however, are observed in certain more flexible regions; such as the N- and C-termini, and, interestingly, the region comprising helix α3 and helix α4 (Figure 3.15).

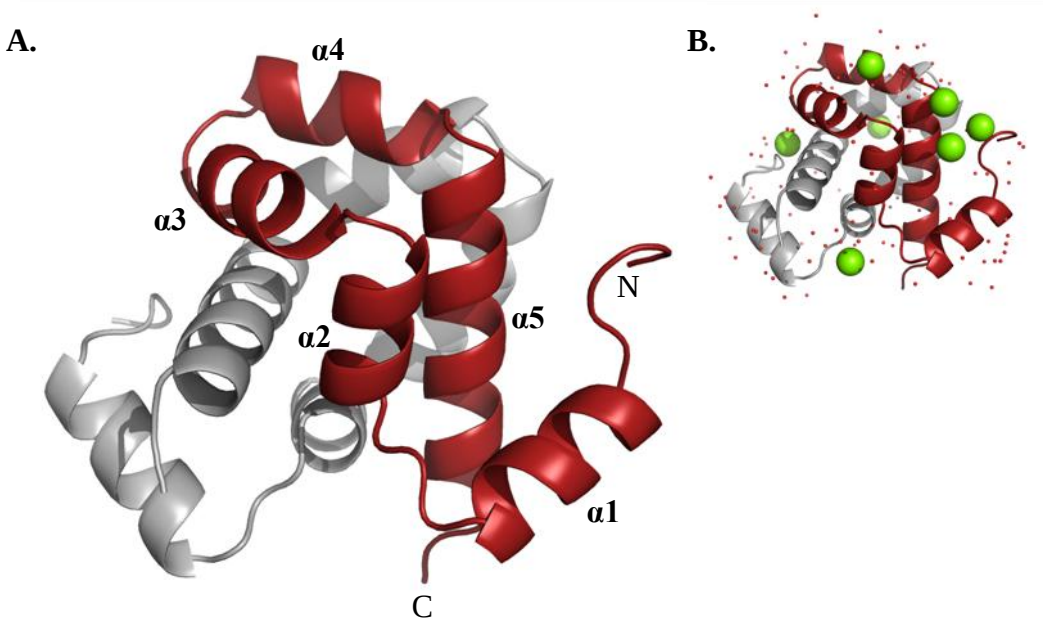

Figure 3.14 Protein structure of the effector domain of PexRD2

(A.) Cartoon ribbon representation of the effector domain of PexRD2 with chain-a coloured in dark red, and chain-b in grey. The N and C termini, as well as helices 1 – 5 (α1 – 5) are labelled on chain-a. **(B.)** Protein structure of PexRD2 effector domain in the same orientation as in A. but showing the locations of the 7 bromide ions (large green spheres), and 127 waters (small red spheres).

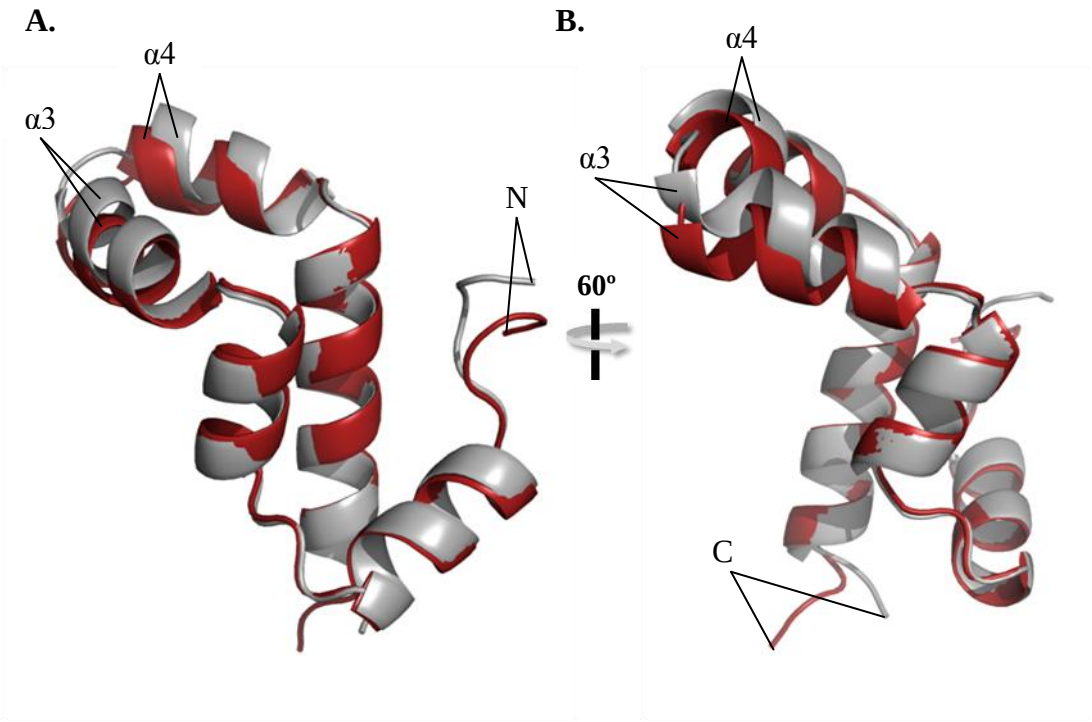

Figure 3.15 Superposition of PexRD2 chain-b onto PexRD2 chain-a

(A.) Cartoon ribbon representation of the superposition of the two polypeptide chains in the asymmetric unit, with chain-a coloured in dark red, and chain-b in grey, and the orientation of chain-a the same as in Figure 3.14. and **(B.)** rotated 60º, anti-clockwise, about the y-axis. The differences in the positioning of the N- and C-termini, as well as helices α3 and α4, are clearly visible.

The solvent exposed surface of the PexRD2 dimer displays a large positively charged region, dominated by a large number of lysines, that wraps around the structure (Figure 3.16 A). Two distinct negatively charged patches are also observed: a large one that maps to a groove in the structure in the proximity of the C-termini of the two chains; and a smaller one in the area spanning helices α4 from both chains. In contrast, the interface between the two PexRD2 monomers is dominated by hydrophobic residues (Figure 3.16 B).

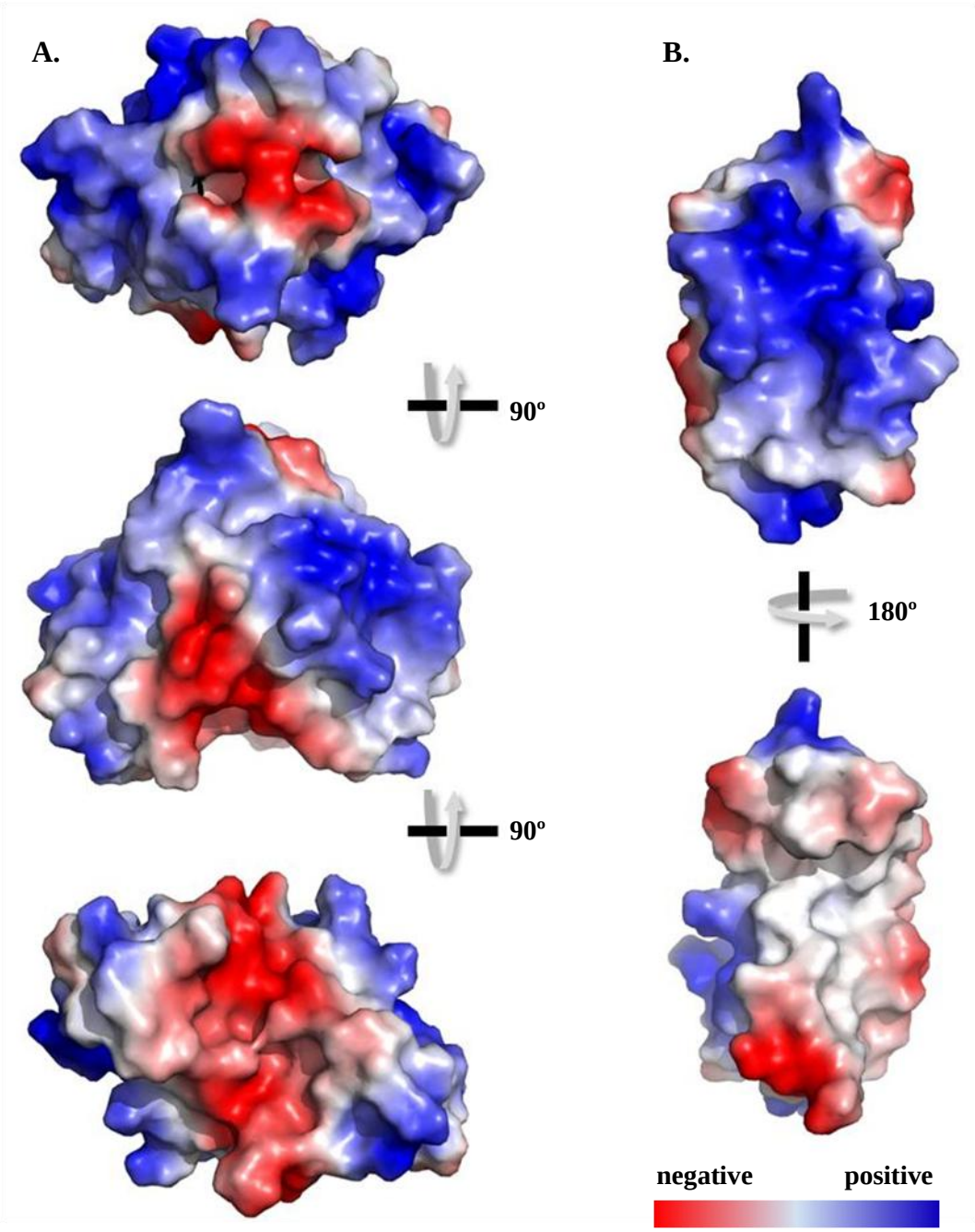

Figure 3.16 Surface charge distribution for PexRD2 dimer and monomer

(A.) (MIDDLE) Electrostatic potential calculated with Pymol for the PexRD2 dimer in the same orientation as Figure 3.14 displaying the large positively charged region. (TOP) This positive charge wraps around the structure, encircling the small patch of negative charge that spans helices α4 from both chains. (BOTTOM) The large negative charged patch maps to a groove in the structure in the proximity of the C-termini of the two chains. **(B.)** Electrostatic potential for a PexRD2 monomer highlighting the contrast between (TOP) the positively charge solvent surface exposed and (BOTTOM) the hydrophobic dimerisation interface.

3.2.7 Oligomeric state of PexRD2 in solution and *in planta*

The observation of dimers of PexRD2 effector domain in protein crystals could represent an artefact of crystallisation. To test whether this was the case, the oligomeric state of PexRD2 was assessed in solution, by size exclusion chromatography (SEC) and analytical ultracentrifugation (AUC), and *in planta*, by co-immunoprecipitation (co-IP).

3.2.7.1 Preparative size exclusion chromatography data support dimerisation of PexRD2 effector domain

Size exclusion chromatography separates macromolecules based on their size and shape (Section 2.5.4.2). A very large macromolecule cannot penetrate the pores within the stationary phase and passes only through the space between the particles within the column, also known as the void volume (V_0). On the other hand, small macromolecules can penetrate the pores, as well as the void volume. Therefore, larger particles will elute earlier, when a volume of mobile phase equal to the V_0 has passed through the column, whilst smaller molecules will elute much later after a greater volume has passed through the column.

By comparing the elution volume (V_e) that corresponds to the A_{280} peak for PexRD2, to a calibration curve of elution volumes of protein standards of known molecular weights, run previously on the same SEC column, a rough estimate for the apparent molecular weight of PexRD2 can be obtained. From the initial purification of PexRD2, with the affinity tag cleaved post 3C protease treatment, an elution volume of 203.9 mL is observed (Figure 3.9). By comparison to a previously generated calibration curve (Figure 3.17), this equates to a predicted molecular weight of 12.7 kDa. Since the molecular weight of monomeric PexRD2 is 7.3 kDa (-5.4 kDa), and a dimer of PexRD2 is 14.7 kDa (+2.0 kDa), this predicted value is closer to that of PexRD2 effector domain eluting as a dimer, rather than a monomer. The deviation between the predicted value and the actual molecular weight likely results from the fact that the standards used to generate the calibration curve and the experimental sample were not run in parallel, as well as the use of a preparative column and not an analytical column.

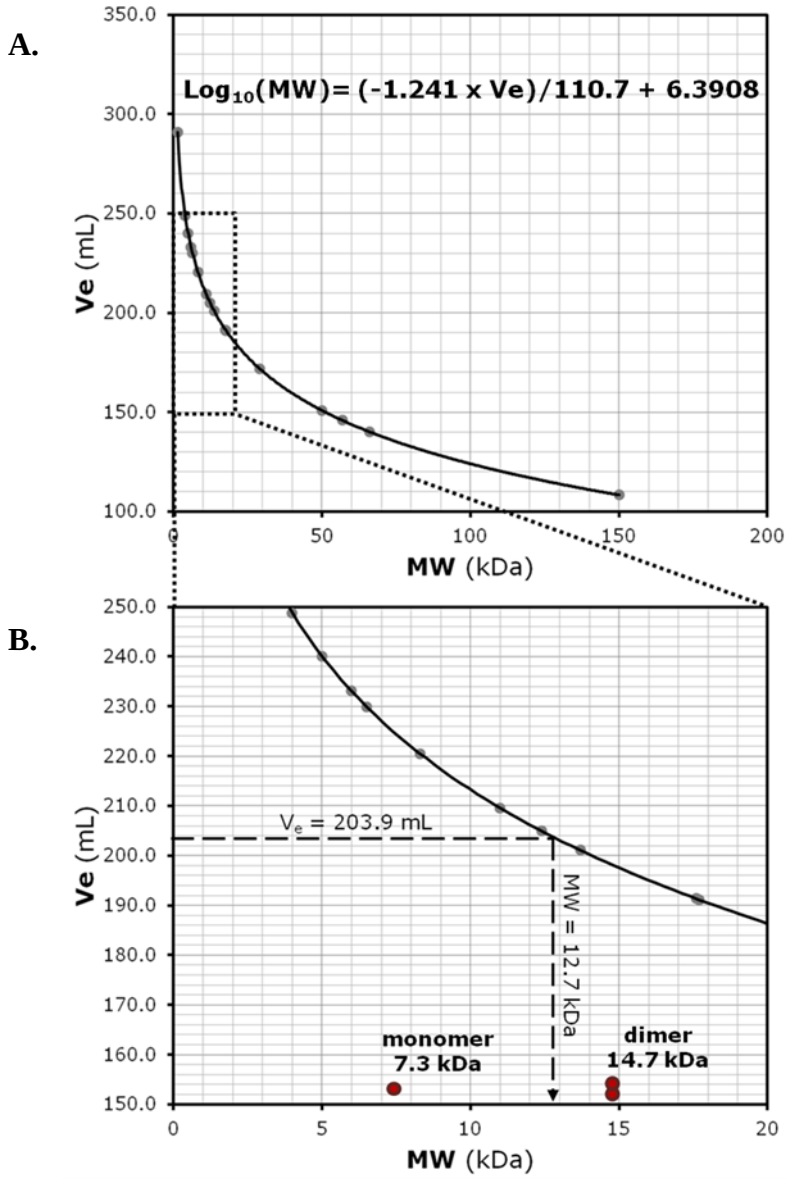

Figure 3.17 The estimated molecular weight of PexRD2, using its Ve from SEC columns, suggests dimerisation in solution.

(A.) A previously generated calibration curve of elution volumes (Ve) of protein standards, as determined using a Hi-Load 26/60 Superdex 75 prep grade gel filtration column, against their molecular weights (MW). V_0 for this column equals 110.7 mL and the calibration of the column was conducted by *Dr. Richard Hughes.* **(B.)** The estimated molecular weight of eluted PexRD2 effector domain, (12.7 kDa), from its elution volume on the same column at a later stage during its purification (203.9 mL), is closer to the value of a PexRD2 dimer (14.7 kDa).

3.2.7.2 Analytical ultracentrifugation (AUC) confirms that dimers of PexRD2 are the dominant species in solution

Note: AUC analysis of PexRD2 effector domain was performed by Dr. Tom Clarke (UEA) with solutions of purified protein as used in crystallisation trials.

Analytical ultracentrifugation is commonly regarded as the 'gold standard' technique for the measurement of the molecular weight of protein and protein complexes in solution. Sedimentation equilibrium experiments were performed at a speed of 99,660 x ***g*.** Optical interference patterns were collected at equilibrium for protein samples at concentrations of 3.0 and 6.0 $mg.mL^{-1}$. Data were fitted using ULTRASCAN (Demeler *et al.,* 2005), with the molecular masses of the species fixed at their theoretical value, to a dimer/tetramer model. The dimeric form predominated in solution, and there was no evidence for any free monomer (Tom Clarke, personal communication, for more details see Supplementary Figure 3, Boutemy *et al.,* 2011).

3.2.7.3 ***Co-immunoprecipitation (Co-IP) experiments confirm PexRD2 self-associates* in planta**

Note: The Co-IP described below was conducted by Dr. Joe Win (TSL).

In addition to the data obtained from purified proteins in solution, the oligomeric state of PexRD2 *in planta* was also assessed. Co-immunoprecipitation experiments are widely considered the gold standard for demonstration of protein-protein interactions *in vivo*. Transient expression, in *N. benthamiana* via agroinfiltration, of both FLAG-epitope-tagged or GFP-fusions of effector proteins, were followed by co-immunoprecipitation from total protein extracts with anti-FLAG M2 affinity gel as described in Section 2.9.4 and by Boutemy *et al.*, (2011). Subsequent western blot analysis of total extracts and immunoprecipitated proteins demonstrated that PexRD2 self-associates *in planta* (Joe Win, personal communication, for more details see Supplementary Figure 3, Boutemy *et al.,* 2011).

3.2.8 Structural similarity searches with PexRD2

One of the benefits of solving the three-dimensional structure of a new protein is that by searching for structural similarity to already characterised proteins in the PDB, it may be possible to infer a biochemical function for the new protein. This approach can often be more successful than searches based on primary sequence data alone since the structure of a protein is more important in determining function and, as such, is often more conserved (Illergård *et al.*, 2009). A structural similarity search with chain-a from the structure of PexRD2 effector domain was conducted using the DALI server (Holm and Rosenström, 2010). Similarity is measured by Dali Z-scores, and structures that have significant similarities have a Z-score above 2, and usually have similar folds.

3.2.8.1 L29 protein, a 50S ribosomal subunit protein

The top hit obtained following a search against a subset of PDB matches, filtered to remove those with 90% sequence identity (PDB90) was to L29: one of the proteins within the large ribosomal subunit of the ribosome of *Haloarcula marimortui*, a halophilic archaeon (1JJ2, chain-u). The Z-score for this hit was 4.6, and the structural alignment with PexRD2 had an r.m.s.d. of 4.6 Å, with 20% sequence identity over the aligned region.

L29 interacts extensively with a kink-turn motif (K-turn or KT), in the 23S ribosomal RNA (25S rRNA) designated KT-7 (Klein *et al.*, 2001). A histidine residue near the N-terminus of this protein, His4, interacts by stacking with the protruded nucleotide in KT-7, A96; and this protein contacts KT-7 on the opposite face to one of the two assembly initiator proteins, L24.

Visual inspection of the superposition of protein L29 onto the chain-a from the structure of PexRD2 effector domain (Figure 3.18) showed clear differences between the two protein folds that likely indicate differences in function. The structure of L29 consists of only three helices; a single short helix followed by two extended helices. The second and third helices run anti-parallel and are linked by a loop of seven residues. In the superposition, the first helix shows a partial overlay with α1 of

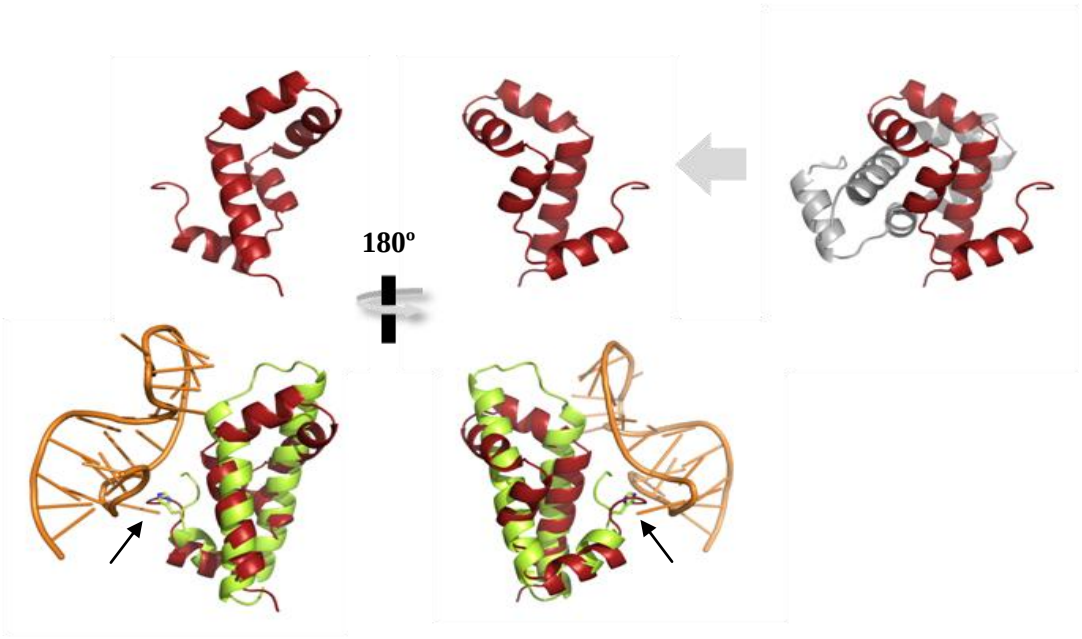

Figure 3.18 Superposition of the 50S ribosomal subunit protein, L29, on to the structure of PexRD2 effector domain

Cartoon representations of a superposition performed using the DaliLite tool for the pairwise alignment of protein structures. The appropriate chain from structure 1JJ2 from the PDB, was aligned with the chain-a from PexRD2. L29 polypeptide chain is coloured in green, and the KT-7 motif of the 25S rRNA is orange. PexRD2 chains are coloured as in Figure 3.14. The black arrow indicates the positioning of His4 from L29 that stacks with the protruded nucleotide A96.

PexRD2, but is misaligned by an angle of approximately 20º. The second helix is overlaid with both α2 and α3, but does not include the articulation observed between these two helices in PexRD2. As such, the alpha carbon atoms of the residues at the end of these two helices (L29 helix 2, and PexRD2 α3) are 9.4 Å apart in the superposition. No part of the structure of L29 is overlaid with α4 from PexRD2, and the third helix only partial overlays with α5, but misaligned by an angle of approximately 16º. These structural differences, combined surface differences, in particular the lack of a residue that could substitute for residue His4 of L29, mean that is highly unlikely that PexRD2 would also interact with ribosomal RNA, and the apparent structural similarity must be deemed coincidental.

3.2.8.2 Sus1, a central component of the yeast 'gene gating' machinery

The second hit obtained following a structural similarity search of PexRD2 against the PDB90 was Sus1[*]: a small nuclear protein from *Saccharomyces cerevisiae* (3KIK, chain-a). The Z-score for this hit was 4.5, and the structural alignment with PexRD2 had a lower r.m.s.d. (3.6 Å) than that with L29, but with only 8% sequence identity over the aligned region.

Sus1 is a central component of the yeast 'gene gating' machinery (Ellisdon *et al.*, 2010). Gene gating refers to the tethering of actively transcribed genes to the nuclear pore complex (NPC) and as such integrates transcription with mRNA nuclear export. Sus1 is part of both the SAGA complex: a 2 MDa protein complex that acts as a co-activator for transcription by RNA polymerase II; and the TREX2 complex; that tethers the SAGA complex to the NPC. Sus1 adopts an "articulated helical hairpin fold" that consists of five alpha helices linked by loops that form putative hinges. This fold is proposed to allow Sus1 to wrap tightly an extended alpha helix of its interacting proteins following 'a surface exposed hydrophobic stripe'. The first helix of Sus1 was shown to not be involved in the interaction with some interacting proteins, and in these cases its positioning was shown to be highly variable.

The overall fold of PexRD2 could also be described as an articulated helical hairpin (Figure 3.19 A), which also wraps around an α-helix, in this case the α5 of the other monomer in the dimer. However, closer visual inspection of the superposition of Sus1 onto the chain-a from PexRD2 (Figure 3.19) shows some clear differences between the two. For example, the second helix of Sus1 is extended by four residues when compared to α2, which results in a dramatic change in the positioning of helices 3 and 4 in Sus1, compared to the corresponding helices in PexRD2 (Figure 3.19 B). These two helices are also both much longer in Sus1 relative to those in PexRD2.

The helix from the Sus1-interacting protein, Sgf11 (Sgf11-h), that was crystallised in complex with Sus1 is also in a drastically different orientation than the corresponding α5 helix from the other PexRD2 in the dimer. Sgf11-h has its N-

[*] Sus1 encoded by *SUS1* (*SUS* = synthetic lethal gene upstream of *Ysa1*)

terminus near to the end of helix 5 from Sus1. Its C-terminus is close to the loop between Sus1 helices 3 and 4 (Figure 3.19 C-D). Whereas, in the PexRD2 dimer, the α5 of the chain-b monomer, starts close to the centre of α4 from chain-a; and ends nearer the start of α2 on chain-a (Figure 3.19 E). These findings suggest that rather than implying a shared function in 'gene gating', the superficial resemblance of PexRD2 to Sus1, may likely result from both proteins converging on a protein fold that mediates protein-protein interactions. The articulated helical hairpin allows tight binding to an α-helix from an interacting partner. In the case of Sus1, it allows heterodimer formation with other proteins involved in the SAGA and TREX2 complexes, but for PexRD2 it appears to mediate homodimerisation.

Figure 3.19 Superposition of Sus1, and an α-helix from an interacting protein, on to the structure of PexRD2

Cartoon representations of a superposition performed using the DaliLite tool for the pairwise alignment of protein structures. The appropriate chain from structure 3KIK from the PDB, was aligned with the chain-a from PexRD2. Sus1 polypeptide chain is coloured in blue, and the helix from the interacting protein (Sgf11) is yellow. PexRD2 chains are coloured as in Figure 3.14.

3.2.8.3 Structural similarity of PexRD2 to other RXLR effectors

Around the same time the crystal structure of PexRD2 from *P. infestans* was published, the three-dimensional structures of four other oomycete RXLR effectors were also released: AVR3a11 (Boutemy *et al.*, 2011), AVR3a4 (Yaeno *et al.*, 2011), ATR1[†] (Chou *et al.*, 2011) and ATR13 (Leonelli *et al.*, 2011). AVR3a11 and AVR3a4 are paralogs from the hemibiotrophic pepper and curbit pathogen *P. capsici* (*Pc*), and are close homologs of arguably the best studied of RXLR effectors, AVR3a from *P. infestans*. ATR1 and ATR13 are RXLR effectors from *Hyaloperonospora arabidopsidis* (*Hpa*), an obligate biotroph of the model plant *Arabidopsis thaliana*.

The effector domains of AVR3a11 (Thr70 - Val132) and AVR3a4 (Gly59 - Tyr122) were determined by X-ray crystallography (Boutemy *et al.*, 2011) and nuclear-magnetic resonance (NMR) (Yaeno *et al.*, 2011), respectively. The structure of AVR3a11 was solved to a sub-angstrom resolution of 0.9 Å, and the solution structure of AVR3a4 had an r.m.s.d. for the backbone atoms in the helical regions of the protein of 0.36 Å. Both were shown to adopt a four-helix bundle, with α-helices connected by loop regions, and with their folds stabilised by a core of hydrophobic residues.

The crystal structure of the ATR1 effector domain (Ala52 - Val311) was solved to a resolution of 2.3 Å. The fold of ATR1 was described as a "two-domain, extended, seahorse like structure" and is comprised of 13 α-helices (Chou *et al.*, 2011). The N-terminal 'head' formed from the first three helices was separated from the larger C-terminal 'body' made up of the other 10 helices, by a nine residue loop referred to as the 'neck' region. Analysis of the structure of the C-terminal body domain of ATR1 revealed that it contained two five-helix structural repeats that were not evident in the primary sequence. The Cα-atoms for helices α4 – α8 could be overlaid on to those of the next five-helix segment (α9 – α13) with r.m.s.d. of 5.1 Å, in spite of only 8% sequence identity between the two repeats.

The solution structure of ATR13 effector domain (Ser54-Gln154), from *Hpa* strain Emco5, has an r.m.s.d. for backbone atoms in the helical regions of the protein of

[†] ATR = *Arabidopsis thaliana* recognized

0.8 Å. The fold consists of a disordered N-terminal region preceding a three-helix bundle containing another large, disordered loop region. The central helix packs against a short helix and turn on one side, and a long C-terminal helix on the other.

A comparison of PexRD2 to the other RXLR structures led to the identification of a three-helix bundle fold that was conserved in four of the five structures (Win *et al.*, 2012, Figure 3.20 B). This conserved fold was observed in the structures of PexRD2, Avr3a11, Avr3a4 and ATR1 (Figure 3.21 B); but not ATR13. These helices were linked by one conserved loop and one variable loop, and the fold was maintained by a hydrophobic core. This conserved fold was called the 'WY-domain' (Boutemy *et al.*, 2011) (Figure 3.21), since it was shown to be composed of two published conserved sequence motifs (the W-motif and the Y-motif) that were known to be prevalent in the C-terminal effector domains of large numbers of RXLR effectors (Dou *et al.*, 2008a). The key residues identified in each motif were buried inside the hydrophobic core of this bundle, and the interaction between these key residues was suggested to maintain the fold's overall structural integrity (Boutemy *et al.*, 2011). The discovery of the WY-fold gave previous mutation analysis of these sequence motifs a structural context. With hindsight, the observation that the mutations at these key residues typically result in the loss of function of the W- and Y-motif containing RXLR effectors (Dou *et al.*, 2008a) can be explained by their likely disruptive impact on the protein folding. Furthermore, although the key residues are likely to be important for effector stability, and hence function, the exact identity of these residues is variable between the different examples of WY-folds observed in the four effectors (Win *et al.*, 2012b). The conserved WY-domain of PexRD2, which consists of helices α1, α2 and α5, has Met66 and Tyr111 in the key residue positions of the W- and Y- motifs, respectively. The WY-domains of AVR3a11 and AVR3a4, which consist of helices α2, α3 and α4, both have tryptophan and tyrosine residues in the key positions (Trp96/Tyr125, and Trp105/Tyr135 respectively). The C-terminal body region of ATR1 contains two WY-domains, with the first (ATR1-WY1) consisting of helices α6, α7 and α8, and the second (ATR1-WY2), helices α11, α12 and α13. The key residues of ATR1-WY1 and ATR1-WY2 are Trp173/Cys208 and Tyr259/Tyr305, respectively. In all cases a hydrophobic core is maintained and

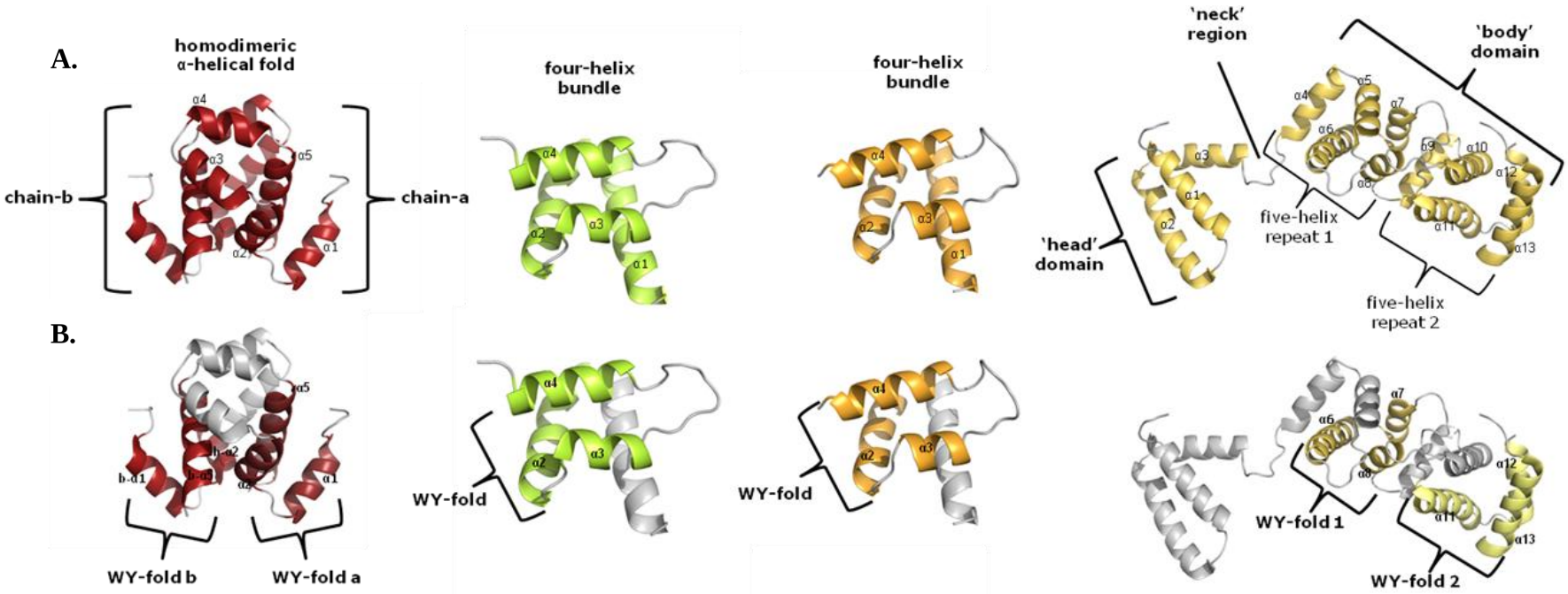

Figure 3.20 Structures of RXLR effectors from different oomycete species show a conserved fold.

(A.) Published structures of RXLR effector domains showing key structural features. From left to right: PexRD2 (PDB ID code: 3ZRG), *Pc*AVR3a11 (3ZR8), *Pc*AVR3a4 (2LCL), and *Hpa*ATR1 (3RMR). **(B.)** The same four structures as above highlighting only the helices that contribute to the conserved WY-folds.

A.

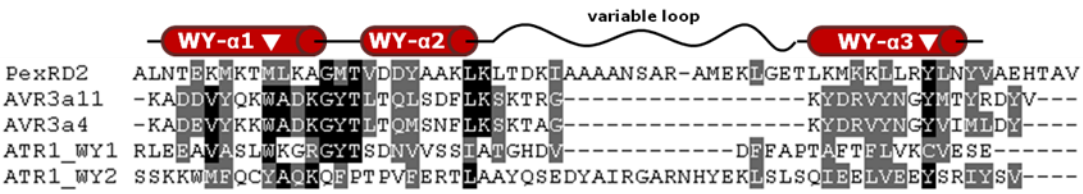

B.

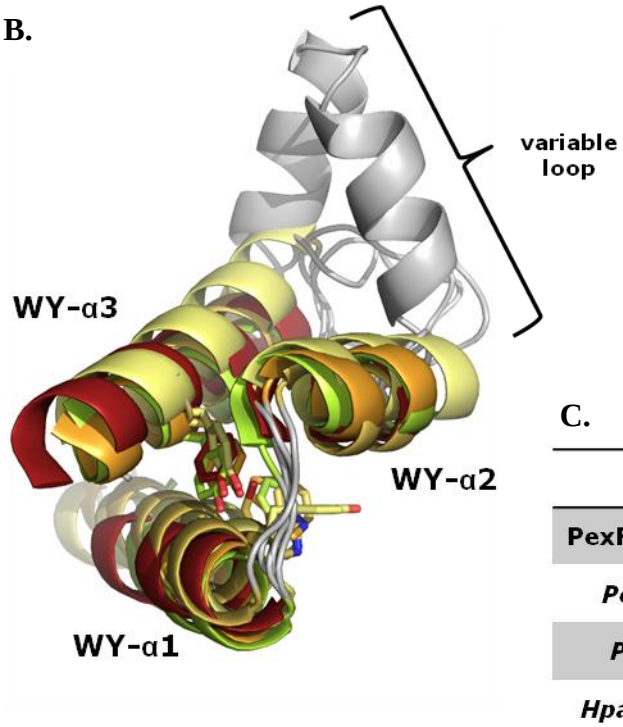

C.

	PexRD2 (chain-a)
PexRD2 (chain-b)	0.30 Å
***Pc*AVR3a11**	0.73 Å
***Pc*AVR3a4**	0.93 Å
***Hpa*ATR1-WY1**	1.30 Å
***Hpa*ATR1-WY2**	0.94 Å

Figure 3.21 Sequence and structural alignments of WY-fold from published RXLR structures.

(A.) Alignment of the five WY-fold sequences found in published structures of RXLR effectors, generated manually from structural alignments. Conserved residues are shaded black, and similar residues shaded grey. The positioning of the three helices that form the fold are shown above the alignment (red cylinders), as is the position of the variable loop region within this fold (wavy line). The key residues, from the W- and Y-motifs, that contribute to the hydrophobic core are highlighted by white triangles. **(B.)** Cartoon representation of superposition of the five WY-folds, with respective helices coloured as in Figure 3.20. 'Loop' regions are shown in grey, and the side-chains of the key residues that form the hydrophobic core of each WY-fold are shown in stick representation. **(C.)** R.m.s.d. values for pair-wise alignments of Cα within the conserved helices of the WY-folds. Performed using the DaliLite server, with additional values as reported in Win *et al.*, (2012)**.**

water is excluded. When residues with large side chains are substituted for smaller ones, complementary mutations are observed at other positions to fill the available space (Win *et al.*, 2012b).

Comparison of the five available structures of WY-folds shows that the overall positions of the three constituent helices are highly conserved. R.m.s.d. for Cα-atoms of overlaid helices varied from 0.73 – 2.12 Å. This comparison also identified a number of ways this conserved fold could be adapted (Boutemy *et al.*, 2011, Win *et al.*, 2012b). With respect to PexRD2, one of the most striking adaptations is a significant insertion in the loop between the second and third helices of the conserved fold. The WY-fold of PexRD2 has an additional 16 residues inserted in this variable loop, compared to the corresponding loop in the structure of AVR3a11. These additional residues contribute to the two unique helices seen in the structure of PexRD2 (α3 and α4). Interestingly, the positioning of these two helices was highlighted previously as one of the regions that showed the greatest differences between the two monomers in the PexRD2 dimer (Section 3.2.6, Figure 3.15). The flexibility in this variable loop region is also evident in the comparison of the structures of the other WY-domains, and can be seen to vary in both length and conformation.

Other significant adaptations of the conserved three-helix bundle fold are extensions on the N- and C-termini. In AVR3a11 and AVR3a4 an additional α-helix at the N-terminus of the WY-fold adapts it into a four-helix bundle; and in the two WY-folds of ATR1, an extension of two α-helices at the N-terminus onto each one cause the five-helix structural repeats. Also in ATR1, the physical linking of two adapted WY-folds in one polypeptide chain, plus the addition of N-terminal 'head' domain, show how this simple fold can be repeated and modified to give a diversity of structures.

The structure of PexRD2 provides another example of how two WY-folds may be functionally linked. The WY-folds present in each of the two PexRD2 monomers are juxtaposed by dimer formation. Interestingly, the two helices (α3 and α4) that form the extended variable 'loop' of PexRD2, contribute a significant number of residues to the hydrophobic dimerisation interface. Therefore it is possible that the extension and formation of ordered helices in this variable loop may be a specific adaptation of

the WY-fold to support oligomerisation. None of the other WY-folds solved to date show any evidence of secondary structure within this region, nor do any show evidence of homo-oligomerisation.

3.2.9 Structural modelling of PexRD2 homologs and family members

Solving the structure of PexRD2 also allowed the use of homology modelling methods to generate predictions for the structures of PexRD2 homologs from other *Phytophthora* species, as well as PexRD2 family members from *P. infestans*.

Analysis of available genome sequences suggests that PexRD2 homologs are restricted to clade 1C of the *Phytophthora* genus (Blair *et al.*, 2008). Within this clade, a clear homolog of PexRD2 was identified in the genome of the closely related species, *Phytophthora mirabilis (Pm)* (Liliana Cano Mogrovejo, personal communication). Species in clade 1C have evolved through host jumps followed by adaptive specialisation on plants belonging to different botanical families (Blair *et al.*, 2008, Raffaele *et al.*, 2010a). *P. mirabilis* is a pathogen of *Mirabilis jalapa*, also known as the four o'clock flower or marvel of Peru. A PexRD2 homolog was cloned from *P. mirabilis* PIC99114 gDNA using primers designed in the flanking regions of the gene, before ligating the amplified product into the pGEM®-T Easy vector and sequencing. This sequence showed signatures of positive selection (*dN/dS* = 1.27) and contained non-synonymous polymorphisms at five positions (Liliana Cano Mogrovejo, personal communication). Comparison to the PexRD2 structure revealed these five residues to be presented on the protein's surface, although they were not co-localised to any one particular surface region (Figure3.22). It was concluded that these polymorphisms in surface exposed residues may have contributed to the adaptation of PexRD2 to a new host species without disrupting the stable WY-fold. These changes may be required to strengthen an interaction with homologs of the effector's predicted virulence target in the new host, or allow the effector to interact with an entirely novel target. Alternatively they may allow evasion of recognition of the effector by the new host immune system.

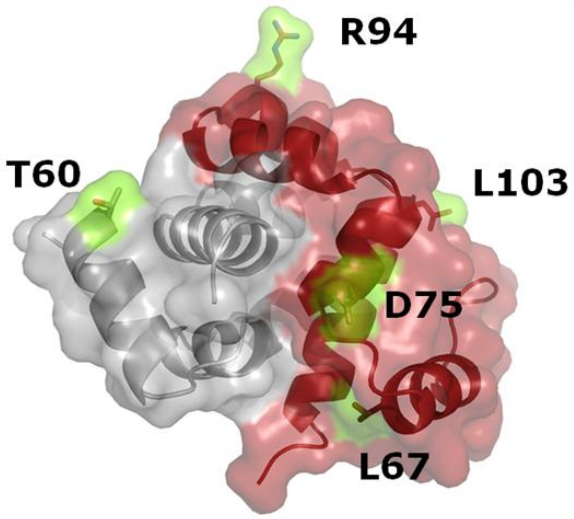

Figurte 3.22

Polymorphic residues of PexRD2 are surface-presented

Surface view of *Pi*PexRD2 effector domain structure highlighting (in green) the positions of the five residues that are polymorphic between *P. infestans* and *P. mirabilis.* homologues

Although PexRD2 appears restricted to the clade 1C species, PexRD2-like effectors can be identified in the reference genomes of *P. infestans* and the more distantly related *P. sojae*, and *P. ramorum*: the causative agents of soybean stem and root rot; and sudden oak death, respectively. A bioinformatic analysis of RXLR effectors from the reference genomes of *P. infestans*, *P. sojae*, and *P. ramorum*, based on homology restricted to within the C-terminal effector domains (Joe Win, personal communication) identified 12 putative PexRD2-like effectors in *P. infestans* using an E-value threshold of e^{-03}; with five putative PexRD2-like effectors identified from *P. sojae*, and six from *P. ramorum*. However, manual inspection of sequence alignments eliminated two candidates from both *P. infestans* (PITG_09739 and PITG_09773) and *P. sojae* (PsG_134359 and PsG_159079), because they showed poor alignment, insertions and/or deletions within the conserved WY-fold of PexRD2. An alignment of PexRD2 with the remaining 19 PexRD2-like effectors is provided in Figure 3.23. A phylogenetic tree based on this alignment and showing the proposed evolutionary relationships within the PexRD2-like effector family is shown in Figure 3.24.

The IntFold2 server allows homology modelling using solved structures as templates (Roche *et al.*, 2011). This server was previously used in a novel automated prediction pipeline to model haustoria-localised proteins from the barley powdery mildew pathogen, *Blumeria graminis* f. sp. *hordei* (Bindschedler *et al.*, 2011). This

homology modelling server, using the deposited PDB file of PexRD2 as a template, was able to generate predictions for the three-dimensional structures of all of the other 19 PexRD2-like effectors. The confidence level and p-values for these predictions of PexRD2-like effectors varied from CERT 9.989E-5 to MEDIUM 3.140E-2, and the corresponding global model quality scores varied from 0.8762 to 0.3230 (for PITG_14787 and PITG_13628 (PexRD27, (Oh *et al.*, 2009)) respectively). A complete set of statistics for all PexRD2-like structure predictions is shown in Table 3.2. The best homology models for all family members were confidently predicted to adopt a WY-fold with similar adaptations in the variable loop region to those seen in PexRD2 (Figure 3.25). The most significant differences observed in the predicted structures compared to the solved structure of PexRD2 tended to occur in regions that had already been identified as displaying some plasticity. Most notably, small insertions or deletions within the variable loop region and extensions at the N- and C-termini were observed. Extensions at the N-terminus tended to be relatively short, between 3 – 9 residues. On the other hand, longer C-terminal extensions of between 10 – 107 residues were also observed. These extensions were largely predicted to be unstructured in the models with the highest confidence, although some of the less confident models did suggest some secondary and tertiary structure within these C-terminal extensions based on potential homology to other proteins in the PDB.

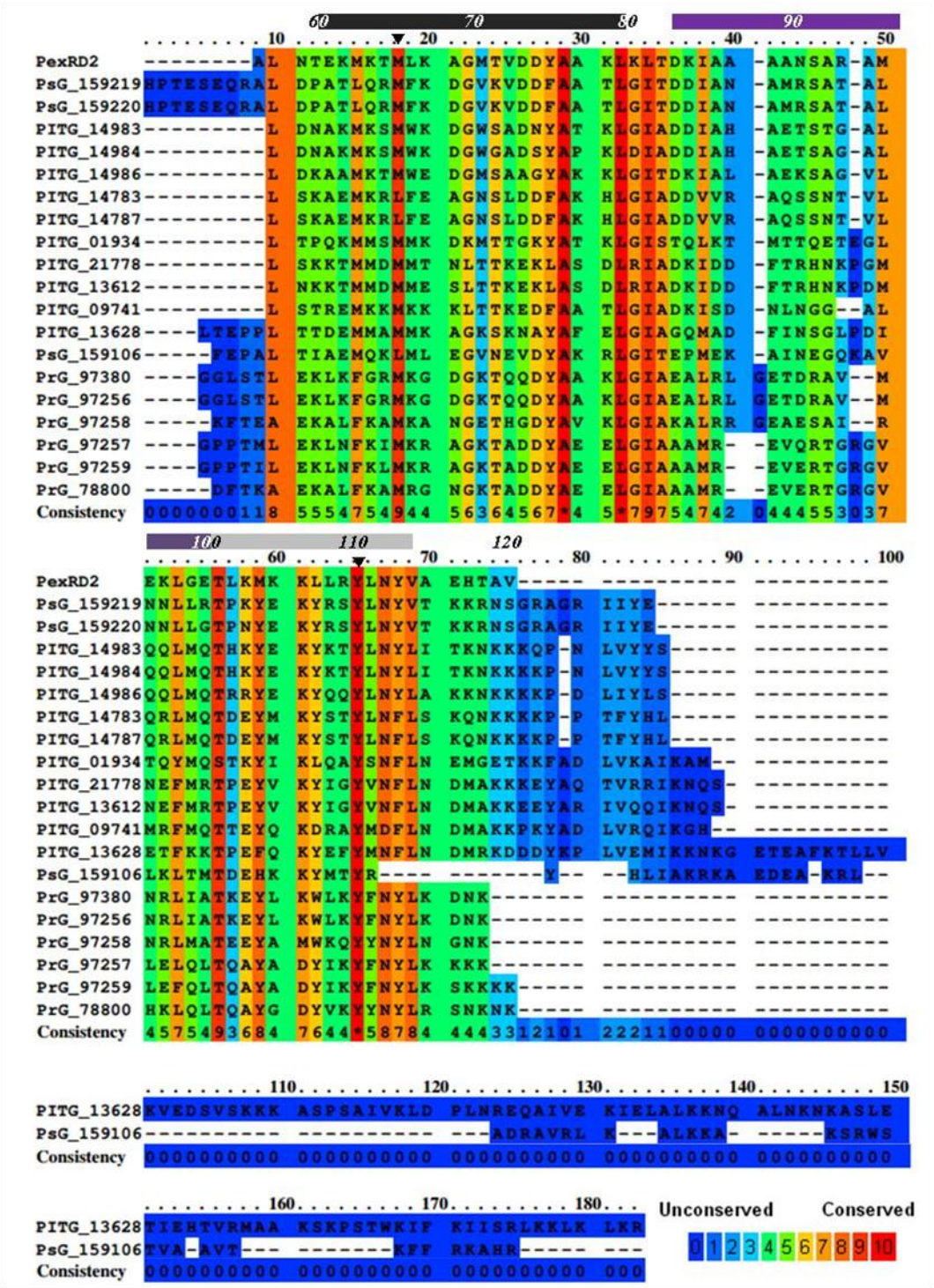

Figure 3.23 Sequence conservation in the effector domains of PexRD2-like effectors from *Phytophthora* spp.

Sequence alignment of the effector domains of the 20 PexRD2-like effector family members created using PRALINE. Sequences are from *P. infestans* (PITG), *P. sojae* (PsG) and *P. ramorum* (PrG). The key features of the WY-fold are indicated as shaded boxes above the alignment (W-motif (dark grey), Y-motif (light grey) and the variable loop region (purple). The location of residues corresponding to Met66 and Tyr111 are indicated with ▼.

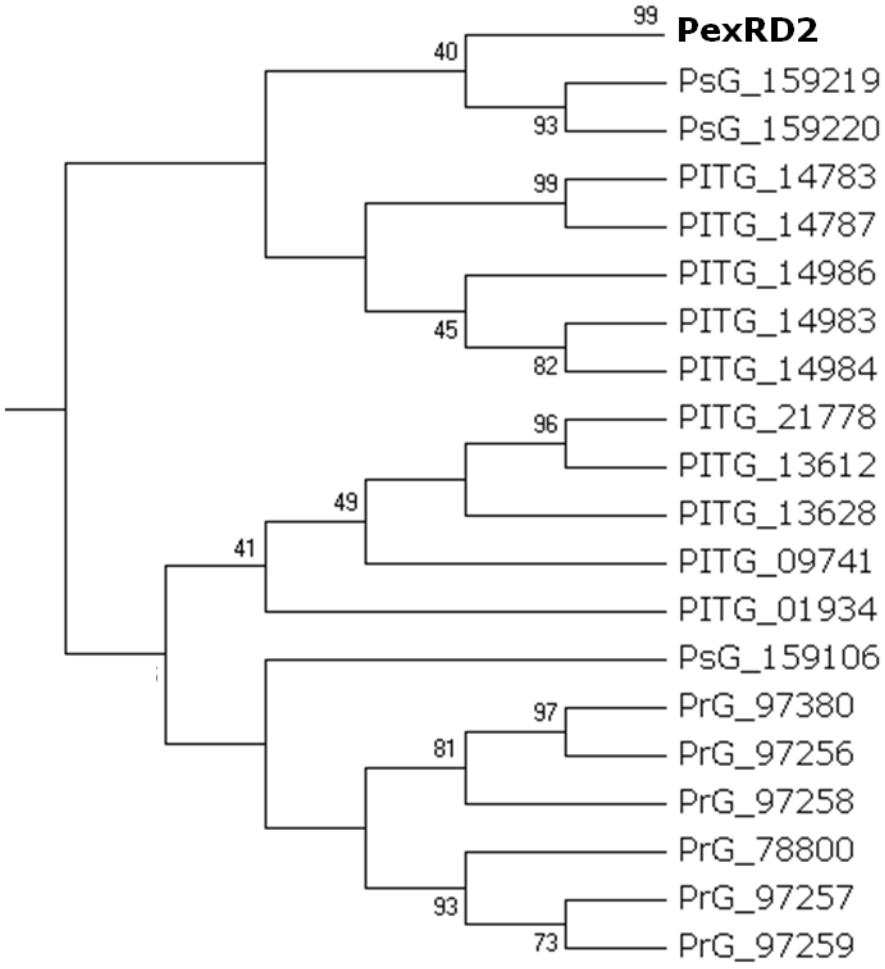

Figure 3.24 The evolutionary relationships between PexRD2 family effectors from *Phytophthora* spp.

Consensus tree by Maximum Likelihood methods as generated using an alignment of effector domains and the MEGA software package (Tamura *et al.*, 2011). Sequences are from *P. infestans* (PITG), *P. sojae* (PsG) and *P. ramorum* (PrG). Sequences previously excluded from PexRD2-like effector family (PITG_09739, PITG_09773, PsG_134359 and PsG_159079) were used as an out-group. Bootstrap values greater than 40% are shown at the appropriate nodes.

Table 3.2 Structural homology modelling statistics for PexRD2-like effectors

Family member	Confidence[a]	P-value[a]	Global model quality score[a]	Sequence identity in aligned region[b]
PITG_14787	CERT	9.989E-5	0.8762	18/62 (29%)
PITG_14986	CERT	1.020E-4	0.8742	27/59 (46%)
PITG_14984	CERT	1.079E-4	0.8688	27/58 (47%)
PITG_14783	CERT	1.160E-4	0.8618	18/62 (29%)
PITG_14983	CERT	1.719E-4	0.8240	26/58 (45%)
PITG_01934	CERT	1.720E-4	0.8239	11/47 (23%)
PITG_21778	CERT	2.007E-4	0.8091	9/39 (23%)
PITG_09741	CERT	2.183E-4	0.8010	12/44 (27%)
PITG_13612	CERT	2.465E-4	0.7893	14/58 (24%)
PsG_159220	CERT	2.488E-4	0.7885	27/59 (46%)
PsG_159219	CERT	2.778E-4	0.7778	28/59 (47%)
PrG_97258	CERT	3.367E-4	0.7593	17/60 (28%)
PrG_78800	CERT	3.659E-4	0.7513	16/53 (30%)
PrG_97380, PrG_97256	CERT	4.491E-4	0.7316	18/57 (32%)
PrG_97259	HIGH	1.302E-3	0.6292	15/53 (28%)
PrG_97257	HIGH	2.404E-4	0.5702	16/53 (30%)
PsG_159106	HIGH	5.221E-3	0.4956	18/56 (32%)
PITG_13628 (PexRD27)	MEDIUM	3.140E-2	0.3230	18/60 (30%)

All statistics listed above are for structures modelled on the published co-ordinates for PexRD2 effector domain (3ZRG), as found by template searching with IntFold server.
[a] Values obtained from the IntFold (Version 2.0) server (Roche *et al.*, 2011)
[b.] Value obtained using BLASTP (Altschul *et al.*, 1990).

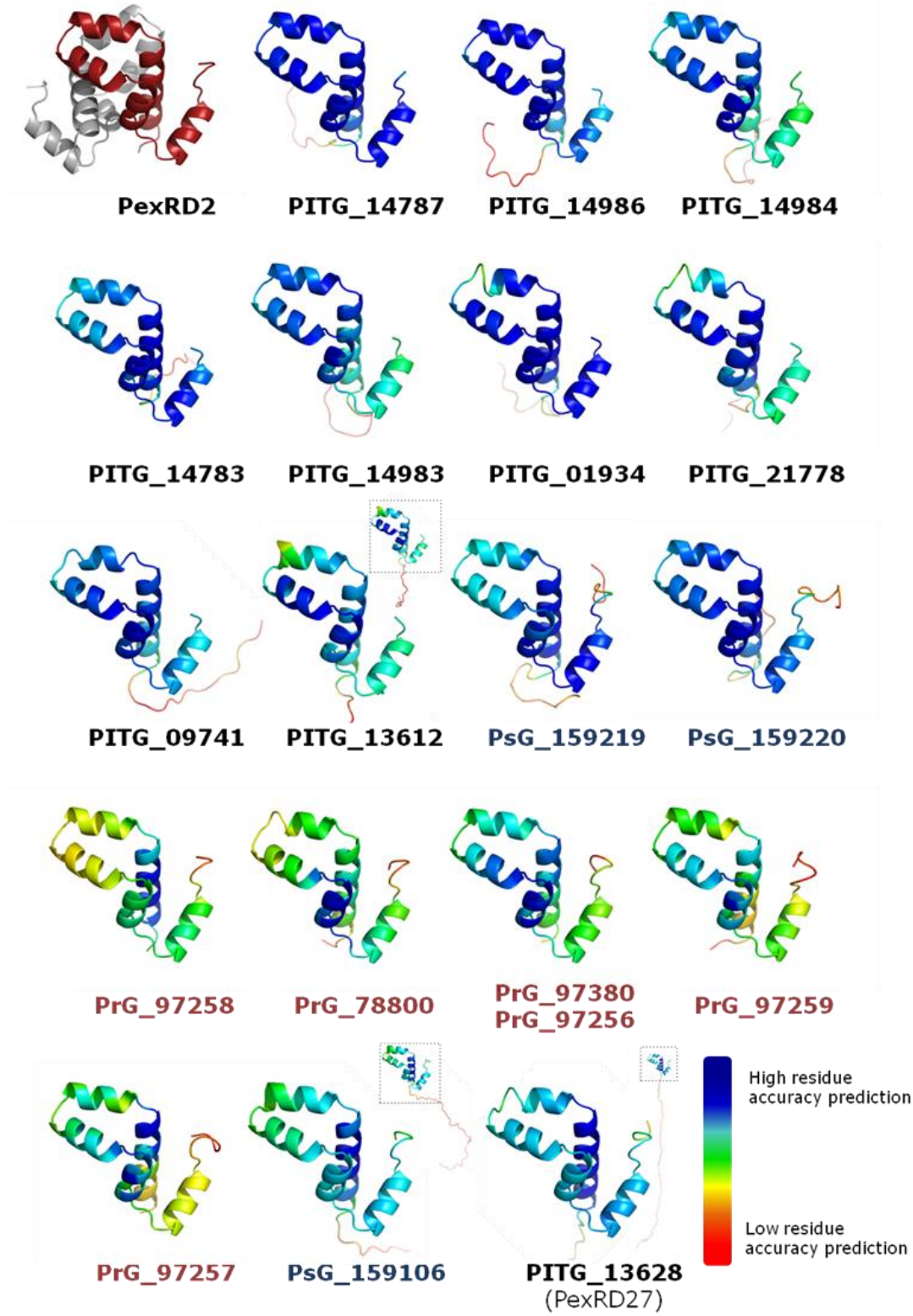

Figure 3.25 Homology models of PexRD2-like effectors

Models generated using the IntFold (v. 2.0) server (Roche *et al.*, 2011) and oriented with the chain-a in PexRD2 (top left). Models are arranged in order of decreasing global model quality score, and coloured by local model quality score (residue accuracy prediction). Where images have been cropped, the full structure is shown to right of the cropped image, with the region displayed highlighted in the dotted square.

3.3 Conclusion

At the start of this project there was no structural information for RXLR effectors. At the time of writing this thesis, the three-dimensional structures of five RXLR effector domains have been published, PexRD2 from *Phytophthora infestans*, Avr3a11 and Avr3a4 from *P. capsici*; and ATR1 and ATR13 from *H. arabidopsidis*.

The decision to omit the N-terminal region of PexRD2, which contains the translocation motifs, from the construct design appears a prudent one, in terms of producing protein for structural study. The structures of all RXLR effectors solved by X-ray crystallography have also excluded these regions. The *Pc*AVR3a4 structure solved by NMR is the full length mature protein (excluding only the signal peptide), and shows the N-terminal region as disordered (Yaeno *et al.*, 2011). Furthermore, NMR analysis of the effector domain of *Pc*AVR3a11 revealed residues 63 – 69 were structurally disordered and impeded crystallisation. Excluding these residues yielded protein that crystallised readily, producing protein crystals that diffracted to sub-angstrom resolution (Boutemy *et al.*, 2011).

Solving the crystal structure of the effector domain of PexRD2 was crucial to the identification of the WY-fold. It demonstrated that a three-helix bundle was the minimal conserved structural motif. The fold is composed of, and hence named after, two sequence motifs previously identified as prevalent in RXLR effector C-terminal domains: the W- and Y- motifs. Bioinformatics revealed that this fold may be present in over 44% of all predicted RXLR effectors (Win *et al.*, 2012b), with some having up to 11 tandem repeats of WY-folds. Also, the WY-domain, like the RXLR motif, was shown to be limited to haustoria-forming phytopathogenic oomycetes.

The prevalence of RXLR effectors containing this conserved fold may have arisen from the extensive gene duplication which is a common mechanism of effector evolution in *Phytophthora* spp. (Haas *et al.*, 2009, Raffaele *et al.*, 2010b). The fold may have been preserved in this large number of effectors because it represents a protein scaffold that is stable in the plant cytosol following translocation; and can be extensively modified to increase its functionality. The adaptation of a simple protein scaffold to achieve a diversity of functions can also be seen both in nature: in the

virion assembly proteins of some bacteriophage (Cardarelli *et al.*, 2010); and in synthetic biology: in libraries of *de novo* designed four-helix bundles that function to complement different lethal mutations in *E. coli* (Fisher *et al.*, 2011).

The WY-fold can be adapted through surface polymorphisms, extensions at the N- and C-termini and changes within the variable loop region between WY-α2 and WY-α3. The structure of PexRD2 demonstrates that insertions within the variable loop region can display secondary structure. It is also unique amongst published RXLR effector structures as it demonstrates how WY-domains can oligomerise, which could further increase their functionality. One could hypothesise that these two observations are linked, since the two helices that are formed by the extension with the variable loop contribute extensively to the hydrophobic dimerisation interface. This suggests that dimerisation is important for this effector's function.

Although the lack of significant structural homology to characterised proteins currently available in the PDB has not aided assignment of a biochemical function to this effector, the structure does provide a useful framework to interpret future results that would otherwise be unavailable. It can also be exploited as a platform for the rational design of structurally informed mutants of PexRD2 that could be used to probe this effectors functioning (see Section 5.2.10).

The effector domain of PexRD2 has been used as a template for the homology modelling of other RXLR effectors within the PexRD2 effector family. As would be expected, all family members were confidently predicted to adopt a WY-fold with similar adaptations to those seen in PexRD2. However, since the WY-fold is highly prevalent within the effectoromes of some oomycetes, the published co-ordinates of PexRD2 may assist in solving of the structures of other, less closely related, RXLR-WY-effectors. The WY-fold of PexRD2 could be used as a search model for molecular replacement methods to solve the phase problem. Since molecular replacement requires no additional experimental procedures or data, and additionally simplifies model-building, it is usually the method of choice for structure determination when a suitable search model is available. In fact, to date, the majority (>60%) of macromolecular crystal structures within the PDB have been solved by molecular replacement.

Chapter 4:

Identifying Potential Host Targets of PexRD2

4 Identifying Potential Host Targets of PexRD2

4.1 Introduction

A central paradigm in the field of plant pathology is that understanding how phytopathogens interact and co-evolve with their host plants is dependent on first determining the virulence, and avirulence, activities of their effectors (Oh *et al.*, 2009). Bioinformatic analysis of the genome sequences of plant pathogenic oomycetes has revealed extensive effector repertoires. For example, the genome sequence of *Phytophthora infestans* strain T30-4 has a total of 563 predicted RXLR effector genes (Haas *et al.*, 2009). The biochemical effector functions of the majority of RXLR effectors remain unknown. However, high-throughput effectoromics combined with in-depth studies of particular effectors have begun to uncover the mechanisms behind the virulence and avirulence activities of these effectors.

The *P. infestans* effector AVR3a is able to suppress the programmed cell death (PCD) response triggered by the PAMP-like molecule INF1 (Bos *et al.*, 2006, Bos *et al.*, 2009). This effector was shown to be essential for the pathogen's virulence. An *AVR3a* stable-silenced line of *P. infestans* 88069 shows significantly reduced virulence and infectivity; which was restored by transient over-expression of AVR3a in the host (Bos *et al.*, 2010b). The virulence activity of AVR3a was inferred to result from this effector's capacity to interact with, and stabilise, the host E3 ubiquitin ligase CMPG1[*] (Bos *et al.*, 2010b). CMPG1 is required for the plant immune response to a diverse range of elicitors, including INF1 (González-Lamothe *et al.*, 2006, Gilroy *et al.*, 2011). The nature of CMPG1 as a virulence target for this effector is supported by evidence from infection of wild-type or *CMPG1*-silenced *Nicotiana benthamiana*; although the data indicated contrasting roles in the biotrophic and necrotrophic stages of infection (Bos *et al.*, 2010b). During the biotrophic stage, AVR3a-mediated stabilisation of CMPG1 suppresses its activity and is hypothesised to allow colonisation of the host. However, CMPG1 is

[*] CMPG1, named according to the first four strictly conserved amino acids: cysteine, methionine, proline, and glycine (Kirsch *et al.*, 2001).

implicated to play a positive role in infection development during the necrotrophic stage, since infections of *CMPG1*-silenced plants showed reduced lesion growth and sporulation.

IPI-O1 (also known as AVRblb1) is a *P. infestans* RXLR effector that is recognised by the Rpi-blb1 late blight resistance (R) protein from the wild potato *Solanum bulbocastanum* in a gene-for-gene manner (Vleeshouwers *et al.*, 2008). The effector protein has also been shown to contain an RGD (arginine-glycine-aspartate) tripeptide sequence which mediates an interaction with the lectin receptor kinase LecRK-I.9 (Senchou *et al.*, 2004, Gouget *et al.*, 2006, Bouwmeester *et al.*, 2011). Interaction of IPI-O1 with this receptor kinase caused disruption of cell wall-plasma membrane adhesions in *Arabidopsis*. Since *Arabidopsis* is a non-host for *P. infestans*, testing this effector-target interaction during infection utilised the *Phytophthora brassicae-Arabidopsis* pathosystem. Plants mutated in the *LecRK-I.9* gene showed a gain-of-susceptibility phenotype, which could be phenocopied by transgenic lines over-expressing IPI-O1 (Bouwmeester *et al.*, 2011), suggesting an important role for this protein in resistance against *Phytopthora* spp.

AVRblb2 is a recognised effector from *P. infestans*, that blocks infection of potato plants carrying the broad-spectrum *R* gene *Rpi-blb2* from *S. bulbocastanum* (Oh *et al.*, 2009). AVRblb2 was shown to interact with the host papain-like cysteine protease C14 (Bozkurt *et al.*, 2011). During infection, both the effector and interacting protease accumulated at the haustoria; and co-expression of AVRblb2 blocked the normal secretion of C14 to the host apoplast (Bozkurt *et al.*, 2011). Transient silencing of C14 in *N. benthamiana* caused increased susceptibility to *P. infestans* (Kaschani *et al.*, 2010, Bozkurt *et al.*, 2011); which was also observed in transgenic plants over-expressing AVRblb2 (Bozkurt *et al.*, 2011). In contrast, transgenic over-expression of C14 conferred increased resistance against *P. infestans*, which could be partially reversed by simultaneous over-expression of AVRblb2 (Bozkurt *et al.*, 2011). These results suggest that AVRblb2 enhances virulence by functioning as an inhibitor of the secretion of the plant immunity associated protease C14.

The potato and tomato orthologs of BSL1 have been shown to associate with both *P. infestans* RXLR effector AVR2 and the *Solanum demissum* R protein R2 to mediate disease resistance (Saunders *et al.*, 2012). *Arabidopsis* BSL1 (BSU1[†]-LIKE PROTEIN1) is a predicted serine/threonine-protein phosphatase, with an N-terminal kelch repeat region and C-terminal phosphatase domain, which is involved in brassinosteroid signal transduction (Mora-García *et al.*, 2004, Kim *et al.*, 2009). The effector domain of AVR2 and putative phosphatase domain of BSL1 were shown to mediate the interaction, and the two proteins were shown to co-localise and accumulate around haustoria during infections (Saunders *et al.*, 2012). Silencing *BSL1* in *N. benthamiana* revealed that it was specifically required for the recognition of AVR2 by R2, and not the other AVR-R recognition events tested (Saunders *et al.*, 2012). *BSL1*-silenced plants showed a loss of R2-mediated resistance following infection with *P. infestans*, but no other effect of *BSL1*-silencing during either compatible or incompatible infections could be observed (Saunders *et al.*, 2012). *In planta* co-IPs revealed an association between BSL1 and R2 only in the presence of AVR2 (Saunders *et al.*, 2012); consistent with indirect recognition of the effector by the R protein, through its interaction with the BSL1 protein as an intermediate. As such BSL1 could represent a 'guarded' virulence target (van der Biezen and Jones, 1998), or represent a 'decoy' that aids the recognition of the effector by R2 (van der Hoorn and Kamoun, 2008). However, further investigation is required to elucidate the function of BSL1 during infection.

The characterisation of the biochemical functions of the RXLR effectors described above has been assisted greatly by the identification of their interacting host proteins. The adaptive function of effectors is to manipulate the host cell function and structure for the benefit of the pathogen, and the means by which effectors achieve this manipulation is likely to result from an interaction with components of the signalling cascades and executors of the plant defence response. To identify PexRD2-interacting host proteins that might provide an insight into the biochemical function of this effector, a yeast two-hybrid screen was conducted using PexRD2 and a cDNA library extracted from infected host tissue.

[†] BSU1 = *bri1* SUPPRESSOR 1, BRI1 = BRASSINOSTEROID-INSENSITIVE 1

4.2 Results and Discussion

4.2.1 Yeast two-hybrid screening – introduction

Yeast two-hybrid (Y2H) screening is a molecular biology technique used to discover protein–protein interactions, by testing for physical interactions between two proteins (Fields and Song, 1989). The principle behind the test is the activation of downstream reporter genes by the binding of a transcription factor onto an upstream activating sequence (UAS). The transcription factor's DNA binding domain (DBD) is responsible for binding to the UAS, and the activation domain (AD) is responsible for activating transcription. The protein of interest is fused to the DBD, and called the 'bait', whilst potential interactors are fused to the AD, and called 'prey'. If the bait and prey interact, they bring the DBD and AD in close enough proximity to each other, to reconstruct the transcription factor and lead to the transcription of the reporter genes.

Y2H screening with PexRD2 was conducted using the ProQuest™ Two-Hybrid System (Invitrogen). This system utilizes *Saccharomyces cerevisiae* MaV203 which has a single copy of each of three GAL4 inducible reporter genes (*HIS3, URA3*, and *lacZ*) integrated into its genome. Activation of the reporter genes can be detected by growth on plates lacking histidine or uracil, or the formation of a blue colouration in the presence of X-gal resulting from the activity of the *lacZ* encoded β-galactosidase enzyme, respectively.

4.2.2 Identification of PexRD2-interacting proteins using the ProQuest™ Two-Hybrid System

Note: The yeast two-hybrid screen, described below, was conducted by Dr. Miles Armstrong at the James Hutton Institute (JHI), Invergowrie, Dundee, Scotland UK. Follow-up Y2H analyses were conducted initially with Dr. Miles Armstrong at JHI, and later independently at JIC.

To identify PexRD2-interacting host proteins (PexRD2PIs), a yeast two-hybrid screen was conducted using a PexRD2 paralog, (PITG_11383^{K104E}, residues 21 –

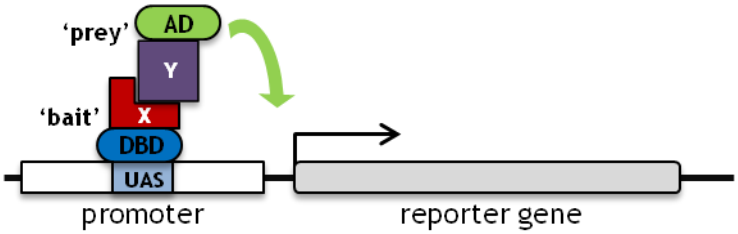

Figure 4.1 Overview of the yeast two-hybrid system

In the Y2H system, the protein of interest (X) is fused to the DNA-binding domain (DBD), to produce the 'bait'; whilst potential interactors (Y) are fused to the activation domain (AD), to produce the 'prey'. An interaction between the two proteins mediates the reconstruction of the transcription factor, which activates transcription of specific reporter genes, containing an upstream activating sequence (UAS) in their promoter regions (Fields and Song, 1989).

121) as the bait. This was screened against a cDNA prey library, prepared from RNA extracted in the early biotrophic and later necrotrophic phases of a susceptible potato interaction (Bos *et al.*, 2010b). Prey plasmids from yeast colonies that grew on selective media lacking histidine were isolated and sequenced using the suggested forward and reverse sequencing primers as described in the manufacturer's manual. PexRD2PIs were identified by using these sequencing results to search the released *Solanum tuberosum* Group Phureja DM1-3 (DM) annotated genome sequence (Potato Genome Sequencing Consortium *et al.*, 2011) and BLAST searches of non-redundant protein databases (Altschul *et al.*, 1990). Following confirmation of the entire gene sequences of interacting yeast clones by iterative rounds of sequencing, four candidate interactors were identified: MAPKKKε; two unknown protein kinases with homology to phylogenetically annotated MAPKKK kinases (MAPKKKKs or MAP4Ks, henceforth PexRD2 interacting MAP4K 1 (PM4K1) and 2 (PM4K2)); and a U-box domain-containing protein with homology to the *Arabidopsis* protein PUB38 (Table 4.1). Each candidate was found as multiple clones.

To confirm the interactions were not false positives, a clone for each candidate interactor was re-transformed and re-screened in Y2H against a PexRD2 bait (PITG_21422, residues 21 – 121), or the a bait vector control (empty pDEST™32).

Each bait/prey combination was tested in assays for each of the three independent reporter genes (Figure 4.2).

Each candidate interactor was confirmed positive for an interaction with PexRD2 by activation of at least two of the three independent reporter genes. None of the candidate interactors were able to activate the reporter genes in the absence of PexRD2, confirming that they were not auto-active. Interestingly the interactions between PexRD2 and PM4K1 or PM4K2 activated the more stringent *URA3* reporter gene, suggesting that these may be stronger interactions, whilst the interaction with the U-box domain containing PUB38-like only showed weak blue colouration in the presence of X-gal, suggesting this may be a weaker interactor. Since the interactions between the host protein kinases and PexRD2 appeared to be the strongest, combined with MAPKKKε having already been identified as a regulator of plant immunity signalling, these interactions were prioritised for further characterisation using a range of protein-protein interaction techniques.

Table 4.1 PexRD2-interacting proteins identified by Y2H screening

ID	Name	PGSC Accession	Best BLASTP match	Score	E value	InterPro domains
PexRD2PI-1	**(MAPKKKε)**	PGSC0003DMP400013529	ref|NP_001234779.1|MAP3K epsilon protein kinase [*Solanum lycopersicum*]	2830	0.0	Serine/threonine- /dual specificity protein kinase, catalytic (IPR002290), Armadillo-like helical (IPR011989), Armadillo-type fold (IPR016024)
PexRD2PI-2	**(PM4K1)**	**NF**	ref|XP_004232298.1|PREDICTED: uncharacterized protein LOC101251534 [*Solanum lycopersicum*]	1388	0.0	Serine/threonine- /dual specificity protein kinase, catalytic (IPR002290)
PexRD2PI-3	**(PM4K2)**	PGSC0003DMP400025019	ref|XP_004235876.1|PREDICTED: uncharacterized protein LOC101251667 [*Solanum lycopersicum*]	1350	0.0	Serine/threonine- /dual specificity protein kinase, catalytic (IPR002290)
PexRD2PI-4	**(PUB38-like)**	PGSC0003DMP400042309	ref|XP_004236147.1|PREDICTED: U-box domain-containing protein 38-like [*Solanum lycopersicum*]	810	0.0	U box (IPR003613), Armadillo-like helical (IPR011989), Armadillo-type fold (IPR016024)

NF = not found. However PM4K1 shows overall sequence identity to the following three predicted proteins: PGSC0003DMP400025018 (49.0%); PGSC0003DMP400025019, (48.8%); PGSC0003DMP400025017, (48.7%).

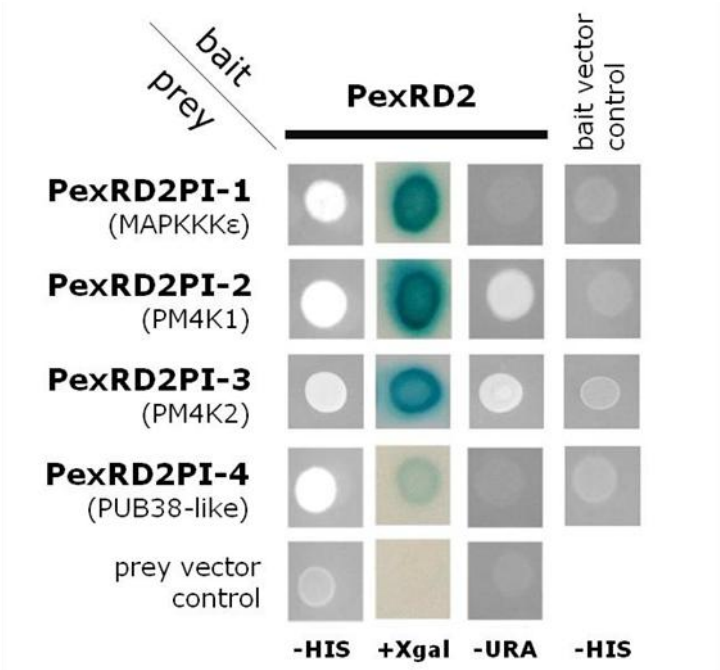

Figure 4.2 PexRD2 interacts with four host proteins in Y2H

Y2H analysis of co-transformants carrying PexRD2 bait and one of the four identified interacting host proteins as indicated. Interaction between PexRD2 and the host protein preys allows growth on plates lacking histidine (–HIS) and blue colouration in the presence of X-gal (+Xgal). The stronger interaction between PexRD2 and PM4K1 or PM4K2 also allow growth on plates lacking uracil (-URA). No growth on –HIS plates was detected for co-transformants carrying empty vector controls, confirming that none of the proteins in question are auto-active. Bait/prey combinations were tested in triplicate and single representative colonies are shown.

4.2.3 MAPKKKε

Kinase signalling-cascades of the mitogen-activated protein (MAP) kinase class play central roles in transmitting external and endogenous signals to downstream targets, and are crucial for the regulation of development, growth and programmed cell death (PCD), as well as responses to both abiotic and biotic stresses. MAP kinase cascade-mediated signalling is an essential step in the establishment of resistance to a diverse range of pathogens (Colcombet and Hirt, 2008, Pitzschke *et al.*, 2009). The MAP kinase core module is highly conserved in eukaryotes and consists of three protein kinases that are sequentially activated by the upstream component to form a 'phospho-relay'. At the bottom of the cascade, a MAP kinase (MAPK or MPK) is activated by the dual phosphorylation of the threonine-x-tyrosine motif located

within the activation loop of its kinase catalytic domain. This phosphorylation is mediated by a MAP kinase kinase (MAPKK or MKK), which, in turn, is activated by phosphorylation by a MAP kinase kinase kinase (MAPKKK or MKKK). In higher plants, roughly 10% of all kinases are involved in MAPK pathways, and MAPKKKs are the most divergent of these three proteins. The genome of the model plant, *Arabidopsis thaliana*, encodes approximately 80 putative MAPKKKs, at least 10 MAPKKs and 20 MAPKs (Ichimura *et al.*, 2002, Colcombet and Hirt, 2008).

The tomato homolog of MAPKKKε was discovered by Melech-Bonfil and Sessa (2010) as a positive regulator of cell death responses associated with plant immunity (see Introduction to Chapter 5 for more details). *Sl*MAPKKKε is a 154 kDa protein with an N-terminal catalytic kinase domain, and a C-terminal domain containing two armadillo (ARM) repeats. ARM repeats are short ~42-amino-acid motifs that have been implicated in mediating protein-protein interactions (Huber *et al.*, 1997). *Sl*MAPKKKε shares 98% amino acid sequence identity with the potato homolog indentified in the Y2H screen, *St*MAPKKKε. If the comparison is limited to the catalytic kinase domains (residues 19 – 273) the two proteins share 100% identity. Phylogenetic analysis revealed that *Sl*MAPKKKε and its homologs belong to the A4 subgroup of plant MAPKKKs (Ichimura *et al.*, 2002). Closely related homologs can also be found in a range of dicot plants, including the wild tomato species, *Solanum pimpinellifolium* (99% amino acid sequence identity), and *N. benthamiana* (*Nb*MAPKKKε1, 90%). More distantly related homologs were found in *Arabidopsis thaliana* (*At*MAPKKKε1, 72%; and *At*MAPKKKε2, 69%) and *Brassica napus* (*Bn*MAPKKKε1, 67%).

4.2.4 The WY-domain of PexRD2 interacts with the catalytic kinase domain of MAPKKKε

To identify which domains of *St*MAPKKKε and PexRD2 were involved in the interaction, different N- and C-terminal truncation of both were sub-cloned into the pENTR™/D-TOPO® entry vector, before being transferred into the Y2H vectors by Gateway® cloning.

Five truncated *St*MAPKKKε prey vector constructs were tested for interaction with PexRD2 (residues 21 – 121). These constructs were tested alongside the almost full length *St*MAPKKKε prey construct identified in the Y2H screen (clone PexRD2PI-1 residues 4 – 1401), and the appropriate empty vector controls as before.

PexRD2 interacted with all three constructs that contained the N-terminal catalytic kinase domain (KD) (N1, residues 2 – 373; N2, residues 2 – 300; and N3, residues 2 – 278), as evidenced by both the growth of co-transformed yeast on media lacking histidine, and the development of blue colouration in the presence of X-gal (Figure 4.3). On the other hand, PexRD2 showed no interaction with the two C-terminal region constructs (C1, residues 279 – 1401; and C2, residues 301 – 1401). These results indicate that the catalytic kinase domain of MAPKKKε is both necessary and sufficient for the interaction with the effector PexRD2. As with the original Y2H-library clone, none of the truncated *St*MAPKKKε prey constructs showed any evidence of auto-activation activity.

To identify whether the effector domain of PexRD2 was sufficient for the interaction with MAPKKKε, the full length mature effector (residues 21 – 121) and two N-terminal truncations of PexRD2 in the Y2H-bait vector were screened for protein-protein interactions with MAPKKKε. The truncated PexRD2 constructs started either immediately after the RXLR translocation motif, but included the 'dEER' motif (residues 42 – 121) or immediately after the 'dEER' motif, and included just the WY-fold containing effector domain (residues 57 – 121). The original almost full length (~FL) PexRD2PI-1 clone, as well as the MAPKKKε-N2 and -N3 truncations were used as known interacting preys. All bait/prey combinations were assessed using the *HIS3*, and *lacZ* reporter gene assays, alongside empty vector controls.

All three PexRD2 constructs were able to interact with the MAPKKKε prey constructs, as evidenced by the activation of both the *HIS3* and *lacZ* reporter genes (Figure 4.4). These results demonstrate that the N-terminal region of PexRD2, containing the translocation motifs is dispensable for the interaction. On the other hand, the effector domain of PexRD2, which contains a WY-fold, mediates the interaction with MAPKKKε KD. As with the original PexRD2 bait, the truncated bait constructs showed no evidence of auto-activation of the reporter genes.

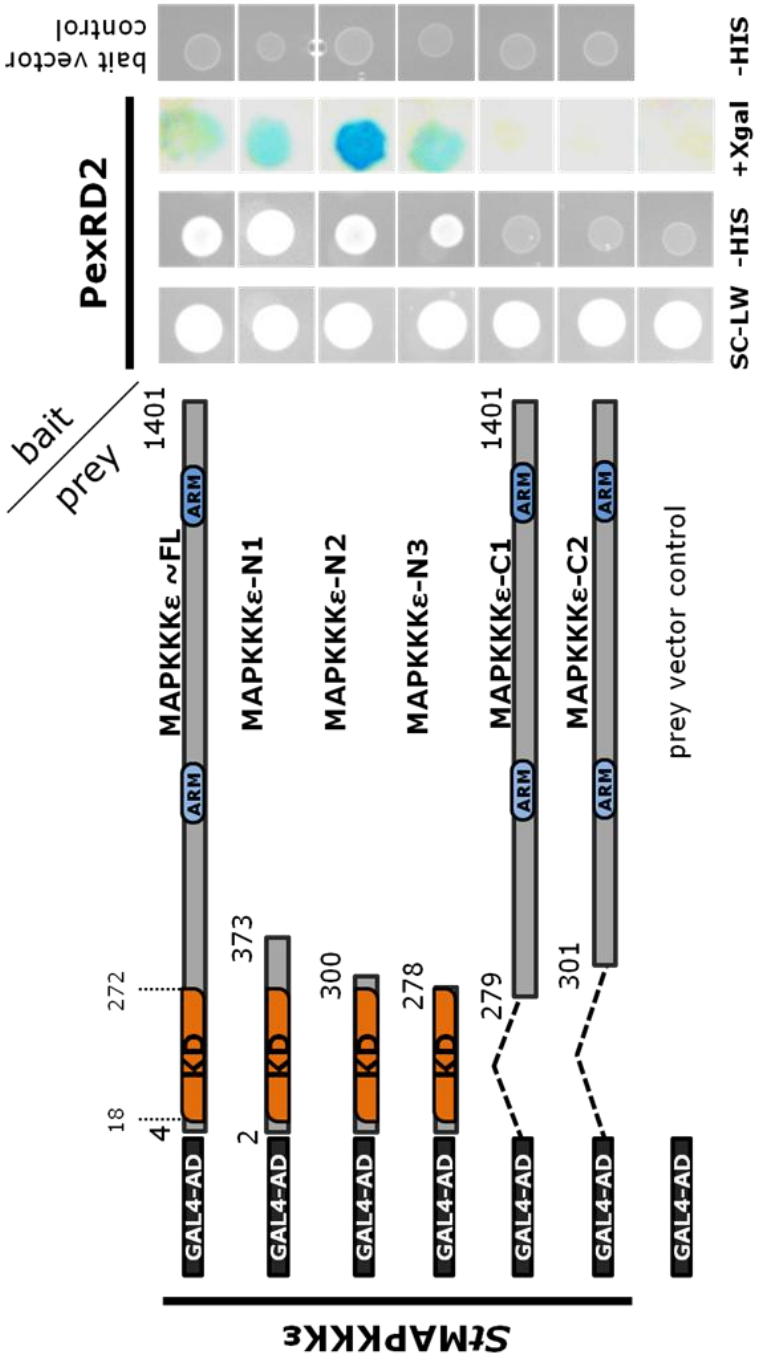

Figure 4.3 The catalytic kinase domain of *St*MAPKKKε is both necessary and sufficient for the interaction with PexRD2

Y2H analysis of co-transformants carrying PexRD2 bait and *St*MAPKKKε truncated preys are indicated. Growth on SC-LW confirms co-transformation. Interaction between and MAPKKKε preys containing the kinase domain (KD) confirmed by growth on plates lacking histidine (–HIS) and blue colouration in the presence of X-gal (+Xgal). Bait/prey combinations were tested in triplicate and single representative colonies are shown.

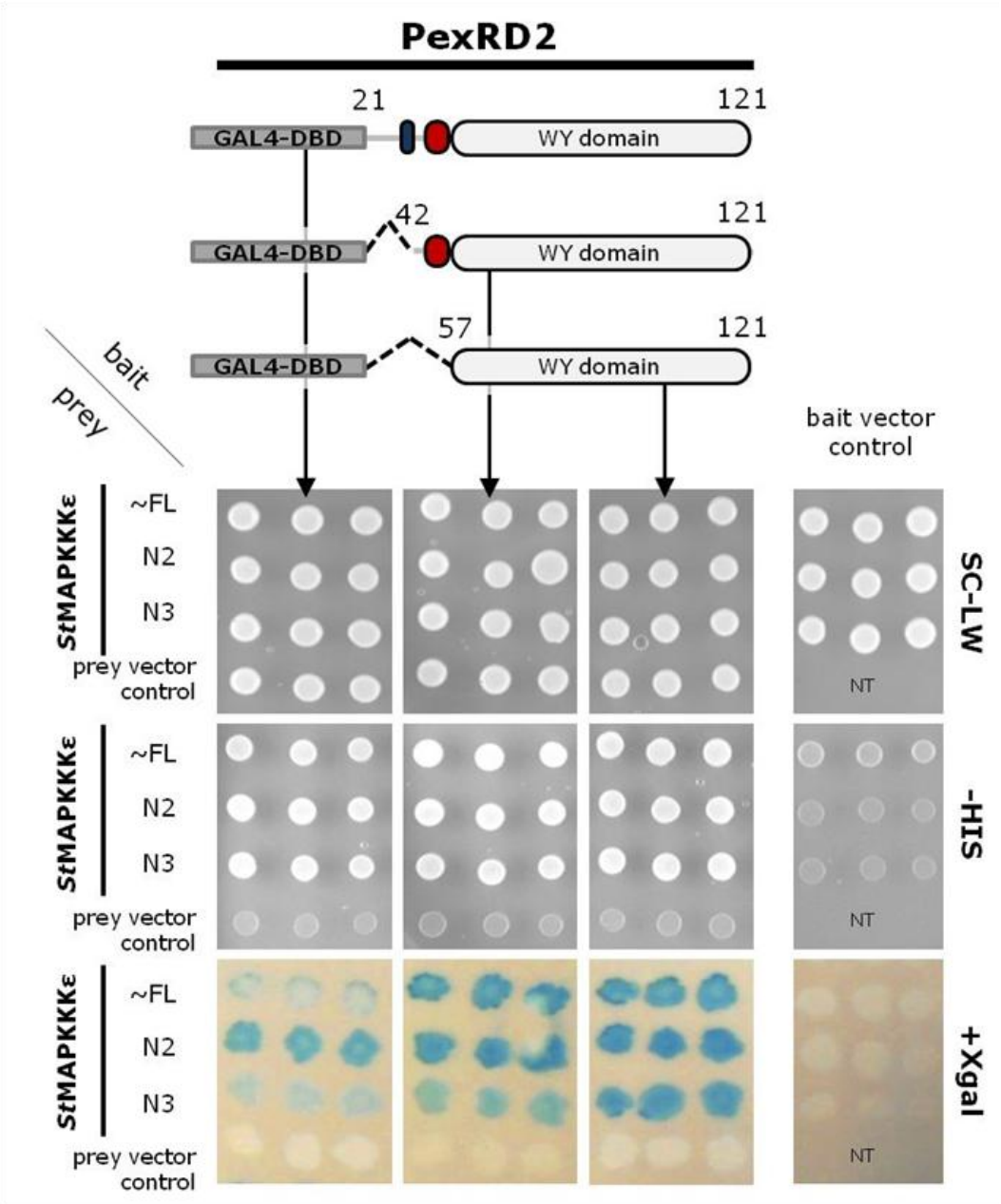

Figure 4.4 PexRD2 WY-domain interacts with MAPKKKε

Y2H analysis of co-transformants carrying PexRD2 baits and *St*MAPKKKε preys are indicated (~FL = residues 4 – 1401, N2 = 2 – 300, N3 = 2 – 278). Growth on SC-LW (TOP panel) confirms co-transformation. Interaction between PexRD2 truncations and MAPKKKε confirmed by activation of (MIDDLE) *HIS3* and (BOTTOM) *lacZ* reporter genes. Bait/prey combinations were tested in triplicate using three single colonies.

4.2.5 PexRD2 specifically interacts with MAPKKKε orthologs

To confirm if the interaction between PexRD2 WY-domain and *St*MAPKKKε KD was specific, interactions between PexRD2 and a MAPKKKε ortholog, or the catalytic kinase domain (KD) of a second, closely related, tomato MAPKKK, *Sl*MAPKKKα, were also assessed. The potato and tomato homologs of MAPKKKε share 100% amino acid sequence identity within the identified minimal interacting domain (MAPKKKε-N3); so instead an interaction between PexRD2 and *At*MAPKKKε1 was tested. This *Arabidopsis* ortholog shares an overall 72% sequence identity with the potato protein, and 94% identity with *St*MAPKKKε-N3. *Sl*MAPKKKα had also been identified as a positive regulator of cell death signalling pathways associated with both plant immunity and disease (del Pozo *et al.*, 2004). Significant homology between MAPKKKε and MAPKKKα is restricted to the catalytic kinase domains, with the two proteins sharing 42% identity within their aligned regions.

An entry clone encoding the full length *At*MAPKKKε1 was provided by Dr Malick Mbengue (The Sainsbury Laboratory, NRP), whereas a sequence encompassing the *Sl*MAPKKKα KD (residues 192 – 467) was sub-cloned into pENTR™/D-TOPO®, from a binary vector provided by Professor Gregory B. Martin (Boyce Thompson Institute for Plant Research (BTI), Ithaca, NY). The respective Y2H-prey constructs were then generated using Gateway® cloning methods.

Prey constructs encoding: *At*MAPKKKε1, *Sl*MAPKKKα KD, *St*MAPKKKε ~FL (PexRD2PI-1), *St*MAPKKKε KD (N2), and an empty prey vector control; were co-transformed with bait vectors: encoding PexRD2, PexRD2 WY-domain, or an empty bait vector control. Yeast cells expressing the PexRD2 and *At*MAPKKKε1 failed to activate the *HIS3* and *lacZ* reporter genes under the same assay conditions used to detect the interaction between PexRD2 and *St*MAPKKKε (Figure 4.5). However, protein-protein interactions between *At*MAPKKKε1 and PexRD2 WY-domain were detectable, as evidenced by the growth on media lacking histidine and the development of a blue colouration in the presence of X-gal, indicating β-galactosidase activity. No interactions between PexRD2 or PexRD2 WY-domain and the kinase domain of *Sl*MAPKKKα were detected.

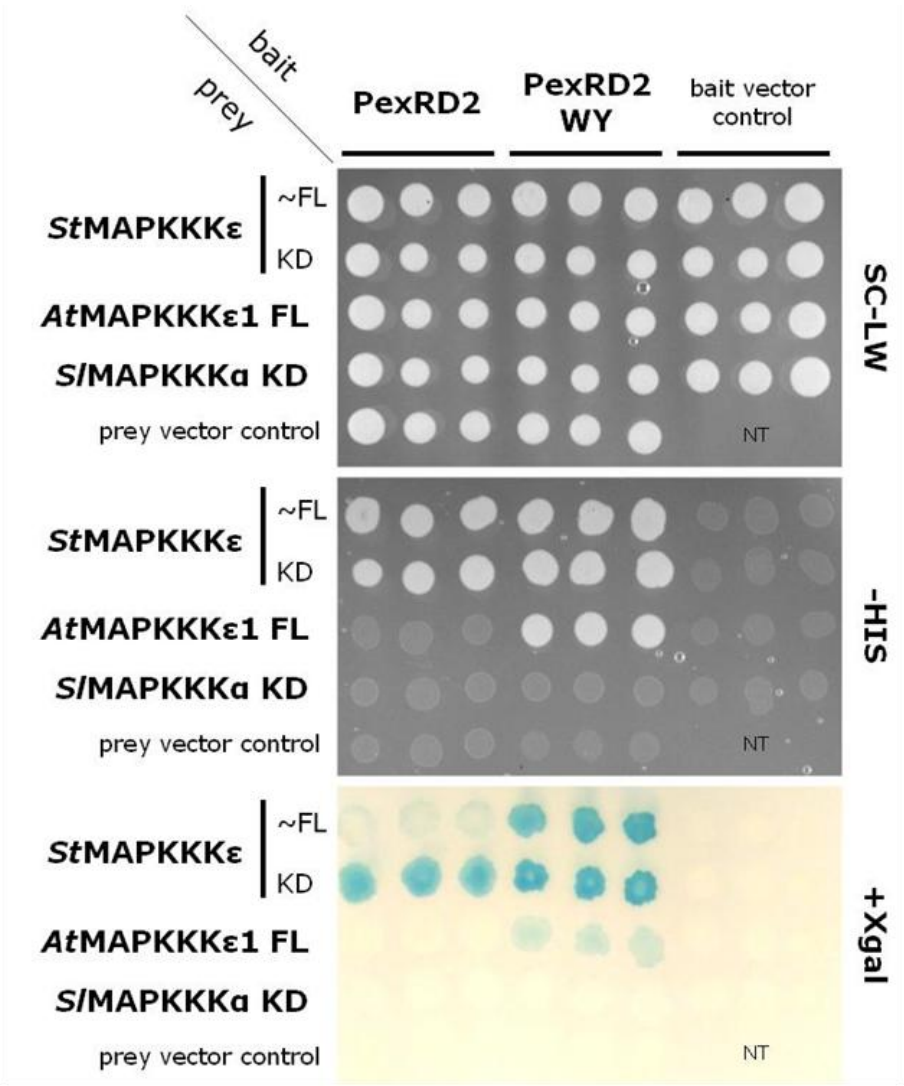

Figure 4.5 PexRD2 interacts specifically with MAPKKKε orthologs

Y2H analysis of co-transformants carrying PexRD2 (FL = residues 21 – 121, WY = 57 – 121) baits and *St*MAPKKKε preys (~FL = residues 4 – 1401, KD = 2 – 300), alongside *At*MAPKKKε1 FL (residues 1 – 1368) and *Sl*MAPKKKα KD (residues 192 – 467) preys. Growth on SC-LW (TOP panel) confirms co-transformation. Interaction between specific baits and preys confirmed by activation of (MIDDLE) *HIS3* and (BOTTOM) *lacZ* reporter genes. Bait/prey combinations were tested in triplicate using three single colonies.

The observation that PexRD2 WY-domain yields a weak, yet detectable interaction with the *Arabidopsis* ortholog, whilst PexRD2 does not, may be explained in a number of ways. It could indicate that the N-terminal region of the effector impinges on the interaction with the *Arabidopsis*, but not the potato, kinase. Alternatively, it could indicate that the interaction between *At*MAPKKKε1 and PexRD2 is existent, but weaker than that between *At*MAPKKKε1 and PexRD2 WY-domain and as such too weak to activate the reporter genes in this experimental system. Of the two explanations, the second is perhaps more favourable, as the interaction between PexRD2 WY-domain and *St*MAPKKKε was shown to give more robust activation of the *lacZ* reporter gene than that with PexRD2 (Figure 4.4).

Together, these results suggest that the WY-domain of PexRD2 specifically interacts with the kinase domains of MAPKKKε homologs and not generically with MAPKKKs. Furthermore, the potentially weaker interaction between PexRD2-WY and the *Arabidopsis* ortholog, compared to PexRD2-WY and the potato ortholog, suggest that the effector is better adapted to interact with the host potato protein, rather than the non-host, *Arabidopsis*, protein. However, confirmation of this would be dependent on determining the expression levels of the two kinase orthologs in yeast.

To further test specificity, a PexRD2 ortholog from the *Phytophthora mirabilis* was tested for an interaction with *St*MAPKKKε. This sequence flanked by the *att*B recombination sites was synthesised supplied in a pUC57 vector by Genscript (USA). The sequence of this effector had originally be confirmed (see Section 3.2.9) by cloning from *P. mirabilis* PIC99114 gDNA (provided by Liliana Cano Mogrovejo (TSL)) Gateway® cloning methods were used to transfer the sequence from the pUC57 vector into the entry vector pDONR™201, and eventually into the Y2H-bait vector as described previously.

In addition, two PexRD2-like effector family members (see Section 3.2.9) were cloned from *P. infestans* T30-4 gDNA (from Liliana Cano Mogrovejo (TSL)) into the pENTR™/D-TOPO® entry vector. The coding sequences of *PITG_14984* and *PITG_14787* (excluding the N-terminal signal peptides), are henceforth referred to as PexRD2-like-1a and PexRD2-like-2a, respectively. These were confirmed by

sequencing; and PexRD2-like-1a was shown to share 47% amino acid sequence identity with the WY-domain of PexRD2; whilst PexRD2-like-2a shared 29% identity. These two effector sequences were then transferred to the pDEST™32 bait vector by Gateway® cloning, and tested for interactions with prey vectors *St*MAPKKKε, or the *St*MAPKKKε-N2 and -N3 truncations as before.

The *P. mirabilis* ortholog of PexRD2 showed activation of both reporter genes indicating an interaction with *St*MAPKKKε preys. In contrast, neither *Pi*PexRD2-like-1a, nor *Pi*PexRD2-like-2a, showed any evidence of interaction with the *St*MAPKKKε preys (Figure 4.6 A). The expression of both PexRD2-like GAL4-DBD fusion proteins in yeast was confirmed by western blot (Figure 4.6 B). Therefore, the lack of detectable interactions is not due to the proteins not being expressed *per se*, although the protein level of PexRD2-like-1a was markedly lower than that of PexRD2 or PexRD2-like-2a. These results further support the conclusion that different PexRD2 homologs, and not other PexRD2-like RXLR effectors, are adapted to interact with MAPKKKε homologs.

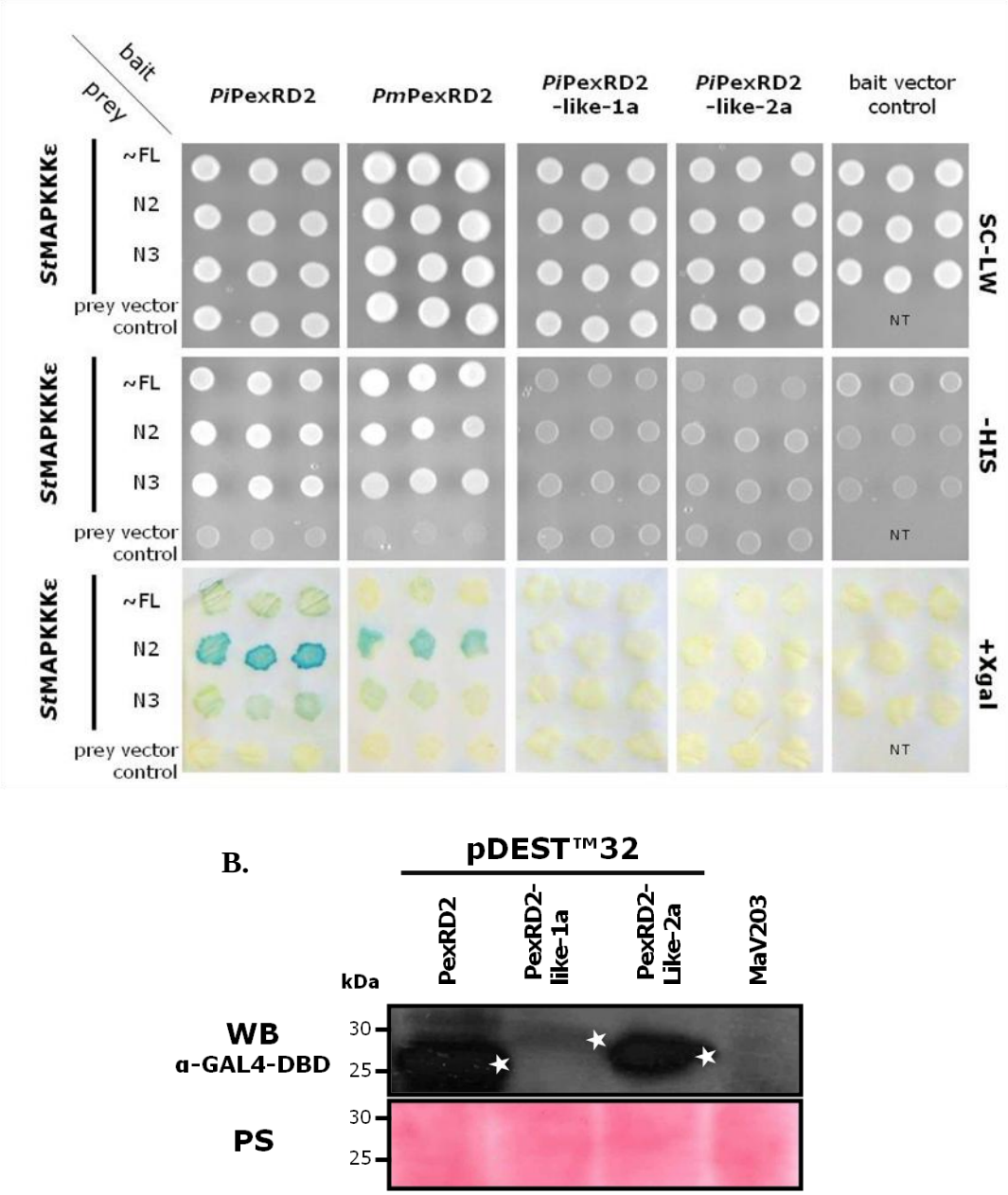

Figure 4.6 PexRD2 orthologs, but not PexRD2-like effectors, interact with MAPKKKε in yeast two-hybrid

(A.) Y2H analysis of co-transformants carrying PexRD2 or PexRD2-like baits and *St*MAPKKKε (~FL = residues 4 – 1401, N2 = 2 – 300, N3 = 2 – 278). Growth on SC-LW (TOP panel) confirms co-transformation. Interaction between PexRD2 baits and MAPKKKε preys confirmed by activation of (MIDDLE) *HIS3* and (BOTTOM) *lacZ* reporter genes. Bait/prey combinations were tested in triplicate using three single colonies. **(B.)** Western blot analysis confirming expression levels of PexRD2 and PexRD2-like baits. White stars indicate the expected sizes of full length fusion proteins. MaV203 represents total proteins from an untransformed yeast and serves as a negative control. PS indicates Ponceau staining to confirm protein loading.

4.2.6 PexRD2 interacts with MAPKKKε *in planta*

Since the interaction between PexRD2 and MAPKKKε was confirmed to be specific in the Y2H system, independent protein-protein interaction experiments were conducted to confirm this *in planta*.

PexRD2 was confirmed to interact with MAPKKKε *in planta* by bimolecular fluorescence complementation (BiFC) (Dr Petra Boevink (JHI), unpublished data). This technique allows the detection of protein-protein interactions in living cells, and is based upon reconstitution of split fragments of a fluorescent protein, primarily yellow fluorescent protein (hence "split YFP"), to form a fluorescent fluorophore (Ghosh *et al.*, 2000, Hu *et al.*, 2002). Co-expression of PexRD2 fused to the N-terminal portion of YFP (YN-), with *St*MAPKKKε-FL fused to the C-terminal portion (YC-), resulted in clear fluorescence, indicating protein-protein interactions. Although weak fluorescence was detected when YN-PexRD2-like-1a or YN-PexRD2-like-2a were co-expressed with YC-*St*MAPKKKε, above that observed in the uninfiltrated control, the level of fluorescence was significantly lower than that observed for co-expression with YN-PexRD2. Switching to use YC-fused effectors and YN-*St*MAPKKKε had no effect on the observed results (Petra Boevink, personal communication).

These results support the conclusion that PexRD2 specifically interacts with MAPKKKε, and show that this interaction can occur within living plant cells. Additional experiments to independently confirm this *in planta* interaction via co-immunoprecipitation (Co-IP) are on-going.

4.2.7 PM4K1 and PM4K2

The signalling components upstream of the MAPKKKs at the top of the three-tiered MAPK cascades, are typically poorly characterised, but a number have been shown to be activated by, so called, MAPKKK kinases (MAPKKKKs or MAP4Ks) (Qi and Elion, 2005). PexRD2 interacts with two protein serine/threonine kinases (named PM4K1 and PM4K2) that show homology to the kinase domains of Ste20p-related protein kinases. Ste20p (Sterile 20 protein) is a putative yeast MAP4K that is known to activate a MAPK cascade by direct phosphorylation of the MAPKKK, Ste11p (Wu *et al.*, 1995, van Drogen *et al.*, 2000). Clear homologs of this protein have been identified in mammals and other organisms, indicating that Ste20-related protein kinases comprise a large, emerging family (Dan *et al.*, 2001). This family can be further divided into the p21-activated kinase (PAK) and germinal centre kinase (GCK) families. They are characterized by the presence of a conserved catalytic kinase domain, located at the C-terminus for PAKs and the N-terminus for GCKs, and a structural diverse non-catalytic region. Ste20p-related kinases have been implicated in a diverse range of intracellular regulatory processes, including the regulation of apoptosis, morphogenesis and rearrangement of the cytoskeleton (Sells and Chernoff, 1997, Bagrodia and Cerione, 1999, Kyriakis, 1999).

A search for conserved protein domains using CD-search (Marchler-Bauer et al., 2011) revealed that PM4K1 and PM4K2 contain serine/threonine kinase catalytic domains (Figure 4.7) with homology to those found in the oxidative stress response kinase (OSR1) and Ste20-related proline alanine-rich kinase (SPAK[**]). OSR1 and SPAK are both GCKs and belong to the GCK-VI subfamily (Dan *et al.*, 2001). These two proteins share distinctive features in their non-catalytic regulatory regions including a putative nuclear localisation signal (NLS), a caspase-cleavage site and a C-terminal region of high conservation required for interaction with their downstream membrane associated protein targets (Piechotta *et al.*, 2003, Delpire and Gagnon, 2008). Although some of the residues comprising the putative NLS are conserved in PM4K1 and PM4K2 (Figure 4.7), the rest of the proposed regulatory regions of the two PexRD2-interacting kinases are generally highly divergent from

[**] also known as PASK (proline-alanine-rich Ste20p-related kinase)

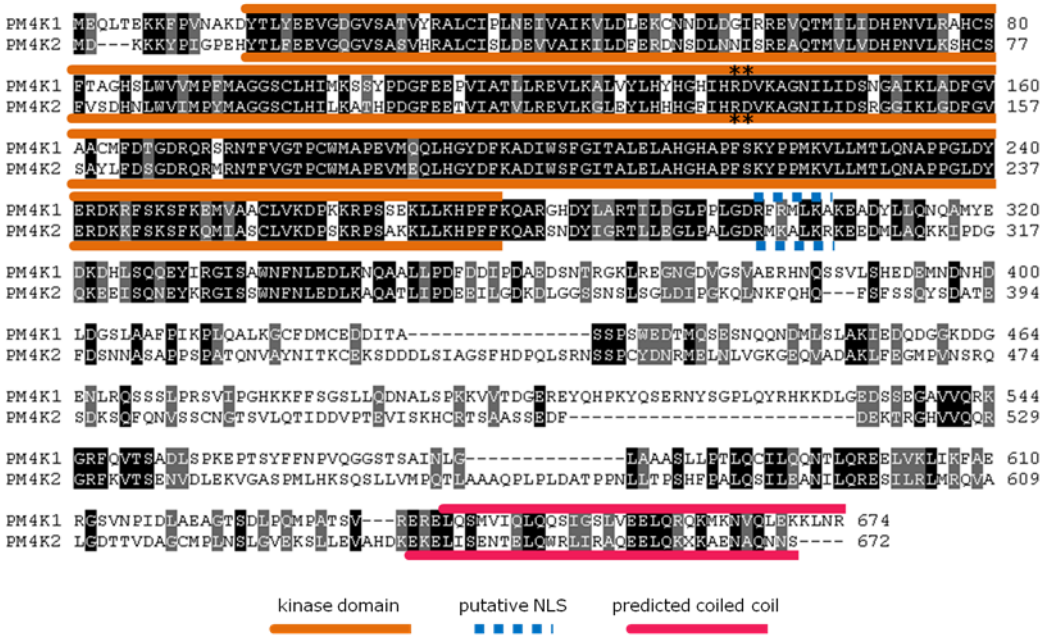

Figure 4.7 PM4K1 and PM4K2 show similar domain organisation

Sequence alignment of full-length protein sequences for the PM4K1 and PM4K2. Conserved residues are shaded in black, similar residues are shaded grey. The position of the conserved catalytic kinases domains (orange), putative NLS (dotted blue) and predicted coiled coils (pink) are indicated above (PM4K1) and below (PM4K2) the alignment. The positions of the catalytic arginine and aspartate residues are indicated with *.

OSR1 and SPAK. This suggests that the potential downstream targets and regulatory mechanisms of PM4Ks are unlikely to be the same as OSR1 and SPAK. Furthermore, unlike OSR1 or SPAK, but in similarity with some other GCKs (Yustein *et al.*, 2003, Callus *et al.*, 2006, Delarosa *et al.*, 2011), both PM4Ks have predicted coiled coils (CCs) at their extreme C-termini (Figure 4.7). These were predicted by using SMART (simple modular architecture research tool) to identify potential signalling domains (Schultz *et al.*, 1998, Letunic *et al.*, 2012). These protein-protein interaction motifs have been implicated in other Ste20-related kinases in mediating homodimerisation, which typically enhances their activity (Delarosa *et al.*, 2011).

Champion *et al.*, (2004b) conducted a phylogenetic analysis based on an extensive survey of MAPKKKs in the Raf[††] superfamily and STE family kinases: which

[††] Raf = RAPIDLY ACCELERATED FIBROSARCOMA

include kinases related to the MAP4K, Ste20p, the MAPKKK, Ste11p; and the MAPKK Ste7p. This revealed that the annotated MAP4Ks formed a monophyletic lineage, which was the sister clade to the CDC[‡‡] subfamily kinases that includes MAPKKKε homologs.

The two PexRD2-interacting PM4Ks identified in the initial Y2H screen share 48% amino acid sequence identity over their entire protein sequences. Restricting the comparisons to the N- and C-terminal regions separately, the two proteins share approximately 78% sequence identity within their N-terminal catalytic kinase domains (PM4K1, residues 1 – 277), and 29% sequence identity within their C-terminal regions (PM4K1, residues 278 – 674). Analysis of the *Solanum tuberosum* Group Phureja DM1-3 (DM) annotated genome sequence (Potato Genome Sequencing Consortium *et al.*, 2011) revealed one sequence sharing 99% amino acid sequence identity with PM4K2. In contrast, no clear candidate sequence for PM4K1 could be found. Three predicted protein sequences in the potato draft genome shared overall sequence identities with PM4K1 of between 48 – 49%, and one of which was the identified PM4K2 sequence (see Table 4.1). The inability to find a clear *PM4K1* candidate likely results from the incomplete nature of the draft genome, since only 86% of the 844 megabase genome has currently been assembled (Potato Genome Sequencing Consortium *et al.*, 2011). In spite of this, orthologous proteins for both PM4K1 and PM4K2 can be found in both tomato: sharing 99% and 97%; and *N. benthamiana*: sharing 92% and 90% sequence identity to the potato proteins, respectively. PM4K1 and PM4K2 only share significant homology with MAPKKKε within the catalytic kinase domains, sharing 34% and 35% amino acid sequence identity with the KD of *St*MAPKKKε. Since the two related PM4Ks show significant sequence similarity, and similar domain organisations, subsequent analyses were restricted to focus on PM4K1.

[‡‡] CDC = CELL DIVISION CYCLE

4.2.8 The WY-domain of PexRD2 specifically interacts with a region containing the kinase domain of PM4K1

To identify which domains of *St*PM4K1 and PexRD2 were involved in the interaction, the full length and different N- and C-terminal truncations were sub-cloned into the pENTR™/D-TOPO® entry vector, before being transferred into the Y2H vectors by Gateway® cloning.

Three truncated PM4K1 prey vector constructs were tested for interaction with PexRD2. These constructs were tested alongside the full length PM4K1 prey construct sub-cloned from the Y2H screen (clone PexRD2PI-2), and the appropriate empty vector controls as before.

PexRD2 interacted with one truncated construct that contained the N-terminal catalytic kinase domain (KD) plus some additional 42 amino acids of the C-terminal region (PM4K1-N1, residues 2 – 319), as evidenced by both the growth of co-transformed yeast on media lacking histidine, and the development of a weak blue colouration in the presence of X-gal (Figure 4.8). This interaction was weaker than that observed with the PM4K1-FL prey, as no growth on media lacking uracil was detected. PexRD2 showed no interaction with the other two prey constructs (PM4K1-N2, residues 2 – 286; and PM4K1-C, residues 287 – 674). These results suggest that, in similarity with MAPKKKε, PexRD2 is interacting with the kinase domain of PM4K1, or a region immediately downstream. In the full length protein, the interaction is potentially being stabilised by weak contacts with residues within the remainder of the C-terminal region, or by potential homodimerisation of the kinase mediated by the predicted C-terminal coiled coil. Alternatively the weaker interaction with PM4K1-N1, compared to PM4K-FL, and lack of interaction with PM4K1-N2 and PM4K-C with might result from reduced stability of these truncations in yeast. As with the original PexRD2PI-2 clone, none of the sub-cloned PM4K1 prey constructs showed any evidence of auto-activation activity.

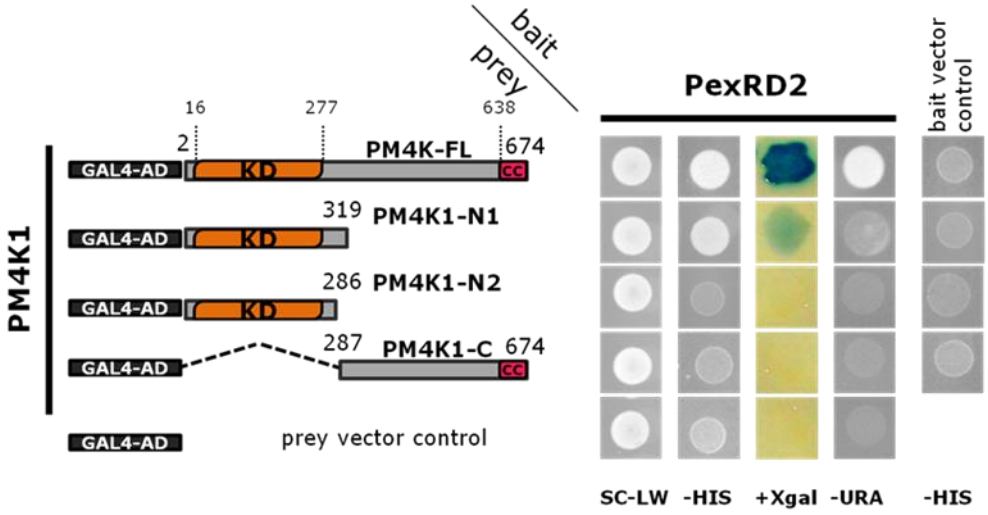

Figure 4.8 Truncated PM4K1 containing catalytic kinase domain interacts with PexRD2, weaker than PM4K1-FL

Y2H analysis of cotransformants carrying PexRD2 bait and PM4K1 truncated preys are indicated. Growth on SC-LW confirms cotransformation. Interactions between PexRD2 and the full length or one truncated PM4K1 preys are confirmed by growth on plates lacking histidine (–HIS) and blue colouration in the presence of X-gal (+Xgal). Growth on media lacking uracil (-URA) only seen for interaction with almost full length PM4K1. KD indicates the catalytic kinase domain and CC indicates a predicted coiled coil. Bait/prey combinations were tested in triplicate and single representative colonies are shown.

Note: Y2H interaction assays conducted between PM4K1 and PexRD2-WY or PexRD2-like effectors were conducted with Benjamin Hall.

To identify whether the effector domain of PexRD2 was sufficient for the interaction with PM4K1, PexRD2 and its WY-domain in the Y2H-bait vector, which had previously been tested for interaction with MAPKKKε, were screened for protein-protein interactions with PM4K1-FL. Full length P4MK1 was chosen since this construct had shown more robust activation of reporter genes than the interacting N-terminal fragment. To test whether this interaction were specific to PexRD2, the two PexRD2-like effectors, PexRD2-like-1a and PexRD2-like-2a, were also included as additional baits. All bait/prey combinations were assessed using the *HIS3*, *lacZ* and *URA3* reporter gene assays, alongside the appropriate empty vector controls.

Consistent with previous results, the WY-domain of PexRD2 was able to interact with PM4K1; as evidenced by the activation of all three reporter genes (Figure 4.4). These results indicate that the N-terminal region of PexRD2, containing the translocation motifs is dispensable for the interaction with PM4K1. This suggests that, as for the interaction between PexRD2 and MAPKKKε, the WY-fold containing effector domain is mediating the interaction with PM4K1. This interaction is specific to the WY-domain of PexRD2, as neither of the two PexRD2-like effector baits showed activation of any of the reporter genes when co-transformed with PM4K1-FL prey. The specificity of PexRD2 for PM4K1 and PM4K2 was further confirmed by the fact that PexRD2 was shown not to interact with another putative potato MAP4K that was identified as an interactor of another predicted RXLR-WY effector (Dr. Miles Armstrong, unpublished data) This non-interacting putative MAP4K shared 46% amino acid sequence identity with PM4K1 KD. These results support the conclusion that PexRD2 interacts specifically with PM4K1.

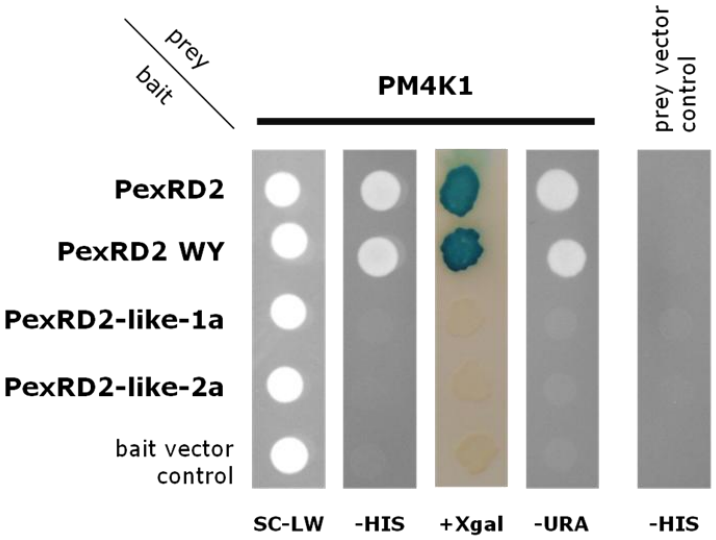

Figure 4.9 PM4K1 interacts specifically with PexRD2

Y2H analysis of co-transformants carrying PexRD2 or PexRD2-like baits and PM4K1-FL prey as indicated. Growth on SC-LW confirms co-transformation. Interactions between PM4K1 and full length or effector domain from PexRD2 are confirmed by growth on plates lacking histidine (–HIS), β-galactosidase activity (+Xgal), and growth on media lacking uracil (-URA). No interactions were detected for PexRD2-like baits. Bait/prey combinations were tested in triplicate and single representative colonies are shown.

4.2.9 PexRD2 interacts with PM4K1 *in planta*

Since the interaction between PexRD2 and PM4K1 was confirmed to be specific in the Y2H system, independent protein-protein interaction experiments were conducted to confirm that the two proteins also interacted *in planta* by co-immunoprecipitation (co-IP). Co-IP experiments are widely considered the gold standard for demonstration of protein-protein interactions *in vivo.* The full length *PM4K1* sequence was transferred into the binary expression vector pK7WGF2 by Gateway® cloning. This vector allows transient expression of transgenes with N-terminally fused GFP expressed under the control of a 35S promoter (Karimi *et al.*, 2002). Agroinfiltation was used to transiently express this GFP-fusion PM4K1-FL or free GFP with either PexRD2, PexRD2-like-2a WY-domain, or the unrelated WY-domain-containing RXLR effector AVR3a. All effectors were expressed with N-terminal FLAG-epitope tags from the pTRBO binary vector (Lindbo, 2007).

Total protein extracts were subjected to GFP-IPs using GFP-Trap® (ChromoTek), and total and immunoprecipitated protein samples were analysed by western blots. Immunoprecipitation of GFP-PM4K1 specifically supported the co-immunoprecipitation of the FLAG-epitope tagged PexRD2, but not the other two RXLR effectors. Immunoprecipitation of free GFP did not support the co-immunoprecipitation of any of the FLAG-epitope tagged effectors (Figure 4.10). This indicates that the interaction between PexRD2 and PM4K1 also occurs *in planta*.

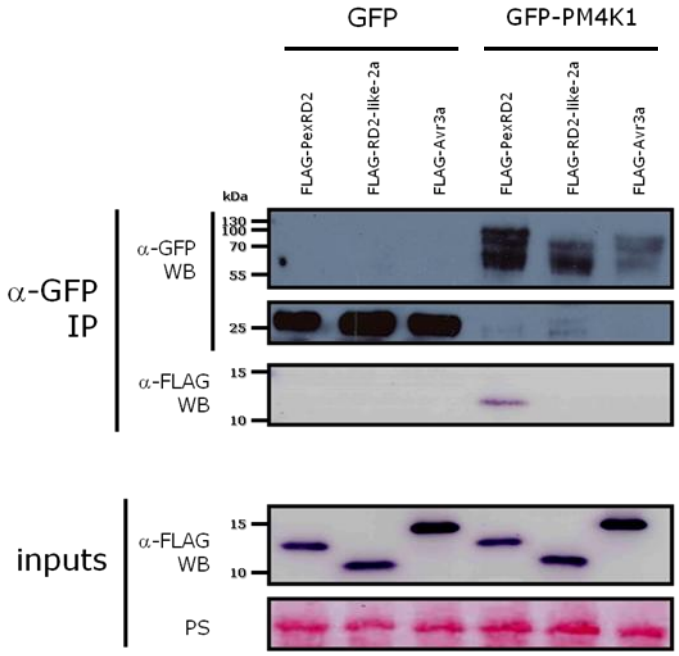

Figure 4.10 PexRD2 interacts with PM4K1 *in planta*

Western blots showing PexRD2 specifically coimmunoprecipitates with PM4K1 *in planta.* Free GFP or GFP-tagged PM4K1 were co-expressed with FLAG-tagged effectors in *N. benthamiana.* Immunoprecipitates (IP) obtained with GFP-Trap® (α-GFP IP) and total protein extracts (inputs) were immunoblotted with antibodies as indicated. PS indicates of Ponceau stain of large RuBisCO subunit to confirm equal protein loading.

4.2.10 PUB38-like

All aspects of cellular physiology and development are controlled by the balance of *de novo* protein synthesis and degradation of existing proteins. The principle proteolytic system found in eukaryotes is the ubiquitin-26S proteasome system, and growing evidence has highlighted the extensive role that this system plays in plant cellular signalling. In this pathway, the ubiquitin (Ub) protein, which is found in all eukaryotes, serves as a reusable 'tag' that directs target proteins for selective degradation. Polymeric ubiquitin (poly-Ub) chains are covalently attached via the C-terminal glycine residue to lysine residues on protein targets. This is achieved by the iterative actions of a three step enzymatic conjugation cascade.

Free ubiquitin moieties are activated by an E1 ubiquitin-activating enzyme by an ATP-dependent mechanism. The activated ubiquitin is then transferred to a cysteine

residue in an E2 ubiquitin-conjugating enzyme. Once conjugated to ubiquitin, the E2 enzyme binds to one of several E3 ubiquitin ligases which are responsible for tethering the Ub-E2 enzyme and the target protein substrate. The close proximity allows transfer of the ubiquitin from the E2 cysteine to a lysine residue on the target protein. Of the three enzyme classes E3 ubiquitin ligases are the most abundant. The *Arabidopsis* genome contains two E1 enzymes, around 45 E2 enzymes and 1415 E3 enzymes. This diversity is required as it is the E3 enzymes that perform target protein recognition and hence specificity.

The nature of the inter-ubiquitin covalent linkages in the poly-Ub tag is key to determining the fate of the ubiquitinated target. Lys48-mediated inter-ubiquitin linkages predominate in cells, and direct target proteins towards degradation by the 2 MDa, ATP-dependent, 26S proteasome. Other inter-Ub linkages have also been observed, and function in non-proteolytic signalling. Lys63-linked poly-Ub chains have been shown to mediate a number of processes including, interestingly, kinase activation.

Within Arabidopsis, *At*PUB-ARM proteins form a family of E3 ligases with 41 members (Azevedo *et al.*, 2001, Mudgil *et al.*, 2004). These proteins are characterised by ~70-amino-acid conserved plant U-box (PUB) domain which is a recognised E3 ubiquitin ligase motif, and between two and 32 ARM repeats. PexRD2 interacts with a potato PUB-ARM domain protein that shows homology to the confirmed E3 ubiquitin ligase *At*PUB38 (Mudgil *et al.*, 2004). *At*PUB38 has N-terminal U-box, and five predicted ARM repeats in its C-terminus. Comparison to the *At*PUB38 and the homologous sequence in the *Solanum tuberosum* Group Phureja DM1-3 (DM) annotated genome sequence (St_{DM}PUB38-like) indicated that the interacting prey identified in the Y2H screen was N-terminally truncated (*St*ΔN-PUB38-like). Overall, *St*PUB38-like shows a similar domain organisation to *At*PUB38, although polymorphisms between the two sequences mean that the fourth Arm repeat is no longer confidently predicted by bioinformatic analysis. *St*ΔN-PUB38-like and *At*PUB38 share an overall amino acid identity of 52%.

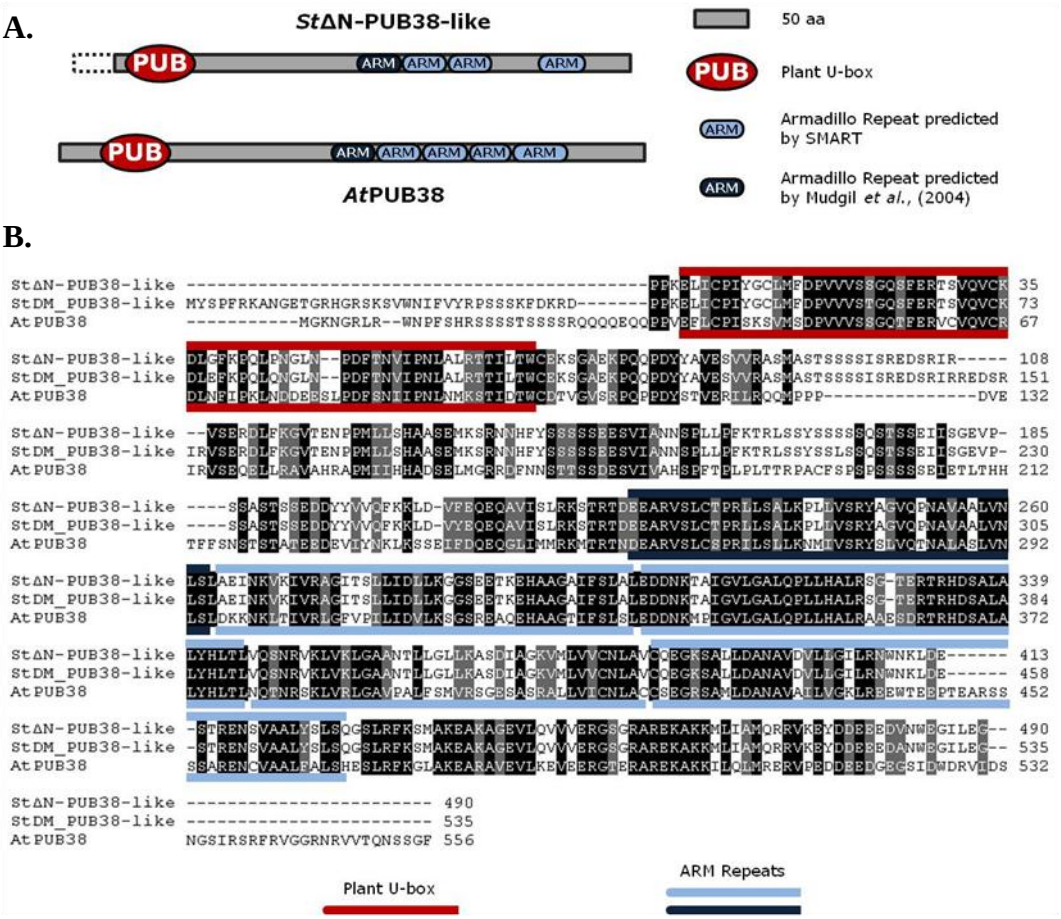

Figure 4.11 Homology between *At*PUB38 and PUB38-like proteins

(A) Domain organisation for the truncated *St*PUB38-like sequence (*St*ΔN-PUB38-like) identified in Y2H clone PexRD2PI-4, and the *Arabidopsis* ortholog *At*PUB38. **(B)** Sequence alignment for the two protein sequences represented in (A), in addition to the predicted full length sequence found in the *Solanum tuberosum* Group Phureja DM1-3 (DM) annotated genome sequence (St_{DM}PUB38-like), highlighting the U-box domain (red) and ARM repeats (blue).

U-box domains are predicted to mediate interactions with E2 ubiquitin-conjugating enzymes (Pringa *et al.*, 2001), whilst the C-terminal ARM repeats are expected to mediate interactions with target proteins (Mudgil *et al.*, 2004). Although, the crystal structure of the mammalian, ARM repeat-containing protein β-cateninin suggests that six repeats constitute a protein interaction domain (Huber *et al.*, 1997), the C-terminal domains of *At*PUB38, which contains only five predicted repeats was shown to interact with the intracellular kinase domains of a number of plant receptor

like kinases (RLKs) (Samuel *et al.*, 2008). A number of other *At*PUB-ARM proteins were also shown to interact with RLK KDs, and these interactions highlighted the potential role of PUB-ARM proteins as downstream signalling proteins for RLKs. The potential for *St*PUB38-like to interact with RLKs remains to be investigated, but the ability of PexRD2 to interact with both protein kinases and an E3 ubiquitin ligase raises the question as to whether these host proteins are also functionally linked and/or exist in a larger, macromolecular complex.

4.2.11 MAPKKKε and PM4K1 can self associate, interact with each other and PUB38-like

To address the potential functional links between PexRD2-interacting host proteins, the ability of *St*MAPKKKε, PM4K1 and *St*PUB38-like to interact with one another in the Y2H system was assessed. The *PM4K1-FL* and *MAPKKKε ~FL* sequences were transferred into the Y2H-bait vector by Gateway® cloning. These constructs were then co-transformed with the previously described *PM4K1-FL*, *StMAPKKKε ~FL* and *ΔN-PUB38-like* prey vectors, and an empty prey vector control. In addition, the WY-domain of PexRD2 was transferred into the Y2H-prey vector by Gateway® cloning, and co-transformed with the two host kinases as baits, as a potential positive interaction control.

Co-transformants were then tested for their ability to grow on media lacking histidine or uracil, as well as for β-galactosidase activity. Preliminary experiments showed that the previously used concentration of 3AT[§§] of 10 mM was insufficient to prevent auto-activation of the *HIS3* reporter gene by the new kinase baits; as evidenced by the growth of yeast cells expressing these baits with the empty prey vector. To combat this, the *HIS3* reporter assay was repeated with the 3AT concentration increased to 50 mM. None of the protein-protein interactions tested were able to allow growth on media lacking uracil, indicating no activation of the more stringent *URA3* reporter gene.

[§§] 3AT (3-amino-1,2,4-triazole) is a competitive inhibitor of the product of the *HIS3* gene, and is used to repress growth caused by unspecific auto-activation of this reporter gene, allowing detection of specific protein-protein interactions.

Activation of *HIS3* and *lacZ* reporter genes (Figure 4.12) indicated protein-protein interactions for *St*MAPKKKε-*St*MAPKKKε and PM4K1-PM4K1 co-expressing yeast, suggesting that these two host kinases might self associate and possible function as homodimers. Weak protein-protein interactions were detected for yeast co-expressing PM4K1 as the bait and MAPKKKε as the prey: as evidenced by activation of the *HIS3* gene and detectable growth on media lacking histidine; but not the *lacZ* gene and hence no development of blue colouration in the presence of X-gal. Weak protein-protein interactions were also detected between either of the host kinases baits and the ΔN-PUB38-like prey. The discovery that the host proteins that interact with PexRD2 can also form homomeric and heteromeric interactions increases the chance that these proteins might be functionally linked, or even exist in large macromolecular complexes within the host cell. Whether PexRD2 interacts

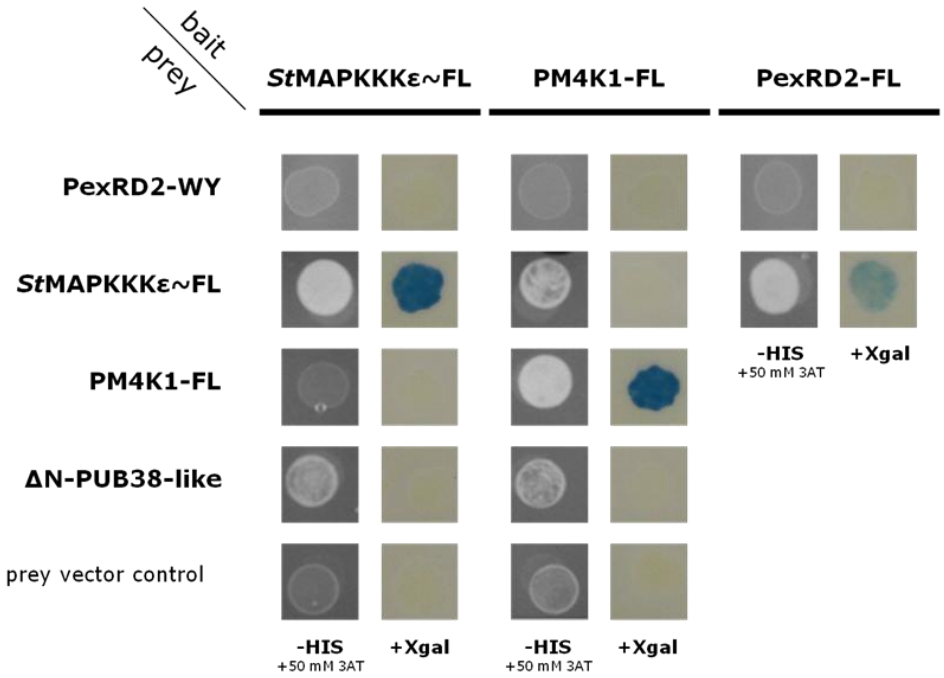

Figure 4.12 Homomeric and heteromeric protein-protein interactions can be detected between the confirmed interactors of PexRD2

Y2H analysis of cot-ransformants carrying bait and prey constructs as indicated. Homomeric interactions between the two host kinases is indicated by growth on plates lacking histidine, but supplemented with 50 mM 3AT (–HIS + 50 mM 3AT) and blue colouration in the presence of X-gal (+Xgal). Weak heteromeric interactions between the two host kinases, and either kinase and the ΔN-PUB38-like prey were indicated by weak growth on –HIS + 50 mM 3AT media. No interactions were detected for the PexRD2-WY prey. All bait/prey combinations were tested in triplicate and single representative colonies are shown.

with the host proteins individually, or as homodimeric, or higher order, complexes remains to be investigated.

Unexpectedly, following the detectable interaction between MAPKKKε and PM4K1, the reciprocal co-transformation (MAPKKKε as the bait and PM4K1 as the prey) did not cause activation of the *HIS3* reporter gene. This could have resulted from steric hindrance of this particular combination of fusion partners, preventing the normal association between the two host proteins. Alternatively the specific geometry of the resultant kinase complex might not be able to promote the recruitment of the transcriptional machinery required to initiate reporter gene expression.

Surprisingly, any co-transformation involving the WY-domain of PexRD2 in the prey vector was unable to activate any of the reporter genes. This was true even when it was co-expressed with PexRD2-FL in the bait vector (Figure 4.12), and when the 3AT concentration was reverted back to 10 mM (data not shown). As PexRD2 is known to self associate this was unpredicted (Section 3.2.6 – 3.2.7). Again, this may indicate that steric hindrance is preventing the association between the different PexRD2 GAL4-fusions, or that the specific geometry of the resultant PexRD2 GAL4-fusion 'heterodimer' cannot promote the recruitment of the transcriptional machinery. However, it may indicate that the PexRD2-WY protein when expressed as a GAL4-AD fusion, but not a DBD fusion, is unstable in yeast. Further work is required to determine which, if any, of these explanations is best describing the situation.

4.3 Conclusion

Y2H hybrid screening revealed that the RXLR-WY effector PexRD2 interacts with four different host proteins. Although other RXLR effectors, such as AVR3a have been shown to interact with multiple host proteins (Bos *et al.*, 2010b), most RXLR effectors tested, to date, using the same Y2H screen have revealed a single interacting host protein (Professor Paul Birch, JHI, personal communication).

Two of the interactions, those between PexRD2 and MAPKKKε, and PexRD2 and PM4K1, have also been confirmed independently *in planta*. This reduces the chance that observed interactions were false positives, validating the Y2H screening approach. For the same interacting proteins, the WY-fold containing effector domain of PexRD2 was shown to be sufficient to mediate these interactions. This validates the biological relevance of the construct used for crystallisation, and means that the solved structure of PexRD2's effector domain should prove an invaluable resource for understanding the molecular nature of these interactions.

Since Y2H analyses have demonstrated that PexRD2 interacts with regions of MAPKKKε and PM4K1 that include the catalytic kinase domains might suggest a shared interaction mechanism. The importance of the N-terminal domains of the three host protein kinases for the interaction with PexRD2 could have been inferred from the sequence of the clones identified in the Y2H screen. The Y2H-prey cDNA library screened was generated by amplification of mRNA transcripts from their 3'-end and N-terminally truncated constructs are frequently observed (i.e. *St*ΔN-PUB38-like). As such, the retrieval of almost exclusively, full length constructs for particularly long genes such as *MAPKKKε* (~4.2 kb) and the two PM4Ks could be considered a strong indicator that the N-terminus of these proteins are important for the interactions in question.

The specific role of the C-terminal regions of these interaction protein kinases, which are predicted to contain known protein-protein interaction motifs (ARM repeats and CC domains), has not been characterised. These regions could potentially mediate interactions with upstream or downstream signalling components, or the homomeric associations observed above (Figure 4.12) allowing regulation and conferring specificity to the activity of the kinases.

*St*PUB38-like also contains ARM repeats within its C-terminus. Although six arm repeats are predicted to be a prerequisite for an effective protein interaction domain, the homologous region of the *Arabidopsis* E3 ubiquitin ligase *At*PUB38, which contains only five repeats, is known to interact with the kinase domains of a range of RLKs. As ARM repeats are often extremely sequence diverse both between and within ARM-repeat containing proteins (Mudgil *et al.*, 2004), the potential for additional repeats with the sequences of *At*PUB38 and PUB38-like proteins cannot be excluded. The weak interactions detected between *St*ΔN-PUB38-like and PM4K1 or MAPKKKε might suggest that this protein is actually able to interact with a broader range of protein kinases, although if the predicted ARM-repeats are required, to mediate these interactions, has yet to be tested.

Following the detection of an interaction between the MAPKKKε, and the putative MAP4K, PM4K1, it is tempting to suggest a role of PM4K1 as an upstream activator of the MAPKKKε MAPK cascade. Whether PM4K1 can phosphorylate and/or activate MAPKKKε has yet to be investigated. Other members of the GCK family are known to associate with MAPKKKs and activate their downstream cascades. However, a GCK has yet to been shown to directly phosphorylate its interacting MAPKKK. Instead they have been proposed to achieve activation of signalling by acting as adaptors or scaffold proteins, rather than genuine MAPKKK kinases (Kyriakis, 1999).

The interaction with MAPKKKε is perhaps most interesting. This host protein was already known to be involved in plant immunity signalling, following recognition of effectors from both bacterial and fungal pathogens (see Introduction to Chapter 5). As such this protein represents a potential convergence point for plant immunity signalling pathways. The detected interactions between MAPKKKε and the other PexRD2-interacting proteins could suggest that this protein is a part of a highly connected cellular hub, similar to other proteins known to be involved in plant cell immunity signalling (Mukhtar *et al.*, 2011). The interaction of PexRD2 with the catalytic kinase domains of this host protein might suggest a potential virulence role of PexRD2 as an inhibitor of said kinase. This finding could suggest that, as proposed for other effector repertoires, effectors from *Phytophthora infestans* are targeting the protein complexes at the points of convergence in plant immunity

signalling cascades (Mukhtar *et al.*, 2011). However, it is important to recognise that interactions between effectors and host proteins, even when validated by multiple protein-protein interaction techniques do not necessarily indicate that the host protein represents a 'target' of the effector.

For an interacting protein to represent a genuine virulence target, one would expect the interaction with the effector to interfere with the normal functioning of the protein, to deliver a benefit to the pathogen. Interacting proteins might alternatively represent examples of decoys (van der Hoorn and Kamoun, 2008). In this model, the effector's interactions with these specific host proteins are not expected to benefit the pathogen. However, in certain host genetic backgrounds containing cognate R proteins, the interaction with the decoy would serve to aid recognition of the effector's presence or activity. Decoys are expected to either be related to or mimic genuine, operative targets; however, confirming a protein's roles as a decoy is likely to be challenging because of the expected redundancy of interactions and reliance on negative results (van der Hoorn and Kamoun, 2008). Other interactors might further represent so called 'helpers' (Win *et al.*, 2012a), and perform some required modification of the effector, to allow it to carry out its virulence function, or serve to deliver it to its eventual sub-cellular localisation, or protein complex, promoting the effector's interaction with its genuine virulence target.

Understanding the importance of the different interactions, described in this chapter, in the context of normal plant cell function, immunity and infection represents the next big challenge. Further characterisation of the interplay between the effector and the identified host proteins *in planta* may help elucidate the adaptive value, if any, of these interactions for either the pathogen or the host. This would aid the determination as to whether the host proteins are targets, decoys or helpers. In the subsequent chapter, the role of the immunity signalling host kinase, MAPKKKε, in the resistance response against *Phytophthora infestans* is assessed. The implication of the interaction of PexRD2 with this kinase for this host protein's activity is also tested, using a range of experiments in the model host plant *N. benthamiana*.

Chapter 5:

MAPKKKε and the Putative Virulence Function of PexRD2

5 MAPKKKε and the Putative Virulence Function of PexRD2

5.1 Introduction

This introduction refers to the state of the knowledge at the start of this aspect of the project in 2011. Subsequent publications relevant to this section are referenced throughout, and discussed at the end of, this chapter.

Mitogen-activated protein (MAP) kinase cascade-mediated signalling, involving three-tiered MAP kinase core modules, is critical for defence responses following the perception of pathogen-associated molecular patterns (PAMPs) and effectors from a range of pathogens (Asai *et al.*, 2002, Nürnberger *et al.*, 2004, Pitzschke *et al.*, 2009). The best characterised MAPK cascades involved in plant immunity are arguably those following perception of the PAMP, flagellin, the principal component of bacterial flagellum (Zipfel, 2008). In *Arabidopsis thaliana*, FLAGELLIN SENSING 2 (FLS2)-mediated perception of the 22-amino-acid peptide of flagellin, flg22, triggers activation of two MAPK cascades (Asai *et al.*, 2002, Nicaise *et al.*, 2009). One involves MEKK1[*], which is likely functionally redundant with at least one other unknown MAPKKK; the MAPKKs, MKK4/MKK5; and MAPKs, MPK3/MPK6. The other comprises MEKK1, MKK1/MKK2, and MPK4 (Figure 5.1). The two act antagonistically; the first contributes positively, and the second negatively, to PAMP-triggered immunity (PTI).

Other PAMPs, such as the peptide elf18 from the bacterial elongation factor Tu (EF-Tu), induce a similar set of responses as flg22, including activation of MKK4/MKK5 and MPK3/MPK6 (Zipfel *et al.*, 2006). Furthermore, perception of oomycete PAMPs, such as the peptide Pep-13 from a *Phytophthora sojae* cell wall transglutaminase or the *P. infestans* sterol-scavenging elicitin INF1, trigger activation of MAPK cascades required for subsequent defence responses (Kroj *et al.*, 2003, Zipfel and Felix, 2005, Asai *et al.*, 2008).

[*] MEKK = MAPK/ERK kinase kinase, ERK = extracellular signal-regulated kinase

MAPK cascades have also been identified as signalling components in R protein-mediated effector-trigger immunity (ETI). In solanaceous plants, NPK1 is a MEKK-like MAPKKK that is required for triggering resistance mediated by the N, Bs2, and Rx resistance (R) proteins (Jin *et al.*, 2002). N-mediated resistance against tobacco mosaic virus (TMV) was also dependent on MEK2[†], WIPK and SIPK[‡] (Jin *et al.*, 2003), which are orthologs of *Arabidopsis* MKK4/MKK5, MPK3, and MPK6 respectively, as well as MEK1, and the MAPK, NTF6[§] (Liu *et al.*, 2004), which function downstream of NPK1 (Soyano *et al.*, 2003).

MAPKKKα was identified as a positive regulator of cell death associated with plant immunity in solanaceous plants (del Pozo *et al.*, 2004). It is required for AvrPto/Pto-triggered hypersensitive response (HR) and is suggested to signal through MEK2, SIPK, MEK1, and WIPK. The signalling ability of MAPKKKα was shown to be enhanced by a 14-3-3 protein, TFT7[**] (Oh *et al.*, 2010). MAPKKKα also positively regulates cell death associated with disease susceptibility (del Pozo *et al.*, 2004).

MAPKKKε is a positive regulator of cell death responses specifically associated with plant immunity (Melech-Bonfil and Sessa, 2010). The tomato homolog was identified as required for the immune response against bacterial pathogens using a virus-induced gene silencing (VIGS)-based screen. Silencing of *Sl*MAPKKKε resulted in a loss of resistance against avirulent *Xanthomonas campestris* pv. *vesicatoria* (*Xcv*) strains and *Pseudomonas syringae* pv. *tomato* (*Pst*) DC3000.

Gene silencing in *N. benthamaina* showed that MAPKKKε was required for eliciting the HR triggered following the recognition of the *Pst* effector AvrPto by the R protein Pto (Melech-Bonfil and Sessa, 2010). Silencing *MAPKKKε* also impaired the HR triggered by the recognition of Avr4 and Avr9 from the fungal pathogen *Cladosporium fulvum* (*Cf*) by Cf4 and Cf9, respectively.

Similar to some other MAPK-cascade components implicated in plant immunity (Yang *et al.*, 2001, del Pozo *et al.*, 2004), the over-expression of MAPKKKε *in planta* results in a pathogen-independent cell death. This response is dependent on

[†] MEK2 = MAPK/ERK kinase 2
[‡] WIPK = wound-induced protein kinase, SIPK = salicylic acid-induced protein kinase
[§] NTF6 = *Nicotiana tabacum* FUS3-like kinase 6
[**] TFT7 = Tomato Fourteen-Three-three protein 7

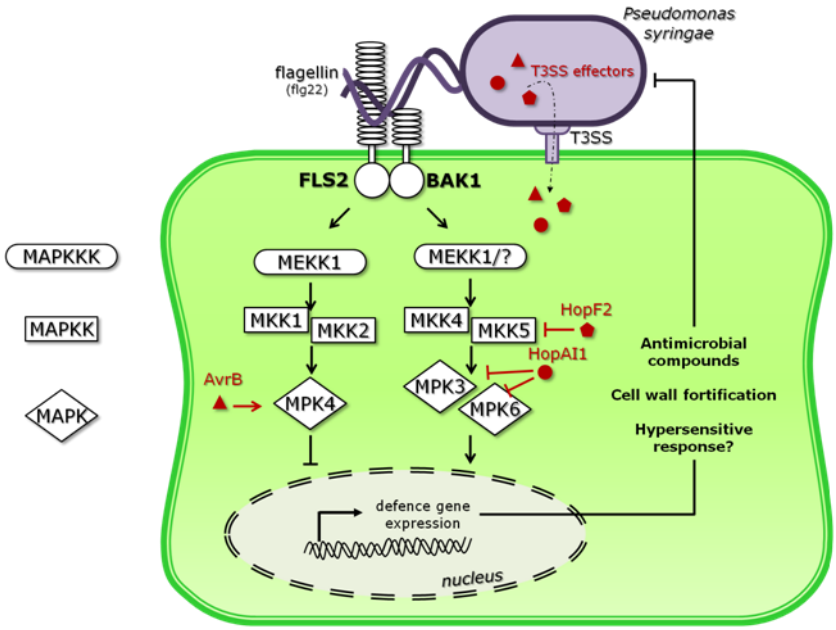

Figure 5.1 MAP kinase cascades involved in PAMP-triggered immunity, are prominent targets of bacterial effectors

Two antagonistically acting MAPK cascades are activated following FLS2-mediated perception of the PAMP-peptide flg22 in *Arabidopsis*. The activity of these cascades triggers a defence response aimed to inhibit growth of invading pathogens. The bacterial phytopathogen *Pseudomonas syringae* injects effector proteins into the plant cytoplasm via it type III secretion system (T3SS) to interfere with this PAMP-triggered immunity (PTI). Three such effectors that specifically target components of MAPK cascades are shown.

the catalytic kinase activity of this protein as it was abolished by substituting the essential lysine in the ATP-binding site with an arginine (K49R).

Epigenetic experiments identified the signalling components downstream of MAPKKKε as MEK2, SIPK and WIPK (Melech-Bonfil and Sessa, 2010). A second MAPKK, SIPKK (SIPK KINASE) was identified as a negative regulator of MAPKKKε-mediated cell death.

As described in Section 4.2.3, *St*MAPKKKε is a multi-domain protein with a catalytic kinase domain at its N-terminus, and a C-terminal domain containing two predicted armadillo (ARM) repeats. Closely related homologs exist in a range of dicots, including cultivated and wild tomato species, *Solanum lycopersicum* and *S. pimpinellifolium*, respectively, and *N. benthamiana*. More distantly related homologs were found in *A. thaliana* and *Brassica napus*.

The most closely related non-plant relatives of MAPKKKε homologs were identified as cell division control (Cdc) proteins from yeast (Jouannic *et al.*, 2001). *Bn*MAPKKKε1 was found to partially complement the *Schizosaccharomyces pombe cdc7* mutant implicating a role in cell division (Jouannic *et al.*, 2001). *At*MAPKKKε1 and *At*MAPKKKε2 were determined to be functionally redundant and required for pollen development (Chaiwongsar *et al.*, 2006). Double mutants had pollen lethality; which together with functional redundancy, limited assessment of their roles in developing or adult plants. However, the observation that both genes were expressed in all tissues (Champion *et al.*, 2004a) suggested that they are likely to play a general role in cellular function rather than a role limited to pollen development (Chaiwongsar *et al.*, 2006). Finally, both tomato and *N. benthamiana* MAPKKKε had been implicated as having a pleiotropic role in growth and development, in addition to immunity (Melech-Bonfil and Sessa, 2010).

The interaction between the catalytic kinase domain of MAPKKKε and PexRD2 raises the possibility that this effector is an inhibitor of this host kinase. For the bacterial phytopathogen *P. syringae*, manipulation of MAPK cascades has emerged as a common strategy for effector-mediated suppression of PTI (see Figure 5.1) (Block *et al.*, 2008, Block and Alfano, 2011, Lindeberg *et al.*, 2012).

For example, the type III secretion system (T3SS)-effector HopAI1 (HRP[††]-dependent outer protein AI1) irreversibly inhibits MPK3 and MPK6 activity via a unique phosphothreonine lyase activity (Zhang *et al.*, 2007). HopF2 also inhibits flg22-triggered immunity (Wang *et al.*, 2010). HopF2 is an ADP-ribosyltransferase that interacts with MKK5, and potentially other MAPKKs. Residues in HopF2 that are critical for either interaction with MKK5, or *in vitro* ADP-ribosylation activity, were also shown to be required for HopF2-mediated PTI-suppression (Wang *et al.*, 2010). Finally, AvrB is a recognised T3SS-effector (Ashfield *et al.*, 1995, Grant *et al.*, 1995, Ashfield *et al.*, 2004), that contributes to virulence in plants lacking cognate R proteins through an association with MPK4 (Cui *et al.*, 2010). AvrB enhances MPK4 phosphorylation and activity which, in turn, negatively regulates plant immunity. The crystal structure of AvrB revealed that it shares features with protein kinases (Desveaux *et al.*, 2007). As such, AvrB may mimic plant MKKs to activate MP4K (Cui *et al.*, 2010), however kinase activity for AvrB has yet to be demonstrated.

To investigate if MAPKKKε represents a genuine virulence target of PexRD2, the involvement of this protein in resistance to *Phytophthora infestans* was assessed using the model plant *N. benthamiana*. The effect of PexRD2 on multiple *in vivo* readouts of MAPKKKε activity was investigated, and the crystal structure of PexRD2 effector domain was interrogated to design mutants that could be used to probe the molecular mechanism of PexRD2 function.

[††] HRP = HYPERSENSITIVE RESPONSE AND PATHOGENECITY

5.2 Results and Discussion

5.2.1 Virus-induced gene silencing (VIGS) – introduction

Following the confirmation of a specific interaction between PexRD2 and MAPKKKε independently using Y2H and *in planta*, VIGS of *MAPKKKε* was used to probe this putative target's role during infection with *P. infestans.* This technique has previously been used to identify other components of the plant immune response against *Phytophthora* including CMPG1 (Bos *et al.*, 2010b), the receptor like kinase SERK3/BAK1 (Chaparro-Garcia *et al.*, 2011), the resistance genes *Rpi-blb1*and *R1* (Brigneti *et al.*, 2004), as well as ten other genes that are highly expressed in potato during the early stages of infection (Du *et al.*, 2013).

VIGS allows investigation of gene function by exploiting the plant's own RNA-mediated antiviral defence mechanism (Lu *et al.*, 2003b). Infection with a wild-type virus, specifically targets the response against the viral genome (Ratcliff *et al.*, 1999, Voinnet, 2001); however, virus-based vectors carrying inserts derived from specific host genes can additionally target the corresponding endogenous mRNA (Burch-Smith *et al.*, 2004, Robertson, 2004). Gene silencing is thought to result from replication of the modified viral genome transiently forming double-stranded RNA (dsRNA) within plant cells. This dsRNA is cleaved by Dicer-like ribonucleases (Blevins *et al.*, 2006), into short interfering RNAs (siRNAs) of 21 - 24 nucleotides in length. These siRNAs guide the RNA-induced silencing complex (RISC) to degrade homologous transcripts (Pantaleo *et al.*, 2007), and 'knock down' gene expression.

The tobacco rattle virus (TRV)-based vectors are the most frequently used for VIGS (Ratcliff *et al.*, 2001, Liu *et al.*, 2002, Valentine *et al.*, 2004). TRV has a bipartite genome and, as such, two different vectors are used: pTRV1, which encodes the replication and movement viral functions while the other; and pTRV2, harbors the coat protein and the sequence used to direct VIGS. Inoculation of *N. benthamiana* with a mixture of *Agrobacterium* strains harbouring each vector results in systemic infection and silencing of homologous target genes.

TRV-based VIGS of MAPKKKε has previously been used to confirm this kinase's involvement in the plant's immune response to bacterial pathogens; as well as in

eliciting the cell death triggered following the recognition of AvrPto, Avr4 and Avr9 by Pto, Cf4 and Cf9 respectively (Melech-Bonfil and Sessa, 2010). A pTRV2 derivative, which included a 411-bp fragment (nucleotides 898 – 1308) from the tomato MAPKKKε cDNA, hereafter TRV:5'MAPKKKε, was obtained from the lab of Professor Guido Sessa (Tel-Aviv University, Tel-Aviv, Israel). To confirm that any phenotypes observed resulted from the silencing of MAPKKKε, a second pTRV2 derivative including a 348-bp fragment (nucleotides 3086 – 3433) from the *Nb*MAPKKKε2 cDNA, hereafter TRV:3'MAPKKKε, was provided by Dr. Hazel McLellan (JHI), along with a pTRV2 derivative encoding a 356-bp fragment of GFP, TRV:GFP, to be used as a negative control, and pTRV1.

5.2.2 Silencing *MAPKKKε* increases susceptibility to *Phytophthora infestans*

N. benthamiana plants were infiltrated with *Agrobacterium* harbouring silencing constructs as described in Section 2.9.6. As observed previously, plants silenced with either fragment of *MAPKKKε* showed a growth inhibition phenotype when compared to the *'GFP'*-silenced control plants. Furthermore, this phenotype was more severe for plants silenced with TRV:3'MAPKKKε – which showed reduced stem growth and smaller, thicker leaves with a darker green pigmentation – compared to those silenced with TRV:5'MAPKKKε (Figure 5.2, and see Section 5.2.9 for quantification of growth defects).

Detached leaves from silenced plants were subsequently infected with *Phytophthora infestans* zoospores as described in Section 2.9.7. Infection assays were conducted with *P. infestans* 88069td, a transgenic isolate of 88069 that expresses tdTomato, a tandem-dimer red fluorescent protein (RFP). The use of this fluorescent derivative strain allowed the observation of the initial biotrophic stages of infection by fluorescence microscopy. The development of necrotic lesions during the necrotrophic stage and sporulation were scored visually and a lesion diameter quantified using image analysis software.

Figure 5.2 Growth inhibition in plants silenced for *MAPKKKε*

Phenotype of *Nicotiana benthamiana* plants 14 days after treatment with either TRV:GFP control, or TRV:5'MAPKKKε, or TRV:3'MAPKKKε. See Section 5.2.9 for quantification of growth defects.

N. benthamiana plants silenced with either fragment of *MAPKKKε* showed increased susceptibility to infection by *P. infestans* 88069td. Fluorescence microscopy repeatedly revealed increased hyphal growth of the pathogen on leaves silenced for *MAPKKKε* that was visible 3 – 4 days post inoculation. The growth of necrotic lesions and progression to sporulation was also accelerated on *MAPKKKε*-silenced plants. Necrotic lesions that developed on leaves silenced with TRV:5'MAPKKKε or TRV:3'MAPKKKε, within the first six days of infection, were significantly larger than those on leaves treated with the TRV:GFP control (Tukey HSD, $P < 0.05$). These results suggest that MAPKKKε is involved in mediating a defence response against *Phytophthora infestans* 88069td that can limit infection by the pathogen.

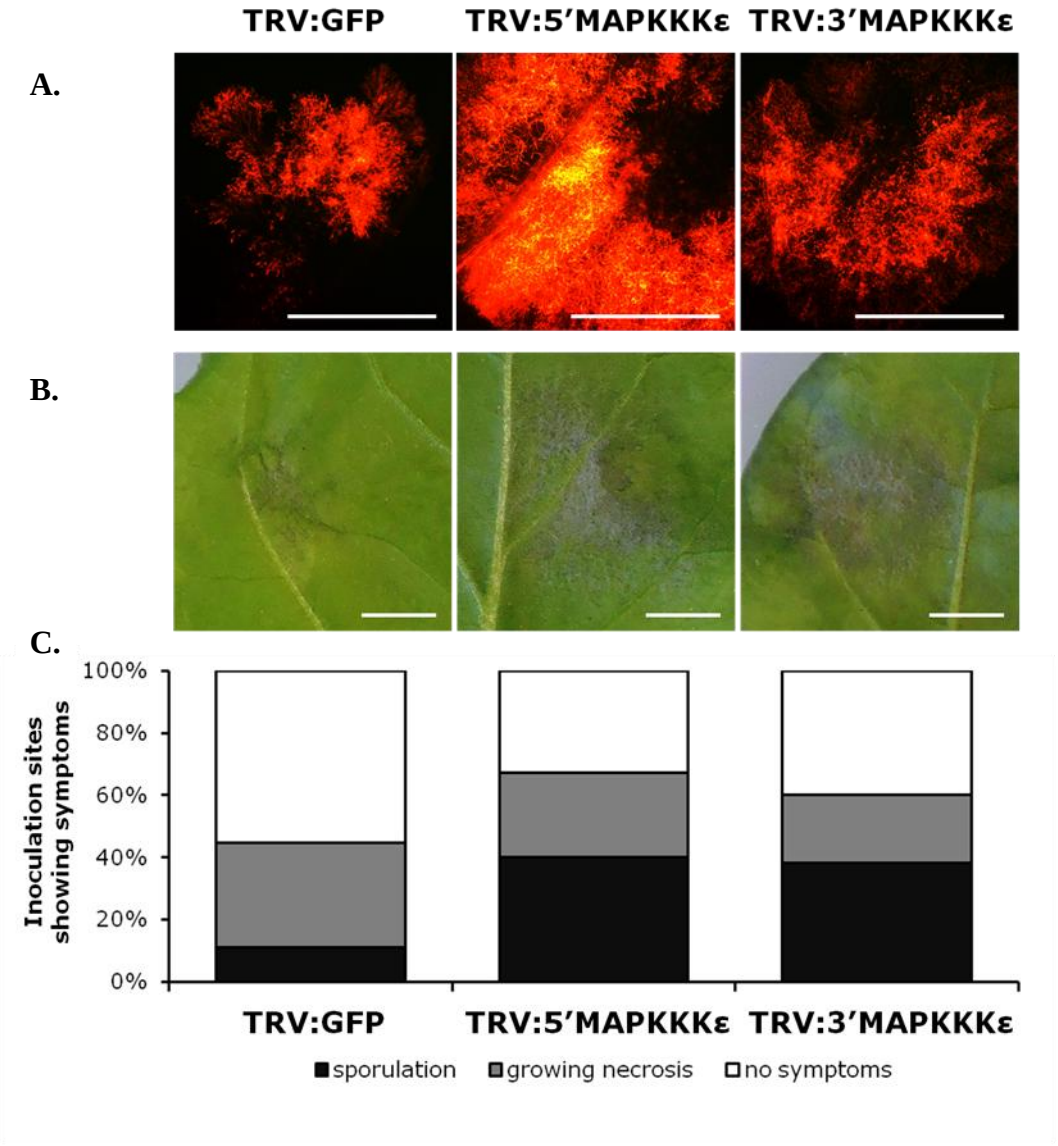

Figure 5.3 Silencing *MAPKKKε* in *N. benthamiana* enhances growth and sporulation of *P. infestans*

(A.) Fluorescence microscopy of red fluorescent *P. infestans* 88069td showing increased hyphal growth on TRV:5'MAPKKKε and TRV:3'MAPKKKε treated plants at 4 days post zoospore inoculation (dpz). **(B.)** White light images of infection sites showing increased necrosis and sporulation on *MAPKKKε*-silenced plants. Images taken 5 dpz. Scale bar = 10 mm. **(C.)** Percentage of inoculation sites showing symptoms at 5 dpz. Results are from at least 50 inoculations per silencing construct.

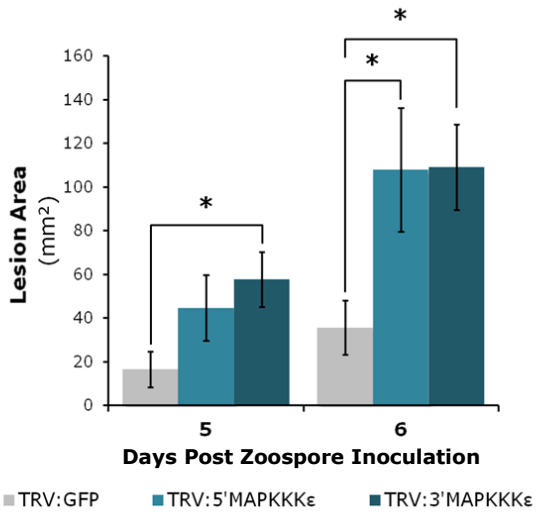

Figure 5.4 Silencing *NbMAPKKKε* increases lesion area of *P. infestans*

Mean lesion area at 5 – 6 days post zoospore inoculation (dpz) for infection with *P. infestans* 88069td. Bars indicate the mean ± SE for 40 inoculations per silencing construct. Asterisks indicate means that are significantly different at a given time point, as determined by Tukey HSD (*, $p<0.05$).

5.2.3 *Testing the target specificity and silencing efficiency of MAPKKKε VIGS constructs*

Note: qRT-PCR analysis was conducted by Dr Hazel McLellan (JHI). The scripts used to search the N. benthamiana *draft genome were written by Dr. Joe Win (TSL). Bioinformatic searches and preliminary analyses of retrieved sequences were conducted with Dr. Joe Win.*

To confirm that the increased susceptibility phenotype observed resulted from a reduction in MAPKKKε expression, the level of silencing in TRV:5'MAPKKKε, TRV:3'MAPKKKε, and TRV:GFP treated plants was assessed by real-time quantitative reverse-transcriptase PCR (qRT-PCR). Successful application of VIGS relies on high target specificity and silencing efficiency, and as such, the potential for off-target silencing of the related MAPKKKα was also assessed. Consistent with observations by Melech-Bonfil and Sessa (2010), qRT-PCR analysis indicated that endogenous transcripts of *NbMAPKKKε* were reduced by approximately 70% in

plants silenced with either TRV:5'MAPKKKε or TRV:3'MAPKKKε. In contrast, the levels of *NbMAPKKKα* were only slightly altered in *MAPKKKε*-silenced plants, suggesting that silencing was specific.

As off-target silencing represents one of the biggest caveats associated with this technique (Xu et al., 2006), analysis of the recently released *N. benthamiana* draft genome (Bombarely et al., 2012) was conducted to identify any bioinformatically predicted off-targets. Since siRNAs guide the RNA-induced silencing complex (RISC) to degrade transcripts (Pantaleo et al., 2007), all 21-nucleotide sequences within the silencing constructs that were predicted to mediate efficient silencing were identified (Section 2.9.6.1). These were then used to find *N. benthamiana* transcripts (henceforth targets) containing sequences with homology to putative efficient siRNAs (henceforth sites). Since mRNAs with only partial complementarity to a siRNA can also be targeted for destruction (Jackson *et al.*, 2003, Haley and Zamore, 2004), the level of mismatch allowed was varied from a zero, meaning perfect complementarity, to five mismatches.

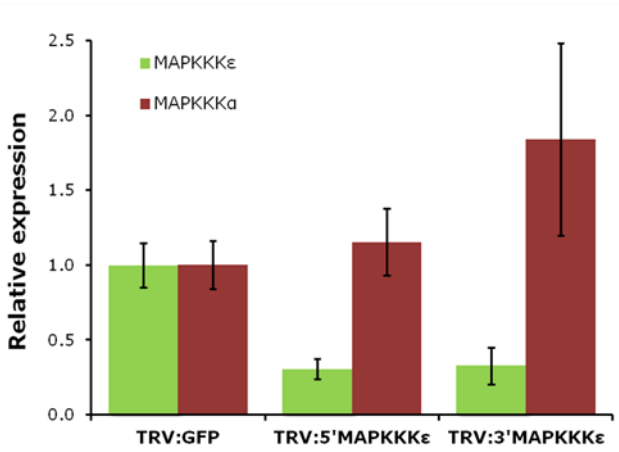

Figure 5.5 Virus-induced gene silencing of *MAPKKKε* in *N. benthamiana* plants is efficient and specific

qRT-PCR analysis of TRV:GFP, TRV:5'MAPKKKε, and TRV:3'MAPKKKε silenced *Nicotiana benthamiana*. The expression of *NbMAPKKKε* and *NbMAPKKKα* in silenced plants was standardised relative to expression of the elongation factor-1 alpha gene (*EF1α*) as an internal reference control (Rotenberg *et al.*, 2006). Values are the average of triplicates ± SE. Experiment was independently repeated with similar results. *Data collected by Dr. Hazel McLellan.*

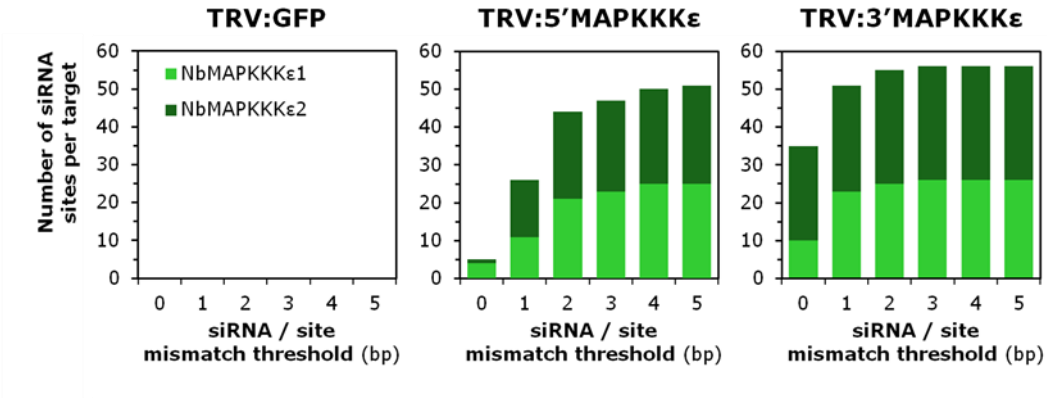

Figure 5.6 Both *MAPKKKε*-silencing constructs contain predicted efficient siRNAs directed against both paralogs of *NbMAPKKKε*

The number of predicted efficient siRNAs from the three TRV constructs used that target sites within either paralog of MAPKKKε as found in the draft *N. benthamiana* genome. Different thresholds of mismatch between the siRNA and site within the transcript are used.

The 356-nt insert in TRV:GFP was predicted to contain 32 putative efficient 21-nt siRNAs, whilst the 411-nt insert in TRV:5'MAPKKKε and the 348-nt insert in TRV:3'MAPKKKε were predicted to contain 43 and 30, respectively. The *N. benthamiana* genome encodes two paralogs of MAPKKKε, *Nb*MAPKKKε1 and the more recently identified *Nb*MAPKKKε2 (Hashimoto *et al.*, 2012), which share 98% DNA and 95% amino acid sequence identity. Unlike TRV:5'MAPKKKε and TRV:3'MAPKKKε, none of the predicted TRV:GFP-derived siRNAs showed any homology to either *MAPKKKε* transcript, even when using the highest level of siRNA/site mismatch threshold tested.

As expected increasing the maximum level of mismatch allowed between the predicted siRNAs and sites in potential target transcripts increased the number of predicted putative off-targets (Figure 5.7). At the maximum level of mismatch tested, the longer TRV:5'MAPKKKε construct has a total of 1431 putative off-targets. The TRV:3'MAPKKKε and TRV:GFP constructs had predicted totals of 581 and 527 putative off-targets, respectively.

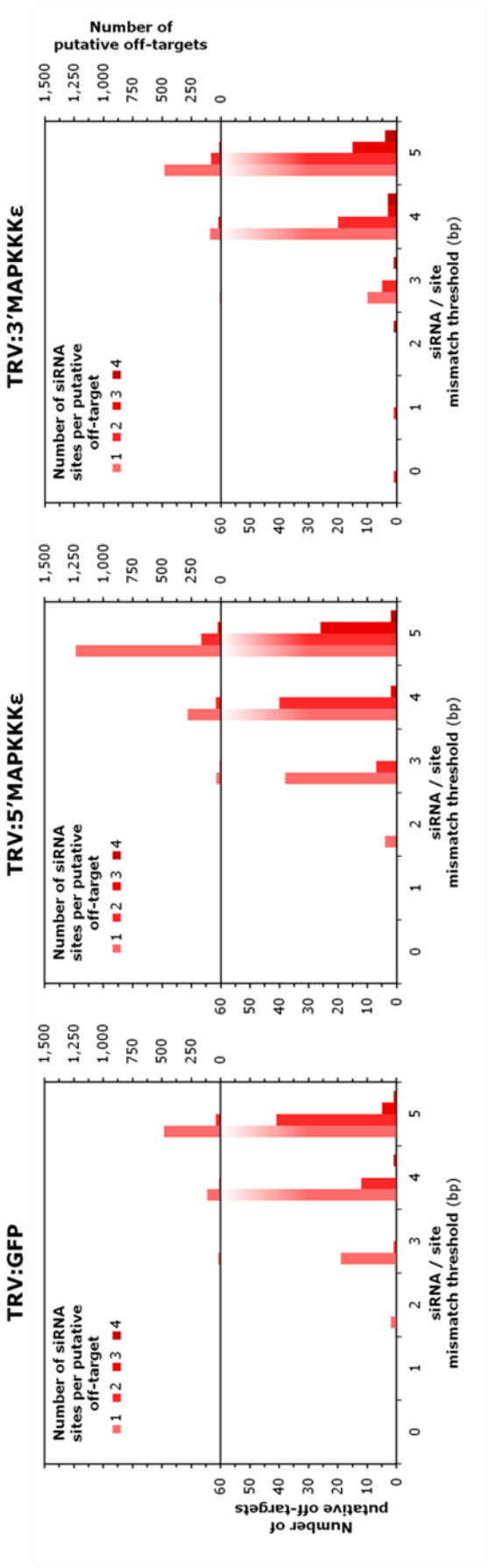

Figure 5.7 Both *MAPKKKε*-silencing constructs also contain predicted efficient siRNAs directed against off-target transcripts

The number of *N. benthamiana* transcripts showing homology to predicted efficient siRNAs from the three TRV constructs, other than the intended *MAPKKKε* paralogs. The number of putative off-targets increases with increased mismatch between the siRNA and sites within the transcript. The number of putative off-targets with multiple siRNA sites also increases with increasing mismatch threshold.

If the analysis is restricted to those targets that show no more than three mismatched base pairs (3 bp) between a predicted siRNA and the target site, TRV:5'MAPKKKε, TRV:3'MAPKKKε and TRV:GFP have predicted totals of 45, 16 and 20 putative off-targets, respectively. Analysis of these 81 putative off-target sequences revealed that they are all unique to their respective silencing constructs (Figure 5.8). Only the two copies of *NbMAPKKKε* are targeted by both TRV:5'MAPKKKε and TRV:3'MAPKKKε, but importantly not TRV:GFP. Together these results indicate that the enhanced susceptibility to *P. infestans*, described above, was likely a result of specific silencing of *MAPKKKε*.

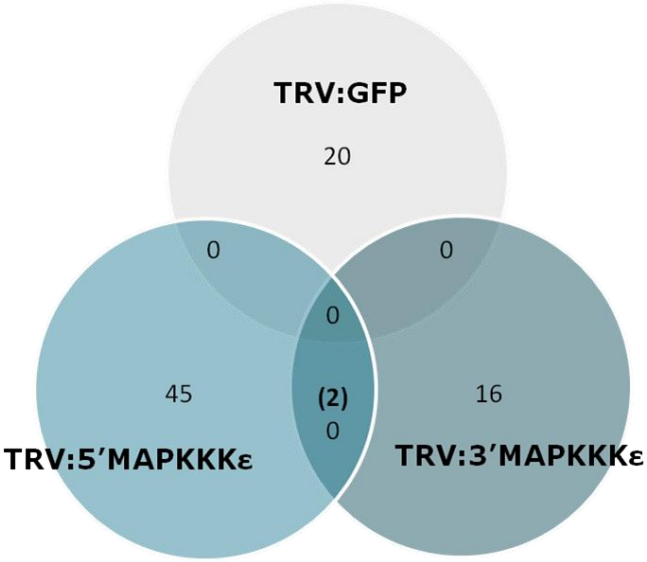

Figure 5.8 No common off-targets are predicted between different TRV constructs using the 3-bp siRNA/site mismatch threshold

Venn diagram showing the number of predicted off-targets in common between the three TRV constructs when analysis is restricted to a maximum of three mismatches between a predicted siRNA and a putative off-target. The number in brackets indicates that the two intended targets (*NbMAPKKKε1* and *NbMAPKKKε2*) are only shared between TRV:5'MAPKKKε and TRV:3'MAPKKKε.

5.2.4 *In planta* transient expression of PexRD2, prior to infection, enhances virulence of *Phytophthora infestans*

The identification of *Nb*MAPKKKε as important component for the plant's immune response against *P. infestans* is consistent with the hypothesis that the effector PexRD2 might function as an inhibitor of this kinase. To test this, the ability of transient expression of PexRD2 *in planta* to phenocopy silencing of *MAPKKKε* during infection assays was tested. This approach is commonly adopted since, although stable transformation of *P. infestans* isolates to over-express or silence specific genes is achievable, it has only been successful in a limited number of research groups (Judelson *et al.*, 1991, Grouffaud *et al.*, 2008, Bos *et al.*, 2010b).

Agroinfiltration was used to transiently express a GFP-fusion of PexRD2 in one half of a leaf, and free GFP (pK7WGF2, empty vector control) in the other half of the same leaf. After 24 h, infiltrated leaves were detached from the plants and infected on both sides of the mid-vein with *P. infestans* 88069 zoospores as described in Section 2.9.7. The growth of necrotic lesions and progression to sporulation were scored as before, see Figure 5.9 A.

Transient expression of PexRD2, prior to zoospore inoculation, enhances infection by *P. infestans* 88069. The percentage of infection sites showing necrosis or sporulation within the first five days of infection was higher for leaf tissue expressing PexRD2 than leaf tissue infiltrated with the vector control (Figure 5.9 B). The mean lesion area at five days post zoospore inoculation (5 dpz) for infection of tissue expressing PexRD2 (251.7 ± 37.5 mm^2) was significantly higher (ANOVA, $P < 0.001$) than for infection of the vector control leaf tissue (83.0 ± 20.4 mm^2) (Figure 5.9 C-D). Conversion of these absolute lesion areas to relative measures revealed that transient expression of PexRD2 *in planta* significantly increased the lesion area, 5.2-fold (± 0.9), relative to infection of the vector control tissue on the same leaf (Tukey HSD, $P < 0.01$, Figure 5.10 A).

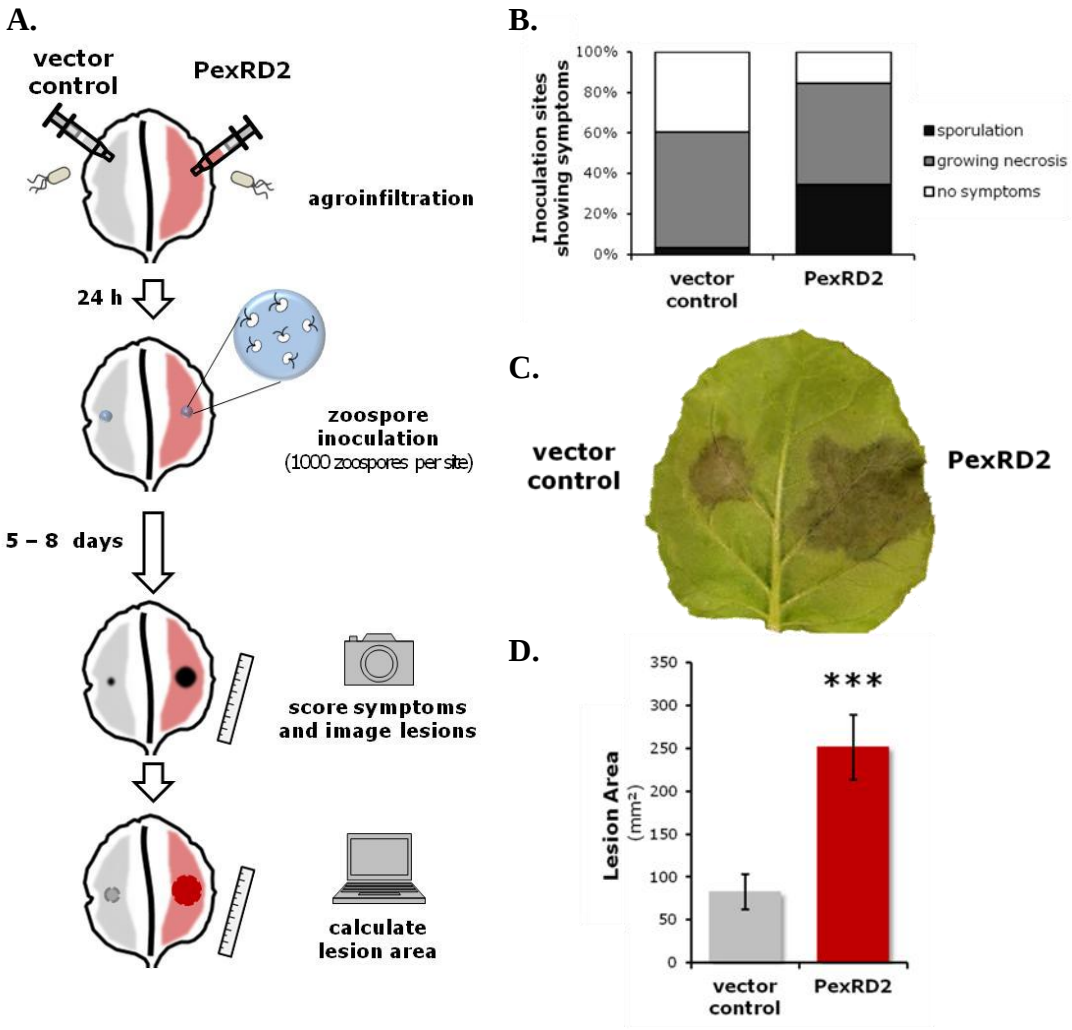

Figure 5.9 Transient expression of PexRD2 in *N. benthamiana* enhances growth and sporulation of *P. infestans*

(A.) *Agrobacterium* strains harbouring *PexRD2* and a vector control are agroinfiltrated into either half of a *N. benthamiana* leaf. After 24 h, leaves are detached and inoculated with *P. infestans* 88069 zoospores (10 µL at 100 zoospores.µL^{-1}) and incubated at room temperature with high humidity. Between 5 – 8 days after zoospore inoculation (dpz), symptoms are scored and leaves images, and the area of each lesion calculated using image analysis software. **(B.)** Percentage of inoculation sites showing symptoms at 5 dpz. Results are from at least 30 inoculations per construct. **(C.)** Representative leaf showing infection of vector control- and *PexRD2*-agroinfiltrated tissue. Image taken 7 dpz. **(D.)** Mean lesion area at 5 dpz for infection with *P. infestans* 88069. Bars indicate the mean ± SE for 51 inoculations, and 17 leaves, per construct. (ANOVA, *** = $P < 0.001$)

This method was also used to test the two PexRD2-like effectors introduced in the previous chapter. These effectors do not interact with MAPKKKε or PM4K1. Nevertheless, as effectors, these proteins are still expected to contribute to pathogen virulence, and qRT-PCR has confirmed that the expression of all three is induced in *P. infestans* 88069 during the early biotrophic stages of infection of potato (Dr. Hazel McLellan (JHI), unpublished data). Conversion of absolute lesion areas to relative measures revealed that transient expression of GFP-fusions of either PexRD2-like effector *in planta* did not significantly enhance the growth of *P. infestans* 88069 (Tukey HSD, P > 0.05 Figure 5.10 A). Western blot analysis confirmed expression of all three GFP-fusion proteins (Figure 5.10 B), and so the lack of a significant enhancement is not due to a lack of expression of the PexRD2-like effectors *in planta*.

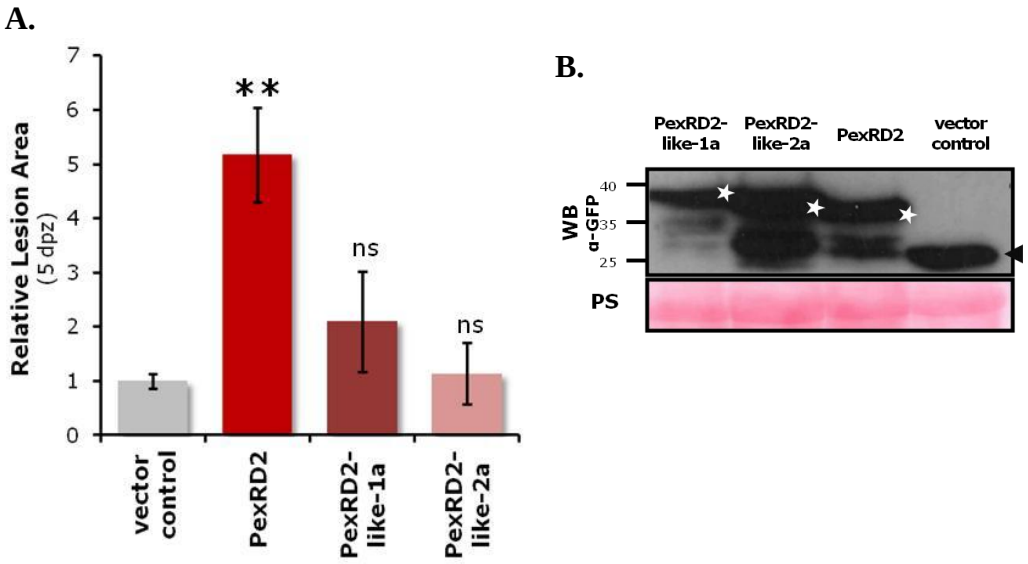

Figure 5.10 PexRD2, but not PexRD2-like effectors, enhances the infection of *N. benthamiana* by *P. infestans* 88069.

(A.) Mean relative lesion area at 5 dpz for infection with *P. infestans* 88069. Relative lesion area is calculated by dividing the lesion area for infection of effector agroinfiltrated tissue, by the lesion area for infection of vector control agroinfiltrated tissue within the same leaf. Each bar represents the mean ± SE of at least 17 leaves per construct. Asterisks indicate means that are significantly different from the standardised value of 1.0 for infection of vector control tissue (Tukey HSD, ** = P < 0.01, ns = not significantly different). **(B.)** Western blot analysis confirming expression levels of GFP-fusions of PexRD2 and PexRD2-like effectors at 3 dpi. White stars indicate expected sizes of full length fusion protein. Black arrow indicates expected size of free GFP. PS indicates Ponceau staining of RuBisCO to confirm protein loading.

These results may be explained in a number of ways. The two PexRD2-like effectors tested might not contribute to the virulence of this specific isolate of the pathogen on this specific host species. Alternatively, and in contrast to PexRD2, the N-terminal GFP fusion might adversely affect these effector's activities *in planta*. It is also possible that the delivery of the endogenous effectors might be carefully regulated to a specific infection stage; or the effectors might require some post-translational modification in the pathogen or plant apoplast prior to translocation to function effectively. Constitutive expression of effectors *in planta* removes this potential for regulation. Finally, the levels of endogenous effector translocated during infection may already be optimal for infection, meaning that no additional effect is observed through further over-expression.

5.2.5 Identification of MAPKKKε-dependent and MAPKKKε-independent cell death responses

Note: Confirmation of the loss of AvrPto/Pto and Avr4/Cf4 triggered hypersensitive response on plants silenced for MAPKKKε was conducted by Dr. Hazel McLellan (JHI). Experiments involving INF1 were conducted at both JHI and JIC.

Gene silencing experiments had previously shown that MAPKKKε was required for mediating the HR following the recognition of the bacterial effector AvrPto by the resistance protein Pto, and the fungal chitin-binding protein Avr4 by the LRR-RLK Cf4 (Melech-Bonfil and Sessa, 2010). This was re-confirmed using transient co-expression assays in *N. benthamiana* plants silenced with the TRV:5'MAPKKKε and TRV:3'MAPKKKε used in this study as described in Section 2.9.8 (Figure 5.11). The role of MAPKKKε as a positive regulator of the plant's immune response against *P. infestans* suggests that it might also mediate a signalling event following the perception of an unknown elicitor from *P. infestans*. As such, a range of cell death events that are associated with *P. infestans* infections were also tested.

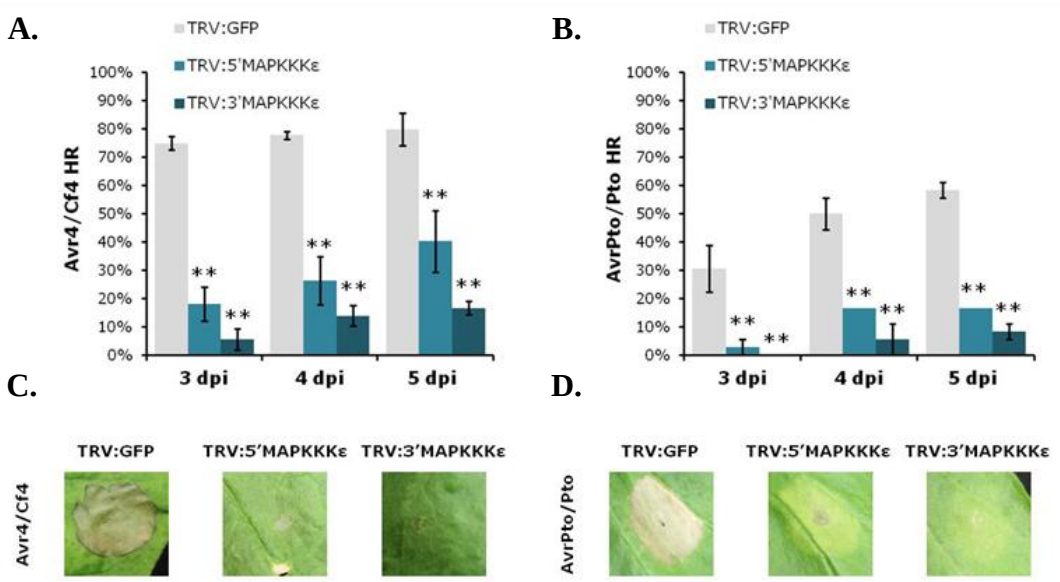

Figure 5.11 Silencing of *MAPKKKε* reduces the hypersensitive response (HR) activated by co-expression of effector protein/R proteins

Mean percentage of agroinfiltration sites in silenced plants with greater than 50% of the agroinfiltrated area showing confluent HR following co-expression of **(A.)** Avr4 and Cf4, or **(B.)** AvrPto and Pto. Bars indicate means ± SE for three plants. Asterisks indicate means that are significantly different from the TRV:GFP control at a given time point, as determined by Tukey HSD (**, P<0.01). Images of representative agroinfiltration sites for each silencing construct following co-expression of **(C.)** Avr4 and Cf4, or **(D.)** AvrPto and Pto, taken at 7 dpi. *Data collected by Dr Hazel McLellan*

In planta transient expression of the secreted oomycete elicitin INF1 results in a cell death response (Kamoun *et al.*, 1998, Kamoun *et al.*, 2003). The level of cell death observed following infiltration with *Agrobacterium* harbouring *INF1* into *N. benthamiana* plants silenced with either TRV:5'MAPKKKε or TRV:3'MAPKKKε, was not significantly different to the level observed for the *TRV:GFP* silencing control plants (Figure 5.12 A-B). This indicates that MAPKKKε is not required for signalling following perception of INF1 leading to the development of INF1-induced cell death (ICD).

Co-expression of the RXLR effector AVR3a^{KI} allele, but not the AVR3a^{EM} allele, with R3a results in HR (Armstrong *et al.*, 2005). Expression of the D2 domain of the translocated effector CRN8 (Haas *et al.*, 2009) also triggers cell death. Both of these cell death responses were also shown to be MAPKKKε-independent; since TRV:5'MAPPPKε-silenced plants showed levels of necrosis that were not

significantly different from those observed in TRV:GFP control plants following the co-expression of AVR3a^{KI} with R3a, or expression of CRN8 (Figure 5.12 C).

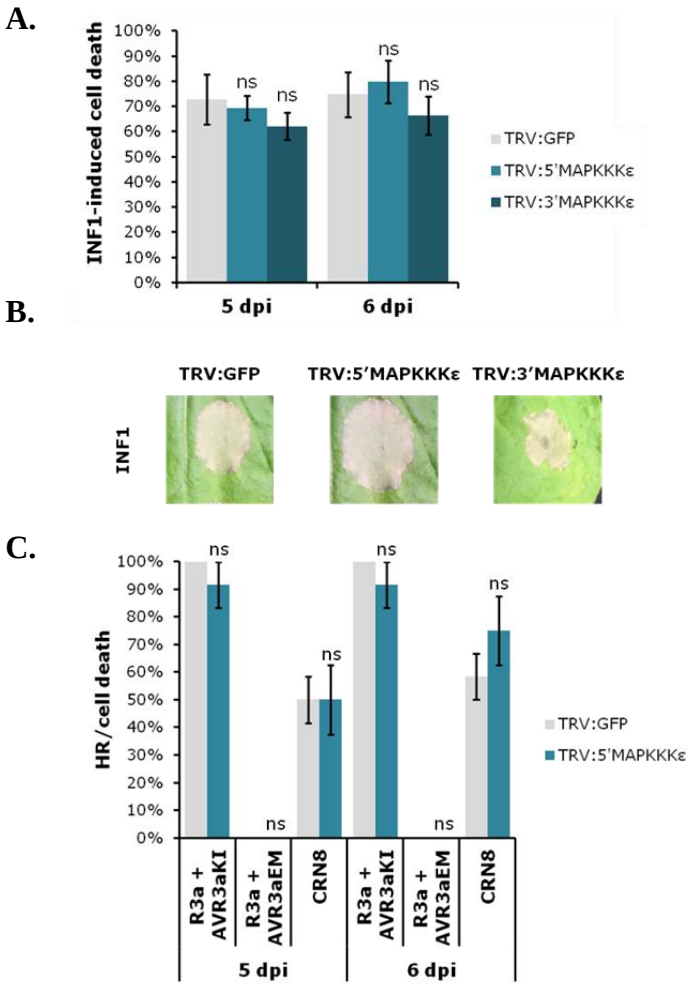

Figure 5.12 MAPKKKε is not required for cell death triggered by INF1, recognition of AVR3a^{KI} by R3a, or CRN8.

(A.) Mean percentage of agroinfiltration sites in silenced plants with greater than 50% of the agroinfiltrated area showing confluent cell death following expression of INF1. Bars indicate means ± SE for at least 10 plants. Values are not significantly different (ns) from the TRV:GFP control, as determined by Tukey HSD (P>0.05). **(B.)** Images of representative agroinfiltration sites for each silencing construct following expression of INF1, taken at 7 dpi. **(C.)** Mean percentage of agroinfiltration sites in silenced plants showing cell death following agroinfiltration of pEAQ-HT:D2 (CRN8) or p35S:R3a with pTRBO:AVR3a^{KI} or pTRBO:AVR3a^{EM}. Bars indicate means ± SE for at least three plants. Values are not significantly different (ns) from the TRV:GFP control, as determined by Tukey HSD (P>0.05).

5.2.5.1 PexRD2-triggered cell death is independent of MAPKKKε

In planta over-expression of PexRD2 from a PVX-based binary vector triggers a weak cell death phenotype (Oh *et al*,. 2009, also see Section 3.1.2). This response was shown to be dose dependent and required the host ubiquitin ligase associated protein SGT1, since VIGS of *SGT1* in *N. benthamiana* suppressed the response. To determine whether PexRD2-triggered cell death was also dependent on MAPKKKε, PexRD2 (residues 21 – 121) or PexRD2 WY-domain (residues 57 – 121[‡‡]) were transiently expressed in *MAPPPKε*-silenced plants. Proteins were expressed with N-terminal FLAG-tags from the TMV-based pTRBO vector (Lindbo, 2007), which is known to deliver high levels of expression in *N. benthamiana*.

In preliminary experiments, pTRBO:PexRD2 and pTRBO:PexRD2-WY were agroinfiltrated into wild-type *N. benthamiana* plants. In parallel, FLAG-tagged RFP and PexRD2-like-2a-WY were expressed by agroinfiltration as additional controls. Transient expression of either PexRD2, or its WY-domain, in *N. benthamiana* plants caused the development of discrete, pale, necrotic lesions in infiltrated tissue. This confirms that the WY-domain of PexRD2 is sufficient to elicit the weak cell death. This response was observable as early as 4 dpi; and was fully developed by 7 dpi (Figure 5.13 A). Unlike the stronger cell death responses of INF1 or CRN8, the weak PexRD2-triggered cell death never achieved confluent necrosis of infiltrated tissue. Neither RFP nor PexRD2-like-2a-WY triggered any observable cell death, confirming that the cell death observed was specific to expression of PexRD2. As seen for other cell death responses, the weak cell death triggered by PexRD2 was also associated with a significant increase in electrolyte leakage, compared to over-expression of the RFP control (two-sample $t = 5.9$, $df = 6$, $P < 0.01$, Figure 5.13 B).

[‡‡] PexRD2 WY-domain was sub-cloned into pTRBO, from pENTR™/D-TOPO®, using a single-tube overlap extension PCR-based epitope tagging strategy with primers 386F, 388F and 389R.

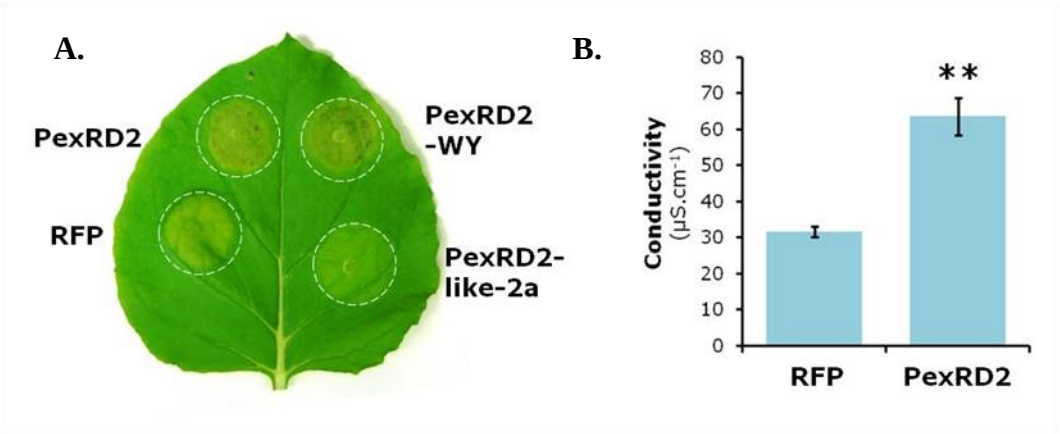

Figure 5.13 PexRD2 induces a weak cell death response *in planta*

(A.) Leaf showing weak cell death activity of PexRD2 or PexRD2 WY-domain as expressed from pTRBO. Image taken at 7 dpi. **(B.)** Quantification of cell death by measuring electrolyte leakage from leaf tissue agroinfiltrated with either *RFP* or *PexRD2*, measured at 4 dpi.Bars represent the mean value ± SE from at least three plants. (t-test, ** = $P < 0.01$).

Following confirmation that pTRBO-driven over-expression was sufficient to trigger a reproducible cell death response, the PexRD2 and RFP constructs described above were agroinfiltrated into *N. benthamiana* plants treated with either TRV:5'MAPKKKε, TRV:3'MAPKKKε, or TRV:GFP. As before, PexRD2 triggered significantly more cell death than the RFP control (Figure 5.14 A), although the percentage of infiltration sites showing PexRD2-triggered cell death at 7 dpi was not significantly different between the *MAPKKKε*-silenced plants and the control plants (Figure 5.14 B). Therefore the previously observed weak cell death activity of PexRD2 is also independent of MAPKKKε. Interestingly, and in contrast to the preliminary experiment with wild-type *N. benthamiana* plants, agroinfiltration of pTRBO:RFP into silenced plants resulted in the occasional development of necrotic lesions. This was not MAPKKKε dependent as it was observed in both control (TRV:GFP) and TRV:5'MAPKKKε-silenced plants, although the level of cell death observed was not statistically significant (Figure 5.14 B).

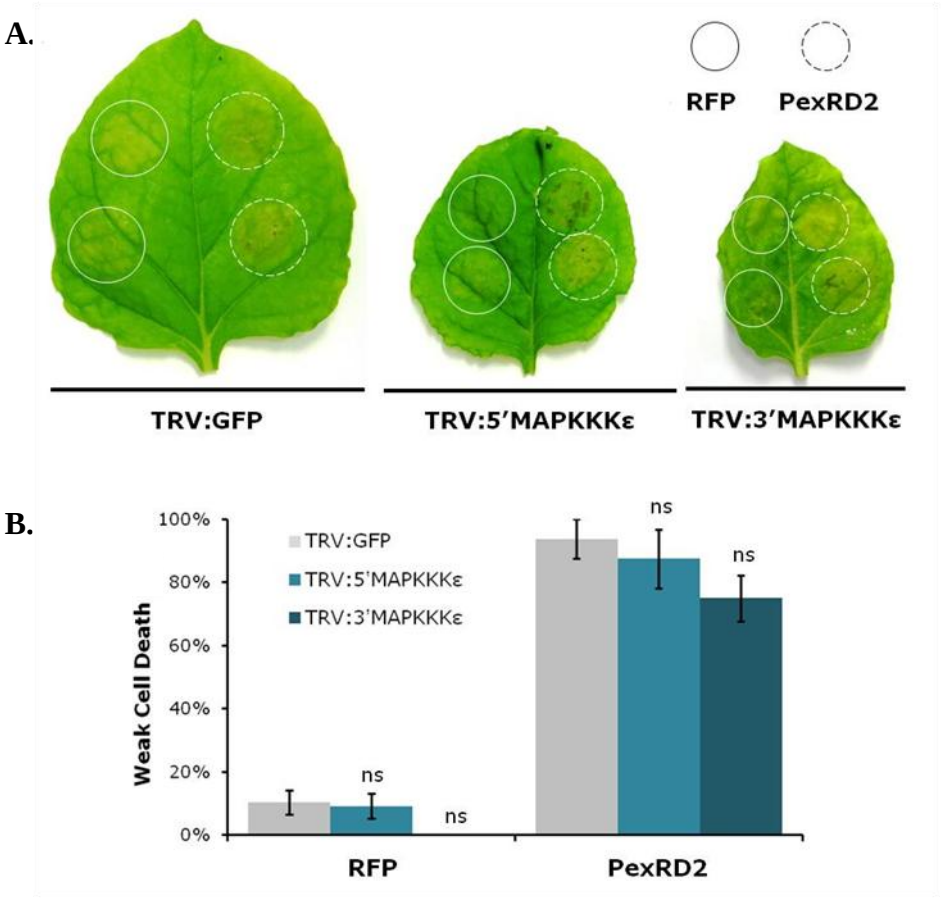

Figure 5.14 PexRD2-trigged cell death is MAPKKKε-independent

(A.) Leaves showing weak cell death activity of PexRD2, but not RFP, in leaves from silenced plant. Images taken at 7 dpi. **(B.)** Mean percentage of agroinfiltration sites in silenced plants displaying weak cell death at 7 dpi. Bars indicate means ± SE for between 3 – 6 plants. Values are not significantly different (ns) from the TRV:GFP control, as determined by Tukey HSD (P>0.05).

5.2.6 *PexRD2 suppresses MAPKKKε-mediated cell death responses*

Note: PexRD2 mediated suppression of AvrPto/Pto triggered hypersensitive response was conducted by Dr. Hazel McLellan (JHI).

To test the hypothesis that the effector PexRD2 functions as an inhibitor of the host kinase MAPKKKε, the ability of PexRD2 to suppress MAPKKKε-dependent cell death responses was assessed. GFP-fusions of PexRD2 were co-expressed in *N. benthamiana*, using co-agroinfiltration, with AvrPto and Pto, or Avr4 and Cf4 (Section 2.9.8). In addition, constructs expressing these pathogen and corresponding host proteins were co-agroinfiltrated with an appropriate empty vector control.

Co-expression of PexRD2 with AvrPto and Pto has a significant effect on the mean level of HR observed between 3 – 5 dpi (ANOVA, $F = 18.83$, $df = 1$, $P < 0.001$)) (Figure 5.15). Furthermore, the mean level of HR observed at 5 dpi for leaves expressing Avr4 and Cf4 with PexRD2 was also significantly reduced (3.6 ± 2.0%) compared to co-agroinfiltration with the empty vector control (60.1 ± 5.1%, (Tukey HSD, $p < 0.01$)) (Figure 5.16 A-B). The HR triggered by the Avr4/Cf4 recognition event was also associated with an increase in electrolyte leakage from leaf tissue (Section 2.9.9), which was also significantly reduced by co-expression with PexRD2 (Tukey HSD, $p < 0.01$, Figure 5.16 C). The ability of PexRD2 to suppress the HR observed following co-expression of both AvrPto and Pto, and Avr4 and Cf4, in *N. benthamiana* supports the hypothesis that PexRD2 can suppress MAPKKKε-dependent cell death responses.

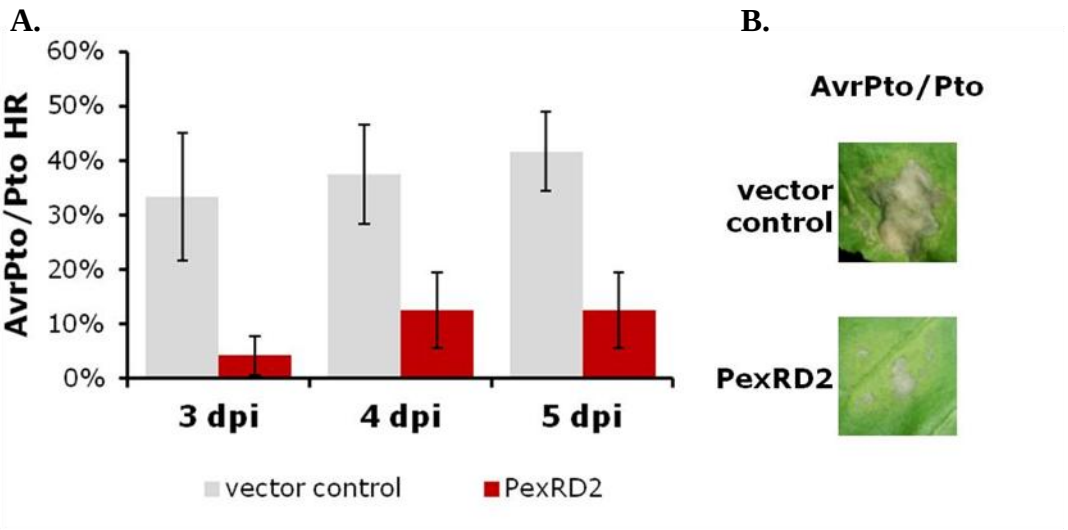

Figure 5.15 PexRD2 suppresses the hypersensitive response (HR) activated by co-expression of AvrPto/Pto

(A.) Mean percentage of agroinfiltration sites with greater than 50% of the agroinfiltrated area showing confluent HR following co-expression of AvrPto/Pto, and PexRD2 or a vector control. Bars indicate means ± SE for four plants. **(B.)** Images of representative agroinfiltration sites taken at 7 dpi. *Data collected by Dr Hazel McLellan*

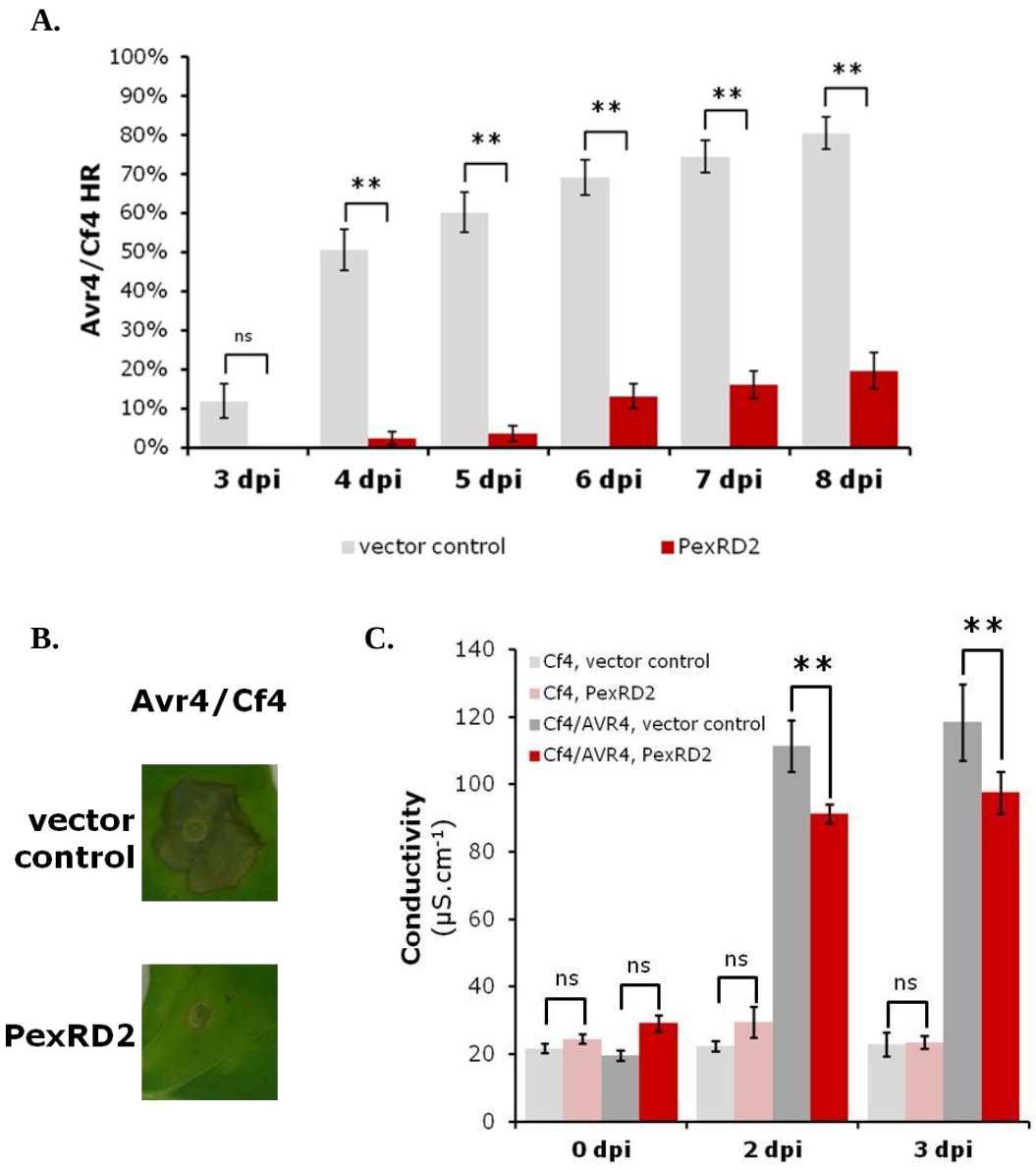

Figure 5.16 PexRD2 suppresses the hypersensitive response (HR) activated by co-expression of Avr4/Cf4

(A.) Mean percentage of agroinfiltration sites with greater than 50% of the agroinfiltrated area showing confluent HR following co-expression of Avr4/Cf4, and PexRD2 or a vector control. Bars indicate means ± SE for at least 20 plants. **(B.)** Images of representative agroinfiltration sites taken at 7 dpi. **(C.)** Quantification of cell death associated with HR by measuring electrolyte leakage from leaf tissue agroinfiltrated as described. Measurements were taken before (0 dpi) or 2 – 3 days post agroinfiltration (2 dpi/3 dpi). Bars represent the mean ± SE from six plants. (Tukey HSD, ** = $P < 0.01$).

To further investigate, PexRD2's function *in planta*, its ability to suppress the MAPKKKε-independent INF1-induced cell death (ICD) and CRN8-triggered cell death was also assessed using the same co-agroinfiltration approach. For either elicitor, no significant difference in the mean level of cell death was observed between the PexRD2 and vector control conditions (Tukey HSD, $P > 0.05$, Figure 5.17). This supports the hypothesis that PexRD2 specifically suppresses MAPKKKε-dependent cell death, and not all cell death responses, consistent with a potential virulence function as a specific inhibitor of this host protein kinase.

The cell death suppression assays described above were all conducted using simultaneous infiltration of the *Agrobacterium* strains (co-agroinfiltration) harbouring *PexRD2* or an empty vector control with other *Agrobacterium* strains

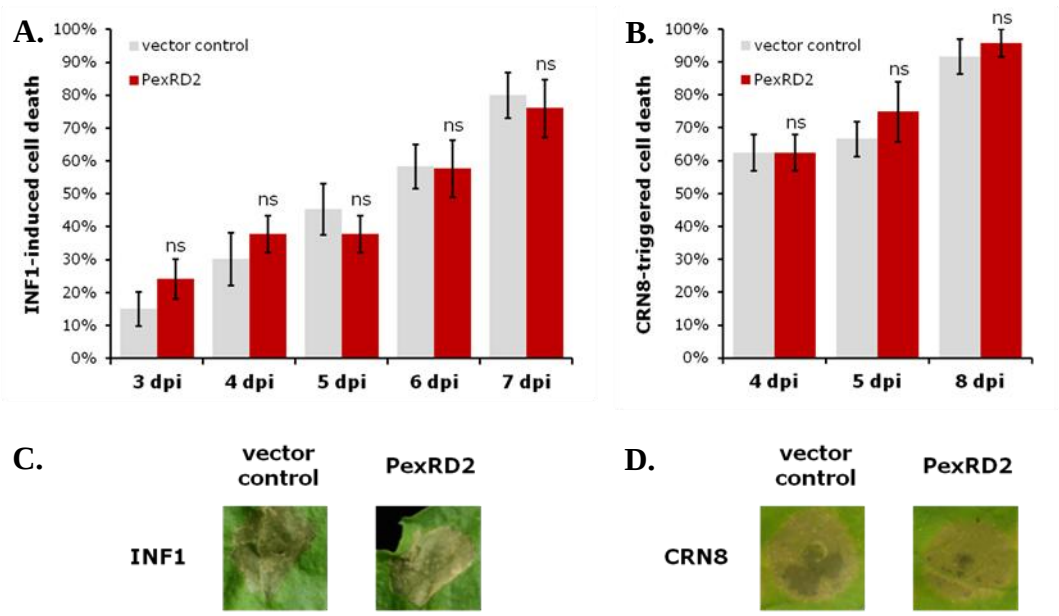

Figure 5.17 PexRD2 does not suppress the cell death triggered by INF1 or CRN8

Mean percentage of agroinfiltration sites with greater than 50% of the agroinfiltrated area showing confluent HR following co-expression of **(A.)** INF1 or **(B.)** CRN8, with PexRD2 or a vector control. Bars indicate means ± SE for at least six plants. Means are not significantly different from the vector control at a given time point, as determined by Tukey HSD ($P>0.05$). Images of representative agroinfiltration sites for co-expression PexRD2 or vector control with **(C.)** INF1 or **(D.)** CRN8. Images taken at 7 - 8 dpi, respectively.

harbouring the relevant cell death elicitors. Agroinfiltration of *PexRD2* or a vector control, prior to agroinfiltration with the cell death elicitors (pre-agroinfiltration) represents an alternative method to test for cell death suppression. Wang *et al.*, (2011) assessed the ability of 169 RXLR effectors from *Phytophthora sojae* for suppression of the programmed cell death (PCR) triggered by the pro-apoptotic mouse protein BAX in *N. benthamiana*. BAX-triggered PCD (BT-PCD) was tested because it physiologically resembles cell death associated with HR. Cell death suppression was assessed using co-agroinfiltration or pre-agroinfiltration assays. Six RXLR effectors could completely suppress BT-PCD when co-agroinfiltrated with the *Agrobacterium* harbouring the *BAX* gene, whilst nine showed a partially suppression of BT-PCD. When infiltrated 12 h prior to *BAX*, 41 and 38 *P. sojae* RXLR effectors could completely or partially suppress BT-PCD, respectively. If a delay of 24 h between infiltrations was used, the number of effectors with cell death suppression activity increased, with 107 effectors consistently suppressing BT-PCD and a further 20 showing partial suppression. Wang *et al.*, (2011) also assessed the ability of 49 of these RXLR effectors for suppression of the INF1-induced cell death (ICD) using pre-agroinfiltration with either a 16 h or 24 h delay between agroinfiltrations. Fifty-one percent of the effectors tested (25 out of 49) were able to suppress ICD when infiltrated prior to agroinfiltration of *INF1*.

Two effectors that were included in Wang *et al.*'s study, and which are interesting with respect to the work described above, are Avh98a and Avh98b. These two effectors were previously introduced as the PexRD2-like effectors PsG_159219 and PsG_159220 respectively (Section 3.2.9, Figures 3.24–25). Agroinfiltration of *Avh98a* 24 h prior to *BAX* could completely suppress BT-PCD, whereas pre-agroinfiltration of *Avh98b* had no effect on BT-PCD. For both effectors, co-agroinfiltration with *BAX* also had no effect on BT-PCD, suggesting that the delay between the two infiltrations was critical for activity. Avh98a was also able to suppress INF1-induced cell death if pre-agroinfiltrated 16 h in advance. Avh98a and Avh98b share 98% sequence identity within their C-terminal effector domains, and share 47% and 46% sequence identity, respectively, with the effector domain of PexRD2.

Since these results were reported to show that PexRD2-like effectors from *P. sojae* were able to suppress a greater range of cell death response if infiltrated prior to the elicitor of the cell death response, similar assays involving PexRD2 were also conducted. The Wang *et al.* study had used PVX-based binary vectors for expression of both the effectors and INF1. As such *Agrobacterium* strains harbouring the PVX-based pGR106:PexRD2 or an appropriate vector control (pGR106:ΔGFP), were either infiltrated either 0 h (co-agroinfiltration) or 16 h (pre-agroinfiltration) prior to *Agrobacterium* harbouring pPGR106:INF1 (Huitema *et al.*, 2005). Co-agroinfiltration of *PexRD2* or the vector control had no effect on INF1-induced cell death, as 100% of infiltrated sites showed confluent cell death at 5 dpi (Figure 5.18). In contrast, pre-agroinfiltration of *PexRD2*, prior to *INF1*, completely suppressed ICD and none of the sites developed necrosis. Of the sites pre-agroinfiltrated with

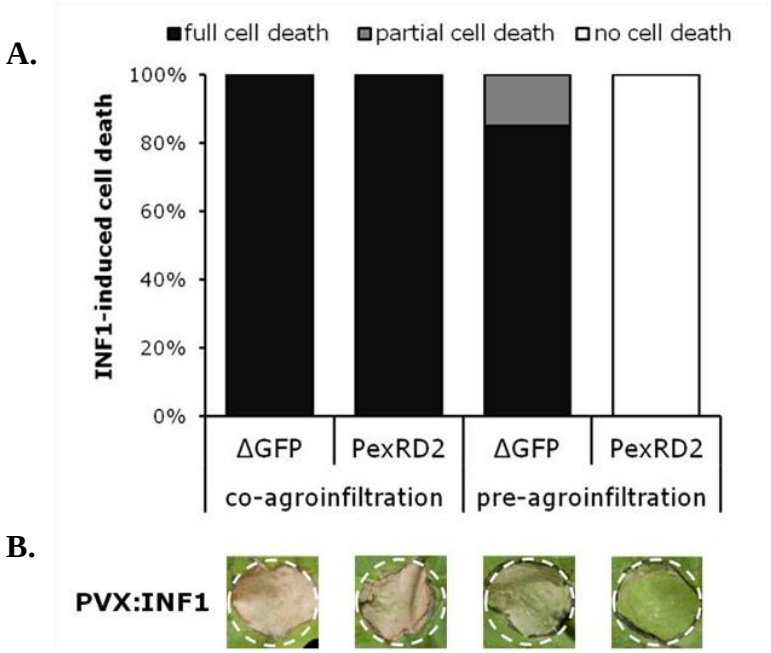

Figure 5.18 Pre-agroinfiltration of *PexRD2* can suppresses the INF1-induced cell death mediated by agroinfiltration

(A.) Percentage of agroinfiltration sites with 100% of the agroinfiltrated area showing confluent cell death (full cell death), or discrete necrotic lesions (partial cell death) following agroinfiltration of pGR106:INF1 either with (co-agroinfiltration) or 16 h after (preagroinfiltration) of PGR106:PexRD2 or a vector control (pGR106:ΔGFP). Data from 20 infiltrations sites per combination, collected at 3 days after agroinfiltration of *INF1* (3 dpi). **(B.)** Images of representative agroinfiltration sites for each treatment taken at 3 dpi.

the vector control, 85% showed confluent cell death, and the remaining 15% showed only discrete necrotic lesions, suggesting partial suppression of ICD.

The rationale for agroinfiltration of RXLR effector prior to elicitins, such as INF1, is that this better reflects the expression patterns of these proteins during an actual infection. Many RXLR effectors show a characteristic increase in expression levels during the early biotrophic stage (Schornack *et al.*, 2009), whilst *INF1* expression is down-regulated during early stages and highest during in late stages of infection when prolific sporulation and tissue necrosis occur (Kamoun *et al.*, 1997). This might explain why a greater number of effectors can demonstrate cell death suppression activity if infiltrated prior to the elicitor. However, one caveat of the pre-agroinfiltration approach, acknowledged by Wang *et al.*, is that the expression level of the second transgene reduces with increasing delay between the first and second infiltrations. This observation can explain why certain effectors can suppress certain cell death responses when pre-agroinfiltrated prior to, but not when co-agroinfiltrated with, the *Agrobacterium* harbouring the elicitor. The reduction in the expression level of the *INF1* transgene, when infiltrated second, could result in a weaker response being triggered which is more easily suppressed by a broader range of effectors, including PexRD2.

To test this hypothesis, the ability of pre-agroinfiltration of PexRD2 to suppress the cell death triggered by direct infiltration of *P. infestans* culture filtrate (provided by Angela Chaparro-Garcia (TSL)) was tested. Crude culture filtrate (CF) was prepared by growing *P. infestans* 88069 in liquid media for 3 months. The media was filtered to remove hyphal tissue, and provide a rich source of secreted elicitins, including the major secreted elicitin of *P. infestans*, INF1. The direct application of secreted protein circumvents the problems associated with transgene expression. Leaf tissue from *N. benthamiana* and *N. tabacum* (tobacco) were agroinfiltrated with GFP-fusions of *PexRD2* or free *GFP* as a negative vector control. A GFP-fusion of the RXLR effector AVR3a^{KI} was used as a positive control, as this effector is known to suppress INF1-induced cell death (Bos *et al.*, 2006, Bos *et al.*, 2009).

Three days after agroinfiltration, to ensure integration of the transgene, a 10-fold dilution series of CF was prepared and infiltrated, alongside a negative control of

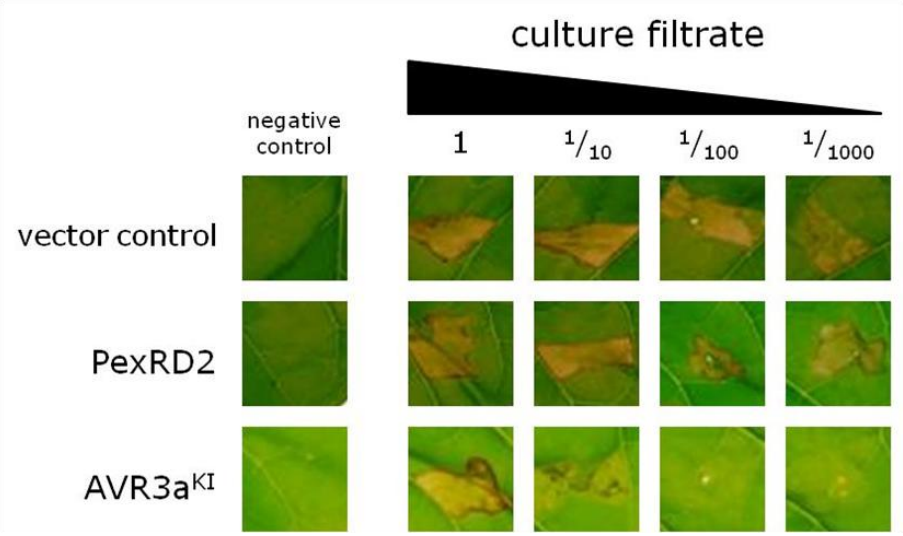

Figure 5.19 Pre-agroinfiltration of *PexRD2* cannot suppresses the induced cell death following infiltration of *P. infestans* culture filtrate

Cell death elicited following infiltration of a 10-fold dilution series of P. infestans culture filtrate into *N. tabacum* leaves, agroinfiltrated 3 days prior with either vector control, PexRD2 or AVR3a^{KI}. Negative control is undiluted sterile culture media. Results are representative of those obtained from three plants.

sterile media, into the pre-agroinfiltrated leaf tissue. CF-induced cell death (CF-ICD) was scored at 7 days post CF-infiltration. Both *N. benthamiana* and *N. tabacum* showed similar responses to CF, although a stronger cell death response was elicited in tobacco. Pre-agroinfiltration of the positive control, *AVR3a^{KI}*, was able to completely suppress CF-ICD at 1000- and 100-fold dilutions, and partially suppress CF-ICD at a 10-fold dilution (Figure 5.19). On the other hand, the same dilutions of CF elicited a clear cell death response in both *PexRD2* and vector control infiltrated tissue. These results support the conclusion that, unlike AVR3a, PexRD2 cannot suppress the MAPKKKε-independent cell death triggered by the elicitin INF1 meaning that the previous observation of cell death suppression if *PexRD2* was pre-agroinfiltrated 16 h prior to *INF1* is potentially an artefact of the experimental approach. However, the use of a crude culture filtrate, and not purified INF1 elicitin, means that this would require further investigation.

The experiments described above raise a number of questions about the current methodology used to assess cell death suppression activity of effectors. In particular,

caution must be taken when comparing conclusions based on co-agroinfiltration versus pre-agroinfiltration of the effector in question. Wherever possible the expression levels of elicitors in suppressed and non-suppressed conditions should be determined to ensure no obvious differences that could explain the results. Furthermore, where extracellular recognition of elicitors occurs, the use of culture filtrates or purified protein provides an alternative to the pre-agroinfiltration approach which may provide more reliable results.

5.2.7 *PexRD2 specifically inhibits MAPKKKε-triggered cell death*

Similar to some other MAPK-cascade components (Yang *et al.*, 2001, del Pozo *et al.*, 2004), the over-expression of MAPKKKε *in planta* results in a pathogen-independent cell death response (Melech-Bonfil and Sessa, 2010). Over-expression (OE) of either full length or the catalytic kinase domain (KD) of the tomato MAPKKKε resulted in a strong cell death response. This response was shown to be dependent on the catalytic kinase activity of this protein since the substitution of the essential lysine in the ATP-binding site with an arginine (K49R) abolished this response. This pathogen-independent cell death can be considered a proxy for a MAPKKKε-mediated HR, and the ability of PexRD2 to suppress MAPKKKε-OE-triggered cell death was assessed *in planta*. The wild-type and kinase-inactive mutant of the tomato MAPKKKε KD, both cloned into the pER8 binary vector (Zuo *et al.*, 2000), were obtained from lab of Professor Guido Sessa (Tel-Aviv University, Tel-Aviv, Israel). These constructs allow transient expression of a C-terminal double haemagglutinin (2xHA) epitope-tag; and under the control of an estradiol inducible promoter (Melech-Bonfil and Sessa, 2010). A GFP-fusion of PexRD2 or free GFP (vector control) was co-expressed, via co-agroinfiltration in *N. benthamiana*, with HA-epitope-tagged *Sl*MAPKKKε KD (*Sl*KD$\varepsilon_{1\text{-}332}$, residues 1 – 332) (Section 2.9.8).

Two days after agroinfiltration, the expression of *Sl*KDε$_{1-332}$ was induced by treatment of infiltrated tissue with 10 µM β-estradiol. The development of MAPKKKε KD-triggered cell death started at 2 days post estradiol treatment (dpt) was scored up to 7 dpt (Figure 5.20 A-B). The mean level of MAPKKKε KD-triggered cell death observed 7 dpt in *PexRD2* co-agroinfiltrated conditions was significantly reduced (6.3 ± 2.9%) compared to co-agroinfiltration with the empty vector control (78.6 ± 4.1%, (two-sample t = 14.3, df = 36, P < 0.001)). Western blot analysis confirmed that MAPKKKε KD accumulated to similar levels in the presence or absence of PexRD2, indicating loss of cell death is not due to loss of expression (Figure 5.20 C).

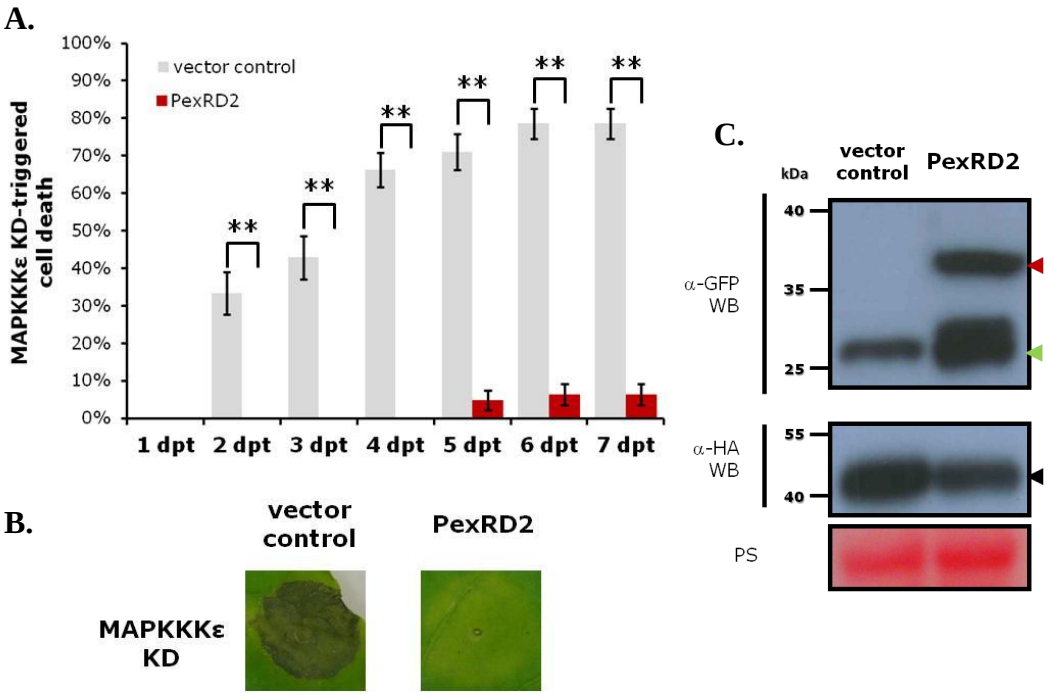

Figure 5.20 PexRD2 suppresses the cell death triggered by over-expression of MAPKKKε kinase domain (KD)

(A.) Mean percentage of agroinfiltration sites with greater than 50% of the agroinfiltrated area showing confluent cell death, follwing treatment with β-estradiol at 2 days post agroinfiltration of PexRD2 or a vector control with *Sl*MAPKKKε KD. Quantification of cell death at 1 – 7 days post estradiol treatment (dpt) to induce kinase expression. Bars indicate means ± SE for at least 20 plants. (Tukey HSD, ** = P < 0.01). **(B.)** Images of representative agroinfiltration sites taken at 7 dpt. **(C.)** Western blot confirming expression of HA-tagged *Sl*MAPKKKε KD (black triangle) in the presence of PexRD2 (red triangle). The green triangle indicates the expected size of free GFP. PS indicates Ponceau staining of RuBisCO to confirm protein loading.

Note: The sub-cloning of potato and Arabidopsis *MAPKKKε kinase domains in the pER8 derivative vector, pERCH, was conducted by Dr. Richard Hughes (JIC)*

To confirm that the cell death suppression activity of PexRD2 is specific to MAPKKKε-mediated cell death, the effect of over-expression the kinase domains from the potato and an *Arabidopsis* homolog in the presence and absence of PexRD2 was also assessed. Two different potato MAPKKKε truncations both containing the kinase domain were tested. *St*KDε$_{1-332}$ (residues 1 - 332) is a portion of the potato protein that corresponds to the region of the tomato homolog previously used for *in planta* expression. *St*KDε$_{1-300}$ (residues 1 - 300) corresponds to the MAPKKKε-N2 truncation that showed the strongest activation of reporter genes in Y2H suggesting a robust protein-protein interaction. The kinase domain of *At*MAPKKKε1 (*At*KDε$_{1-300}$) was also included in the analysis. DNA sequences for all three kinase domains were ligated into XhoI/PacI double digested derivative of the pER8 vector, pERCH (pER8 with C-terminal HA-tag, see Section 2.4.8.6). The three new constructs were transiently expressed in *N. benthamiana* using agroinfiltration together with PexRD2 or an empty vector control as before. The previously described *Sl*KDε$_{1-332}$ and *Sl*KDε$_{1-332}^{K49R}$ expressing constructs were also included as appropriate positive and negative controls, respectively.

At 7 dpt, all four active kinases were capable of triggering cell death when co-agroinfiltrated with the vector control; and no significant differences were observed for the level of cell death triggered (Tukey HSD, $P > 0.05$) (Figure 5.21). Co-expression of PexRD2 with any of the MAPKKKε KD homologs caused a complete inhibition of this cell death (Tukey HSD, $P < 0.01$). Consistent with published results no cell death was observed following OE of the kinase inactive *Sl*KDε$_{1-332}^{K49R}$.

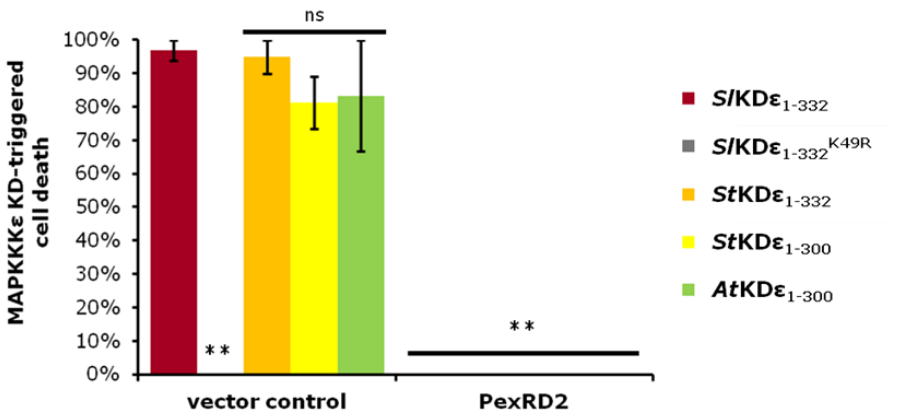

Figure 5.21 PexRD2 suppresses the cell death triggered by over-expression of MAPKKKε kinase domains (KD) from potato and *Arabidopsis* orthologs.

Mean percentage of agroinfiltration sites with greater than 50% of the agroinfiltrated area showing confluent cell death, following treatment with β-estradiol at 2 days post agroinfiltration. PexRD2 or a vector control were co-agroinfiltrated with wild-type *Sl*MAPKKKε KD (*Sl*KDε$_{1-332}$), catalytically inactive *Sl*MAPKKKε KD (*Sl*KDε$_{1-332}^{K49R}$), two potato MAPKKKε KD constructs (*St*KDε$_{1-332}$ and *St*KDε$_{1-300}$), and the *Arabidopsis* ortholog KD (*At*KDε$_{1-300}$). Quantification of cell death at 7 days post estradiol treatment (dpt). Bars indicate means ± SE for at least three plants. Asterisks indicate values that are significantly different from the *Sl*KDε$_{1-332}$/vector control condition (Tukey HSD, ** = $P < 0.01$).

To further test the specificity of the cell death suppression activity of PexRD2, its ability to suppress cell death triggered by the over-expression of other MAPK cascade components was also tested. The over-expression of a catalytically active kinase domain of a second tomato MAPKKK, MAPKKKα, also triggers a cell death *in planta* (del Pozo *et al.*, 2004). In similarity with MAPKKKε, MAPKKKα signals as part of a MAPK-cascade, involving the downstream MAPKK, MEK2 (or MKK2). Over-expression of a constitutively active mutant of MEK2, MEK2^{DD}, where Thr215 and Ser221 in the activation loop have been substituted with phosphomimetic aspartates, also induces a HR-like cell death (Oh and Martin, 2011). Over-expression of *Nt*MEK2^{DD} induces expression of defence genes, and generation of nitric oxide and reactive oxygen species (Yang *et al.*, 2001, Liu *et al.*, 2007). These responses are preceded by the MEK2-mediated activation of endogenous WIPK and SIPK (Yang *et al.*, 2001). Interestingly, transgenic potato plants carrying MEK2^{DD} driven by a pathogen-inducible promoter show enhanced resistance to *Phytophthora infestans* (Yamamizo *et al.*, 2006).

The effect of co-expression of PexRD2 on *Sl*MAPKKKα KD-triggered and *Sl*MEK2^{DD}-triggered cell death was tested as before. PexRD2 or an appropriate empty vector control was co-agroinfiltrated in *N. benthamiana*, with double HA-epitope-tagged versions of the two kinases, under the control of estradiol inducible promoters (provided by Professor Gregory Martin (BTI)). Two days after agroinfiltration the expression of the protein kinases was induced with 10 μM β-estradiol, and the development of cell death was scored up to 7 dpt. Consistent with previous observations by Melech-Bonfil and Sessa (2010), MAPKKKα KD-triggered and MEK2^{DD}-triggered cell death developed faster than that triggered by MAPKKKε. For both kinases, cell death was observable at the earliest time-point (1 dpt), and 100% of infiltrated sites showed full cell death at 4 dpt and 3 dpt respectively (Figure 5.22 A-B). No significant difference was observed in the mean level of cell death observed in *PexRD2* co-agroinfiltrated compared to empty vector control co-agroinfiltration with the for either MAPKKKα KD or MEK2^{DD}.

These results are consistent with PexRD2 interacting with MAPKKKε homologs to function as a specific inhibitor of MAPKKKε-mediated cell death responses at the MAPKKK level of the signalling cascade.

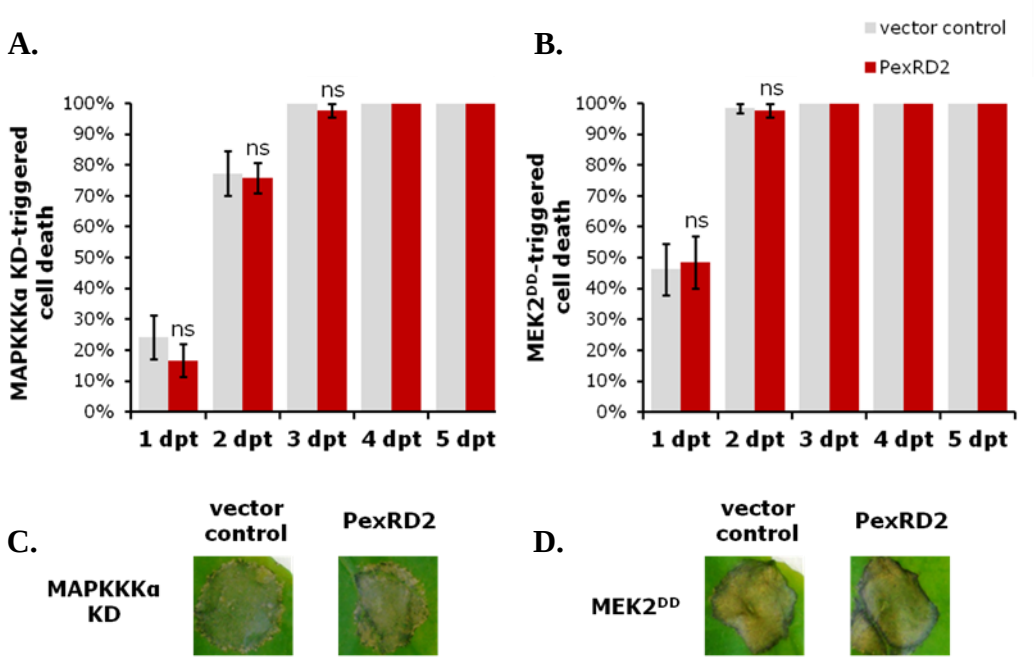

Figure 5.22 PexRD2 cannot suppress the cell death triggered by over-expression of MAPKKKα KD or a constitutively active mutant of MEK2 (MEK2^{DD})

(A.) Mean percentage of agroinfiltration sites with greater than 50% of the agroinfiltrated area showing confluent cell death, follwing treatment with β-estradiol at 2 days post agroinfiltration of PexRD2 or a vector control with *Sl*MAPKKKα KD or MEK2^{DD}. Quantification of cell death at 1 – 5 days post estradiol treatment (dpt) to induce kinase expression. Bars indicate means ± SE for at least 10 plants. (Tukey HSD, P> 0.05). **(B.)** Images of representative agroinfiltration sites taken at 7 dpt.

5.2.8 *PexRD2 inhibits MAPKKKε-mediated activation of MAPK*

To determine if PexRD2 could inhibit other MAPKKKε-mediated responses prior to the development of macroscopic cell death, the phosphorylation of downstream signalling components following MAPKKKε over-expression was assessed; first in the absence, and subsequently in the presence, of PexRD2.

Phosphorylation and activation of the MAPKs, WIPK and SIPK, is known to precede the HR-like cell death and defence gene induction triggered by over-expression of the constitutively active MEK2^{DD} (Yang *et al.*, 2001). Epigenetic experiments have implicated MEK2, SIPK and WIPK as the downstream components of the MAPKKKε signalling cascade, as they are required for MAPKKKε-OE-triggered cell death (Melech-Bonfil and Sessa, 2010). As such the

phosphorylation of the endogenous WIPK and/or SIPK represents a potential surrogate measure for MAPKKKε activity *in vivo*. MAPKs are activated following phosphorylation of threonine and tyrosine residues within the TEY motif in their activation loops. As such their activation can be detected using phosphospecific antibodies that cross react with only the dually phosphorylated pTEpY motif (anti-pTEpY) (Segonzac *et al.*, 2011).

To determine if MAPK activation could be detected following MAPKKKε KD over-expression in *N. benthamiana*, leaf tissue was agroinfiltrated with *MAPKKKε KD* or the catalytically inactive mutant, *MAPKKKε KD*^{K49R}. Expression of the kinases was induced by treatment with estradiol at 48 hpi (0 hpt). Leaf disks from infiltrated tissue were collected at 0, 6, and 24 hpt.

Endogenous MAPK activation was detected by western-blot analysis as described by Segonzac *et al.*, (2011) and in Section 2.9.10. Estradiol-induced expression of MAPKKKε kinase domains was confirmed using an anti-HA antibody. Consistent with previous experiments in *N. benthamaiana* (Segonzac *et al.*, 2011), a single band between 40 – 55 kDa was detected with anti-pTEpY antibody. This band was detectable at both 6 and 24 hpt for tissue expressing MAPKKKε KD, but not the catalytically inactive MAPKKKε KD^{K49R}, consistent with MAPK activation occurring after MAPKKKε KD over-expression and preceding the development of MAPKKKε-OE-triggered cell death (Figure 5.23 A).

To confirm that the band detected corresponded to activated endogenous SIPK or WIPK, *N. benthamiana* leaf disks were treated with peptide corresponding to the epitope of the bacterial PAMP flagellin, flg22. Recognition of flg22 by FLS2 is also known to trigger activation of SIPK and WIPK (Segonzac *et al.*, 2011). In parallel, *N. benthamiana* leaf disks were treated with a 100-fold dilution of *P. infestans* culture filtrate, which contains the oomycete PAMP-like elictin INF1. INF1-induced cell death is also known to involve signalling through MAPK (Asai *et al.*, 2008). Treatment with either flg22 or diluted *P. infestans* culture filtrate also resulted in detection of a single band of 40 – 55 kDa using the anti-pTEpY antibody (Figure 5.23 B), confirming that signal detected is likely the result of detection of activate SIPK or WIPK.

To determine if PexRD2 can inhibit MAPKKKε-mediated activation of MAPK in *N. benthamiana*, leaf tissue was agroinfiltrated with *MAPKKKε KD,* either alone or co-agroinfiltrated with *Agrobacterium* expressing a GFP-fusion of PexRD2 or a free GFP control. As before, expression of the kinase was induced by treatment with β-estradiol, and leaf disks were collected at 0, 6, and 24 hpt. For tissue infiltrated with MAPKKKε alone or co-agroinfiltrated with the GFP control, western blot analysis revealed clear bands corresponding to activated MAPKs detected at both 6 and 24 hpt. Co-agroinfiltration with PexRD2 dramatically reduced the signal observed, consistent with reduced MAPKKKε-mediated activation of MAPK in the presence of PexRD2 (Figure 5.23 C). Anti-GFP and anti-HA western blot analysis confirmed expression of GFP-PexRD2 or free GFP, and induction of MAPPKKKε KD, respectively. These results confirm that PexRD2 can inhibit the MAPKKKε-mediated phosphorylation of downstream signalling components that occur prior to the onset of macroscopic cell death.

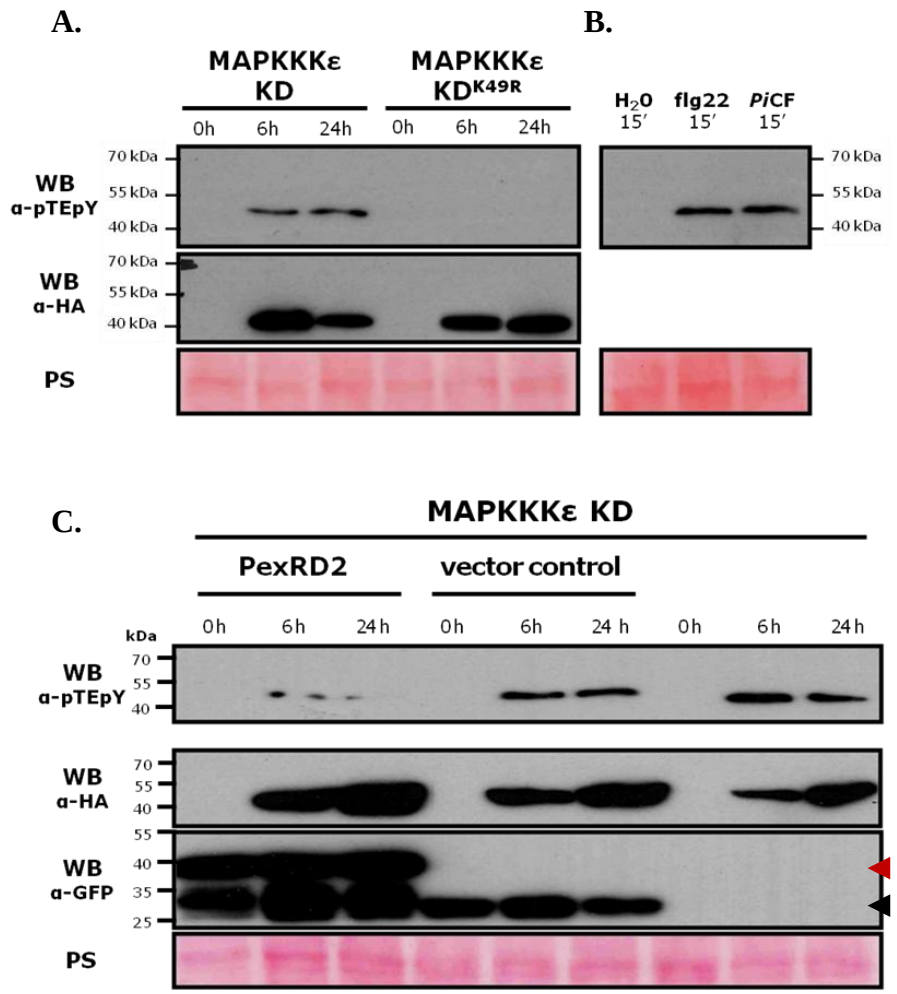

Figure 5.23 Over-expression of MAPKKKε kinase domain (KD) triggers activation of MAPKs, that is suppressed by co-expression with PexRD2

(A.) Western blot showing that over-expression of *Sl*MAPKKKε KD in *N. benthamaina*, but not the catalytically inactive mutant *Sl*MAPKKKε KD^{K49R}, triggers phosphorylation of MAPKs as detected with the phosphopeptide-specific anti-pTEpY antibody. **(B.)** The same size band is detectable following treatment of *N. benthamaina*, leaf disks with 100 nM flg22 peptide or 100-fold diluted *P. infestans* culture filtrate (PiCF) for 15 minutes. **(C.)** Co-expression of PexRD2, but not the vector control (pK7WGF2) reduces levels of phosphorylated MAPKs following inducation of MAPKKKε KD expression. Anti-HA western blot confirms induction of kinase expression. Anti-GFP western blot confirms expression of PexRD2 fusion protein (red arrow) and free GFP (black arrow). PS indicates Ponceau staining of RuBisCO to confirm protein loading.

5.2.9 *PexRD2 inhibits cell expansion* in planta

The results described above indicate that PexRD2 can inhibit MAPKKKε-mediated signalling in plant immunity. However, MAPKKKε has been implicated as having pleiotropic roles in both plant immunity and development. Therefore, the effect of PexRD2 on plant development was also assessed.

VIGS of MAPKKKε in *N. benthamiana* and tomato causes an obvious growth inhibition phenotype (Melech-Bonfil and Sessa, 2010). Growth is the product of cell division and expansion, and reduced growth can therefore result from a reduction in cell number, cell size or both. Although the *mapkkkε-1;mapkkkε-2* double-mutant in *Arabidopsis* causes pollen lethality, use of an ethanol-inducible promoter construct rescued this lethal phenotype (Chaiwongsar *et al.*, 2012). In the absence of ethanol, homozygous double-mutant plants showed significantly reduced root elongation and leaf expansion, resulting from reduced cell expansion and division. Application of ethanol, to induce expression of the transgenic MAPKKKε could partially rescue the reduced cell expansion in leaf epidermal cells.

To further characterise the role of MAPKKKε in plant development in solanaceous plants, the effect of silencing *MAPKKKε* in *N. benthamiana* on leaf cell size and number was assessed (Section 2.9.11). The mean leaf area for plants silenced using TRV:5'MAPKKKε was significantly smaller than that of TRV:GFP-treated control plants (23.98 ± 2.34 cm^2 vs 44.21 ± 2.94 cm^2, t-test $t = 5.39$, $df = 17$, $P < 0.001$ (Figure 5.24 A-B)).

Microscopy of epidermal cells on the abaxial surface of leaves revealed that silencing *MAPKKKε* reduces cell size (Figure 5.24C-D). Leaf epidermal cells from TRV:5'MAPKKKε silenced *N. benthamaiana* plants had a mean cell area of 1931 ± 160 μm^2, compared to 4089 ± 1020 μm^2 for TRV:GFP silenced plants (t-test, $t = 5.39$, $df = 181$, $P < 0.01$). Division of leaf areas by mean cell area gives an estimate for the total number of cells per leaf. In contrast to its effect on cell expansion, silencing *MAPKKKε* has no significant effect on number of cells per leaf (Figure 5.24 E), suggesting cell division is occurring as normal. Therefore consistent with *AtMAPKKKε1* and *AtMAPKKKε2*, *N. benthamaiana* homologs of MAPKKKε are also positive regulators of cell expansion, and hence plant growth.

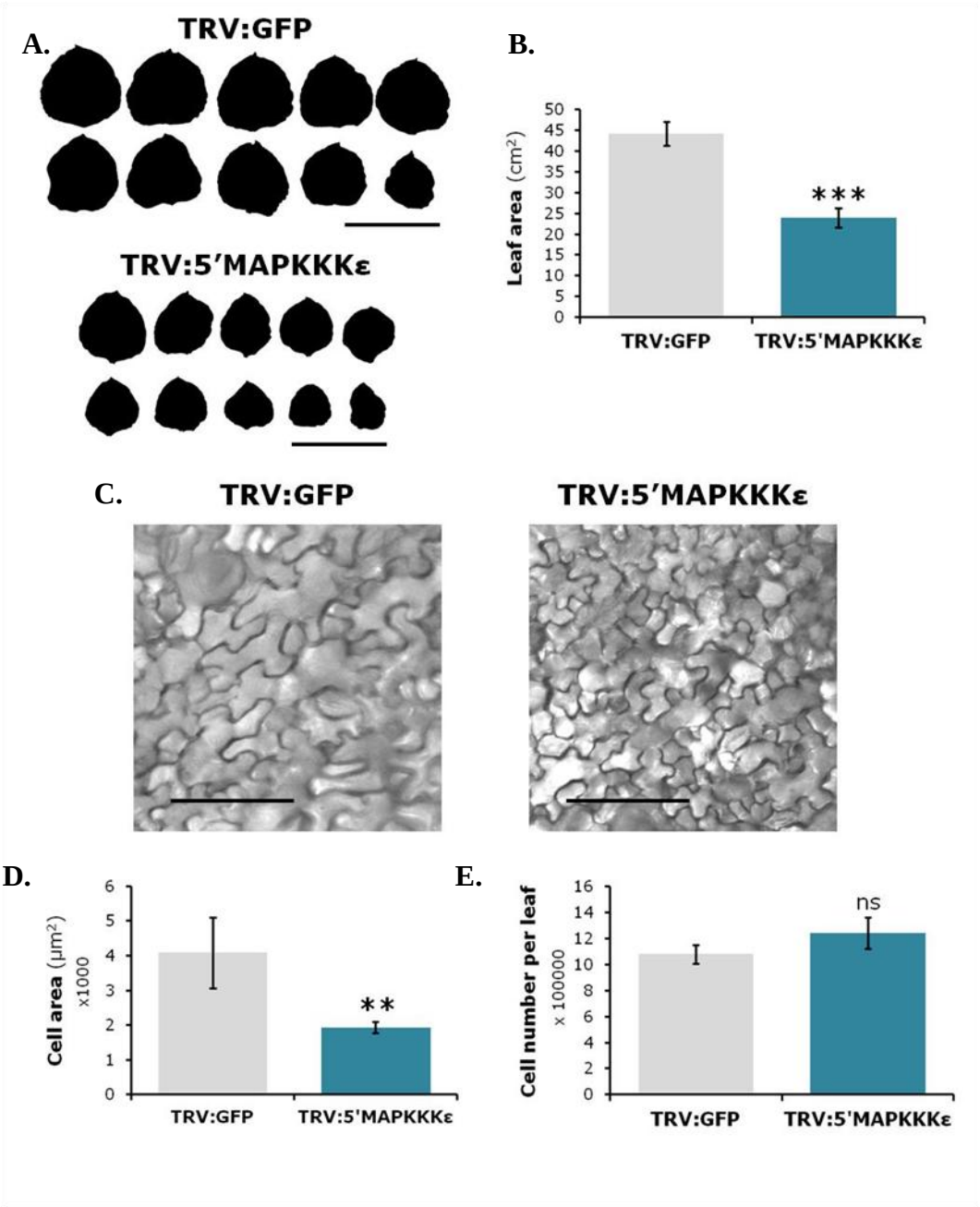

Figure 5.24 Silencing MAPKKKε inhibits cell expansion, and hence growth

(A.) Overall size and shape of *N. benthamiana* leaves 14 days after treatment with either TRV:GFP or TRV:5'MAPKKKε. Scale bars = 10 cm **(B.)** Mean total area for 10 leaves (± SE). **(C.)** Representative microscopy images of abaxial epidermal cells. Scale bars = 100 µm. **(D.)** Mean cell area for 50 – 150 (±SE). **(E.)** Mean estimated number of epidermal cells per leaf (±SE). (t-test, ns = non significant $P>0.05$, ** = $P < 0.01$, *** = $P < 0.001$).

To determine if PexRD2 could inhibit MAPKKKε-mediated responses other than those involved in plant defence, the effect of transient expression of PexRD2 on plant development was also assessed. PexRD2 was expressed from the binary vector pEAQ-HT in one half of leaves of 28-day old *N. benthamaiana* plants, prior to leaf expansion. Seven days subsequent to agroinfiltration (7 dpi), the un-agroifiltrated half of each leaf was fully expanded whilst tissue expressing PexRD2 was not, resulting in a striking curvature of the mid-vein of the leaf (Figure 5.25 A). Control leaves, where half of each leaf was infiltrated with *Agrobacterium* harbouring an empty vector control (pEAQ-HT:EV), showed no reduction in tissue expansion.

To confirm that PexRD2-mediated inhibition of leaf expansion did not result from the previously published weak cell death activity of PexRD2 (Oh *et al.*, 2009), accumulation of autofluorescent phenolic compounds that are associated with cell death was visualized under ultraviolet (UV) light. The levels of ion leakage from infiltrated leaf tissue, which also correlates with cell death, were also measured (Section 2.9.9). Transient expression of D2 domain of CRN8, which is known to cause a strong death response *in planta* (Haas *et al.*, 2009), see Section 6.1.2, was used as a positive control. In similarity with PexRD2, leaf tissue expressing CRN8-D2 failed to expand resulting in clear curvature of the mid-vein, however, unlike pEAQ-HT:PexRD2-infiltrated tissue, pEAQ-HT:D2-infiltrated tissue showed extensive necrosis (Figure 5.25 A). *CRN8*-agroinfiltrated leaf tissue showed clear auto fluorescence (Figure 5.25 B), and high levels of ion leakage (Figure 5.25 C), consistent with the observed cell death. PexRD2-agroinfiltrated tissue did not visibly fluoresce more than the vector control-agroinfiltrated tissue (Figure 5.25 B), nor were the ion leakage levels significantly different for PexRD2 (Figure 5.25 C). As such, the reduced tissue expansion caused by PexRD2 cannot be explained by detectable cell death activity. The fact that transient expression of PexRD2 *in planta* appears to phenocopy the developmental effects of silencing *MAPKKKε* suggests that PexRD2 could also inhibit MAPKKKε's role involved in plant development.

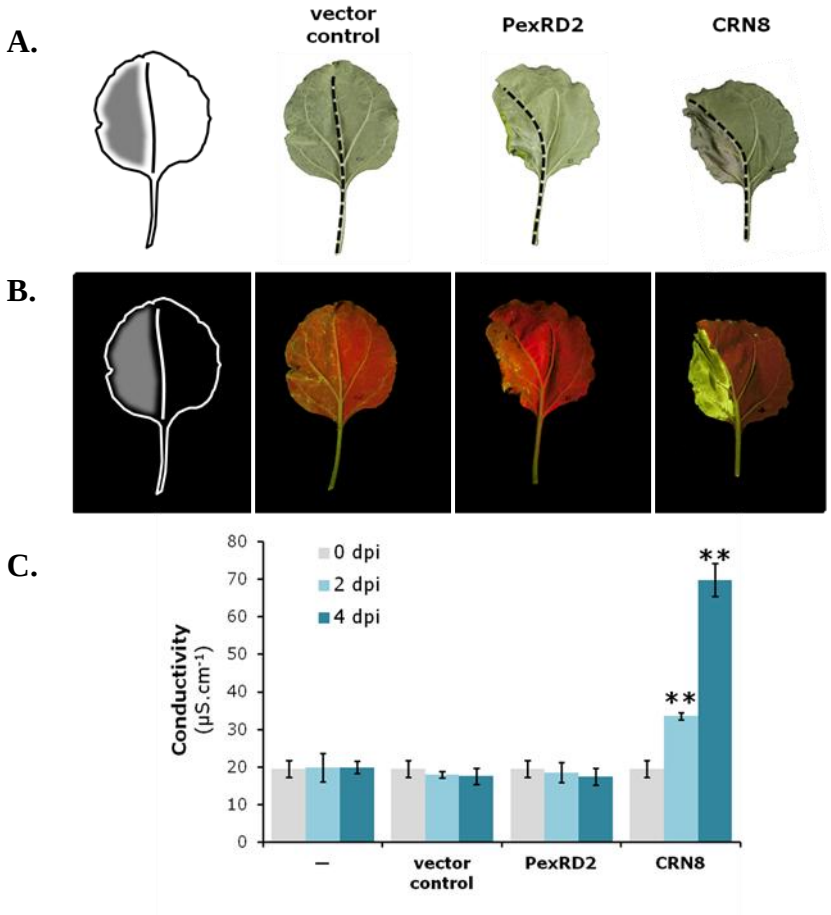

Figure 5.25 Transient expression of PexRD2 also inhibits leaf expansion, which is not caused by cell death activity

(A.) Transient expression of PexRD2 via agroinfiltration into half a leaf of a 28-day old *N. benthamaiana* plant inhibits leaf expansion, resulting in curvature of mid-vein, without visible necrosis of infiltrated tissue, unlike CRN8. **(B.)** Visualization of leaves under ultraviolet (UV) light (480/40 nm excitation filter; 510 nm barrier) confirms lack of accumulation of autofluorescent phenolic compounds that are associated with cell death for PexRD2, but not CRN8. Photographs were taken at 7 dpi. **(C.)** Quantification of cell death by measuring electrolyte leakage from leaf tissue confirms lack of cell death for PexRD2-infiltrated tissue. Bars represent the mean value ± SE from at least three plants. Asterisks indicate means that are significantly different from the 0 dpi sample (Tukey HSD, ** = $P < 0.01$).

The results presented above support the role of PexRD2 as a specific inhibitor of MAPKKKε-mediated signalling events, in both plant immunity and development (Figure 5.26 A). Whether PexRD2's inhibition of cell expansion has any biological relevance to the host-pathogen interaction during an infection, or is simply an unavoidable effect of PexRD2 targeting MAPKKKε-mediated immunity signalling to achieve effector triggered susceptibility (Figure 5.26 B), is yet to be determined.

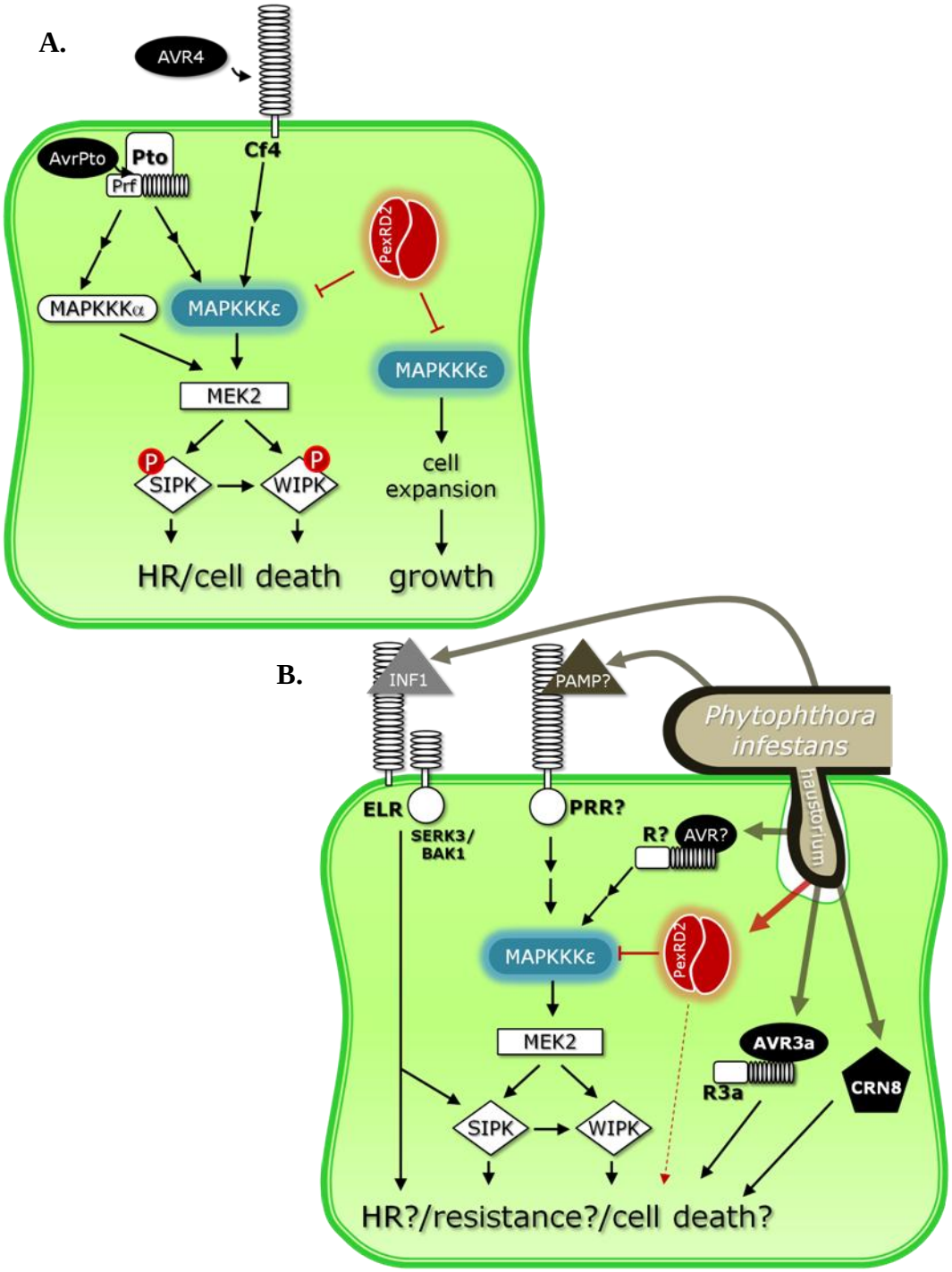

Figure 5.26 Model for PexRD2's effect on known MAPKKKε-mediated signalling responses *in vivo*, and proposed virulence function during infection

(A.) Schematic representation of PexRD2-mediated inhibition of MAPKKKε activity required for cell death associated with plant immunity and plant development. **(B.)** MAPKKKε's role in the restriction of growth of *P. infestans* suggests that it is required for triggering a defence response following perception of an as yet unknown oomycete elicitor (PAMP?, AVR?). PexRD2 is proposed to function as an inhibitor of this kinase to confer effector-triggered susceptibility, and enhance colonisation.

5.2.10 *Mutations in PexRD2 disrupt the interaction with MAPKKKε*

To help develop a more mechanistic understanding of PexRD2's interaction with MAPKKKε, and the importance of this interaction for the effector's virulence function, a series of mutant PexRD2 effectors were designed. These mutants were either generated by whole-plasmid mutagenesis (Section 2.4.6.1) or synthesised by Genscript (USA), before testing to identify those that disrupted the interaction with MAPKKKε. Since the WY-fold containing effector domain of PexRD2 was sufficient to mediate the interaction with MAPKKKε KD, only residues within this region were targeted. The structure of PexRD2's effector domain, together with sequence alignments of PexRD2 and the two 'non-interacting' PexRD2-like effectors, were used to design structurally-informed mutants. These mutants were intended to investigate the importance of different features of PexRD2 in mediating the interaction with MAPKKKε, without disrupting the conserved WY-fold.

Amongst the published WY-fold effectors, dimerisation is uniquely observed in PexRD2. Co-immunoprecipitation experiments had confirmed that this oligomerisation was also observed for PexRD2 *in planta* (see Figure 3.18 B). The crystal structure reveals that this homodimerisation is mediated by an interface dominated by hydrophobic residues. To investigate the importance of this interface for dimerisation and effector function, two leucine residues with side-chains that contributed to this surface (Leu109 and Leu112) were individually mutated to aspartates (Figure 5.27 B). A similar approach had been used to investigate the importance of the observed dimerisation in the crystal structure of the bacterial effector AvrRps4 (Sohn *et al.*, 2012). In that study, replacement of a hydrophobic isoleucine, within the predicted dimerisation interface, to a charged aspartate abolished dimer formation and confirmed that monomeric effector is sufficient to activate plant immunity pathways.

Other individual point mutations in PexRD2 were designed to either abolish or reverse the charge of ten residues with side-chains that were solvent exposed in the crystal structure and as such not involved in the dimerisation interface (Figure 5.27 A). It was hypothesised that the residues that are solvent exposed in the crystal structure might mediate the interactions with the host targets. Five of the ten

mutations targeted negatively charged surface features; namely a glutamate present at the start of the first α-helix of the WY-fold (Glu61, (E61A)); two aspartates (Asp74 and Asp75, (D74A and D75A)) that contribute to part of the large negatively charged groove observed in the structure; and two glutamates (Glu97 and Glu101, (E97Q and E101Q)) that map to the smaller negatively charged patch that spans helices α4. Furthermore five lysines (Lys79, Lys81, Lys85, Lys104, and Lys107), which contribute to the large positive region that wraps around the structure, were mutated to negatively charged glutamates. The mutation of surface exposed lysines to glutamates has also been applied to study the function of AVR3a, targeting residues that were predicted to be surface exposed based on a homology model (Yaeno *et al.*, 2011).

All twelve mutants were transferred to the pDEST™32 bait vector by Gateway® cloning, and tested for interactions with the prey vector encoding *St*MAPKKKε KD or the appropriate empty vector control. The loss of interaction with MAPKKKε KD was assessed using the *HIS3*, and *lacZ* reporter gene assays. Only the two mutants differing in the dimerisation interface, PexRD2^{L109D} and PexRD2^{L112D}, had any observable effect on the interaction with this host protein. Neither mutant was able to interact with the MAPKKKε prey construct, as evidenced by the lack of activation of either the *HIS3* or *LacZ* reporter genes (Figure 5.27 C), although anti-GAL4-DBD western blot analysis confirmed expression to levels comparable to wild-type PexRD2 (Figure 5.28 C). The other ten single point mutations targeting surface exposed residues did not interfere with PexRD2's interaction with MAPKKKε. As with the wild-type PexRD2 bait, none of the mutant bait constructs showed any evidence of auto-activation activity.

These results indicate that an intact dimerisation interface is crucial for PexRD2's interaction with MAPKKKε KD. This could suggest that PexRD2 interacts with the kinase exclusively as a dimer; or that this hydrophobic surface on PexRD2 is a dual-purpose interaction interface mediating either homodimerisation or binding to host targets.

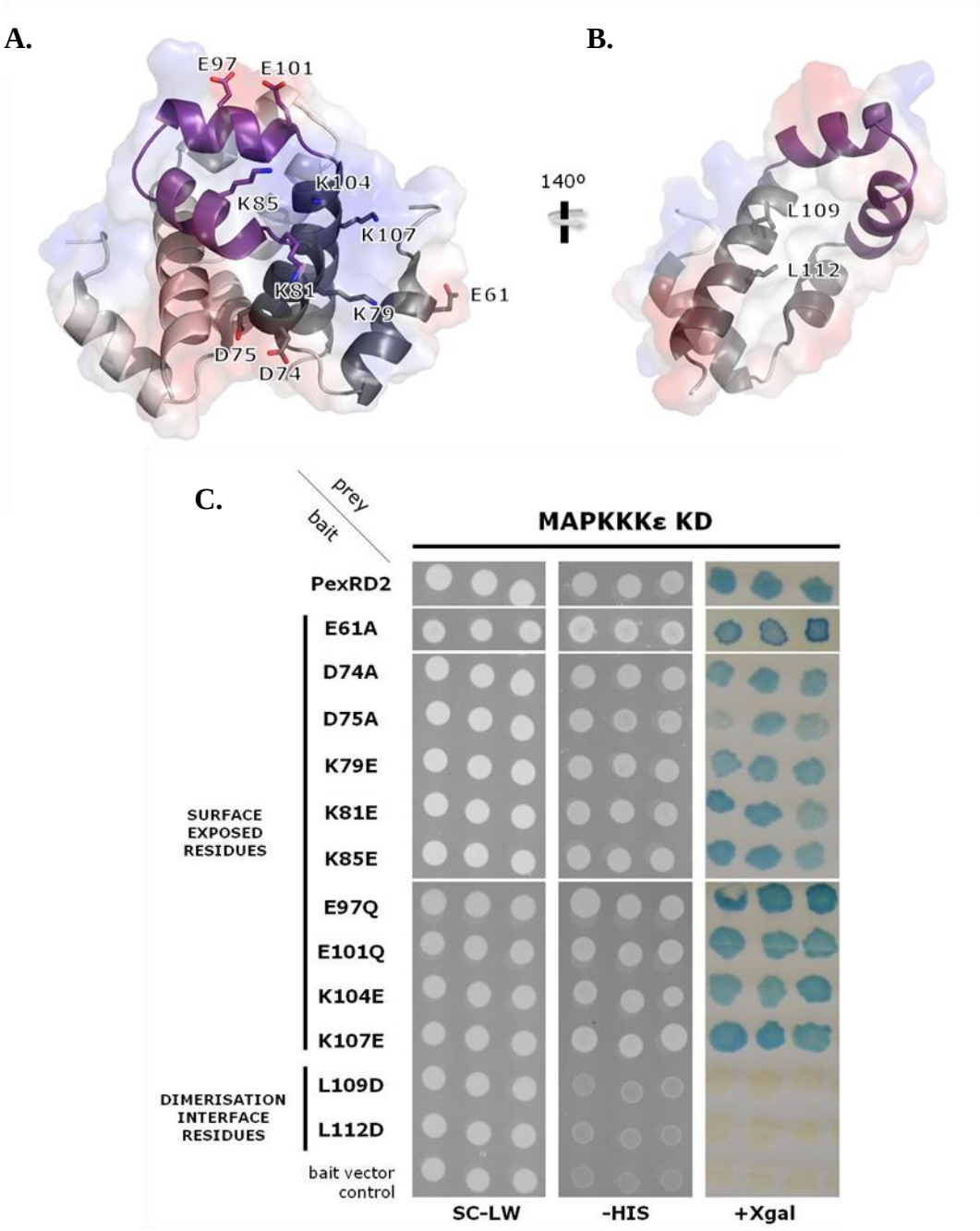

Figure 5.27 Point mutations in PexRD2 dimerisation interface abolish interaction with MAPKKKε KD in yeast two-hybrid

Cartoon ribbon representation with electrostatic surface of the effector domain of PexRD2 with WY-fold on chain-a coloured in dark grey and variable loop highlighted in purple. and chain-b in grey. **(A.)** Homodimer highlighting surface exposed residues targeted by mutagenesis. **(B.)** Dimerisation interface of monomer showing dimerisation interface residues targeted by mutagenesis. **(C.)** Y2H analysis of cotransformants carrying wild-type or mutant PexRD2 baits and StMAPKKKε KD (residues 1 – 300) prey. Growth on SC-LW confirms cotransformation. Interactions between baits and prey are confirmed by growth on plates lacking histidine (–HIS) and blue colouration in the presence of X-gal (+Xgal). Bait/prey combinations were tested in triplicate.

The inability of any single point mutation to alter the interaction between PexRD2 and kinase is perhaps not surprising. The *P. mirabilis* homolog of PexRD2, contains five polymorphisms in its effector domain when compared to *Pi*PexRD2, and is still able to interact with MAPKKKε. Therefore more dramatic mutants, simultaneous targeting multiple residues, were designed using a structurally informed approach. The natural variation between PexRD2 and the non-interacting PexRD2-like-1a was exploited to identify residues that may be important in mediating the interaction. As noted above for PexRD2-like effectors (Section 3.2.9), the variable loops and C-termini were identified as regions of the two proteins that showed the greatest variation.

Interrogation of the crystal structure revealed eight residues within the variable loop region with solvent exposed side-chains. A mutated version of PexRD2 in which all eight of these residues were mutated to their corresponding residues from the variable loop of PexRD2-like-1a was designed, henceforth PexRD2$^{vloop-8}$ (Figure 5.28 B). The appropriate DNA sequence was then synthesised, flanked by the attB recombination sites, and supplied in a pUC57 vector by Genscript (USA). Of the selected eight residues, Ala90 was the closest to the dimerisation interface and its mutation to the corresponding glutamate from PexRD2-like-1a could potentially be quite disruptive. As such the mutated Glu90 of PexRD2$^{vloop-8}$ was reverted back to the wild-type alanine to generate PexRD2$^{vloop-7}$ using whole plasmid mutagenesis.

PexRD2-like effectors can show substantial extensions to the conserved WY-fold at their C-termini. PexRD2-like-1a has an additional nine residues compared to PexRD2. To investigate if these C-terminal extensions in PexRD2-like effectors impede the interactions of these effectors with MAPKKKε, the last three residues of PexRD2 (119-TAV-121) were replaced with the last 12 residues of PexRD2-like-1a (121-NKKKKPNLVYYS-132). The resultant mutant is henceforth referred to as PexRD2$^{long-tail}$. The reciprocal swap in PexRD2-like-1a yielded the mutant PexRD2-like$^{short-tail}$, and was used to investigate if removal of the long C-terminal extension could cause a gain of interaction of PexRD2-like effectors with MAPKKKε KD. The appropriate DNA sequence for PexRD2$^{long-tail}$ and PexRD2-like$^{short-tail}$ were synthesised, flanked by the attB recombination sites, and supplied in a pUC57 vector by Genscript (USA). These four additional PexRD2/PexRD2-like

mutants were then transferred to the pDEST™32 bait vector by Gateway® cloning, and tested for interactions with the prey vector encoding MAPKKKε KD or the appropriate empty vector control. The loss of interaction with MAPKKKε KD was assessed using the *HIS3,* and *lacZ* reporter gene assays

PexRD2$^{long\text{-}tail}$ showed wild-type interactions with MAPKKKε KD, and PexRD2-like$^{short\text{-}tail}$ did not gain the ability to interact with the host kinase domain (Figure 5.28 A). These results show that the residues comprising the short C-terminal tail of PexRD2 are neither required nor sufficient to mediate the interaction; and that extensions at the C-terminus of PexRD2 can be accommodated without impacting the interaction with the host kinase.

In contrast, the PexRD2$^{vloop\text{-}7}$ mutant showed a reduced interaction with MAPKKKε KD, as evidenced by the weak growth on media lacking histidine, but not the development of a blue colouration in the presence of X-gal (Figure 5.28 A). Furthermore, the PexRD2$^{vloop\text{-}8}$ showed no interaction with MAPKKKε KD; co-transformants failed to activate either the *HIS3* and *lacZ* reporter genes. Western blot analysis using anti-GAL4-DBD confirmed expression of PexRD2$^{vloop\text{-}7}$ to levels similar to wild-type PexRD2, whilst PexRD2$^{vloop\text{-}8}$ accumulated to slightly lower levels (Figure 5.28 C). This suggests that the A90E mutation, present in PexRD2$^{vloop\text{-}8}$ but not PexRD2$^{vloop\text{-}7}$, has an additive effect in reducing the strength of interaction between PexRD2 and MAPKKKε, possibly through reducing protein stability. Furthermore, the composition of surface exposed residues in the variable loop region of PexRD2 is important for the effector's ability to interact with MAPKKKε.

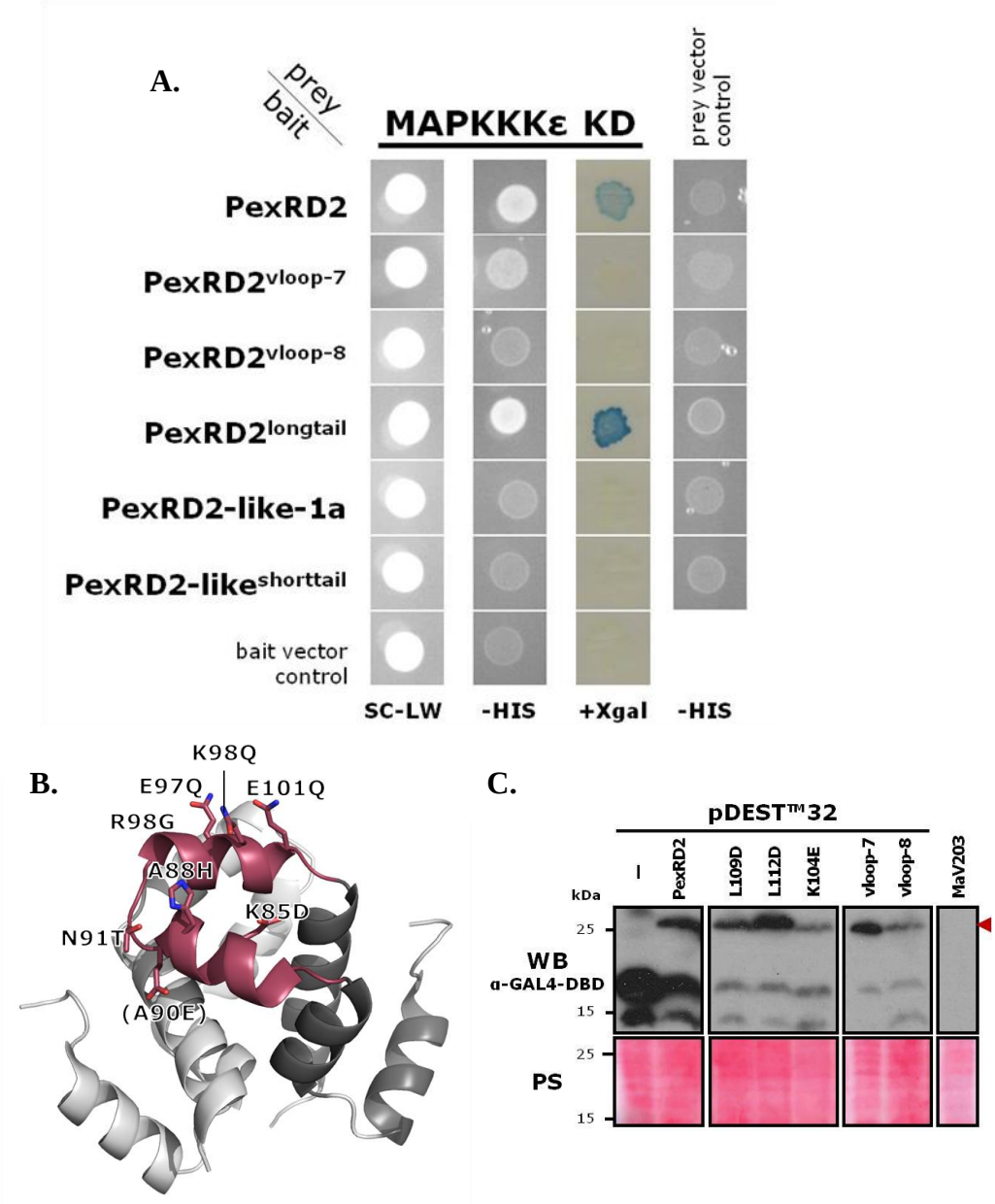

Figure 5.28 More drastic mutations in PexRD2 reduce interaction with MAPKKKε KD in yeast two-hybrid

(A.) Y2H analysis of cotransformants carrying wild-type or mutant effector baits and StMAPKKKε KD (residues 1 – 300) prey. Growth on SC-LW confirms cotransformation. Interactions between baits and prey are confirmed by growth on plates lacking histidine (–HIS) and blue colouration in the presence of X-gal (+Xgal). Bait/prey combinations were tested in triplicate, and a single respresentative colony is shown. **(B.)** Cartoon ribbon representation PexRD2 dimer with WY-fold on chain-a coloured in dark grey and variable loop highlighted in reddish-purple. Mutations present in both PexRD2vloop-7 and PexRD2vloop-8, or just PexRD2vloop-8 are shown without or within brackets respectively. **(C.)** Western blot analysis confirming expression levels of wild-type or mutant PexRD2 baits. Red arrow indicates expected size of fusion protein. MaV203 represents total proteins from an untransformed yeast and serves as a negative control. PS indicates Ponceau staining to confirm protein loading.

5.2.11 *Non-interacting mutants do not suppress MAPKKKε-dependent HR, or MAPKKKε-triggered cell death*

Following identification of mutants of PexRD2 that reduce or abolish its interaction with MAPKKKε, the ability of these mutants to suppress MAPKKKε-mediated cell death *in planta* was assessed. Cell death suppression assays were repeated using these mutants as described in Sections 2.9.8, 5.2.6, and 5.2.7. The PexRD2^{K104E} mutant that still interacts with MAPKKKε KD in Y2H significantly suppressed the HR triggered by recognition of Avr4 by Cf4, to the same level as that achieved by wild-type PexRD2 (Figure 5.29 A-B). In contrast, co-expression of the two non-interacting point mutants, PexRD2^{L109D} or PexRD2^{L112D}, with Avr4 and Cf4 in *N. benthamiana* did not significantly suppress the level of HR observed, compared to the empty vector control, although western blot analysis confirmed their expression to levels comparable to wild-type PexRD2 (Figure 5.29 C).

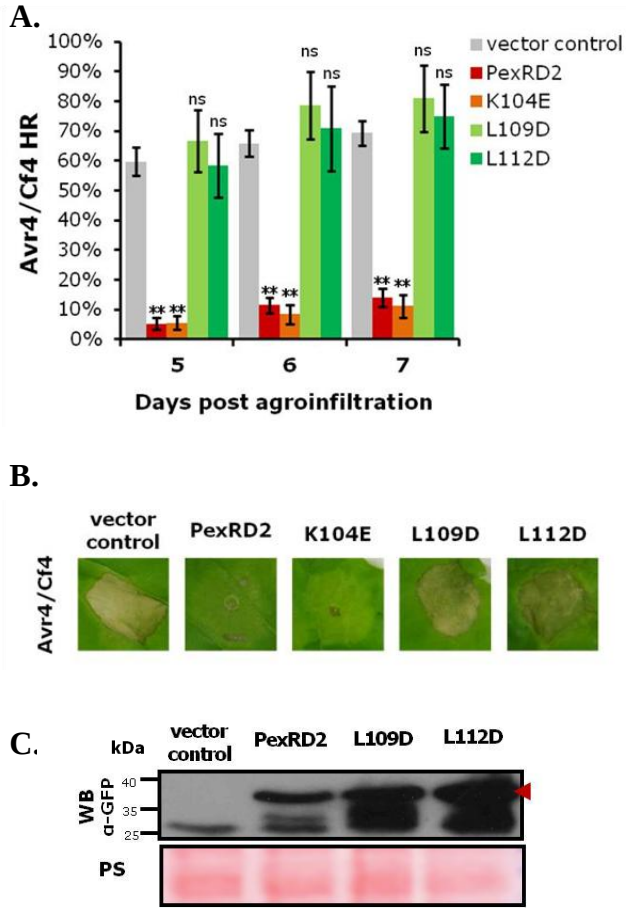

Figure 5.29

'Dimerisation interface mutants' of PexRD2 do not suppress Avr4/Cf4-triggered HR

(A.) Mutations in the dimerisation interface of PexRD2 (L109D or L112D) abolish the effector's ability to suppress Avr4/Cf4-triggered HR. Data represents the mean ± SE from at least three plants. Superscripts above means indicate the significance level of the difference compared to the vector control at a given time point, as determined by Tukey HSD. **(B.)** Images of representative levels of HR/HR suppression for each condition, taken 7 dpi. **(C.)** Western blot analysis confirming expression levels of GFP-fusions of wild-type and mutant PexRD2 at 3 dpi. Red arrow indicates expected size of full length fusion protein. PS indicates Ponceau staining of RuBisCO to confirm protein loading.

Co-expression of the same non-interacting point mutants, PexRD2^{L109D} and PexRD2^{L112D}, with the kinase domain of *Sl*MAPKKKε had no significant effect on the level of cell death observed following estradiol treatment (Figure 5.30). In similar with wild-type PexRD2, the PexRD2^{K104E} mutant could significantly suppress the MAPKKKε KD-triggered cell death.

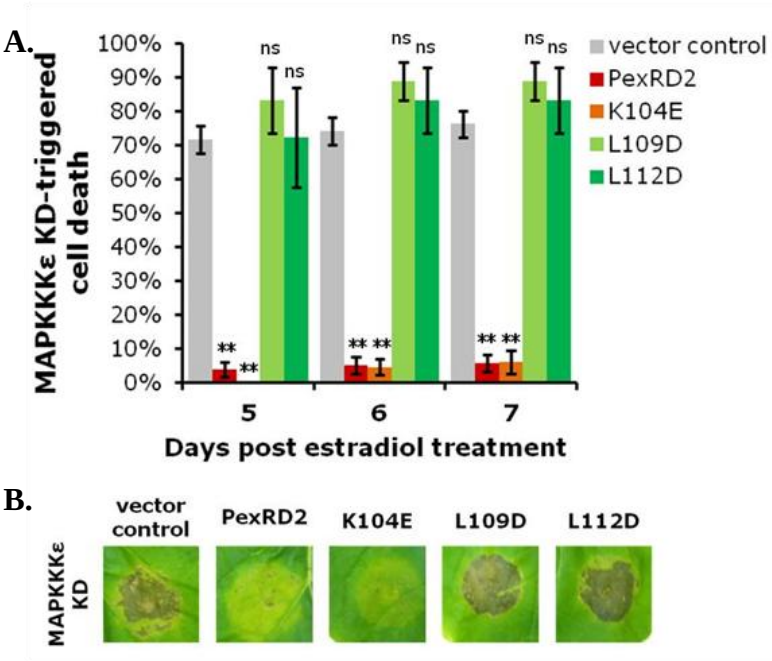

Figure 5.30 'Dimerisation interface mutants' of PexRD2 do not suppress the cell death triggered by MAPKKKε KD

(A.) Mutations in the dimerisation interface of PexRD2 (L109D or L112D) also abolish the effector's ability to suppress MAPKKKε KD -triggered cell death. Data represents the mean ± SE from at least four plants. Superscripts above means indicate the significance level of the difference compared the vector control at a given time point, as determined by Tukey HSD. **(B.)** Images of representative levels of MAPKKKε-triggered cell death/cell death suppression for each condition, taken 7 dpt.

Furthermore, mutations within the variable loop region which negatively affected the interaction with MAPKKKε KD in Y2H, also negatively affected PexRD2-mediated suppression of the MAPKKKε KD-triggered cell death. The PexRD2$^{vloop-8}$ mutant, which does not interact with MAPKKKε KD in Y2H, did not suppress MAPKKKε KD-triggered cell death *in planta* (Figure 5.31 A-B). The level of cell death observed

was not significantly different from the negative control. In contrast, the PexRD2$^{vloop-7}$ mutant, which still shows a very weak interaction with MAPKKKε KD in Y2H, showed a reduction in, but not complete loss of, cell death suppression activity. The level of MAPKKKε KD-triggered cell death when co-expressed with PexRD2$^{vloop-7}$ was significantly different from both the vector control and wild-type PexRD2 conditions. It was also significantly different from the level of cell death observed following co-expression with PexRD2$^{vloop-8}$ (Figure 5.31 A-B). Western blot analysis confirmed that both mutants accumulated to similar levels to wild-type PexRD2 *in planta* (Figure 5.31 C). This intermediate level of cell death suppression activity indicates that the ability of PexRD2 to suppress MAPKKKε-mediated cell death can be positively correlated with the strength of interaction between the effector and host protein, as estimated by the Y2H.

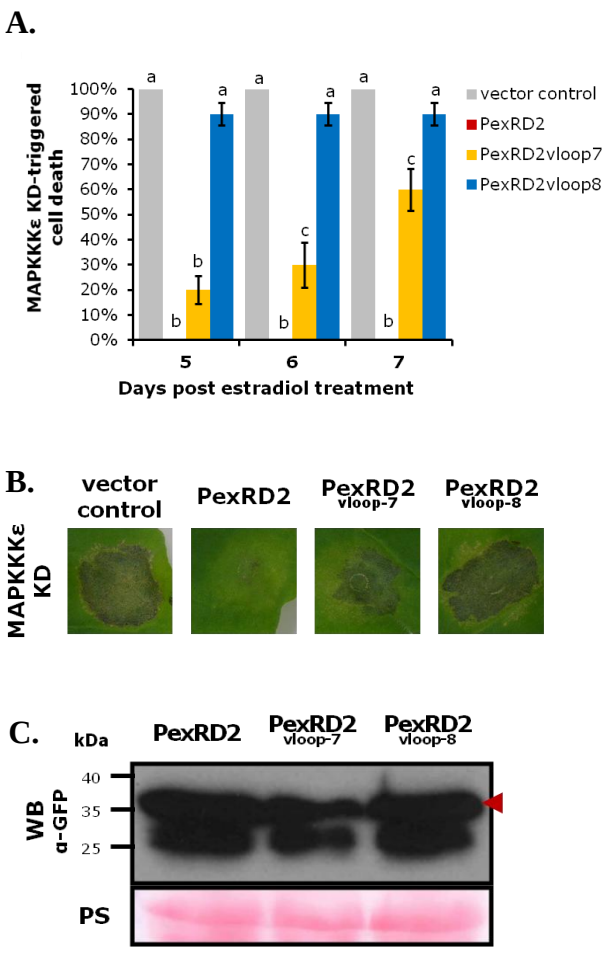

Figure 5.31

'Variable loop mutants' of PexRD2 do not suppress the cell death triggered by MAPKKKε KD

(A.) Mutations in the variable loop region of PexRD2 significantly reduce the effector's ability to suppress MAPKKKε KD-triggered cell death. Data represents the mean ± SE from at least five plants. Different letters above two means indicate they are significantly different from each other at that given time point, as determined by Tukey HSD ($P<0.05$). **(B.)** Images of representative levels of MAPKKKε-triggered cell death/cell death suppression for each condition, taken 7 dpt. **(C.)** Western blot analysis confirming expression levels of GFP-fusions of wild-type and mutant PexRD2 at 4 dpi. Red arrow indicates expected size of full length fusion protein. PS indicates Ponceau staining of RuBisCO to confirm protein loading.

5.2.12 *Non-interacting mutants of PexRD2 do not enhance growth* of Phytophthora infestans

Since non-interacting PexRD2 mutants show less suppression of cell death responses that are dependent on MAPKKKε-mediated signalling, which was shown to limit the spread of infection with *P. infestans*, their ability to enhance infection was also tested. As described for wild-type PexRD2 in Section 5.2.4, agroinfiltration was used to transiently express PexRD2 mutants in one half of a leaf, and vector control in the other half of the same leaf. After 24 h, detached leaves were infected with *P. infestans* 88069 zoospores and the growth of necrotic lesions was scored as before.

Wild-type PexRD2 enhanced infection by *P. infestans* 88069, as measured by lesion area, approximately five-fold relative to infection of the vector control tissue (Figure 5.10 A). In contrast, prior expression of any of the four mutants: that show no (PexRD2^{L109D}, PexRD2^{L112D}, and PexRD2$^{vloop-8}$) or significantly reduced (PexRD2$^{vloop-7}$) ability to suppress MAPKKKε-mediated signalling, did not significantly enhance infection by the *P. infestans* 88069 (Figure 5.32). The lesion area achieved for infection of leaf tissue expressing any of the four mutants was not significantly different from the lesion area of infections in the same leaf on tissue infiltrated with vector control (Tukey HSD, P > 0.05).

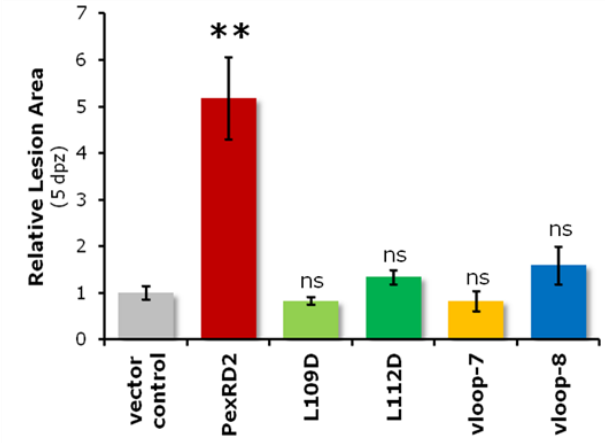

Figure 5.32 ***In planta*** **expression of non-interacting mutants does not enhance infection by** ***P. infestans***

Mean relative lesion area at 5 dpz for infection with *P. infestans* 88069. Relative lesion area is calculated as in Figure 5.10. Each bar represents the mean ± SE of at least 16 leaves per construct. Asterisks indicate means that are significantly different from the standardised value of vector control tissue (Tukey HSD, ** = P < 0.01, ns = not significantly different, P>0.05)

5.2.13 *PexRD2^{L109D} mutant displays dominant negative activity*

To further explore the mechanism of PexRD2's virulence function, the ability of a structurally-informed mutant PexRD2 that no longer interacts with MAPKKKε, nor inhibits MAPKKKε-mediated signalling, to function in a dominant negative manner was tested. Previous studies had shown that co-expression of catalytically inactive mutants of the translocated kinase effector CRN8, or the bacterial effector HopAO1, with the wild-type effectors could inhibit the wild-type effectors' activities. To determine if PexRD2^{L109D} (L109D) displays dominant negative activity, *Agrobacterium* harbouring *3xHA-PexRD2* was mixed with other *Agrobacterium* harbouring either empty vector control (pK7WGF2) or *GFP-L109D* in various ratios to achieve a combined OD_{600} of 0.3. These agroinfiltration mixtures were then co-agroinfiltrated with *Sl*MAPKKKε KD into *N. benthamiana* leaves and the level of cell death following estradiol treatment was scored (Section 2.9.8).

Co-expression of 3xHA-PexRD2 alone with MAPKKKε KD significantly suppressed the triggered cell death, indicating that different N-terminally tagged variants of PexRD2 retain activity (Figure 5.33 A). Co-expression of a mixture of wild-type PexRD2 and the empty vector control, at any ratio, still significantly suppressed the MAPKKKε KD-triggered cell death, to similar levels to expression of PexRD2 alone (Figure 5.33 B). However, co-expression of a mixture of PexRD2 and L109D, at any ratio, did not suppress the MAPKKKε KD-triggered cell death. The level of MAPKKKε KD-triggered cell death achieved following co-expression with L109D was not significantly different either in the presence or absence of PexRD2. Interestingly the cell death that occurred when co-expressed of L109D was accelerated relative to that that occurred when MAPKKKε KD was co-agroinfiltrated with the vector control (see Figure 5.36 A).

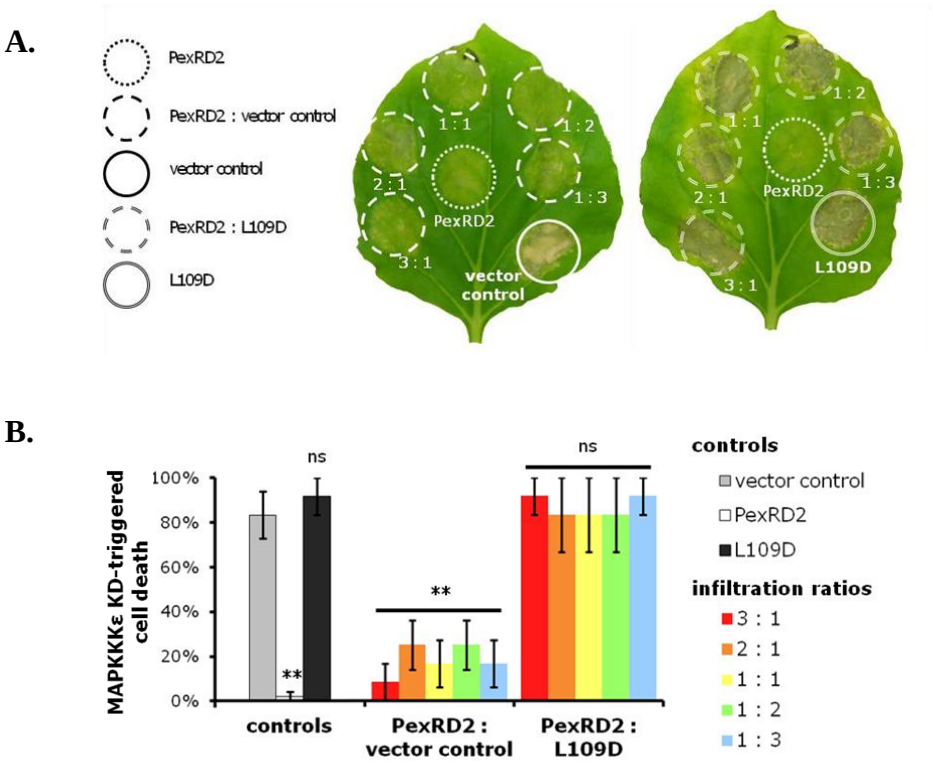

Figure 5.33 PexRD2^{L109D} displays dominant negative activity.

(A.) Co-expression of PexRD2^{L109D} (L109D), but not a vector control, with wild-type PexRD2 *in* planta prevents PexRD2-mediated suppression of MAPKKKε KD-triggered cell death. Leaves were imaged at 5 days post estradiol treatment (dpt). **(B.)** Level of MAPKKKε KD-triggered cell death observed at 5 dpt. Results presented represent the percentage of infiltration sites per plant with greater than 50% of area showing cell death. Bars represent the mean ± SE from at least five plants. Asterisks indicate means that are significantly different from the vector control alone condition (Tukey HSD, ** = $P < 0.01$, ns = not significantly different, $P>0.05$)

These above results demonstrate that PexRD2^{L109D} does display dominant negative activity, and is able to apparently inhibit the activity of the wild-type PexRD2. This dominant negative activity could result from a number of different mechanisms, which are outlined in Figure 5.34: (Section 5.2.13.1) L109D could out compete wild-type PexRD2 for the interaction surface on MAPKKKε KD without suppressing MAPKKKε-mediated signalling; (Section 5.2.13.2) L109D could render PexRD2 non-functional either through destabilisation of wild-type protein or formation of non-functional heterodimers; (Section 5.2.13.3) expression of L109D could trigger an altered physiological state *in planta* that unspecifically accelerates cell death responses; or (Section 5.2.13.4) L109D could out compete wild-type PexRD2 for a third unknown factor that is required for PexRD2-mediated suppression of MAPKKKε-mediated signalling.

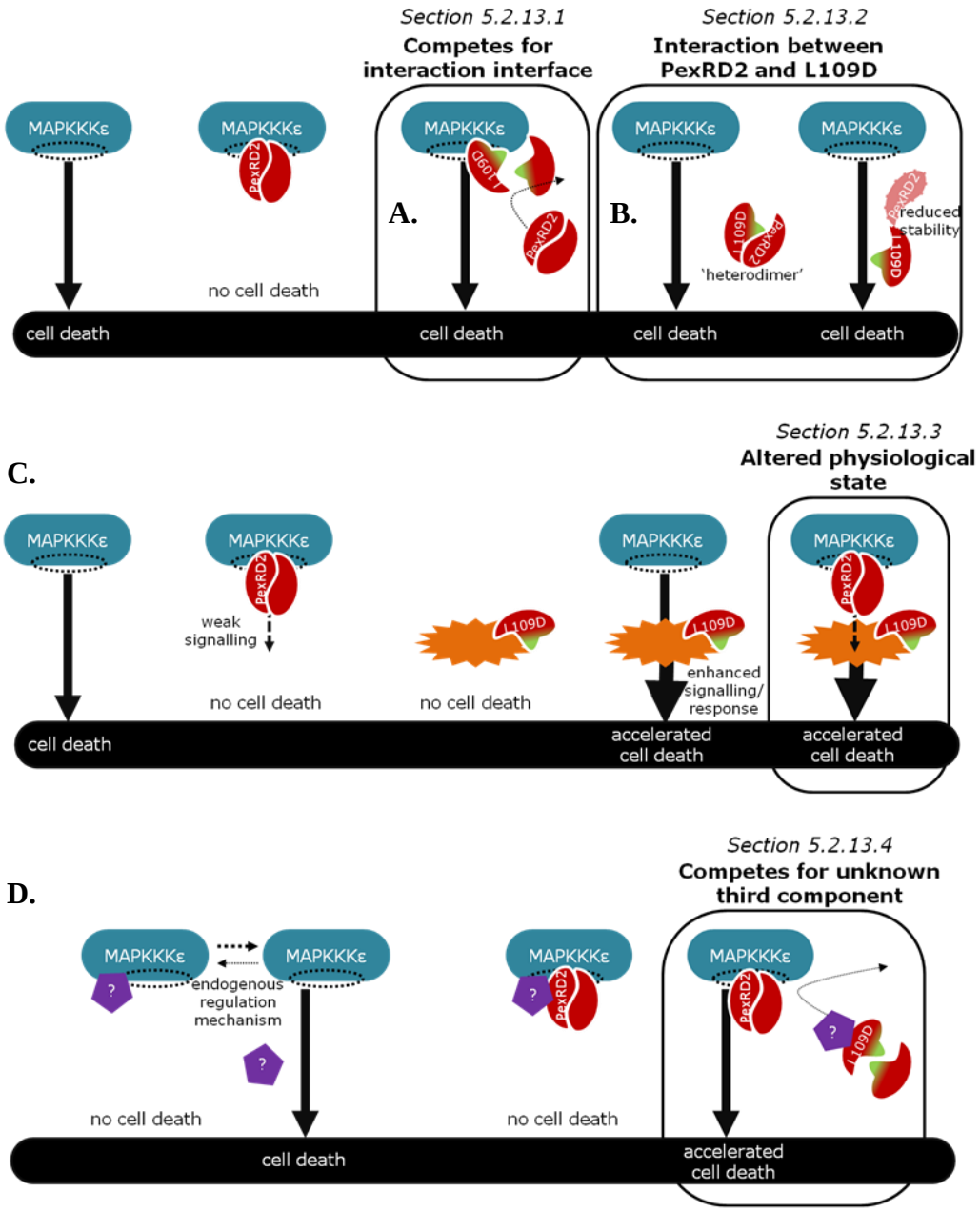

Figure 5.34 Potential mechanisms behind dominant negative activity of PexRD2^{L109D} mutant

Schematic representation of the proposed means by which PexRD2^{L109D}'s (L109D) domain negative activity might result. **(A.)** L109D might block the binding interface on MAPKKKε without inhibiting the kinase's activity. **(B.)** L109D might form non-function heterodimers with or otherwise destabilise the wild-type PexRD2. **(C.)** PexRD2 might reduce MAPKKKε-mediated signalling below the threshold required for elicitation of cell death. L109D might cause an altered physiological state that reduces the threshold required for elicitation of cell death resulting in accelerated cell death, even in the presence of PexRD2. **(D.)** PexRD2 might require a third unknown component (purple pentagon) to mediate inhibition of MAPKKKε-mediated cell death. L109D might compete with PexRD2 for this unknown component, preventing PexRD2-mediated inhibition of MAPKKKε.

5.2.13.1 Does L109D compete with wild type PexRD2 for the interaction interface on the host target?

Dominant negative activity could result from L109D competing with wild type PexRD2 for the interaction interface on the host target, without being able to inhibit the kinase's activity itself. However, this explanation can be deemed unlikely. For L109D to block the interaction surface on MAPKKKε KD one should expect it be able to interact with the host kinase with at least an equal, if not greater, affinity than the wild-type PexRD2. The protein-protein interaction studies described above (Section 5.2.10) have confirmed a loss of detectable interaction between L109D and MAPKKKε KD.

5.2.13.2 Does L109D interact with PexRD2 and prevent the interaction with the host target?

A second explanation is that the L109D mutant interacts with the wild-type PexRD2 and prevents it from interacting with its proposed virulence target. L109D might achieve this through forming non-functional heterodimers with PexRD2, or by the mutant destabilising the wild-type protein.

An interaction between PexRD2 and L109D is plausible, because the crystal structure of PexRD2 revealed that this protein homodimerises. This oligomerisation of wild-type PexRD2 was reconfirmed by multiple independent techniques (Section 3.2.7). To assess for the potential for heterodimerisation, or destabilising effects, 3xHA-PexRD2, or 3xHA-L109D, were co-expressed in planta, with either free GFP, GFP-PexRD2 or GFP-L109D by co-agroinfilitration. Total protein extracts were obtained from infiltrated tissue and analysed by western blotting.

Co-expression of 3xHA-PexRD2 with GFP-L109D had no effect on the accumulation of the wild-type protein compared to co-expression with GFP or GFP-PexRD2 (Figure 5.35). This means that the dominant negative activity of L109D is unlikely to result from any destabilising effect, however, unlike wild-type PexRD2, no expression of 3xHA-L109D was detected, even after anti-HA

immunoprecipitation, suggesting that this particular construct has reduced expression or stability, although this requires further investigation.

The potential for PexRD2 and L109D to form non-functional heterodimers remains a possibility. Immunoprecipitation of 3xHA-PexRD2, using anti-HA affinity matrix, did not co-immunoprecipitate GFP-L109D, but neither did it co-immunopreciptiate, wild-type GFP-PexRD2 (Figure 5.35). As such experiments designed to assess potential for heterodimerisation remain inconclusive.

One way that this could be assess in the future, would be to switch the HA-tag for a FLAG-tag and reassess for heterodimerisation, as GFP-PexRD2 was previously shown to co-IP with FLAG-PexRD2 (Boutemy *et al.*, 2011). Co-expression or co-purification of the two proteins expressed recombinantly in *E. coli*, followed by biophysical characterisation, represents another strategy to assess the potential for homo- and heterodimerisation of L109D.

Yeast two-hybrid does not represent a suitable assay to assess for PexRD2 oligomeriation since the homodimeric interaction between wild-type PexRD2 was not detectable (Figure 4.13). However, the potential for L109D to disrupt PexRD2's interaction with MAPKKKε could be tested using yeast three-hybrid (Zhang and Lautar, 1996, Werner *et al.*, 2004, Moriyoshi, 2009).

These first two explanations are based on the assumption that the dominant negative actitivty of L109D is reliant on it preventing PexRD2 from interacting with MAPKKKε. Although these explanations cannot be excluded, they both do not explain why the cell death triggered by MAPKKKε KD is accelerated when co-expressed with L109D, compared to when co-expressed with the vector control, even in the absence of PexRD2.

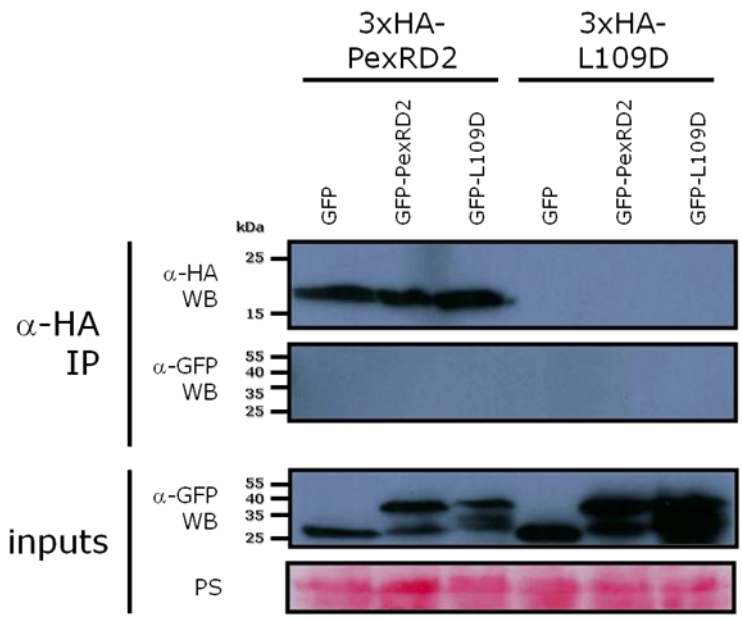

Figure 5.35 L109D does not destabilise PexRD2 *in planta*, although attempts to assess heterodimerisation remain inconclusive

Western blots showing immunoprecipitation of 3xHA-PexRD2. 3xHA-PexRD2 was coexpressed with free GFP, GFP-tagged PexRD2 or L109D in *N. benthamiana.* Immunoprecipitates (IP) obtained with Anti-HA affinity matrix (α-HA IP) and total protein extracts (inputs) were immunoblotted with antibodies as indicated. PS indicates of Ponceau stain of large RuBisCO subunit to confirm equal protein loading.

5.2.13.3 Does expression of L109D trigger an altered physiological state that accelerates the development of cell death?

L109D might act as a non-specific sensitizer to cell death responses. Although L109D itself doesn't trigger a detectable necrosis, it may alter the physiological state within the cell such that the responses triggered by cell-death elicitors are enhanced and accelerated in an unspecific manner. This explanation is consistent with the significantly accelerated MAPKKKε KD-triggered cell death in the presence of L109D (Figure 5.36). This cell death response reaches its maximum with L109D within 3 dpt, compared to 5 dpt with the empty vector control.

If the apparent dominant negative activity of this mutant effector is due to an unspecific, altered physiological state, one might expect the responses triggered by other cell-death elicitors to also be accelerated by L109D. To test this, the effect of L109D on cell death responses that are known to be MAPKKKε-independent was assessed. The cell death responses triggered by the translocated effector CRN8 and the elicitin INF1 have been shown to be independent of *MAPKKKε* in *N. benthamiana* (Section 5.2.5, Figure 5.12). These cell death responses were also not suppressed by co-agroinfiltration with PexRD2 (Section 5.2.6, Figure 5.17). The development of cell death following co-expression of either elicitor with L109D was compared to that following co-expression of the two elicitors with an empty vector control. The level of cell death triggered by CRN8 or INF1 was not significantly affected by co-expression with L109D. This result is consistent with a specific response, and not a general, altered physiological state as described above. However, caution should be taken when drawing conclusion based on negative results.

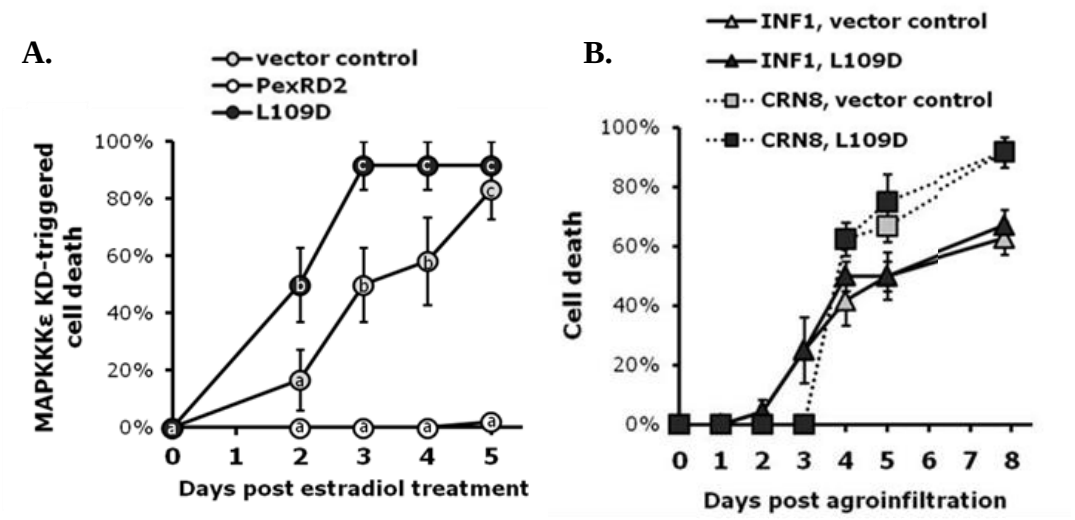

Figure 5.36 PexRD2^{L109D} specifically accelerates cell death triggered by MAPKKKε KD

(**A**) Co-expression of PexRD2^{L109D} (L109D, black circles) accelerates the cell death triggered by over-expression of MAPKKKε KD compared to co-expression with the vector control (grey circles). Values represent the mean ± SE for at least six plants. Different letters within the circles indicate means that are significantly different from each other, as determined by Tukey HSD ($P<0.05$). (**B**) The development of cell death triggered by INF1 (triangles) or CRN8 (squares) is not effected by co-expression of L109D. Values represent the mean ± SE for at least six plants.

5.2.13.4 Does L109D compete with PexRD2 for an unknown factor that is required for suppression of MAPKKKε?

It is possible that PexRD2 mediates its inhibition of MAPPPKε-mediated signalling through an interaction with a third unknown component that forms part of the effector-target complex. For example, PexRD2 might stabilise an interaction with an endogenous negative regulator of the host kinase. One could speculate that, in the absence of any elicitors, activity of the kinase may be inhibited through interaction with this proposed negative regulator. Over-expression of this kinase is sufficient to overcome this baseline level of negative regulation resulting in the pathogen-independent cell death. PexRD2 could inhibit MAPPPKε-mediated signalling by stabilising the interaction with said unknown negative regulator and MAPKKKε. The L109D mutant cannot interact with MAPKKKε, meaning that it cannot inhibit the kinases activity. However, if it could still interact with the proposed negative regulator, this might prevent the putative endogenous regulation mechanism that would otherwise slow the cell death progression. When PexRD2 and L109D are co-expressed together with MAPKKKε KD, the mutant could compete with the wild-type effector for this potential negative regulator. Although this explanation is highly speculative, it is also consistent with the accelerated MAPKKKε-triggered cell death observed when co-expressed with L109D.

To further investigate this potential explanation, the ability of the L109D mutant to interact with other identified putative targets of PexRD2, was assessed using Y2H. These known interactors of PexRD2 and MAPKKKε might be likely candidates for the third unknown component. Yeast co-transformants harbouring the L109D mutant bait and either *St*PM4K1 or *St*ΔN-PUB38-like preys were tested using all three reporter gene assays, alongside co-transformants harbouring the wild-type PexRD2 bait or the appropriate empty vector controls.

Unlike wild-type PexRD2, co-expression of the L109D bait with either the *St*PM4K1 or *St*ΔN-PUB38-like preys failed to activate any of the reporter genes (Figure 5.37). This indicates that mutation of this residue in the dimerisation interface also abolishes the interactions with these other host targets. This suggests that these host proteins are unlikely candidates for the proposed unknown component required for

PexRD2-mediated suppression of MAPKKKε. Further analysis would be required to identify host proteins that interact with both PexRD2 and L109D, and could represent the proposed unknown component.

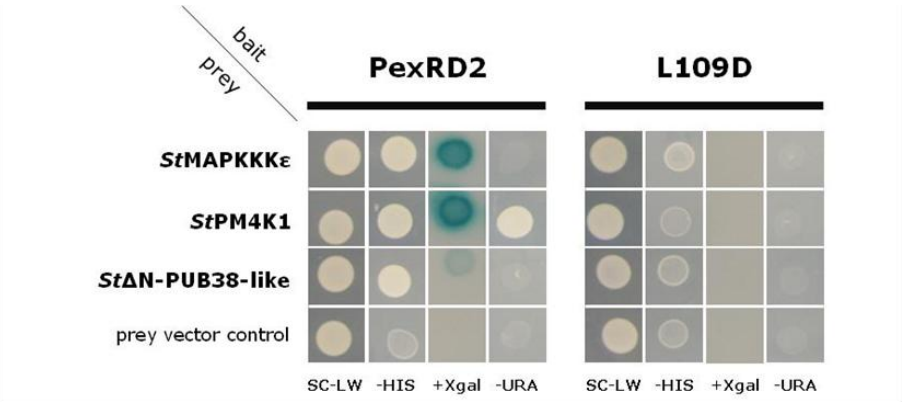

Figure 5.37 PexRD2^{L109D} does not interact with PM4K1 or PUB38-like

Y2H analysis of co-transformants carrying PexRD2 or L109D baits and identified interacting host proteins (PexRD2PIs) as indicated. Interactions allow growth on plates lacking histidine (-HIS) or uracil (-URA) and blue colouration in the presence of X-gal (+Xgal). Bait/prey combinations were tested in triplicate and single representative colonies are shown.

5.2.14 Cell death suppression assays can be adapted to identifiy PexRD2-insensitive MAPKKKε kinase domains from a randomly-generated library

The involvement of MAPKKKε in the plant's resistance response to *P. infestans* (Section 5.2.2), and the suggested role of PexRD2 as a specific inhibitor of this host protein (Section 5.2.6 – 5.2.9), suggest that mutant MAPKKKε that can function even in the presence of PexRD2 could be deployed to provide novel resistance mechanisms to this pathogen. To identify such a mutant, the MAPKKKε KD-triggered cell death suppression assay described in Section 5.2.7 was adapted and optimised for a medium- to high-throughput screening format.

The wild-type sequence for the potato MAPKKKε kinase domain (residues 1 – 332, *St*KDε$_{1\text{-}332}$) was expressed with under the control of the estradiol inducible promoter in the pERCH vector (see Section 5.2.7). This protein had been confirmed to cause a strong cell death response that was robustly suppressed by PexRD2 (Figure 5.21). This protein was co-expressed with N-terminally 3xHA tagged PexRD2, to provide a

PexRD2-sensitive MAPKKKε condition, whilst a 'PexRD2-insensitive mutant' was simulated by co-expressing *St*KDε$_{1-332}$ with the N-terminally 3xHA tagged, non-interacting, PexRD2^{L109D} mutant that does not suppress MAPKKKε KD-triggered cell death (Section 5.2.11 and 5.2.13).

The rate at which mutant MAPKKKεs could be screened in a medium- to high-throughput agroinfiltration-based assay could be increased if the *Agrobacterium* infiltration mixes could be prepared a day in advance. The effect of incubation of *Agrobacterium* in infiltration buffer for prolonged periods (>16 h) prior to infiltration into leaf tissue, was compared to the previously used 1 – 2-h incubation period. When using prolonged incubation, the effect of adding 0.2% (w/v) sucrose, as a source of carbon, to the standard infiltration buffer was also assessed.

Overnight (>16 h) incubation in infiltration buffer, prior to agroinfiltration and estradiol treatment to induce kinase expression, significantly reduced the level of cell death observed in the 'PexRD2-insensitive mutant' simulated condition, compared to the standard < 2-h incubation period (Figure 5.38 A). Addition of sucrose to

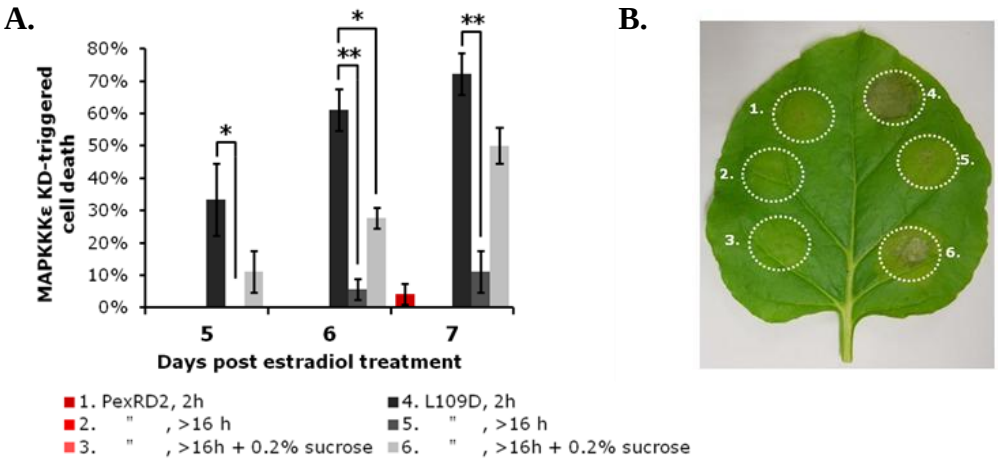

Figure 5.38 Overnight incubation of agroinfiltration mixes reduces subsequent MAPKKKε KD-triggered cell death

(A.) The effect of prolonged incubation in infiltration buffer on the mean level of cell death triggered by *St*MAPKKKε KD (residues 1 – 332) in the presence of PexRD2 or L109D, with or without the addition of 0.2% (w/v) sucrose to infiltration buffer. Bars indicate the mean ± SE for three plants. Asterisks indicates means that are significantly different from the standard 2 h incubation condition (Tukey HSD, * = P<0.05, ** = P<0.01). **(B.)** Image of a representative leaf with conditions numbered as in (A.) taken at 7 dpt.

infiltration buffer used for overnight incubation had some effect in restoring the level of cell death observed, although it was still dramatically reduced compared to the standard incubation period. These results likely indicate a reduction in *Agrobacterium* mediated transformation efficiency. Based on these results prolonged incubation was deemed unsuitable for the subsequent preliminary mutant screening, and the standard incubation period was used instead.

Note: Mutant library construction was conducted by Dr Richard Hughes (JIC). Preliminary screening was conducted with Dr Richard Hughes and Benjamin Hall (JIC). Subsequent screening will be conducted by Benjamin Hall.

Mutants were generated by error-prone-PCR, cloned into pERCH, and transformed into *Agrobacterium* by Dr Richard Hughes (JIC). *Agrobacteria* harbouring mutant clones were grown, mixes as described and prepared as described in Section 2.9.8, and infiltrated into the leaves of *N. benthamiana*. Each leaf infiltrated contained four different mutant clones co-agroinfiltrated with PexRD2, as well as, wild-type *St*KDε$_{1\text{-}332}$ and PexRD2, as a PexRD2-sensitive control and wild-type *St*KDε$_{1\text{-}332}$ and PexRD2^{L109D}, as a surrogate 'PexRD2-insensitive' control. Any mutants that triggered a higher level of cell death than the PexRD2-sensitive negative control were deemed a potential hit.

This assay design means that since cell death induction is most likely dependent on kinase activity, any mutants identified will likely be catalytically active. In the preliminary pilot screen 286 *Agrobacterium* clones were screened, and nine putative PexRD2-insensitive MAPKKKε mutants were identified. Putative hits were repeated to confirm the results and sequenced to identify the mutated residues. The success rate of this primary screen (~3%) provided a manageable number of candidate mutants, that following additional rounds of screening and confirmation in a secondary screen, could be tested for their ability to confer increased resistance to *P. infestans*. Knowledge of the identity of the mutated residues, combined with structural information from homology modelling of the kinase domain, may also give key insights into the PexRD2-MAPKKKε-interaction interface. This information could also provide a unique perspective on the potential molecular mechanism of PexRD2's inhibition of MAPKKKε signalling.

5.3 Conclusion

Plant MAP kinase cascades are increasingly being recognised as key components of immunity signalling; transmitting and amplifying signals following the perception of a diversity of PAMPs and effectors to result in altered gene expression and anti-microbial defence responses (Pitzschke *et al.*, 2009). They have also been identified as a prominent target for interference by effector proteins leading to the suppression of PAMP-triggered immunity (Zhang *et al.*, 2007, Cui *et al.*, 2010, Wang *et al.*, 2010). MAPKKKε is a known positive regulator of cell death responses associated with plant immunity, being shown to be required for resistance to virulent and avirulent bacterial phytopathogens, and for signalling following the recognition of elicitors from bacterial and fungal pathogens (Melech-Bonfil and Sessa, 2010).

A yeast two-hybrid screen revealed that the potato ortholog of MAPKKKε interacts with the RXLR effector PexRD2. This interaction was independently confirmed *in planta*, and shown to be specific. Silencing of this host gene in infection assays using the *Phytophthora infestans-Nicotiana benthamiana* model pathosystem has revealed that this kinase is also required for some level of resistance against the late blight pathogen.

Transient over-expression of the effector *in planta* prior to infection was able to phenocopy the effect of silencing *MAPKKKε*. However, infection of tissue expressing two PexRD2-like effectors, which do not interact with MAPKKKε, did not have the same effect. This potentially highlights the importance of this effector-target interaction for the outcome of infection by *P. infestans*.

The requirement of MAPKKKε for the HR triggered by the AvrPto/Pto and Avr4/Cf4 recognition events was confirmed. The cell death events triggered by the recognition or activity of *P. infestans* proteins tested, so far, were, on the other hand, shown to be MAPKKKε-independent. However, a large number of other oomycete elicitors are yet to be tested.

Perception of the PAMP-like elicitin, INF1, is known to activate MAPK cascades (Asai *et al.*, 2008); however, INF1-induced cell death was shown to not require MAPKKKε. The involvement of MAPKKKε in signalling other oomycete PAMP

responses, such as the peptide Pep-13 from a cell wall transglutaminase (Halim *et al.*, 2004, Halim *et al.*, 2009), or the cell wall glycoprotein, CBEL (Gaulin *et al.*, 2002, Khatib *et al.*, 2004) that also elicit necrosis and defence response *in planta*, is yet to be tested.

The recognition of $Avr3a^{KI}$ by R3a was one of the cell death events that was confirmed to be independent of MAPKKKε, however, to date, 68 *R* genes from *Solanum* spp. that confer resistance to potato late blight have been identified (Rodewald and Trognitz, 2013), and MAPKKKε could theoretically be required for the downstream signalling that leads to resistance for any one of them. Alternatively MAPKKKε may be required for signalling following the recognition of an as yet, unidentified recognised effector (avirulence factor) or for signalling following a recognition event that contributes towards resistance without the typical cell death associated with the hypersensitive response.

In addition, although, the cell death triggered by the translocated kinase effector, CRN8, was also shown to be MAPKKKε-independent, four other domains within the CRN family of effectors are also known to elicit cell death responses *in planta*.

Finally the previously published weak cell death activity of PexRD2 itself is also not dependent on the activity of MAPKKKε. This cell death response was only robustly seen when PexRD2 was expressed from viral-based binary vectors that deliver high levels of protein expression. The biological relevance of PexRD2-triggered weak cell death has yet to be characterised, and it is unclear if it represents a plant immune response following a recognition event, or simply a more general toxic effect as has been proposed for the *Phytophthora* cell death–inducing Nep1-like proteins (NLPs) (Kanneganti *et al.*, 2006).

The virulence function of PexRD2 appears to be as an inhibitor of MAPKKKε-mediated signalling. PexRD2 specifically suppresses the cell death and ion leakage associated with the HR, as well as the activation of MAPKs for events that are dependent on MAPKKKε. Cell deaths that are independent of MAPKKKε-signalling were, generally, not suppressed by PexRD2. One point of potential confusion appears to be the cell death induced by INF1. Pre-agroinfiltration, but not co-agroinfiltration, of *PexRD2* completely suppressed INF1-induced cell death, when

INF1 was expressed subsequently by agroinfiltration. Similar activity has been reported for other RXLR effectors including PexRD2-like effectors from *Phytophthora sojae* (Wang *et al.*, 2011). Pre-agroinfiltration of PexRD2 had no effect on the cell death triggered when crude culture filtrate, containing INF1 protein, was delivered directly into plant tissue. It is possible that this cell death may result from the recognition of pathogen-derived molecules other than INF1 (which is also suppressed by AVR3a^{KI}); however, another plausible explanation for this discrepancy is that prior expression of PexRD2 appears to inhibit delivery or expression of subsequent transgenes. Although, this observation raises questions as to the best current practices in the field of plant pathology for assessing effector-mediated cell death suppression, it might also provide interesting insights into the mechanisms of *Agrobacterium*-mediated transformation of plants. These bacteria have been reported to 'hijack' MAPK cascade signalling, by using the MPK3-induced translocation of VIP1[§§] to shuttle their T-DNA into the nucleus (Djamei *et al.*, 2007). As such, if PexRD2 can interfere with T-DNA transfer it could implicate MAPKKKε as an important component in this delivery process. However, the ability to transiently express proteins via agroinfiltration in *MAPKKKε*-silenced plants would suggest otherwise.

Whether the responses triggered by over-expression of MAPKKKε kinase domain alone are the same as those that follow activation of the full length protein during normal immunity signalling remains to be determined. This is important since the C-terminal, non-catalytic regions of MAPKKKs are often implicated in regulatory roles and mediating substrate specificity (Suarez-Rodriguez *et al.*, 2007). Regardless of this, the ability of PexRD2 to inhibit the cell death triggered by over-expression of the MAPKKKε KD provides strong support for its proposed function as a specific inhibitor of MAPKKKε-mediated signalling at this level of the cascade.

Furthermore, although epigenetic experiments have positioned MEK2, SIPK and WIPK as the downstream components for MAPKKKε-mediated signalling that leads to cell death, whether these proteins represent the minimal functional signalling cascade is also yet to be determined. The proposed three-tier modules of MAPK

[§§] VIP1 = VirE2-Interacting Protein 1

cascades are increasingly being recognised as an oversimplification. Hashimoto *et al.*, (2012) revealed that two novel phylogenetically annotated MAPKKKs, MAPKKKβ and MAPKKKγ from *N. benthamiana*, formed a linear signalling pathway upstream of the previously identified MAPKKKα, with signalling through this pathway leading to HR-like cell death. Furthermore, Kong *et al.*, (2012), identified MEKK2 from *Arabidopsis* as an annotated MAPKKK that is phosphorylated and negatively regulated by MPK4. MEKK2 in turn was implicated as a positive regulator of plant immune responses. These recent studies highlight the prevalence of sequential or parallel signalling in, and cross-talk between, MAPK cascade modules, suggesting that their signalling should more accurately be interpreted as networks. Screens to identify additional interactors of MAPKKKε: combined with more *in planta* epigenetic experiments and *in vitro* protein biochemistry assays; would be useful in identifying the true extent of the MAPKKKε-mediated signalling network.

Uncovering the molecular mechanism behind PexRD2-mediated inhibition of MAPKKKε represents the next big challenge. Unlike the examples of bacterial effectors discussed in the introduction (see Section 5.1 and Figure 5.1), PexRD2 is not predicted to display enzymatic activity. As such PexRD2 might be predicted to interact with MAPKKKε to either block or promote interactions with other host proteins that interfere with this host kinases activity. Interestingly, other RXLR effectors are being implicated as inhibitors of MAPK-mediated signalling responses. The unrelated RXLR effector, Avh238 from *P. sojae* P7076, has been shown to suppress the pathogen-independent cell death triggered by over-expression of a MAPKKK, NPK1, and a MAPKK, MKK1; as well as INF1-induced cell death (Wang *et al.*, 2011). Avh238 is not predicted to contain a WY-domain (Boutemy *et al.*, 2011), and the host targets of Avh238, and hence the mechanism by which this effector achieves this cell death suppression, remain unknown. However, since Avh238 can suppress cell death triggered by both a MAPKKK and MAPKK, it is plausible that its activity is targeting downstream signalling components (Wang *et al.*, 2011). A second *P. sojae* RXLR effector Avh331, which does contain predicted W and Y motifs (Wang *et al.*, 2011), was also shown to be able to suppress a number of responses known to be downstream of MAPK cascade signalling (Cheng *et al.*,

2012). However, activation of MPK3 and MPK6 was unaffected in *Arabidopsis* expressing Avh311 suggesting that the actual mechanism of action is also downstream of the MAPKs.

The structure of the WY-domain of PexRD2 has been invaluable in guiding the design of structurally informed mutants that no longer interact with MAPKKKε, nor suppress *in vivo* responses that are dependent on MAPKKKε-mediated signalling. This work has shown that the nature of a number of the surface exposed residues and the N- and C-termini of the WY-fold are flexible with regards mediating the interaction with MAPKKKε. In contrast, mutation of residues within the dimerisation interface or variable loop region caused a reduced or complete loss of interaction with MAPKKKε. This could be correlated with a loss of cell death suppression and enhancement of pathogenic growth. These results further strengthen the model that MAPKKKε is a genuine virulence target for PexRD2.

One non-interacting mutant, PexRD2^{L109D}, showed dominant negative activity, although the exact mechanism by which it achieves this still remains unclear. This result might indicate that the mechanism of inhibition might be more complex than initially proposed. Furthermore, since this mutant effector was also unable to interact with either the PM4K1 or PUB38-like proteins, it highlights the need to characterise these host proteins potential involvement in plant immunity.

It would be interesting to see if the dominant negative activity of this mutant effector could be exploited to enhance resistance to late blight. If so, the identification of this mutant effector, in addition to potential PexRD2-insensitive variants of the virulence target, could open new avenues for the engineering of resistance to the challenging late blight pathogen in economically important crop species.

Chapter 6:

Heterologous Expression of CRN8

6 Heterologous Expression of CRN8

6.1 Introduction

6.1.1 CRN8, a translocated effector with homology to protein kinases

CRN8 is a member of a second major family of host translocated effectors, the CRNs (*cr*inkling and *n*ecrosis, or 'Crinklers' (Torto *et al.*, 2003)). It was identified in an comparative analysis of 150 full length cDNA sequences from *Phytophthora infestans* (Win *et al.*, 2006). It was shown to possess the hallmark feature of this family, a conserved N-terminal LFLAK domain (Haas *et al.*, 2009). CRN8, in common with most CRN and RXLR effectors has modular domain architecture (Figure 6.1). The LFLAK domain harbours a LXLFLAK translocation motif (Schornack *et al.*, 2010) (46-LQLFLAK-52). This domain is preceded by an N-terminal signal peptide (residues 1 - 13) and followed by the DWL domain, which ends with conserved HVLVXXP motif (110-HVLVALP-116).

The C-terminal effector domain of CRN8 was designated a D2 domain by Haas et al (2009). The D2 domain shows significant similarity to serine/threonine protein kinases. CRN8 is an RD kinase since the predicted catalytic domain, including residues 454 to 573, has an arginine residue (Arg469, or R469) preceding the conserved catalytic aspartate (Asp470, or D470) (van Damme *et al.*, 2012). In CRN8, the D2 domain is followed by a predicted nuclear localisation signal (NLS, 590-KGVRKKHRRA-599), which is observed in 5 out of the 10 paralogs of CRN8 in the *P. infestans* reference genome strain (T30-4). Three paralogs of CRN8 are also present in the *P. ramorum* reference genome, all of which also have a similar predicted NLS, but, in contrast, preceding the D2 domain. The *P. infestans* paralogs show a high degree of sequence conservation in their D2 domains (97 – 99% identity).

Figure 6.1 CRN8 displays modular domain organisation.

Cartoon of domain organisation of CRN8 from *Phytophthora infestans* isolate 88069 highlighting the signal peptide (yellow), LFLAK domain (light green) and DWL domain (dark green). The C-terminal D2 domain (red), with the catalytic kinase domain (dark red) and positions of the catalytic residues are also highlighted, as is the predicted nuclear localisation signal (orange). Numbers indicate the residues at the boundary between domains.

6.1.2 CRN8 triggers cell death *in planta*

The D2 domain of CRN8 was also identified as one of five conserved C-terminal domains from CRN effectors that were capable of triggering the eponymous necrosis phenotype when expressed inside host cells (Haas *et al.*, 2009). Deletion analysis conducted by van Damme et al., (2012) lead them to conclude that an intact D2 domain and C-terminal NLS (residues 118 – 599) was required for cell death induction (Figure 6.2 A). Any further truncation at the N-terminus resulted in no cell death; whilst deletion of the NLS, by truncating the C-terminus back to residue 582 caused a partial loss of activity, which was again completely abolished by any further truncation. The requirement of the NLS for cell death induction suggests that CRN8 triggers cell death by acting within the plant nucleus. This is consistent with the observation that CRN8, and other CRN effectors, accumulate in the plant nucleus (Figure 6.2 B), and that the addition of a functional nuclear export signal (NES) to exclude CRN8 from the plant nucleus also abolishes its ability to cause cell death (Schornack *et al.*, 2010).

6.1.3 CRN8 is an active kinase, and phosphorlyated *in planta*

In vitro assays demonstrated that CRN8 was a functional kinase, with auto-phosphorylation activity (Figure 6.2 C). Epitope-tagged wild-type and mutant CRN8 (where the catalytic residues had been substituted for non-functional residues (D470N or R469A/D470A)); were expressed *in planta*, and purified by

immunoprecipitation. *In vitro* kinase assays with γ-P^{32}-ATP revealed detectable phosphorylation only with the wild-type CRN8, and not the mutant variants (van Damme *et al.*, 2012). Similarly, only the wild-type effector was stained using phosphorylation-specific staining of crude extracts and immunoprecipitated material. *In planta* expression of kinase inactive mutants of CRN8, revealed that whilst the R469A/D470A double mutation abolished the cell death activity, the D470N mutant still caused the characteristic cell death response. This suggests that kinase activity, *per se*, is not required for CRN8-induced cell death.

Mass spectrometry revealed five phosphorylated serine residues within the D2 domain of CRN8 expressed *in planta* (van Damme *et al.*, 2012). The substitution of either three or five of these serines for alanines either greatly reduced or abolished CRN8's cell death activity, suggesting that this activity is the result of the phosphorylated state of CRN8 rather than its kinase activity directly (Figure 6.2 D).

Interestingly, co-expression of the kinase inactive mutant $CRN8^{R469A/D470A}$ with the wild-type CRN8 interfered with CRN8-induced cell death suggesting that this mutant may have dominant negative activity (Figure 6.2 E), through an effect of the mutant protein destabilising the wild-type protein *in planta* (van Damme *et al.*, 2012). This observed destabilisation suggested an interaction between CRN8 and $CRN8^{R469A/D470A}$, which was confirmed by co-immunoprecipitation experiments. This self association *in planta* lead van Damme et al., (2012) to conclude that, in similarity with other kinases, CRN8 forms dimers.

6.1.4 CRN8 enhances virulence of *P. infestans*

Pathogenicity assays using detached leaves from the model host *Nicotiana benthamiana* revealed that *Agrobacterium*-mediated transient expression of CRN8 enhanced infection by the *P. infestans* (van Damme *et al.*, 2012). Infiltration of *Agrobacterium* harbouring *CRN8*, two days after zoospore infection, increased the growth rate of the pathogen, compared to infiltration of *Agrobacterium* harbouring a vector control (Figure 6.2 F). In contrast, transient expression of the kinase inactive mutant $CRN8^{R469A/D470A}$ caused a reduction in the growth rate of the pathogen, consistent with the dominant negative activity of this mutant.

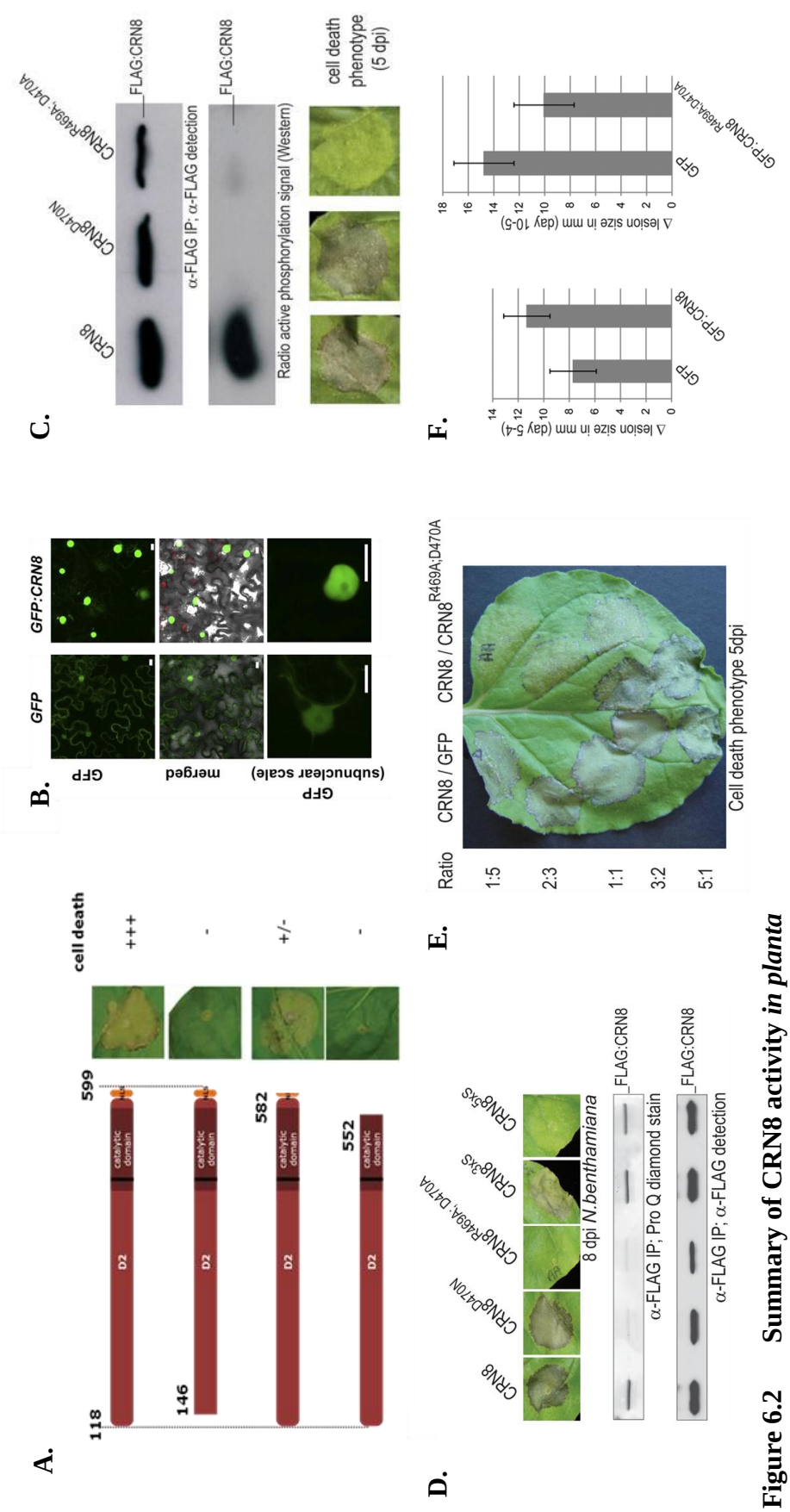

Figure 6.2 Summary of CRN8 activity *in planta*

(A.) The entire CRN8 effector domain (residues 118 to 599) is required for full cell death induction. **(B.)** CRN8-D2 is nuclear localised *in planta*. **(C.)** Catalytic site mutants show loss of autophosphorylation activity, although only D469A/R470A mutant losses cell death induction activity. **(D.)** Five serine residues are required for cell death induction. **(E.)** Kinase inactive mutant CRN8$^{D469A/R470A}$ shows dominant negative activity **(F.)** CRN8 enhances growth of *Phytophthora infestans*, whilst dominant negative CRN8$^{D469A/R470A}$ impedes pathogen growth. *Figure adapted from Schornack et al., (2010) and van Damme et al., (2012).*

To assist development of a mechanistic understanding of the kinase activity of CRN8, and its relationship to its virulence activity, conditions for the heterologous expression and purification of CRN8 protein were assessed. If successful, the resultant pure protein would then be used for *in vitro* biophysical analysis and structural characterisation to support the *in vivo* and enzyme assays already conducted and described above.

6.2 Results and Discussion

6.2.1 Cloning and mutagenesis in pOPIN expression vectors

The sequence of the C-terminal effector domain of CRN8 (the D2 domain and NLS) was synthesised and codon optimised for *E. coli* expression by GenScript USA Inc (Figure 6.3). This synthesised DNA was then used as a template to clone sequences encoding either the full effector domain (CRN8^{-}D2, residues 118 – 599) or a truncated version encompassing the predicted, structured, catalytic kinase domain (CRN8-KD, residues 337 – 599 (Figure 6.4)) into either pOPINF, pOPINJ or pOPINM expression vectors (Berrow *et al.*, 2007), as described in Section 2.4.8.1. The N-terminal regions, containing the translocation motifs, were omitted because work by van Damme et al, (2012) had shown they were dispensable for function, and because adopting a similar approach had proved successful with other cytoplasmic effectors (Boutemy *et al.*, 2011). As described previously (Section 3.2.1), proteins cloned into pOPINF are expressed with an N-terminal hexa-histidine affinity tag that is cleavable owing to the presence of a 3C protease site in the linker region (see Figure 3.6 B). pOPINJ confers an N-terminal dual hexa-histidine Glutathione S-transferase (GST) affinity tag, whilst pOPINM confers an N-terminal dual hexa-histidine maltose binding protein (MBP) affinity tag. As in pOPINF, the affinity tags from pOPINJ and pOPINM are cleavable by 3C protease. As well as aiding purification, the addition of these larger affinity tags has been shown to improve the solubility of the protein of interest fusion partner (Esposito and Chatterjee, 2006).

The over-expression of functional kinases is often toxic to bacterial cells (Haacke *et al.*, 2009). As such, site-directed mutagenesis of the codon optimised *CRN8-D2* was

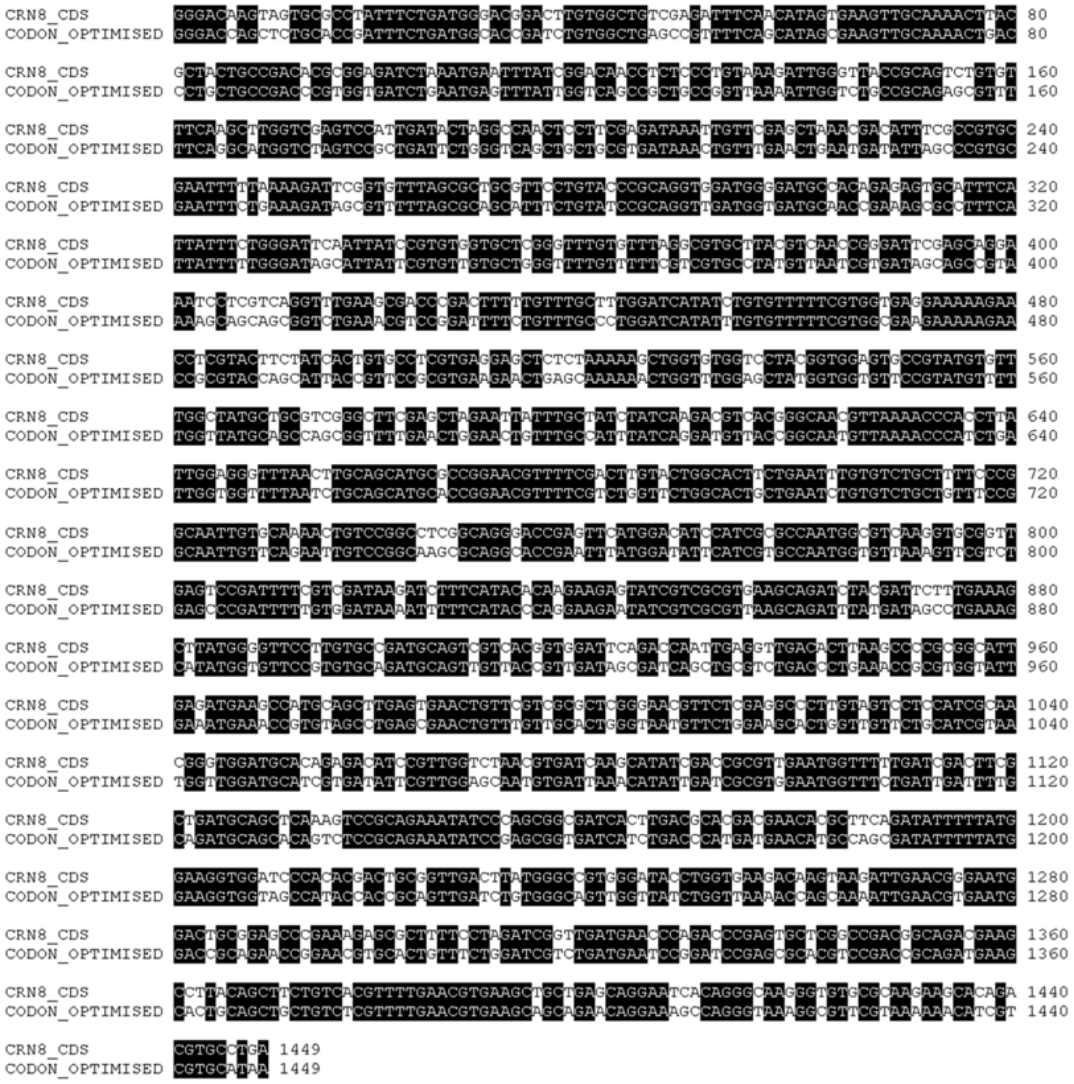

Figure 6.3 Wild-type vs. codon optimised CRN8 DNA sequences

A sequence alignment of effector domain coding sequence (CDS) for CRN8 from *P. infestans* 88069 against the synthesised codon optimised DNA sequence. Conserved nucleotide bases are shaded in black.

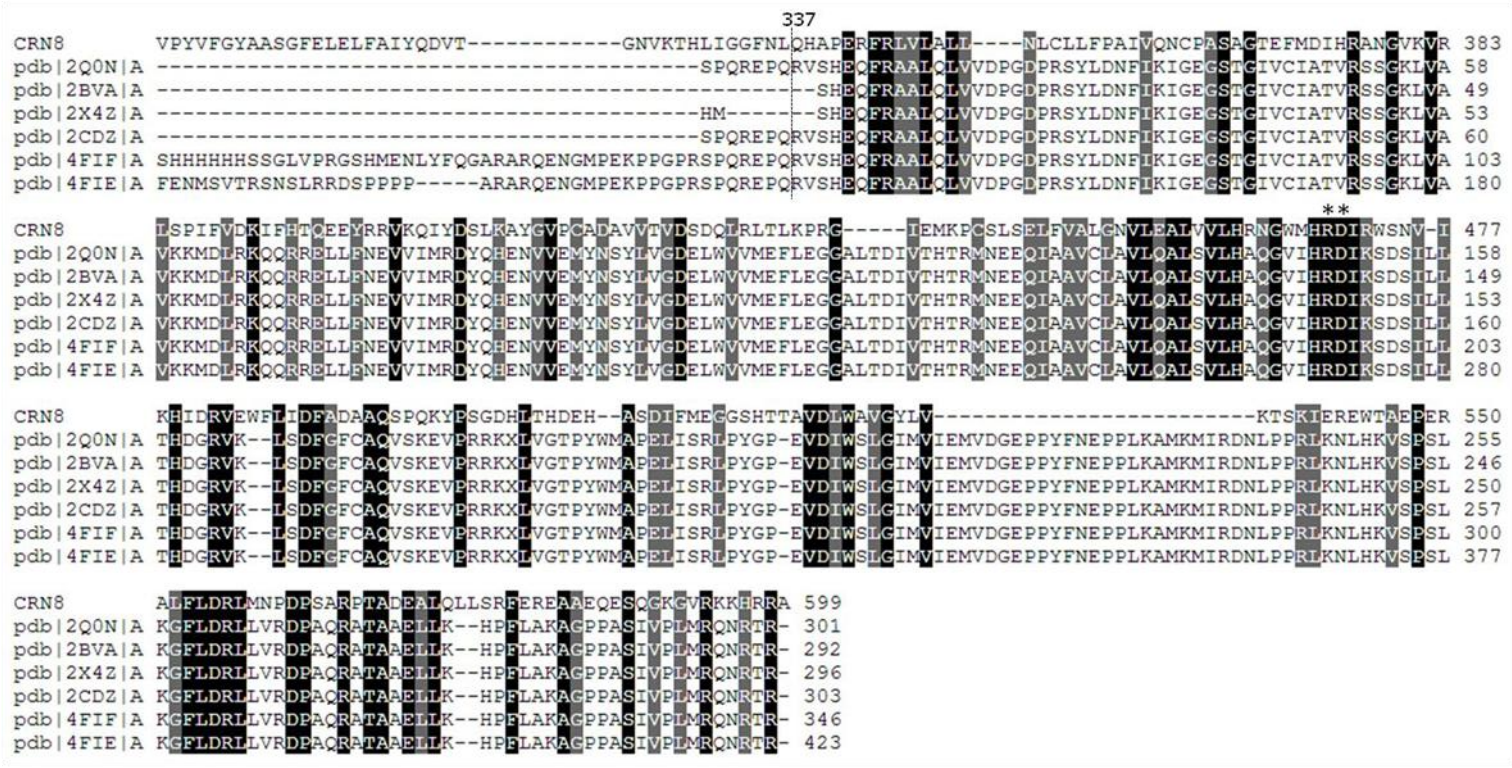

Figure 6.4 Alignment of catalytic domain within CRN8-D2 domain with PDB protein kinase structures

A protein sequence alignment including the region of D2 domain of CRN8 that shows its homology to serine/threonine protein kinases. Multiple sequence alignment was performed using COBALT (Papadopoulos and Agarwala, 2007), following BLASTP (Altschul *et al.*, 1990) search of protein sequences of structures deposited in PDB. Conserved residues are shaded in black, similar residues are shaded in grey. Gln337, which was chosen as the N-terminus for CRN8-KD constructs, is indicated. The positions of the catalytic residues, Arg496 and Asp470, are highlighted with asterisks.

used to specifically substitute both the catalytic arginine and aspartate residues in positions 469 and 470, respectively, with alanines to generate the kinase inactive CRN8$^{R469A/D470A}$. Using an overlap extension polymerase chain reaction (oe-PCR) strategy, *CRN8-D2*$^{R469A/D470A}$ PCR product was generated (Section 2.4.6.2, Figure 6.5) and subsequently cloned into the pOPIN expression vectors outlined above. A mutagenesised CRN8-D2 construct was used as a template to sub-clone CRN8-KD$^{R469A/D470A}$ into the same expression vectors. All CRN8 *E. coli* expression constructs created as described above are listed in Table 6.1 and Appendix Table D.

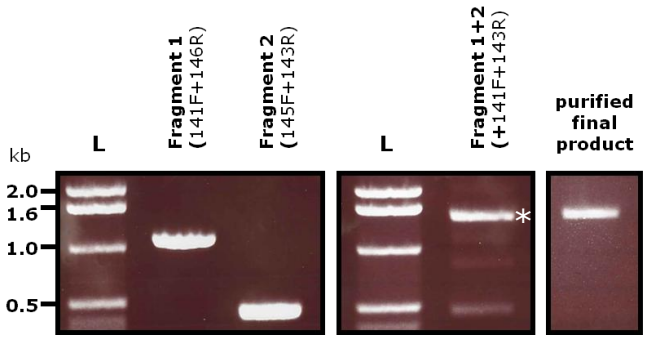

Figure 6.5 Overlap extension PCR to generate *CRN8-D2*$^{R469A/D470A}$

The left panel shows the two PCR fragments amplified using either primers 141F and 146R, or 145F and 143R. The two fragments have homologous overlap in the region containing the desired mutation. The middle panel shows the products formed following the overlap extension reaction and subsequent amplification using primers 141F and 143R. The main product (*) is the full length *CRN8-D2*$^{R469A/D470A}$ fragment. The right panel shows the purified final product. L indicates lanes containing 1kb DNA ladders.

Table 6.1 Constructs for *E. coli* expression of CRN8 proteins

Construct name	Expressed Fusion Protein[a.b.c.d.]	Predicted molecular weight (kDa)[e.]
pOPINF:D2	His_6-3C-CRN8-D2	**56.6**
pOPINF:D2-AA	His_6-3C-CRN8-D2$^{R469A/D470A}$	**56.5**
pOPINF:KD	His_6-3C-CRN8-KD	**32.1**
pOPINF:KD-AA	His_6-3C-CRN8-KD$^{R469A/D470A}$	**32.0**
pOPINJ:D2	His_6GST-3C-CRN8-D2	**82.4**
pOPINJ:D2-AA	His_6GST-3C-CRN8-D2$^{R469A/D470A}$	**82.3**
pOPINJ:KD	His_6GST-3C-CRN8-KD	**57.7**
pOPINJ:KD-AA	His_6GST-3C-CRN8-KD$^{R469A/D470A}$	**57.6**
pOPINM:D2	His_6MBP-3C-CRN8-D2	**97.2**
pOPINM:D2-AA	His_6MBP-3C-CRN8-D2$^{R469A/D470A}$	**97.1**
pOPINM:KD	His_6MBP-3C-CRN8-KD	**72.6**
pOPINM:KD-AA	His_6MBP-3C-CRN8-KD$^{R469A/D470A}$	**72.5**

a. His_6- indicates a hexa-histidine affinity tag
b. GST indicates a Glutathione S-transferase affinity tag
c. MBP indicates a maltose binding protein affinity tag
d. -3C- indicates a cleavable linker containing the 3C protease cleavage site (LEVLFQ▼GP)
e. Molecular weight predictions, given to 1 dp, were calculated using "Compute pI/Mw" tool via the ExPASy Proteomics Server

6.2.2 Small scale expression screening in *E. coli*

The CRN8 expression constructs listed in Table 6.1 were transformed into the BL21(DE3) expression strain, and small scale expression tests of recombinant proteins were conducted as described previously (Section 2.4.3). Protein expression was tested in LB media or auto-induction media (AIM) using either post-induction incubation at 37ºC for 3 – 4 h, or 18ºC for approximately 16 h.

SDS-PAGE analysis of whole cell extract and soluble fraction samples from each expression condition revealed that whilst fusion proteins were clearly over-expressed, no protein was visible in the soluble fraction (Figure 6.6). This indicates that the protein was likely folding incorrectly and being localised to inclusion bodies.

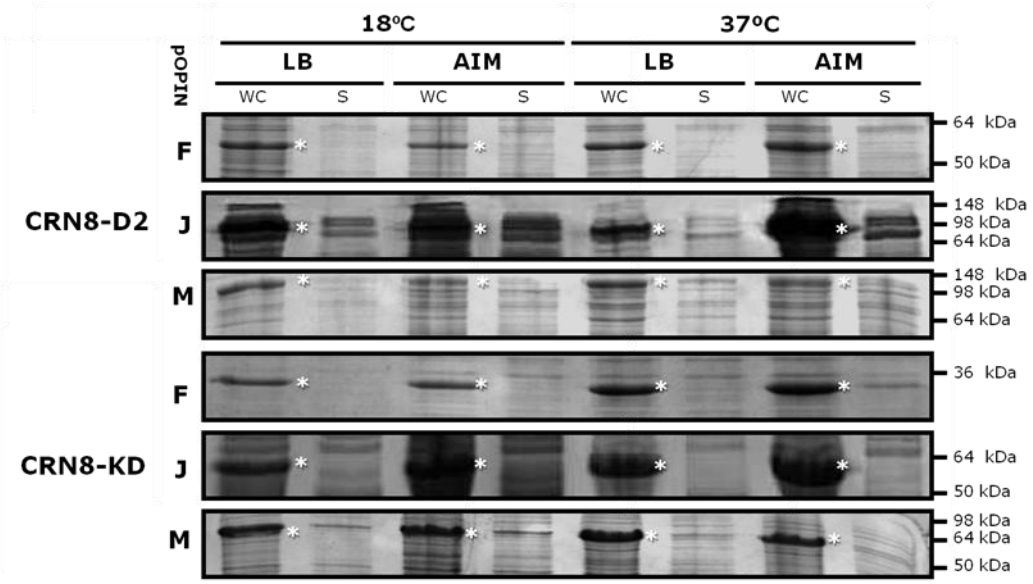

Figure 6.6 Small scale expression tests with CRN8 fusion proteins

17% SDS-PAGE analysis of whole cell (WC) and soluble fractions (S) collected following small scale expression trials of CRN8 fusion proteins. Protein expression was tested in LB or auto-induction media (AIM) using either post-induction incubation at 37ºC for 3 – 4 h, or 18ºC for approximately 16 h. Asterisks indicate an over-expressed protein of the predicted size. In all cases, this was present in the whole cell, but absent in the soluble fraction, indicating insoluble protein. Data shown are for wild-type CRN8 proteins, although expression trials with the kinase inactive CRN8$^{R469A/D470A}$ showed qualitatively the same results of insoluble expression (data not shown).

Performing IPTG induction at higher cell densities has been suggested as a possible method of enhancing soluble over-expression of heterologous proteins in *E. coli* (Berrow *et al.*, 2006). To investigate whether this technique would improve soluble expression of CRN8 fusion proteins in BL21(DE3); scaled-up over-expressions of His_6-CRN8-D2 or His_6-CRN8-KD were conducted in 50 mL cultures of LB media at 37°C. The method used was the same as that for the small scale expression tests, with minor alterations. Cultures were incubated to either a cultural density of OD_{600} = 0.5, as was used in previous expression tests, or the higher OD_{600} = 1.2, prior to induction. Samples were subsequently taken at regular intervals post induction and analysed using SDS-PAGE as before.

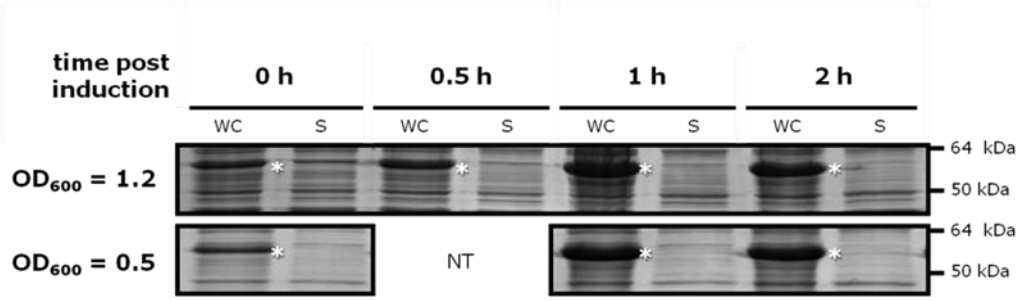

Figure 6.7 Expression tests using high OD_{600} induction

17% SDS-PAGE analysis of time series of whole cell (WC) and soluble fractions (S) collected following over-expression of His_6-CRN8 fusion protein in LB media (AIM) at 37ºC. IPTG induction was conducted at a cultural density (OD_{600}) of 0.5 or 1.2. Asterisks indicate an over-expressed protein of the predicted size. In all cases, this was present in the whole cell, but absent in the soluble fraction, indicating insoluble protein. Data shown are for wild-type D2 domain, although expression trials with the CRN8-KD showed qualitatively the same results of insoluble expression at all time points (data not shown).

The results showed that expression of CRN8 fusion proteins was successfully enhanced following IPTG induction, although in all cases, CRN8 fusion proteins remained insoluble (Figure 6.7). Therefore, under these conditions, inducing at a higher cell density did not enhance solubility of the expressed proteins. Interestingly, a band corresponding to the fusion protein was also visible in protein samples taken prior to induction (0 h), indicating that there is 'leaky' expression from the T7 promoter in the pOPIN vectors.

6.2.3 Denaturation and refolding studies

The use of strong denaturants, such as 6–8 M urea, to solubilise insoluble protein present in inclusion bodies followed by the subsequent removal of the denaturant to promote refolding of denatured proteins has been demonstrated as a valid technique to obtain soluble protein suitable for crystallographic analysis (Badarau *et al.*, 2008). Interestingly, inclusion bodies tend to show high polypeptide purity, and the addition of temperature promoted aggregation tags to drive inclusion body formation has been suggested as one method for the purification of recombinant proteins (Meyer and Chilkoti, 1999). To investigate whether denaturation and refolding of insoluble CRN8 fusion protein represented a suitable strategy for generating stable, soluble

protein, large scale over-expressions of His_6-CRN8-$KD^{R469A/D470A}$ were conducted using 1-litre cultures of AIM. These were initially grown at 37°C for 4 h, prior to overnight incubation at 18°C for approximately 20 h. The cells were harvested by centrifugation, and lysed using a cell disrupter (Section 2.5.4). The resultant lysate was centrifuged, and the supernatant discarded, to obtain an insoluble cell pellet including protein-containing inclusion bodies.

Purification of inclusion bodies, and subsequent solubilisation in urea, was conducted as described in Section 2.5.6. His_6-CRN8-$KD^{R469A/D470A}$ was highly enriched in the solubilised inclusion bodies (Figure 6.8, Lane 3). Although some remained in the insoluble material that was then removed by centrifugation (Figure 6.8, Lane 4). The solubilised material was purified by IMAC using buffers containing 8.0 M urea at room temperature. The eluted protein co-eluted with a number of contaminants, although His_6-CRN8-$KD^{R469A/D470A}$ was clearly the most dominant species (Figure 6.8, Lane 6). Interestingly, a significant proportion of CRN8-fusion protein was visible in the unbound flow through (FT) (Figure 6.8, Lane 5) and this was likely due to saturation of the metal ions in the IMAC column; since subsequent re-purification of this FT showed that the denatured CRN8-KD protein could indeed bind a Ni^{2+}-charged affinity column (data not shown).

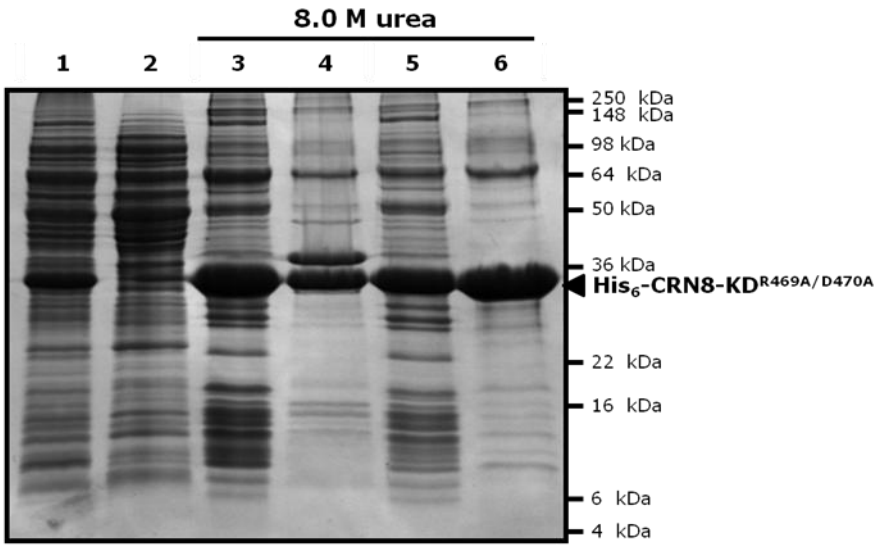

Figure 6.8 Denaturation and purification of kinase inactive CRN8-KD

17% SDS-PAGE analysis of solubilisation and purification under denaturing conditions of CRN8-KD$^{R469A/D470A}$ expressed from pOPINF. Lane 1: whole cell lysate. Lane 2: soluble fraction of cell lysate. Lane 3: solubilised inclusion bodies Lane 4: pelleted insoluble material. Lane 5: unbound flow-through (FT) after passing through nickel affinity column (IMAC). Lane 6: pooled elution from IMAC. Lanes 3 – 6 represent samples collected under denaturing conditions (in the presence of 8.0 M urea). The size of His_6-CRN8-KD$^{R469A/D470A}$ is indicated by the black triangle.

The eluted fractions containing the denatured protein were then pooled and a small-scale screen of refolding buffers was completed to determine the conditions that should minimise aggregation during the refolding stage (Figure 6.9). A range of different pH levels: 4.0, 6.0, 8.0, and 10.0; as well as two different salt concentrations: 150 mM sodium chloride and 500 mM sodium chloride; were tested using a fully factorial design. Aggregation during refolding was measured in three ways: by observing the turbidity of the diluted protein solutions; through visual comparison of insoluble material pellet size following centrifugation; and by performing SDS-PAGE analysis on the supernatant to determine relative soluble protein content.

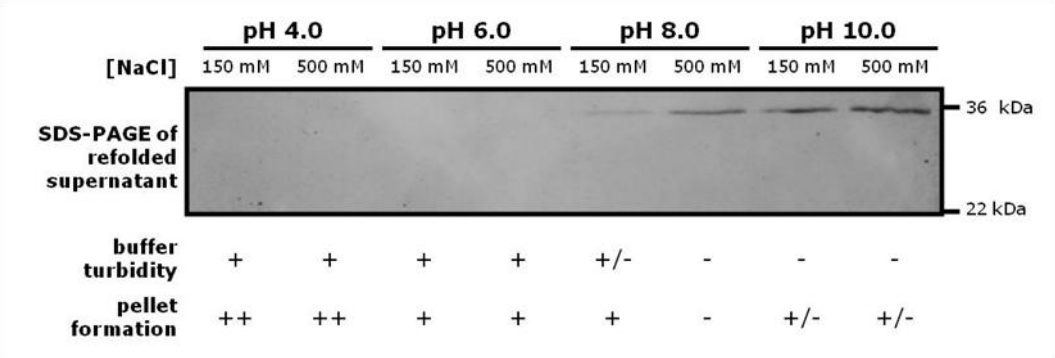

Figure 6.9 Refolding condition screen using rapid dilution method and denatured kinase inactive CRN8-KD fusion protein

17% SDS-PAGE analysis of 'refolded' His_6-CRN8-$KD^{R469A/D470A}$ (32.0 kDa) using refolding buffer conditions at varying pH and sodium chloride concentration [NaCl] as indicated above. Visual scoring for buffer turbidity and pellet formation following centrifugation are scored below each lane.

The results of this screen indicated that the lower levels of aggregate formation during refolding were associated with the higher pH conditions with a possible beneficial effect of high salt concentration. As such the pooled protein was refolded by rapid dilution, in a refolding buffer containing 50 mM Tris-HCl pH 8.5 and 500 mM sodium chloride. The 'refolded' protein solution was then clarified by centrifugation and the supernatant purified using IMAC at 4°C (Section 2.5.4.1, Figure 6.10) and size exclusion chromatography (Section 2.5.4.2)

At all stages, samples were taken and the protein content visualised using SDS-PAGE (Figure 6.8, Figure 6.10). Protein was detectable at all stages prior to the final size exclusion chromatography – however, the only discernible peak on the A_{280} absorbance trace for this stage corresponded to the void volume of the column (data not shown), suggesting that the 'refolding' method had generated incorrectly folded protein, which was forming soluble aggregates.

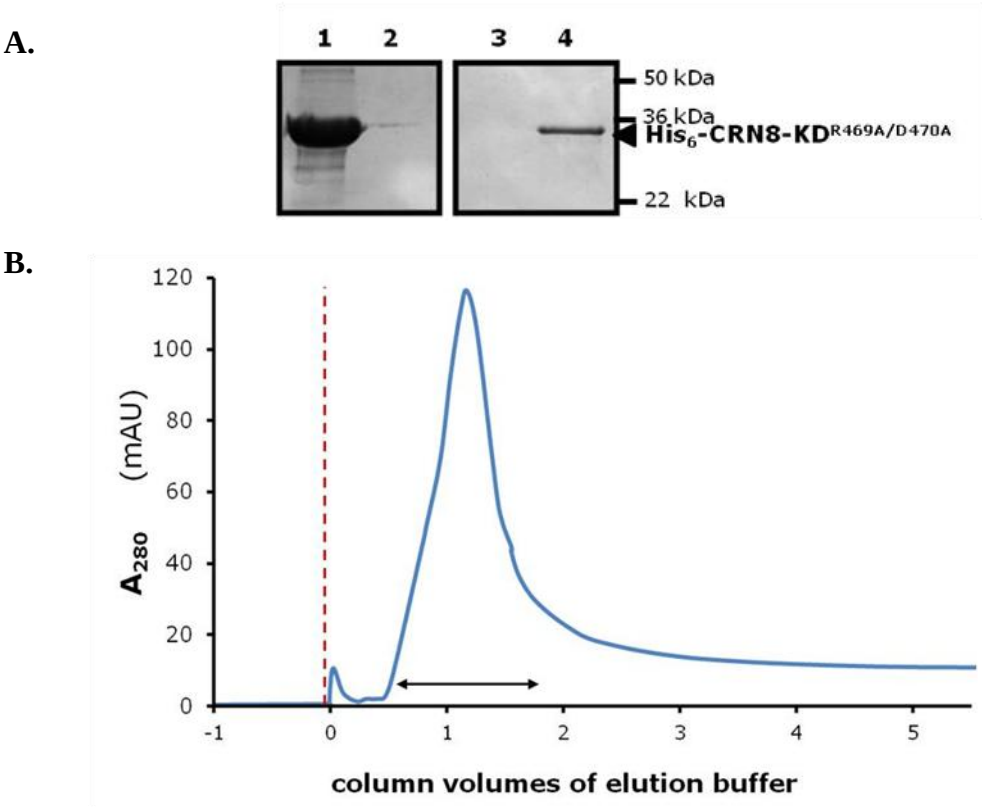

Figure 6.10 Refolding and purification of kinase inactive CRN8-KD

(A.) 17% SDS-PAGE analysis of Lane 1: denatured 'refolded' His_6-CRN8-$KD^{R469A/D470A}$. Lane 2: soluble protein following refolding by rapid dilution. Lane 3: unbound flow-through (FT) after passing through nickel affinity column (IMAC). Lane 4: pooled elution from IMAC. **(B.)** Representation of A_{280} elution profile for refolded CRN8-fusion profile. Red dashed line indicates switch to elution buffer. The black arrow spans the fractions that were pooled and analysed by SDS-PAGE (see **A**, Lane 4)

6.2.4 Cloning and expression tests using pEAQ-HT expression system

As all attempts to produce soluble CRN8 fusion proteins in *E. coli* had proved unsuccessful, a different expression system was tested. CRN8 D2 domain was known to be stably expressed and active *in planta*, and said activity was known to be unaffected by N-terminal tagging of this domain (Schornack *et al.*, 2010, van Damme *et al.*, 2012). As such, the domains that had been used for *E. coli* expression attempts were cloned into the plant binary expression vector pEAQ-HT (Sainsbury *et al.*, 2009). This vector uses a modified 5'UTR and the 3'UTR from Cowpea mosaic

virus (CPMV) RNA2 to increase mRNA stability and translation (Sainsbury and Lomonossoff, 2008) as well as incorporating the P19 suppressor of post-transcriptional-gene-silencing within the same T-DNA region. Co-infiltration with P19 had previously been shown to increase expression of a number of transgenes *in planta* (Voinnet *et al.*, 2003). However, its inclusion onto the same T-DNA region as the transgene of interest eliminates the need to co-infiltrate a separate *Agrobacterium* strain. This ensures that all transformed plant cells will possess both the transgene and P19.

PCR products encoding CRN8-D2 and CRN8-KD were amplified from a wild-type, non-codon optimised sequence as a template, and subsequently ligated into XmaI- and StuI-digested pEAQ-HT binary expression vector (Section 2.4.8.2). The cloning of inserts between these restriction sites results in the expression of N-terminal hexa-histidine-tagged proteins.

These two constructs, along with an empty vector and GFP control vector (Table 6.2), were then transformed into electrocompetent *Agrobacterium tumefaciens* GV3101 (Section 2.402), and infiltrated into *N. benthamiana* using an OD_{600} of 0.3 (Section 2.9.2). For preliminary expression trials, leaf discs from tissue infiltrated with *Agrobacterium* harbouring either pEAQ-HT:D2 or pEAQ-HT:KD were

Table 6.2 Constructs for *in planta* expression of CRN8 proteins

Construct name	Expressed Fusion Protein[a.]	Predicted molecular weight (kDa)[b.]
pEAQ-HT:EV	n/a (empty vector)	n/a
pEAQ-HT:GFP	His_6GFP	**28.0**
pEAQ-HT:D2	His_6CRN8-D2	**55.4**
pEAQ-HT:KD	His_6CRN8-KD	**31.1**

a. His_6- indicates a hexa-histidine affinity tag

b.. Molecular weight predictions, given to 1 dp, were calculated using "Compute pI/Mw" tool via the ExPASy Proteomics Server

collected at 2, 3 and 4 days-post-infiltration (dpi). In parallel, strains harbouring all four construct listed in Table 6.2 were individually infiltrated into sections of other leaves to investigate the development of phenotype development following protein expression.

Only leaf tissue infiltrated with *Agrobacterium* harbouring pEAQ-HT:D2 developed the characteristic leaf crinkling and necrosis phenotype, which was fully developed as early as 4 dpi (Figure 6.11). This is consistent with the work of van Damme et al., (2012), who identified the full D2 domain (residues 118 – 599) as the minimal region of CRN8 required induction of cell death.

CRN8 fusion protein expression in leaf extracts (Section 2.9.3) were separated using 12% SDS-PAGE, and detected using an α-HIS primary antibody followed by a HRP-conjugated secondary antibody (Sections 2.7.1 and 2.7.4). His_6CRN8-D2 was detected in infiltrated leaf tissue, with higher levels of protein detectable at 2 dpi compared with 3 dpi (Figure 6.12). No His_6-tagged protein was detected in the pEAQ-HT:KD infiltrated tissue, which indicates that the protein may either not be being expressed or, if expressed, is not stable.

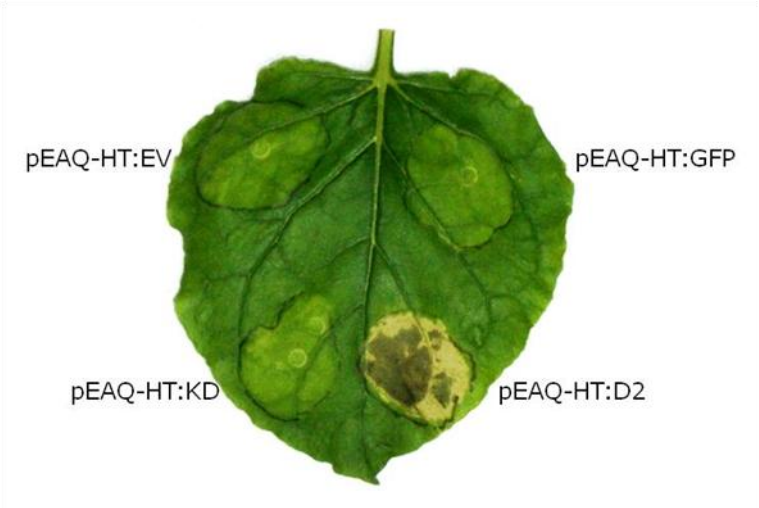

Figure 6.11 Effect of transient expression of CRN8 domains *in planta*

Phenotypes of *Nicotiana benthamiana* leaf tissue infiltrated with *Agrobacterium* harbouring the constructs as labelled. Only CRN8-D2-expressing tissue displays necrosis. Image taken at 7 dpi.

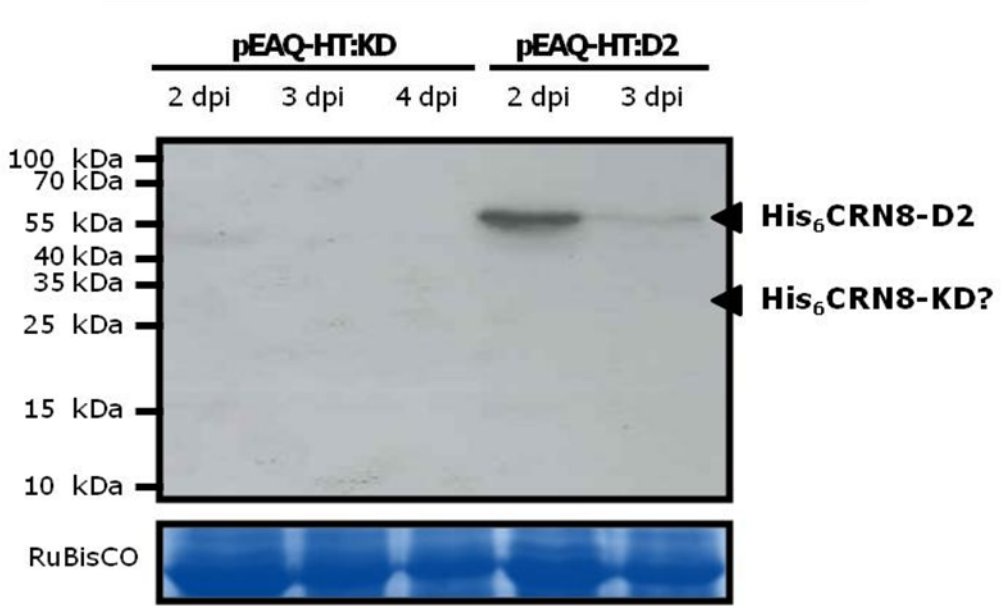

Figure 6.12 Preliminary expression test for CRN8 in *N. benthamiana*

α-HIS western blot (TOP) of protein extracts taken from leaf tissue infiltrated with *Agrobacterium* harbouring the constructs as labelled, at between 2 - 4 dpi. Predicted sizes of fusion proteins are marked with black triangles and labelled appropriately. 4 dpi sample for pEAQ-HT:D2 infiltrated tissue was not collected due to occurrence of extensive cell death. The bottom panel shows the band corresponding to the RuBisCO large subunit on Coomassie stained SDS-PAGE gel to confirm protein loading.

Follow-up expression tests were conducted using pEAQ-HT:D2 and confirmed that optimal expression of His_6-CRN8-D2 occurred at 2 dpi (Figure 6.13). For these follow up trials a pEAQ-HT:GFP-agroinfiltrated tissue was used as an positive control, and un-infiltrated and pEAQ-HT:EV-agroinfiltrated tissue were used as negative controls. Detection of His_6-tagged was conducted using western blots or InVision™ His-Tag In-Gel Stain (Invitrogen) in accordance with manufacturer's protocols. This in-gel stain displayed a high level of unspecific background staining. In particular a strong band corresponding to the ribulose-1,5-bisphosphate carboxylase/oxygenase large subunit (52.9 kDa) was observed. However, a slightly larger band which corresponded to the HisCRN8-D2 fusion protein (55.4 kDa) was detected in pEAQ-HT:D2 infiltrated tissue, and absent in the control samples. The reduced protein levels for the pEAQ-HT:D2 sample taken 4 dpi are likely a result of the occurrence of CRN8-induced cell death at this time point.

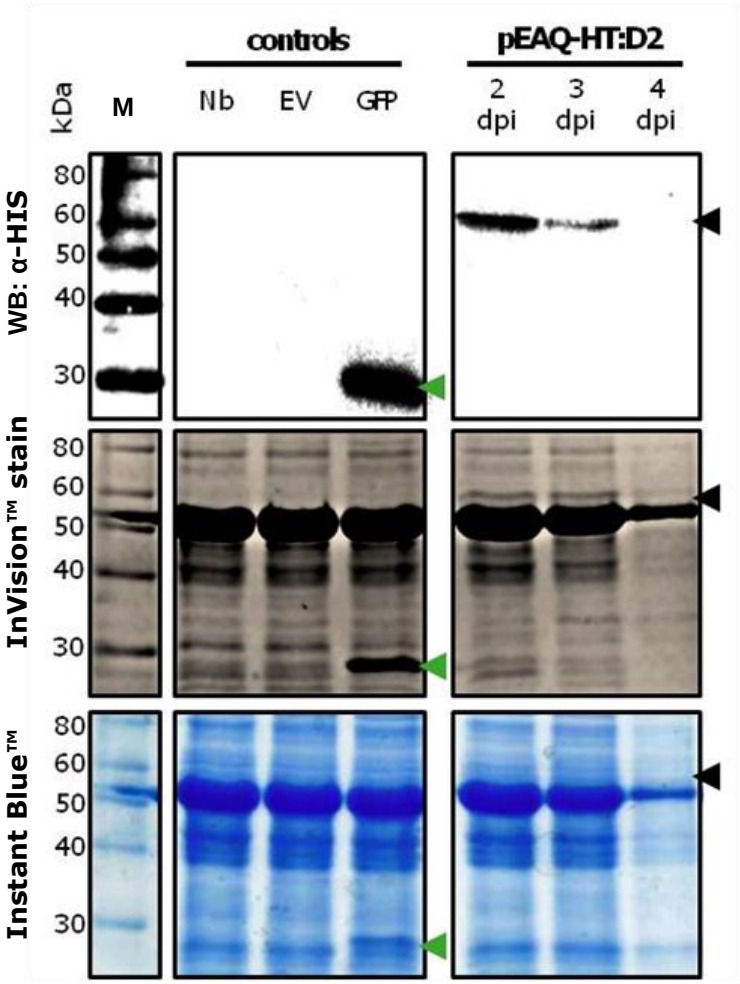

Figure 6.13 Expression test for His_6-tagged CRN8-D2 in *N. benthamiana*

Protein extracts taken from un-infiltrated (Nb) or leaf tissue infiltrated with *Agrobacterium* pEAQ-HT:EV, GFP or D2. His_6-tagged proteins were visualised using α-HIS western blot (TOP) or InVision™ His-tag in gel stain (MIDDLE). Total protein is stained by Instant Blue (BOTTOM). Predicted sizes of D2 domain and GFP are marked with black or green triangles, respectively. M indicates BenchMark™ His-tagged Protein Standard.

6.2.5 Purification of CRN8-D2 expressed *in planta*

Based on the results of initial expression tests with CRN8 fusion proteins using the pEAQ-HT vector and *N. benthamiana*, a larger scale agroinfiltration was conducted to generate pure of CRN8-D2 suitable for further biophysical and potentially structural characterisation. Leaf material from ten 4- to 5-week old plants was infiltrated with *Agrobacterium* harbouring pEAQ-HT:D2, and harvested as before (Section 6.2.4) A small sample of this material was analysed by western blotting and in-gel staining, as above, and confirmed expression of the correct sized fusion protein. Large scale protein extraction and IMAC purification of protein using a gradient elution was conducted as described in Section 2.9.5. Samples corresponding to the crude protein extract prior to loading on the Ni^{2+}-IMAC column (LOAD), the unbound proteins in the flow-through (FT) and eluted protein from the A_{280} peak (ELUATE) were prepared for SDS-PAGE analysis followed by Coomassie staining for total protein and α-HIS western blotting to detect affinity-tagged protein.

His_6CRN8-D2 purified by IMAC from plant extracts eluted as a single peak starting at a concentration of ~116 mM imidazole (Figure 6.14 A). The concentration of protein within the pooled peak was too low to be visible on the Coomassie stained gel. However, the α-HIS western blot showed a distinct band at around 55 kDa, which corresponded to the purified fusion protein (Figure 6.14 B). No such band was present in the FT sample indicating good recovery of protein. Longer exposure of the α-HIS blot, revealed unspecific smaller bands that were present in the crude extract sample, and the FT, but not the pooled fractions of eluted CRN8-D2 supporting the conclusion that IMAC had successful purified away the contaminating proteins.

Protein concentration calculations using purified His_6CRN8-D2 estimated an overall yield of 6.2 ng per gram of fresh leaf tissue. This yield was rather disappointingly low as previous proteins had been expressed to levels three orders of magnitude higher (up to 1.0 mg of fusion protein per gram of fresh leaf tissue), using the same expression system (Sainsbury *et al.*, 2009). The low yield obtained confirmed that obtaining sufficient material for further biophysical or structural characterisation of CRN8 using this expression system was not feasible.

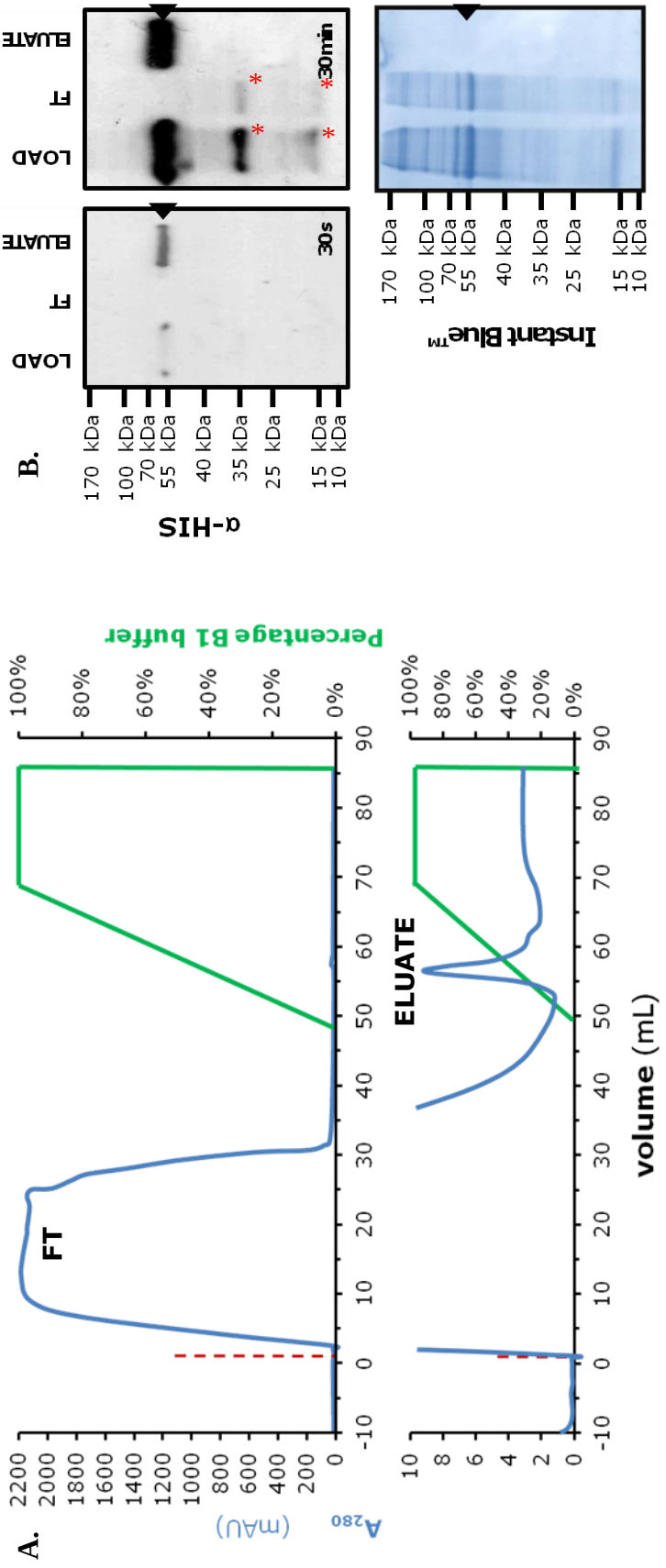

Figure 6.14 Purification of His_6CRN8 expressed transiently in *Nicotiana benthamiana* using Ni^{2+}-IMAC

(A.) Representation of A_{280} profile for IMAC purification of His_6CRN8-D2 from plant crude extract (blue line). Red dashed line indicates injection of crude extract on to the column. FT indicates the washing of the column with A1 buffer to remove unbound proteins, and ELUATE indicates the elution peak corresponding to His_6CRN8-D2. The concentration of B1 buffer is also shown (green line). **(B.)** 12% SDS-PAGE analysis of samples from different stages of purification,; followed by α-HIS western blotting to detect affinity-tagged protein, and Instant Blue™ staining for total protein. Exposure times for western blots are indicated on the figure. Black triangles indicate the size of His_6CRN8-D2, whereas red asterisks indicate major unspecific contaminants that are absent following IMAC.

6.3 Conclusion

CRN8 is a host translocated enzyme effector, with protein kinase activity (Schornack *et al.*, 2010, van Damme *et al.*, 2012). This kinase activity could be predicted based on sequence homology. Although translocated serine/threonine kinases have been identified as important virulence determinants for the human parasite *Toxoplasma gondii* (Boothroyd and Dubremetz, 2008), CRN8 is in contrast to the vast majority of oomycete host-translocated effectors, which lack sequence similarity to known proteins (Schornack *et al.*, 2009, Oliva *et al.*, 2010). One other notable exception is the RXLR effector AVR3b from *Phytophthora sojae*. This effector contains a Nudix motif in its C-terminal domain and was shown to have phosphohydrolase activity (Dong *et al.*, 2011). The Nudix motif was shown to be crucial for the virulence activity although was dispensable for AVR3b-dependent activation of the resistance protein Rps3b. Nevertheless, since CRN8 is unusual in that it was known to possess catalytic kinase activity, it was an exciting potential target for characterisation by structural biology.

Although it is well established that the catalytic domains of kinases adopt similar folds, subtle differences confer specificity (Scheeff and Bourne, 2005). Identifying these differences by solving the three-dimensional structure of CRN8 could give insights into important characteristics such its mechanism of activation. Furthermore, analysis of the solvent exposed surface features of the structure could indicate which residues mediate CRN8 oligomerisation, or its interaction with substrate proteins. The structure would also provide a useful tool for the interpretation of either naturally occurring polymorphisms or engineered mutations that affect CRN8 function, similar to insights gained from the structures of PexRD2 (see Chapter 4, and Boutemy et al., 2011), *Hpa*ATR1 (Chou *et al.*, 2011) and AVR3a homologs (Boutemy *et al.*, 2011, Yaeno *et al.*, 2011).

Unfortunately, structural characterisation of CRN8 has been hampered by a number of problems. Heterologous expression of recombinant CRN8 in *E. coli* expression strain BL21(DE3) consistently yielded only insoluble protein. Expression of CRN8-D2 domain or the truncated predicted kinase domain as GST- or MBP-fusion proteins did not improve solubility. Expression at low temperatures also had no

effect on protein solubility. The insolubility of CRN8 was unlikely to be due to toxic effects of kinase activity, as the kinase inactive mutant, R469A/D470A, was also consistently insoluble. Attempts to purify correctly folded recombinant CRN8 protein from *E. coli* inclusion bodies also proved fruitless. Although significant material could be obtained by solubilisation of purified IB in 8.0 M urea, subsequent refolding by rapid dilution of the denaturant did not yield stable, folded protein.

The insoluble expression of CRN8-fusion proteins in *E. coli* was disappointing, although not surprising. Bacterial protein expression systems are popular because of their simplicity and ability to produce high yields of recombinant protein. However, multi-domain eukaryotic proteins expressed in bacteria often are non-functional because these cells are not equipped to accomplish the required post-translational modifications or molecular folding (Geisse *et al.*, 1996). Eukaryotic expression systems are preferable in these cases. Previous studies outlined above had confirmed soluble expression of active CRN8-D2 domain in *Nicotiana benthamiana,* and hence this seemed a promising alternative to *E. coli* based expression. A number of binary vectors are available that allow high expression levels of recombinant proteins in planta (Lindbo, 2007, Sainsbury *et al.*, 2009). The pEAQ-HT expression system was chosen since it was shown to achieve high expression of transgenes, up to 1.0 mg per gram of fresh leaf weight. It also allowed N-terminal tagging with a hexa-histidine tag to aid subsequent purification. Although CRN8-D2 domain expressed from the pEAQ-HT expression vector was soluble and could be easily purified from plant extracts by IMAC, the low yields prohibited use of this expression system to produce material for structural characterisation.

The difficulties described above deterred further work in this area. Furthermore, solving the structure of PexRD2 effector domain lead to the prioritising the functional characterisation of this RXLR effector, as described in the previous chapters. However, there are a number of options that could have been pursued to potentially solve the problems that impeded structural characterisation of CRN8.

The low yield *in planta* was possibly a result of having to harvest infiltrated material only 2 days post infiltration, whereas other proteins that have been expressed using this vector have typically been obtained from tissue harvested 5 – 8 dpi, to allow

greater accumulation of transgene mRNA and hence higher recombinant protein levels. CRN8-induced cell death necessitated the 2 dpi harvest, and as such, the expression of a mutant CRN8 that is deficient in its cell death activity may prove beneficial, by allowing tissue to be harvested at later time points. Although the dominant negative kinase inactive mutant CRN8$^{R469A/D470A}$ does not cause host cell death, van Damme *et al.*, (2012) demonstrated it to be less stable in planta. A more suitable alternative may be provided by the quintuple serine to alanine mutant, also characterised by van Damme *et al*. This mutant was also deficient in cell death induction; however it accumulated to wild-type levels when expressed transiently *in planta*.

Another alternative approach could also be devised, based on the observation that the ubiquitin associated protein SGT1 has been shown to required to trigger a wide variety of cell death responses *in planta* (Peart *et al.*, 2002, Oh *et al.*, 2009). If SGT1 is also required for CRN8-induced cell death, expression of wild-type CRN8-D2 domain in plants that had been silenced for SGT1 using virus-induced gene silencing may also allow tissue to be harvested at latter time points. This, again, would allow greater time for protein accumulation. To my knowledge, the silencing of SGT1 or other host genes required for diverse cell death responses (e.g. HSP90 (Lu *et al.*, 2003a)) has not been used to enhance transient expression of cell-death inducing proteins to date. This could be because silencing these genes often has significant developmental effects, typically reduced growth, that may negate any potential benefits. In turn, a possible way of overcoming these detrimental pleiotropic effects would be to transiently silence the genes in mature expanded leaves using RNA hairpin vectors (Watson *et al.*, 2005).

Although a small number of published structures in the Protein Data Bank have been solved using protein expressed in *Nicotiana benthamiana* (15 at the point of writing this thesis), it is unlikely that the measures described above would be sufficient to increase the obtained yield to allow structural characterisation of full length CRN8-D2 domain. They should, however, allow further analysis such as partial trypsin digests to remove flexible regions of the protein and identify suitable sub-domains that could be more amenable to structural characterisation. If such a sub-domain could be identified, this could be used to redesign expression constructs for

heterologous over-expression in plants, *E. coli*, or other eukaryotic expression systems, such as yeast, mammalian or insect cells.

In addition to re-designing constructs to eliminate unstructured regions of the protein, cloning into expression vectors that use other fusion partners to aid solubility could be used to re-investigate *E. coli* expression. The small ubiquitin-like modifier (SUMO) is being increasing recognised as a good choice to enhance expression and solubility of recalcitrant proteins (Butt *et al.*, 2005, Panavas *et al.*, 2009). The pOPIN suite of vectors now includes the vector pOPINS3C, which includes a hexa-histidine tagged SUMO fusion partner for IMAC purification, and a 3C protease site to remove the tag from the protein of interest (Bird, 2011).

Additionally, expression could be screened using different strains of *E. coli*. Strains that have mutations to increase protein expression (BL21 Star™(DE3) (Invitrogen)) or enhanced solubility (SoluBL21(DE3) (GenLantis, Inc.), or strains carrying a second vector producing the chaperonin GroEL/GroES (Yan *et al.*, 2012) would be good choices. Alternatively cells that have tighter regulation of protein expression (BL21(DE3)pLysE) should reduce the observed 'leaky' expression of proteins from the pOPIN vectors (Figure 6.7), which may be impairing *E. coli* growth and protein folding. Furthermore the reducing conditions of the *E. coli* cytoplasm impair disulphide bond formation (de Marco, 2009). Disulphide bonds can stabilise protein structure, and the sequence of the D2 domain of CRN8 contains six cysteine residues. The correct folding of proteins that require disulphide bond formation can be increased by targeting the expressed protein to the oxidising environment of the bacterial periplasm or by expression in strains that have mutations that alter the redox state of their cytoplasm (Derman *et al.*, 1993, Stewart *et al.*, 1998, Bessette *et al.*, 1999) (e.g. Origami (Novagen)).

Other conditions that could be tested would include the choice of expression media and the use of additives. The slower growth in minimal media could improve solubility, whereas the addition of chemical chaperones, such as DMSO or glycerol (Papp and Csermely, 2006), or induction of molecular chaperones, by stressing the cells with ethanol (Winter *et al.*, 2000), have also been shown to enhance recombinant protein solubility.

Chapter 7:

General Discussion

7 General Discussion

One of the most intriguing features about effectors is that although their genes reside in the genome of the pathogen, the proteins function outside the pathogen within the tissues, or even cells, of the host. Therefore effectors provide some of the most vivid examples of genes with *extended phenotypes* (Dawkins, 1982). Effectors have been uncovered in the genomes of phytopathogenic microbes including bacteria, fungi, oomycetes, viruses and viroids (Amari *et al.*, 2012, Bozkurt *et al.*, 2012, Deslandes and Rivas, 2012, Rafiqi *et al.*, 2012), as well as arthropod and nematode pests (Bos *et al.*, 2010a, Haegeman *et al.*, 2012), and even in parasitic plants (Lee *et al.*, 2013). The evolution of effectors has been shaped by their interaction with host plants. Natural selection would favour arsenals of effectors that benefit the pathogen by interacting with host targets and subverting host processes, whilst also evading recognition or nullifying elicited defence responses. The plant immune system has in turn evolved to continue to recognise invading pathogens and counteract this manipulation. As such, an adaptation in either the pathogen, or the host, would in turn change the selection pressure experienced by the other. This would give rise to antagonistic co-evolution, or a *co-evolutionary arms race*; a concept that was perhaps most elegantly described by the Red Queen Hypothesis (Van Valen, 1973, Clay and Kover, 1996).

Since effectors play pivotal roles in determining the outcome of an infection, understanding the mechanistic basis of their function should lead to novel strategies for enhancing crop species' resistance to pathogen infection. Genomics approaches have been extremely successful in identifying a plethora of putative effectors. However, many effectors have eluded functional annotation on the basis of primary amino-acid sequence data alone. As described in previous chapters, solving the three-dimensional structures of effectors, as well as identifying host proteins that interact with specific effectors, has been critical to assigning putative virulence activities to several effector proteins.

This thesis describes structure-function studies aimed at understanding the virulence functions of two translocated effector proteins from the late blight pathogen. Prior to starting this project, extensive screening of conditions for the heterologous

expression of oomycete translocated effectors had been conducted by Dr. Laurence Boutemy and Dr. Richard Hughes in the Banfield group. This initial screening had provided significant insights into *E. coli* expression construct design, as well as determining conditions that permitted the soluble expression of the effector domain of the RXLR effector PexRD2. This significantly accelerated the start of this aspect of the project, since obtaining pure, well-folded, soluble protein amenable for crystallography often represents a bottleneck in the structural characterisation of proteins. Some of the potential techniques that can be utilised to promote protein solubility are discussed in Chapter 6 of this thesis, with regards heterologous expression of the *P. infestans* translocated effector CRN8.

For PexRD2, following scaling-up of the pre-determined expression conditions and subsequent purification of the recombinant protein, the crystal structure of this protein's effector domain was solved to 1.75 Å resolution (see Chapter 3). Around the same time, Dr. Laurence Boutemy was performing NMR characterisation of another RXLR effector *Pc*AVR3a11, which eventually led to a re-designed expression construct that crystallised to yield sub-angstrom resolution data. Comparison of the solved structures of PexRD2 and *Pc*AVR3a11 with each other, and eventually with the structures of other RXLR effectors, which were solved by other research groups, led to the discovery of the conserved WY-fold (Boutemy *et al.*, 2011, Win *et al.*, 2012b). This fold was postulated to represent a stable, yet adaptable, protein scaffold. PexRD2 was crucial in identifying a three-helix bundle as the minimal conserved structural motif, as well as providing a unique example of how WY-domains might oligomerise to increase their functional diversity.

Searches for structurally similar proteins for PexRD2 and the other RXLR effectors did not provide clear insights into assigning a function for these proteins; however, the deposition of these structures' co-ordinates into the Protein Data Bank allows comparison with future deposited structures that may shed light onto these proteins' activities. These published co-ordinates may also assist in the solving of other protein structures by molecular replacement, and have already allowed structural predictions of PexRD2-like effectors from several *Phytophthora* spp.

Yeast two-hybrid (Y2H) screening identified four potato proteins that interacted with PexRD2 (see Chapter 4). These interactions were shown to be specific and two of these interactions were also re-confirmed using independent protein-protein interaction techniques. This provides validation for the Y2H screening approach, which has frequently been criticised as yielding high levels of false positives (Bartel *et al.*, 1993, Serebriiskii *et al.*, 2000). PexRD2-interacting proteins were also shown to interact with one another, highlighting the possibility that this effector is targeting host protein complexes involved in plant immunity.

The biological relevance of interaction between PexRD2 and the potato MAPKKK, MAPKKKε, was characterised further and suggested a potential virulence activity for PexRD2 as an inhibitor of this host kinase (see Chapter 5). MAPKKKε homologs had previously been identified as positive regulators of cell death events associated with plant immunity (Melech-Bonfil and Sessa, 2010), with pleoitropic roles in cell division and expansion, and hence plant development (Jouannic *et al.*, 2001, Chaiwongsar *et al.*, 2006, Chaiwongsar *et al.*, 2012). Gene silencing experiments have implicated *MAPKKKε* as required for mediating at least partial resistance in the *P. infestans–N. benthamiana* model pathosystem. Transient expression of PexRD2 *in planta*, appeared to phenocopy silencing of *MAPKKKε*, and also enhanced virulence of the pathogen. PexRD2 was shown to inhibit a diverse range of read-outs of MAPKKKε activity, supporting this effector's role as a specific inhibitor.

The biological relevance of other PexRD2-interacting proteins remains to be investigated, but one could speculate that they may also regulate plant immunity. If this is so, this would provide an example of how effector proteins can be used as molecular probes to identify novel components of plant immunity signalling and defence responses (Bozkurt *et al.*, 2012).

The structure of PexRD2 WY-domain provided a useful framework for the rational design of structurally informed mutations to interrogate this effector's function *in planta* (see Sections 5.2.10 – 5.2.13). Mutational analysis showed that the ability to suppress MAPKKKε-mediated signalling could be positively correlated with the ability of PexRD2 mutants to interact with MAPKKKε kinase domain; and non-interacting mutants of PexRD2 no longer enhanced growth of the pathogen *in planta*.

These mutational studies highlighted specific residues in the dimer interface and the so-called *variable loop region* as important for PexRD2 functioning. One non-interacting mutant, PexRD2^{L109D}, was further shown to possess dominant negative activity and potential mechanisms by which this could occur were discussed (Section 5.2.13). Further work is required to determine the exact mode of action of both the wild-type PexRD2 and this dominant negative mutant.

Future work in this project will be focused at characterising this interaction *in vitro* using a range of biochemical, biophysical and structural biology techniques. Specifically, structural characterisation of an oomycete translocated effector in complex with its host target would be a significant achievement and likely have high impact within the scientific community. Such data would provide an atomic level resolution of the molecular frontline of the co-evolutionary arms race between pathogen and host. Furthermore ongoing work will investigate the potential to exploit knowledge gained regarding this effector-target interaction to enhance late blight resistance in crop plants, such as tomato and potato. In particular, the possibility of deploying structurally-predicted dominant negative mutants of effectors, and/or effector-insensitive variants of host targets (Section 5.2.14) could represent novel management strategies. Whether these previously unexploited methods would provide durable, effective resistance against *Phytophthora infestans* would only be revealed in the field in due course. However, these additional resources might help crop breeders and growers to at least keep pace with this devastating *plant destroyer* in the continued co-evolutionary arms race.

Appendix

Table A **Entry clones used in this study**

Construct name	Vector backbone	Insert/Description	START CODON	STOP CODON	Source
pENTR:PexRD2	pENTR™-D/TOPO®	PITG_21422, residues 21 - 121	•	•	sub-cloned by PCR from pK7WGF2:PexRD2
pENTR:ΔRXLR-PexRD2	pENTR™-D/TOPO®	PITG_21422, residues 42 - 121	•	•	sub-cloned by PCR from pK7WGF2:PexRD2
pENTR:PexRD2-WY	pENTR™-D/TOPO®	PITG_21422, residues 57 - 121	•	•	sub-cloned by PCR from pK7WGF2:PexRD2
pDONR: *Pm*PexRD2	pDONR™201	PexRD2, *Phytophthora mirabilis* ortholog, residues 21 - 121	•	•	sub-cloned by BP reaction from pUC57:PmPexRD2
pENTR: PexRD2-like-1a	pENTR™-D/TOPO®	PITG_14984, residues 21 - 132	•	•	cloned from *P. infestans* T30-4 gDNA
pENTR: PexRD2-like-2a	pENTR™-D/TOPO®	PITG_14787, residues 21 - 130	•	•	cloned from *P. infestans* T30-4 gDNA
pDONR:E61A	pDONR™201	PITG_21422, residues 21 - 121, Glu61 to Ala	•	•	sub-cloned by BP reaction from pUC57:E61A

Construct name	Vector backbone	Insert/Description	START CODON	STOP CODON	Source
pENTR:D74A	pENTR™-D/TOPO®	PITG_21422, residues 21 - 121, Asp74 to Ala	•	•	mutagenised from pENTR:PexRD2 by Genscript (US)
pENTR:D75A	pENTR™-D/TOPO®	PITG_21422, residues 21 - 121, Asp75 to Ala	•	•	mutagenised from pENTR:PexRD2 by Genscript (US)
pENTR:K79E	pENTR™-D/TOPO®	PITG_21422, residues 21 - 121, Lys79 to Glu	•	•	mutagenised from pENTR:PexRD2 by Genscript (US)
pENTR:K81E	pENTR™-D/TOPO®	PITG_21422, residues 21 - 121, Lys81 to Glu	•	•	mutagenised from pENTR:PexRD2 by Genscript (US)
pENTR:K85E	pENTR™-D/TOPO®	PITG_21422, residues 21 - 121, Lys85 to Glu	•	•	mutagenised from pENTR:PexRD2 by Genscript (US)
pENTR:E97Q	pENTR™-D/TOPO®	PITG_21422, residues 21 - 121, Glu97 to Gln	•	•	mutagenised from pENTR:PexRD2 by Genscript (US)
pENTR:E101Q	pENTR™-D/TOPO®	PITG_21422, residues 21 - 121, Glu101 to Gln	•	•	mutagenised from pENTR:PexRD2 by Genscript (US)
pENTR:K104E	pENTR™-D/TOPO®	PITG_21422, residues 21 - 121, Lys104 to Glu	•	•	mutagenised from pENTR:PexRD2 by Genscript (US)

Construct name	Vector backbone	Insert/Description	START CODON	STOP CODON	Source
pENTR:K107E	pENTR™-D/TOPO®	PITG_21422, residues 21 - 121, Lys107 to Glu	•	•	mutagenised from pENTR:PexRD2 by Genscript (US)
pENTR:L109D	pENTR™-D/TOPO®	PITG_21422, residues 21 - 121, Leu109 to Asp	•	•	mutagenised from pENTR:PexRD2 by Genscript (US)
pENTR:L112D	pENTR™-D/TOPO®	PITG_21422, residues 21 - 121, Leu112 to Asp	•	•	mutagenised from pENTR:PexRD2 by Genscript (US)
pDONR:longtail	pDONR™201	PITG_21422, residues 21 - 118, plus 12 residues from C-terminus of PITG_14984 (-NKKKKPNLVYYS)	•	•	sub-cloned by BP reaction from pUC57:longtail
pDONR:shorttail	pDONR™201	PITG_14984, residues 21 - 129, plus 3 residues from C-terminus of PITG_21422 (-TAV)	•	•	sub-cloned by BP reaction from pUC57:shorttail
pDONR:vloop-8	pDONR™201	PITG_21422, residues 21 - 121, with 8 residue substitutions in variable loop region (K85D, A88H, A90E, N91T,R94G, E97Q, K98Q, E101Q)	•	•	sub-cloned by BP reaction from pUC57:vloop-8
pDONR:vloop-7	pDONR™201	PITG_21422, residues 21 - 121, with 7 residue substitutions in variable loop region (K85D, A88H, N91T,R94G, E97Q, K98Q, E101Q)	•	•	mutagenised from pDONR:vloop-8 by Quick-change method

Construct name	Vector backbone	Insert/Description	START CODON	STOP CODON	Source
pENTR: *St*MAPKKKε~FL	pENTR™-D/TOPO®	MAPKKKε, potato ortholog, residues 2 - 1400* (*in-del resulted in loss of C-terminal Leu)		•	sub-cloned by PCR from pEXP32:PexRD2PI-1
pENTR: *St*MAPKKKε-N1	pENTR™-D/TOPO®	MAPKKKε, potato ortholog, residues 2 - 373		•	sub-cloned by PCR from pEXP32:PexRD2PI-1
pENTR: *St*MAPKKKε-N1	pENTR™-D/TOPO®	MAPKKKε, potato ortholog, residues 2 - 300		•	sub-cloned by PCR from pEXP32:PexRD2PI-1
pENTR: *St*MAPKKKε-N1	pENTR™-D/TOPO®	MAPKKKε, potato ortholog, residues 2 - 278		•	sub-cloned by PCR from pEXP32:PexRD2PI-1
pENTR: *St*MAPKKKε-C1	pENTR™-D/TOPO®	MAPKKKε, potato ortholog, residues 279 - 1401		•	sub-cloned by PCR from pEXP32:PexRD2PI-1
pENTR: *St*MAPKKKε-C2	pENTR™-D/TOPO®	MAPKKKε, potato ortholog, residues 301 - 1401		•	sub-cloned by PCR from pEXP32:PexRD2PI-1
pENTR: *At*MAPKKKε1	pENTR™-D/TOPO®	MAPKKKε1, *Arabidopsis* ortholog (AT3G13530), residues 1 - 1368	•	•	Dr. Malik Mbengue (TSL), unpublished

Construct name	Vector backbone	Insert/Description	START CODON	STOP CODON	Source
pENTR: *Sl*MAPKKKα-KD	pENTR™-D/TOPO®	MAPKKKα, tomato homolog, residues 192 - 467	•	•	sub-cloned by PCR from pER8:SlMAPKKKα KD
pENTR:PM4K1-FL	pENTR™-D/TOPO®	PM4K1, residues 2 - 674		•	sub-cloned by PCR from pEXP32:PexRD2PI-2
pENTR:PM4K1-N1	pENTR™-D/TOPO®	PM4K1, residues 2 - 319		•	sub-cloned by PCR from pEXP32:PexRD2PI-2
pENTR:PM4K1-N2	pENTR™-D/TOPO®	PM4K1, residues 2 - 286		•	sub-cloned by PCR from pEXP32:PexRD2PI-2
pENTR:PM4K1-C	pENTR™-D/TOPO®	PM4K1, residues 287 - 674		•	sub-cloned by PCR from pEXP32:PexRD2PI-2

All entry clones listed in this table confer kanamycin resistance.

Table B **Yeast two-hybrid vectors and clones used in this study**

Construct name	Vector backbone[a]	Insert/Description	Source
pEXP32: PITG_11383^{K104E}	pEXP™32	PexRD2 paralog (PITG_11383), residues 21 - 121, Lys104 to Glu	Birch lab (JHI), unpublished
pDEST32 (bait vector control)	pDEST™32	*attR*1-ccdB-CmR-*attR*2	Invitrogen™
pEXP32:PexRD2	pEXP™32	PexRD2 (PITG_21422), residues 21 - 121	sub-cloned by LR reaction from entry clone
pEXP32: ΔRXLR-PexRD2	pEXP™32	PexRD2 (PITG_21422), residues 42 - 121	sub-cloned by LR reaction from entry clone
pEXP32:PexRD2-WY	pEXP™32	PexRD2 (PITG_21422), residues 57 - 121	sub-cloned by LR reaction from entry clone
pEXP32: *Pm*PexRD2	pEXP™32	PexRD2, *Phytophthora mirabilis* ortholog, residues 21 - 121	sub-cloned by LR reaction from entry clone
pEXP32: PexRD2-like-1a	pEXP™32	PITG_14984, residues 21 - 132	sub-cloned by LR reaction from entry clone

Construct name	Vector backbone[a]	Insert/Description	Source
pEXP32: PexRD2-like-2a	pEXP™32	PITG_14787, residues 21 - 130	sub-cloned by LR reaction from entry clone
pEXP32:E61A	pEXP™32	PITG_21422, residues 21 - 121, Glu61 to Ala	sub-cloned by LR reaction from entry clone
pEXP32:D74A	pEXP™32	PITG_21422, residues 21 - 121, Asp74 to Ala	sub-cloned by LR reaction from entry clone
pEXP32:D75A	pEXP™32	PITG_21422, residues 21 - 121, Asp75 to Ala	sub-cloned by LR reaction from entry clone
pEXP32:K79E	pEXP™32	PITG_21422, residues 21 - 121, Lys79 to Glu	sub-cloned by LR reaction from entry clone
pEXP32:K81E	pEXP™32	PITG_21422, residues 21 - 121, Lys81 to Glu	sub-cloned by LR reaction from entry clone
pEXP32:K85E	pEXP™32	PITG_21422, residues 21 - 121, Lys85 to Glu	sub-cloned by LR reaction from entry clone
pEXP32:E97Q	pEXP™32	PITG_21422, residues 21 - 121, Glu97 to Gln	sub-cloned by LR reaction from entry clone

Construct name	Vector backbone[a]	Insert/Description	Source
pEXP32:E101Q	pEXP™32	PITG_21422, residues 21 - 121, Glu101 to Gln	sub-cloned by LR reaction from entry clone
pEXP32:K104E	pEXP™32	PITG_21422, residues 21 - 121, Lys104 to Glu	sub-cloned by LR reaction from entry clone
pEXP32:K107E	pEXP™32	PITG_21422, residues 21 - 121, Lys107 to Glu	sub-cloned by LR reaction from entry clone
pEXP32:L109D	pEXP™32	PITG_21422, residues 21 - 121, Leu109 to Asp	sub-cloned by LR reaction from entry clone
pEXP32:L112D	pEXP™32	PITG_21422, residues 21 - 121, Leu112 to Asp	sub-cloned by LR reaction from entry clone
pEXP32:longtail	pEXP™32	PITG_21422, residues 21 - 118, plus 12 residues from C-terminus of PITG_14984 (-NKKKKPNLVYYS)	sub-cloned by LR reaction from entry clone
pEXP32:shorttail	pEXP™32	PITG_14984, residues 21 - 129, plus 3 residues from C-terminus of PITG_21422 (-TAV)	sub-cloned by LR reaction from entry clone
pEXP32:vloop-7	pEXP™32	PITG_21422, residues 21 - 121, with 7 residue substitutions in variable loop region (K85D, A88H, N91T,R94G, E97Q, K98Q, E101Q)	sub-cloned by LR reaction from entry clone

Construct name	Vector backbone[a]	Insert/Description	Source
pEXP32:vloop-8	pEXP™32	PITG_21422, residues 21 - 121, with 8 residue substitutions in variable loop region (K85D, A88H, A90E, N91T,R94G, E97Q, K98Q, E101Q)	sub-cloned by LR reaction from entry clone
pEXP32: *St*MAPKKKε~FL	pEXP™32	MAPKKKε, potato ortholog, residues 2 - 1400	sub-cloned by LR reaction from entry clone
pEXP32:PM4K1-FL	pEXP™32	PM4K1, residues 2 - 674	sub-cloned by LR reaction from entry clone
pDEST22 (prey vector control)	pDEST™22	*attR*1-ccdB-CmR-*attR*2	Invitrogen™
pEXP22:PexRD2PI-1	pEXP™22	MAPKKKε, potato ortholog, residues 4 - 1401, (MAPKKKε~FL)	Birch lab (JHI), unpublished
pEXP22:PexRD2PI-2	pEXP™22	PM4K1, potato ortholog, residues 4 - 676	Birch lab (JHI), unpublished
pEXP22:PexRD2PI-3	pEXP™22	PM4K2, potato ortholog, residues 4 - 672	Birch lab (JHI), unpublished
pEXP22:PexRD2PI-4	pEXP™22	PUB38-like, potato ortholog, residues 39 - 490, (StΔN-PUB38-like)	Birch lab (JHI), unpublished

Construct name	Vector backbone[a]	Insert/Description	Source
pEXP22:MAPKKKε-N1	pEXP™22	MAPKKKε, potato ortholog, residues 2 - 373	sub-cloned by LR reaction from entry clone
pEXP22:MAPKKKε-N2	pEXP™22	MAPKKKε, potato ortholog, residues 2 - 300	sub-cloned by LR reaction from entry clone
pEXP22:MAPKKKε-N3	pEXP™22	MAPKKKε, potato ortholog, residues 2 - 278	sub-cloned by LR reaction from entry clone
pEXP22:MAPKKKε-C1	pEXP™22	MAPKKKε, potato ortholog, residues 279 - 1401	sub-cloned by LR reaction from entry clone
pEXP22:MAPKKKε-C2	pEXP™22	MAPKKKε, potato ortholog, residues 301 - 1401	sub-cloned by LR reaction from entry clone
pEXP22:*At*MAPKKKε1	pEXP™22	MAPKKKε1, *Arabidopsis* ortholog (AT3G13530), residues 1 - 1368	sub-cloned by LR reaction from entry clone
pEXP22:*Sl*MAPKKKα-KD	pEXP™22	MAPKKKα, tomato homolog, residues 192 - 467	sub-cloned by LR reaction from entry clone
pEXP22:PM4K1-FL	pEXP™22	PM4K1, residues 2 - 674	sub-cloned by LR reaction from entry clone

Construct name	Vector backbone[a]	Insert/Description	Source
pEXP22:PM4K1-N1	pEXP™22	PM4K1, residues 2 - 319	sub-cloned by LR reaction from entry clone
pEXP22:PM4K1-N2	pEXP™22	PM4K1, residues 2 - 286	sub-cloned by LR reaction from entry clone
pEXP22:PM4K1-C	pEXP™22	PM4K1, residues 287 - 674	sub-cloned by LR reaction from entry clone
pEXP22:PexRD2-WY	pEXP™22	PexRD2 (PITG_21422), residues 57 - 121	sub-cloned by LR reaction from entry clone

[a] pEXP™32 confers resistance to gentamycin in bacteria, and complements leucine auxotrophy in yeast. pEXP™22 confers resistance to carbenicillin in bacteria, and complements tryptophan auxotrophy in yeast.

Table C **Binary vectors and *Agrobacterium* strains used in this study**

Construct name	Vector backbone	Insert/Description	Antibiotic Selection[a]			Strain	Source, Reference
			Kan^R	$Spec^R$	Cm^R		
p35S:Avr4	pMOG800	*PR1aSP:Av4* fusion, cloned into XbaI/EcoRI sites	•			GV3101	Prof. Pierre De Wit (Wageningen UR), (van der Hoorn *et al*., 2000)
p35S:AvrPto	pMD1	binary plasmid containing *AvrPto*	•			GV3101	Dr. John Rathjen (The Australian National University, Acton), (Schofield *et al.*, 1996)
p35S:Cf4	pMOG800	*Cf4* cloned into BamHI/KpnI sites	•			GV3101	Prof. Pierre De Wit (Wageningen UR), (van der Hoorn *et al*., 2000)
p35S:INF1	pAvr9	*PR1aSP:INF1* cloned into NcoI/SacI sites	•			GV3101	Kamoun Lab (TSL), (Kamoun *et al.*, 2003)
pJL3-P19	pCB301 derivative	*p19* cloned into the PacI/XbaI sites	•			GV3101	Kamoun Lab (TSL), (Lindbo, 2007)

Construct name	Vector backbone	Insert/Description	Antibiotic Selection[a]			Strain	Source, Reference
			Kan^R	$Spec^R$	Cm^R		
p35S:Pto	pTFS-40	*Pto*, cloned into EcoRI/HindIII sites	•			GV3101	Dr. John Rathjen (The Australian National University, Acton), (Rathjen *et al.*, 1999)
p35S:R3a	pCB302-3	*R3a*, cloned into BamHI/SpeI sites	•			GV3101	Kamoun Lab (TSL), (Kamoun *et al.*, 2013)
p35S:3HA-PexRD2	pB7WGH2	PITG_21422, residues 21 - 121, sub-cloned from pENTR:PexRD2		•		GV3101	This work
p35S:3HA-L109D	pB7WGH2	PITG_21422, residues 21 - 121, Leu109 to Asp, sub-cloned from pENTR:L109D		•		GV3101	This work
pEAQ-HT:EV	pEAQ-HT	empty vector control	•			GV3101	Eva Thuenemann (JIC), (Sainsbury *et al.*, 2009)
pEAQ-HT:GFP	pEAQ-HT	GFP, cloned into the XmaI/XhoI sites.	•			GV3101	Eva Thuenemann (JIC), (Sainsbury *et al.*, 2009)

Construct name	Vector backbone	Insert/Description	Antibiotic Selection[a]			Strain	Source, Reference
			Kan^R	$Spec^R$	Cm^R		
pEAQ-HT:KD	pEAQ-HT	CRN8 kinase domain residues 337 - 599, cloned into the XmaI/StuI sites.	•			GV3101	This work
pEAQ-HT:D2	pEAQ-HT	CRN8 D2 domain residues 118 - 599, cloned into the XmaI/StuI sites.	•			GV3101	This work
pEAQ-HT:PexRD2	pEAQ-HT-DEST2	PITG_21422, residues 21 - 121, sub-cloned from pENTR:PexRD2	•			GV3101	This work
pER8:*Sl*KDε$_{1-332}$	pER8	MAPKKKε, tomato ortholog, residues 1 - 332, with C-terminal 2xHA tag and cloned into XhoI/SpeI sites		•		GV3101	Prof. Guido Sessa (Tel-Aviv Uni), (Melech-Bonfil and Sessa, 2010)
pER8: *Sl*KDε$_{1-332}^{K49R}$	pER8	MAPKKKε, tomato ortholog, residues 1 - 332, Lys49 to Arg, with C-terminal 2xHA tag and cloned into XhoI/SpeI sites		•		GV3101	Prof. Guido Sessa (Tel-Aviv Uni), (Melech-Bonfil and Sessa, 2010)
pER8:MEK2^{DD}	pER8	MEK2, tomato ortholog, residues 1 - 359, Thr215 to Asp, Ser221 to Asp, with N-terminal 2xHA tag		•		GV3101	Prof. Gregory Martin (BTI), (Oh and Martin, 2011)

Construct name	Vector backbone	Insert/Description	Antibiotic Selection[a]			Strain	Source, Reference
			Kan^R	$Spec^R$	Cm^R		
pER8:MAPKKKα KD	pER8	MAPKKKα, tomato ortholog, residues 192 - 467, with N-terminal 2xHA tag		•		GV3101	Prof. Gregory Martin (BTI), (del Pozo *et al.*, 2004)
pERCH: *St*KDε$_{1-332}$	pERCH	MAPKKKε, potato ortholog, residues 1 - 332, cloned into XhoI/PacI sites		•		GV3101	This work
pERCH: *St*KDε$_{1-300}$	pERCH	MAPKKKε, potato ortholog, residues 1 - 300, cloned into XhoI/PacI sites		•		GV3101	This work
pERCH: *At*KDε$_{1-300}$	pERCH	MAPKKKε1, *Arabidopsis* ortholog, residues 1 - 300, cloned into XhoI/PacI sites		•		GV3101	This work
pGR106:ΔGFP	pGR106	fragment of *GFP* gene cloned into ClaI/NotI sites	•			GV3101	Kamoun Lab (TSL), (Bos *et al.*, 2006)
pGR106:INF1	pGR106	*PR1aSP:inf1* fusion sequence cloned into ClaI site	•			GV3101	Kamoun Lab (TSL), (Huitema *et al.*, 2005)

Construct name	Vector backbone	Insert/Description	Antibiotic Selection[a]			Strain	Source, Reference
			Kan^R	Spec^R	Cm^R		
pGR106:PexRD2	pGR106	PITG_21422, from P.infestans 88069, residues 21 - 121, cloned into ClaI/NotI sites	•			GV3101	Kamoun Lab (TSL), (Oh *et al.*, 2009)
pK7WGF2	n/a	used as empty vector control, expresses eGFP *(p35S:eGFP:attR*1-ccdB-CmR-*attR*2)		•	•	GV3101	Kamoun Lab (TSL), (Karimi *et al.*, 2002)
p35S:GFP-PexRD2	pK7WGF2	PITG_21422, from *P.infestans 88069*, residues 21 - 121		•		GV3101	Dr Sebastien Schornack (TSL), (Boutemy *et al.*, 2011)
p35S:GFP-PexRD2-like-1a	pK7WGF2	PITG_14984, residues 21 - 132, sub-cloned from pENTR:PexRD2-like-1a		•		GV3101	This work
p35S:GFP-PexRD2-like-2a	pK7WGF2	PITG_14787, residues 21 - 130, sub-cloned from pENTR:PexRD2-like-2a		•		GV3101	This work
p35S:GFP-K104E	pK7WGF2	PITG_21422, residues 21 - 121, Lys104 to Glu, sub-cloned from pENTR:K104E		•		GV3101	This work

Construct name	Vector backbone	Insert/Description	Antibiotic Selection[a]			Strain	Source, Reference
			Kan^R	$Spec^R$	Cm^R		
p35S:GFP-L109D	pK7WGF2	PITG_21422, residues 21 - 121, Leu109 to Asp, sub-cloned from pENTR:L109D		•		GV3101	This work
p35S:GFP-L112D	pK7WGF2	PITG_21422, residues 21 - 121, Leu112 to Asp, sub-cloned from pENTR:L112D		•		GV3101	This work
p35S:GFP-vloop-7	pK7WGF2	PITG_21422, residues 21 - 121, with 7 residue substitutions in variable loop region, sub-cloned from pDONR:vloop-7		•		GV3101	This work
p35S:GFP-vloop-8	pK7WGF2	PITG_21422, residues 21 - 121, with 8 residue substitutions in variable loop region, sub-cloned from pDONR:vloop-8		•		GV3101	This work
p35S:GFP-AVR3a^{KI}	pK7WGF2	Avr3a^{KI}, residues 23 - 147, sub-cloned from entry clone		•		GV3101	Dr Sebastien Schornack (TSL), (Boutemy *et al.*, 2011)
p35S:GFP-PM4K1	pK7WGF2	PM4K1, residues 2 - 674, sub-cloned from pENTR:PM4K1-FL		•		GV3101	This work

Construct name	Vector backbone	Insert/Description	Antibiotic Selection[a]			Strain	Source, Reference
			Kan^R	$Spec^R$	Cm^R		
pTRBO: PexRD2	pTRBO	PITG_21422, residues 21 - 121, synthesised with N-terminal FLAG tag and cloned into PacI/NotI sites	•			GV3101	Kamoun Lab (TSL), (Boutemy *et al.*, 2011)
pTRBO: PexRD2-WY	pTRBO	PITG_21422, residues 57 - 121, subcloned from pENTR:PexRD2 with N-terminal FLAG tag and cloned into PacI/NotI sites	•			GV3101	This work
pTRBO: PexRD2-like-2a	pTRBO	PITG_14787, residues 57 - 130, synthesised with N-terminal FLAG tag and cloned into PacI/NotI sites	•			GV3101	Dr Joe Win (TSL), unpublished
pTRBO:AVR3a^{KI}	pTRBO	Avr3a^{KI}, residues 23 - 147, synthesised with N-terminal FLAG tag and cloned into PacI/NotI sites	•			GV3101	Kamoun Lab (TSL), (Boutemy *et al.*, 2011)
pTRBO:AVR3a^{EM}	pTRBO	Avr3a^{EM}, residues 23 - 147, synthesised with N-terminal FLAG tag and cloned into PacI/NotI sites	•			GV3101	Kamoun Lab (TSL), (Boutemy *et al.*, 2011)
pTRBO:RFP	pTRBO	RFP synthesised with N-terminal FLAG tag and cloned into PacI/NotI sites	•			GV3101	Kamoun Lab (TSL), (Bozkurt *et al.*, 2011)

Construct name	Vector backbone	Insert/Description	Antibiotic Selection[a]			Strain	Source, Reference
			Kan^R	$Spec^R$	Cm^R		
pTRV1	n/a	binary vector encoding TRV RNA1 sequence	•			AGL1	Dr Hazel McLellan (JHI), (Liu *et al.*, 2002)
pTRV2:GFP	pBinTRV-2b-GFP_{VIGS}	TRV RNA2 derivative containing antisense *GFP* gene	•			LBA4404	Dr Hazel McLellan (JHI), (Valentine *et al.*, 2004)
pTRV2: 5'MAPKKKε	pTRV2	411-nt fragment of *SlMAPKKKε* cloned in antisense orientation into XbaI/BamHI sites	•			LBA4404	Prof. Guido Sessa (Tel-Aviv Uni), (Melech-Bonfil and Sessa, 2010)
pTRV2: 3'MAPKKKε	pBinTRV-2b-GFP_{VIGS}	348-nt fragment of *NbMAPKKKε2* cloned in antisense orientation into EcoRI/HpaI sites	•			LBA4404	Dr Hazel McLellan (JHI), unpublished

[a] Binary vectors listed above confer either resistance to kanamycin (Kan^R), spectinomycin/streptinomycin ($Spec^R$) and/or chloramphenicol (Cm^R). Rifampicin was used for all *Agrobacterium* strain, and gentamycin was used with GV3101.

Table D pOPIN expression vectors used in this study

Construct name	Vector backbone[a]	Insert/Description	Tag/Fusion partner[b]				Source
			His_6	GST	MBP	3C	
pOPINF:PexRD2	pOPINF	codon optimised sequence of PexRD2, residues 57 - 121	•			•	Dr. Laurence Boutemy (JIC), (Boutemy *et al*., (2011))
pOPINF:D2	pOPINF	codon optimised sequence of CRN8, residues 118 - 599,	•			•	sub-cloned by PCR from template synthesised by Genscript (US), into In-Fusion site
pOPINF:D2-AA	pOPINF	codon optimised sequence of CRN8, residues 118 - 599, with Arg469 to Ala, and Asp470 to Ala	•			•	mutagenesised by oe-PCR, subcloned into In-Fusion site
pOPINF:KD	pOPINF	codon optimised sequence of CRN8, residues 337 - 599	•			•	sub-cloned by PCR from template synthesised by Genscript (US), into In-Fusion site
pOPINF:KD-AA	pOPINF	codon optimised sequence of CRN8, residues 337 - 599, with Arg469 to Ala, and Asp470 to Ala	•			•	sub-cloned by PCR from pOPINF:D2-AA, into In-Fusion site

Construct name	Vector backbone[a]	Insert/Description	Tag/Fusion partner[b]				Source
			His_6	GST	MBP	3C	
pOPINJ:D2	pOPINJ	codon optimised sequence of CRN8, residues 118 - 599,	•	•		•	sub-cloned by PCR from template synthesised by Genscript (US), into In-Fusion site
pOPINJ:D2-AA	pOPINJ	codon optimised sequence of CRN8, residues 118 - 599, with Arg469 to Ala, and Asp470 to Ala	•	•		•	mutagenesised by oe-PCR, subcloned into In-Fusion site
pOPINJ:KD	pOPINJ	codon optimised sequence of CRN8, residues 337 - 599	•	•		•	sub-cloned by PCR from template synthesised by Genscript (US), into In-Fusion site
pOPINJ:KD-AA	pOPINJ	codon optimised sequence of CRN8, residues 337 - 599, with Arg469 to Ala, and Asp470 to Ala	•	•		•	sub-cloned by PCR from pOPINF:D2-AA, into In-Fusion site
pOPINM:D2	pOPINM	codon optimised sequence of PexRD2, residues 57 - 121	•		•	•	sub-cloned by PCR from template synthesised by Genscript (US), into In-Fusion site
pOPINM:D2-AA	pOPINM	codon optimised sequence of CRN8, residues 118 - 599, with Arg469 to Ala, and Asp470 to Ala	•		•	•	mutagenesised by oe-PCR, subcloned into In-Fusion site

Construct name	Vector backbone[a]	Insert/Description	Tag/Fusion partner[b]				Source
			His_6	GST	MBP	3C	
pOPINM:KD	pOPINM	codon optimised sequence of CRN8, residues 337 - 599	•		•	•	sub-cloned by PCR from template synthesised by Genscript (US), into In-Fusion site
pOPINM:KD-AA	pOPINM	codon optimised sequence of CRN8, residues 337 - 599, with Arg469 to Ala, and Asp470 to Ala	•		•	•	sub-cloned by PCR from pOPINF:D2-AA, into In-Fusion site

[a] pOPIN expression constructs listed above confer resistance to carbenicillin

[b] 'His_6' indicates N-terminal epitope tag. 'GST' indicates additional glutatione S-transferase fusion partner. 'MBP' indicates additional maltose-binding protein fusion partner. '3C' indicates 3C protease cleavable linker

Table E Miscellaneous vectors used in this study

Construct name	Vector backbone	Insert/Description	Antibiotic Selection[a]			Purpose	Source
			Kan^R	$Gent^R$	Cm^R		
pUC57: *Pm*PexRD2	pUC57	PexRD2, *Phytophthora mirabilis* ortholog, residues 21 - 121, flanked by *att*B sites	•			for generation of entry clone	synthesised by Genscript (US)
pUC57:E61A	pUC57	PITG_21422, residues 21 - 121, Glu61 to Ala, flanked by *att*B sites	•			for generation of entry clone	synthesised by Genscript (US)
pUC57:longtail	pUC57	PITG_21422, residues 21 - 118, plus 12 residues from C-terminus of PITG_14984 (-NKKKKPNLVYYS), flanked by *att*B sites	•			for generation of entry clone	synthesised by Genscript (US)
pUC57:shorttail	pUC57	PITG_14984, residues 21 - 129, plus 3 residues from C-terminus of PITG_21422 (-TAV), flanked by *att*B sites	•			for generation of entry clone	synthesised by Genscript (US)
pUC57:vloop-8	pUC57	PITG_21422, residues 21 - 121, with 8 residue substitutions in variable loop region (K85D, A88H, A90E, N91T,R94G, E97Q, K98Q, E101Q), flanked by *att*B sites	•			for generation of entry clone	synthesised by Genscript (US)

Construct name	Vector backbone	Insert/Description	Antibiotic Selection[a]			Purpose	Source
			Kan^R	$Gent^R$	Cm^R		
pGEMT: *Pm*PexRD2	pGEM®-T Easy	PexRD2, Phytophthora mirabilis ortholog, plus flanking sequence	•			confirmation of PmPexRD2 sequence	cloned for *P. mirabilis* PIC99114 gDNA
pGEMT:H1	pGEM®-T Easy	double haemagglutin tag flanked by PacI and SpeI restriction sites	•			for amplification of 2xHA epitiope tag	sub-cloned by PCR from pBTEX:AvrPto-2xHA
pER8	n/a	n/a		•		binary vector for estadiol-inducible expression	Prof. Guido Sessa (Zou *et al.*, 2000)
pERCH	pER8	double haemagglutin tag cloned between PacI and SpeI sites		•		binary vector for estadiol inducible-expression of C-terminally 2xHA tagged protein	sub-cloned by PCR from pGEMT:H1
pB7WGH2	n/a	*attR*1-ccdB-CmR-*attR*2		•	•	binary vector for p35S-driven expression of N-terminally 3xHA epitope tagged protein	Banfield Lab, unpublished

[a] Vectors listed above confer either resistance to kanamycin (Kan^R), spectinomycin/streptinomycin ($Spec^R$) and/or chloramphenicol (Cm^R).

Table F PCR primers used in this study

Primer ID[a]	Sequence (5' → 3')[b]	Purpose
141F	*AAGTTCTGTTTCAGG*CCCGGGGACCAGCTC... ...TGCACCGAT	Cloning **CRN8-D2** into pOPIN vectors starting from residue 118
142F	*AAGTTCTGTTTCAGG*CCCGCAGCATGCAC... ...CGGAACGTTTT	Cloning **CRN8-KD** into pOPIN vectors starting from residue 337
143R	*ATGGTCTAGAAAGCTTTA*TGCACGAC... ...GATGTTTTTTACGAAC	Cloning **CRN8** into pOPIN vectors ending at C-terminus
145F	CGTAATGGTTGGATGCATgcgGcgATTCGT... ...TGGAGCAATGTG	SDM of **Arg469 to Ala/Asp470 to Ala** in CRN8
146R	CACATTGCTCCAACGAATcgCcgcATGCAT... ...CCAACCATTACG	SDM of **Arg469 to Ala/Asp470 to Ala** in CRN8
147F	GAGAGACCCGGGACAAGTAGTGCGCCTATT... ...TCTGATGGGACG	Cloning **CRN8-D2** into pEAQ-HT starting from residue 118, contains XmaI site
148F	GAGAGACCCGGGCAGCATGCGCCGGAACG... ...TTTTCGACTTGTAC	Cloning **CRN8-KD** into pEAQ-HT starting from residue 337, contains XmaI site
149R	GAGAGACTCGAGTCAGGCACGTCTGTGCTT... ...CTTGCGCACACC	Cloning **CRN8** into pEAQ-HT ending at C-terminus

Primer ID[a]	Sequence (5' → 3')[b]	Purpose
266F	**CACC**ATGCTCTCGACGAACACGGGTGTTCAG	Cloning **PexRD2** into pENTR™/D-TOPO® starting from residue 21
267R	TCAAACTGCTGTGTGTTCAGCCACATAG... ...TTGAGG	Cloning **PexRD2** into pENTR™/D-TOPO® ending at C-terminus
268F	**CACC**ATGAAACACTACACGGCAGCTGA... ...AAACGACG	Cloning **PexRD2** into pENTR™/D-TOPO® starting from residue 42
269F	**CACC**ATGGCCCTGAATACAGAGAAGAT... ...GAAAACG	Cloning **PexRD2** into pENTR™/D-TOPO® starting from residue 57
379F	GAACCAGCGGTACCTCTGATC	Cloning ***P. mirabilis* homolog of PexRD2**, primes in 5' flanking sequence
381R	CAACCGCAGCGGTGTAG	Cloning ***P. mirabilis* homolog of PexRD2**, primes in 3' flanking sequence
386F	CGTTAATTAAATGGACTACAAGGACGACGA... ...TGACAAAGTCAAGCTTCTCGAGAATTCC	Adding **N-terminal FLAG tag** with linker for cloning into pTRBO, contains PacI site
388F	TCAAGCTTCTCGAGAATTCCGCTCTGAA... ...TACAGAGAAGATGAA	Adding linker **PexRD2** for cloning into pTRBO with N-terminal FLAG tag, starting at residue 57

Primer ID[a]	Sequence (5' → 3')[b]	Purpose
389R	CGGCGGCCGCTCATTTGTACAAGAAA... ...GCTGGGTC	Universal cloning from pENTR into pTRBO, contains NotI site
411R	AGAAAGCTGGGTGTCACAAATAATCATGT... ...CCTCGTGCTTGT	Cloning ***StP*M4K1** into pENTR™/D-TOPO® ending at residue 286
438F	**CACC**TCTAGGCAAATGGCAAATGCTG	Cloning ***St*MAPKKKε** into pENTR™/D-TOPO® starting from residue 2
439R	TTACAAAACTGTGTTTATGTGGAGAGC	Cloning ***St*MAPKKKε** into pENTR™/D-TOPO® ending at C-terminus
440F	**CACC**GAACAGCTAACAGAGAAAAAGTTC	Cloning ***StP*M4K1** into pENTR™/D-TOPO® starting from residue 2
441R	TCAGCGATTCAATTTCTTTTCCAACTG	Cloning ***StP*M4K1** into pENTR™/D-TOPO® ending at C-terminus
462aR	TTATCAAGCCGATCCATCTTCTTCTATATT	Cloning ***St*MAPKKKε** into pENTR™/D-TOPO® ending at residue 300
463F	**CACC**GTCAGAGAGGCATCAAATGA	Cloning ***St*MAPKKKε** into pENTR™/D-TOPO® starting from residue 301

Primer ID[a]	Sequence (5' → 3')[b]	Purpose
464F	**CACC**ATGGCACGTACAATCCTTGATGG	Cloning ***StP*M4K1** into pENTR™/D-TOPO® starting from residue 287
475R	TTATCACCTTGAATTTTGTATCCAAGGATG	Cloning ***St*MAPKKKε** into pENTR™/D-TOPO® ending at residue 278
476R	TTATCACTCATGAATTGCTAAAGTTGGAAC	Cloning ***St*MAPKKKε** into pENTR™/D-TOPO® ending at residue 373
481F	**CACC**CGTGCTTTGCAGTCCTCACTC	Cloning ***St*MAPKKKε** into pENTR™/D-TOPO® starting from residue 279,
482R	TTATCAATACATTGCCTGGTTCTGTAAAAG	Cloning ***StP*M4K1** into pENTR™/D-TOPO® ending at residue 319
523F	CGCTTAATTAATCCTTACCCATACGACGTTC	Cloning **C-terminal HA-tag** into pER8, contains PacI site
524R	GTGACTAGTTCAAGCGTAGTCTGGAACGTC	Cloning **C-terminal HA-tag** into pER8, contains SpeI site
527F	**CACC**GCTGAAGGCGCAAAC	Cloning ***Sl*MAPKKKα KD** into pENTR™/D-TOPO® starting from residue 192

Primer ID[a]	Sequence (5' → 3')[b]	Purpose
528aR	TTATTAAGCAACTTTTGCTGTAC	Cloning ***Sl*MAPKKKα KD** into pENTR™/D-TOPO® ending at residue 467
576R	TTATAAATGGTAGAAAGTAGGTGGCTTC	Cloning **PexRD2-like-2a** into pENTR™/D-TOPO® ending at C-terminus
578R	TTATGAGTAGTAGACAAGATTCGGCTTC	Cloning **PexRD2-like-1a** into pENTR™/D-TOPO® ending at C-terminus
579F	**CACC**ATGCTCGTGAACTCGAAC	Cloning **PexRD2-like-2a** into pENTR™/D-TOPO® starting from residue 21
580F	**CACC**ATGCTCGTGAGCTCAAAGC	Cloning **PexRD2-like-1a** into pENTR™/D-TOPO® starting from residue 21
612F	GATATTGCACACGCAGcAACTTCTGCAGGCGCG	SDM of **Glu90 to Ala** in PexRD2^{vloop8} to produce PexRD2^{vloop7}
613R	CGCGCCTGCAGAAGTTgCTGCGTGTGCAATATC	SDM of **Glu90 to Ala** in PexRD2^{vloop8} to produce PexRD2^{vloop7}
614F	CAGCTCGAGCTATGTCTAGGCAAATGG... ...CAAATGC	Cloning ***St*MAPKKKε KD** into pERCH starting from N-terminus, contains XhoI site

Primer ID[a]	Sequence (5' → 3')[b]	Purpose
615R	GGATTAATTAAAGCCGATCCATCTTCTT... ...CTATATTTC	Cloning ***St*MAPKKKε KD** into pERCH ending at residue 300, contains PacI site
618F	CAGCTCGAGCTATGGCGCGGCAAATGA... ...CGTCATCTC	Cloning ***At*MAPKKKε** into pERCH starting from N-terminus, contains XhoI site
619R	GGATTAATTAAACTTGCAGTGGCTTCCTTC	Cloning ***At*MAPKKKε** into pERCH ending at residue 300, contains PacI site
682R	GGATTAATTAATTCAGGTGGTGCCAAT	Cloning ***St*MAPKKKε KD** into pERCH ending at residue 332, contains PacI site

[a] 'F' refers to a forward primer, 'R' refers to a reverse primer, with regards to the orientation of the coding sequence

[b] DNA sequence of primers. Start codons are coloured in green and termination codons in red. **Bold** type indicates CACC sequence required for directional TOPO® cloning. Underlined sequences indicate restriction sites used for cloning. Double-underlined sequences indicate homologous linker sequence used for epitope-tagging of PCR products. *Italics* indicate sequences homologous to In-Fusion sites. Lower case letters indicate substitutions introduced by site-directed mutagenesis (SDM).

Publication arising from this thesis

BOUTEMY, L. S., KING, S. R., WIN, J., HUGHES, R. K., CLARKE, T. A., BLUMENSCHEIN, T. M., KAMOUN, S. & BANFIELD, M. J. 2011. Structures of *Phytophthora* RXLR effector proteins. *Journal of Biological Chemistry*, **286,** 35834-35842.

References

ADL, S., SIMPSON, A., FARMER, M., ANDERSEN, R., ANDERSON, O., BARTA, J., BOWSER, S., BRUGEROLLE, G., FENSOME, R. & FREDERICQ, S. 2005. The new higher level classification of eukaryotes with emphasis on the taxonomy of protists. *Journal of Eukaryotic Microbiology,* 52**,** 399.

AGRIOS, G. N. 2005. *Plant Pathology,* Elsevier Academic Press.

ALFANO, J. R. & COLLMER, A. 2004. Type III secretion system effector proteins: double agents in bacterial disease and plant defense. *Annu. Rev. Phytopathol.,* 42**,** 385-414.

ALTSCHUL, S. F., GISH, W., MILLER, W., MYERS, E. W. & LIPMAN, D. J. 1990. Basic local alignment search tool. *Journal of molecular biology,* 215**,** 403-410.

AMARI, K., VAZQUEZ, F. & HEINLEIN, M. 2012. Manipulation of plant host susceptibility: an emerging role for viral movement proteins? *Frontiers in plant science,* 3, 10.

ARMSTRONG, M. R., WHISSON, S. C., PRITCHARD, L., BOS, J. I. B., VENTER, E., AVROVA, A. O., REHMANY, A. P., BOHME, U., BROOKS, K., CHEREVACH, I., HAMLIN, N., WHITE, B., FRASERS, A., LORD, A., QUAIL, M. A., CHURCHER, C., HALL, N., BERRIMAN, M., HUANG, S., KAMOUN, S., BEYNON, J. L. & BIRCH, P. R. J. 2005. An ancestral oomycete locus contains late blight avirulence gene Avr3a, encoding a protein that is recognized in the host cytoplasm. *Proceedings of the National Academy of Sciences of the United States of America,* 102**,** 7766-7771.

ASAI, T., TENA, G., PLOTNIKOVA, J., WILLMANN, M. R., CHIU, W.-L., GOMEZ-GOMEZ, L., BOLLER, T., AUSUBEL, F. M. & SHEEN, J. 2002. MAP kinase signalling cascade in *Arabidopsis* innate immunity. *Nature,* 415**,** 977-983.

ASAI, S., OHTA, K. & YOSHIOKA, H. 2008. MAPK signaling regulates nitric oxide and NADPH oxidase-dependent oxidative bursts in *Nicotiana benthamiana*. *The Plant Cell Online,* 20**,** 1390-1406.

ASHFIELD, T., KEEN, N. T., BUZZELL, R. I. & INNES, R. W. 1995. Soybean resistance genes specific for different *Pseudomonas syringae* avirulence genes are allelic, or closely linked, at the RPG1 locus. *Genetics,* 141**,** 1597-1604.

ASHFIELD, T., ONG, L. E., NOBUTA, K., SCHNEIDER, C. M. & INNES, R. W. 2004. Convergent evolution of disease resistance gene specificity in two flowering plant families. *The Plant Cell Online,* 16**,** 309-318.

AZEVEDO, C., SANTOS-ROSA, M. J. & SHIRASU, K. 2001. The U-box protein family in plants. *Trends in plant science,* 6**,** 354-358.

BADARAU, A., FIRBANK, S. J., WALDRON, K. J., YANAGISAWA, S., ROBINSON, N. J., BANFIELD, M. J. & DENNISON, C. 2008. FutA2 Is a Ferric Binding Protein from *Synechocystis* PCC 6803. *Journal of Biological Chemistry,* 283**,** 12520-12527.

BAGRODIA, S. & CERIONE, R. A. 1999. Pak to the future. *Trends in cell biology,* 9**,** 350.

BALDAUF, S. L., ROGER, A. J., WENK-SIEFERT, I. & DOOLITTLE, W. F. 2000. A Kingdom-Level Phylogeny of Eukaryotes Based on Combined Protein Data. *Science,* 290**,** 972-977.

BARTEL, P., CHIEN, C. T., STERNGLANZ, R., & FIELDS, S. 1993, Elimination of flase positives that arise using the two-hybrid system. *Biotechniques*, 14, 920-924.

BERROW, N., BUSSOW, K., COUTARD, B., DIPROSE, J., EKBERG, M., FOLKERS, G., LEVY, N., LIEU, V., OWENS, R. & PELEG, Y. 2006. Recombinant protein expression and solubility screening in *Escherichia coli*: a comparative study. *Acta Crystallographica Section D: Biological Crystallography,* 62**,** 1218-1226.

BERROW, N. S., ALDERTON, D., SAINSBURY, S., NETTLESHIP, J., ASSENBERG, R., RAHMAN, N., STUART, D. I. & OWENS, R. J. 2007. A versatile ligation-independent cloning method suitable for high-throughput expression screening applications. *Nucleic acids research,* 35**,** e45.

BERROW, N. S., ALDERTON, D. & OWENS, R. J. 2009. The Precise Engineering of Expression Vectors Using High-Throughput In-Fusion™ PCR Cloning. *High Throughput Protein Expression and Purification.* Springer.

BERTANI, G. 1951. STUDIES ON LYSOGENESIS I.: The Mode of Phage Liberation by Lysogenic *Escherichia coli*1. *Journal of Bacteriology,* 62**,** 293.

BESSETTE, P. H., ÅSLUND, F., BECKWITH, J. & GEORGIOU, G. 1999. Efficient folding of proteins with multiple disulfide bonds in the *Escherichia coli* cytoplasm. *Proceedings of the National Academy of Sciences,* 96**,** 13703-13708.

BINDSCHEDLER, L. V., MCGUFFIN, L. J., BURGIS, T. A., SPANU, P. D. & CRAMER, R. 2011. Proteogenomics and *in silico* structural and functional annotation of the barley powdery mildew *Blumeria graminis* f. sp. *hordei*. *Methods,* 54**,** 432-441.

BIRCH, P., REHMANY, A., PRITCHARD, L., KAMOUN, S. & BEYNON, J. 2006. Trafficking arms: oomycete effectors enter host plant cells. *Trends in Microbiology,* 14**,** 8-11.

BIRCH, P., BOEVINK, P., GILROY, E., HEIN, I., PRITCHARD, L. & WHISSON, S. 2008. Oomycete RXLR effectors: delivery, functional redundancy and durable disease resistance. *Current Opinion in Plant Biology,* 11**,** 373-379.

BIRCH, P., ARMSTRONG, M., BOS, J., BOEVINK, P., GILROY, E., TAYLOR, R., WAWRA, S., PRITCHARD, L., CONTI, L. & EWAN, R. 2009. Towards understanding the virulence functions of RXLR effectors of the oomycete plant pathogen *Phytophthora infestans*. *Journal of Experimental Botany,* 60**,** 1133.

BIRD, L. E. 2011. High throughput construction and small scale expression screening of multi-tag vectors in *Escherichia coli*. *Methods,* 55**,** 29-37.

BIRNBOIM, H. & DOLY, J. 1979. A rapid alkaline extraction procedure for screening recombinant plasmid DNA. *Nucleic acids research,* 7**,** 1513-1523.

BJERRUM, O. J. & SCHAFER-NIELSEN, C. 1986. Buffer systems and transfer parameters for semidry electroblotting with a horizontal apparatus. *Electrophoresis,* 86**,** 315-327.

BLAIR, J. E., COFFEY, M. D., PARK, S.-Y., GEISER, D. M. & KANG, S. 2008. A multi-locus phylogeny for *Phytophthora* utilizing markers derived from complete genome sequences. *Fungal Genetics and Biology,* 45**,** 266-277.

BLEE, K. A., YANG, K.-Y. & ANDERSON, A. J. 2004. Activation of defense pathways: synergism between reactive oxygen species and salicylic acid and consideration of field applicability. *European Journal of Plant Pathology,* 110**,** 203-212.

BLEIN, J., COUTOS-THÉVENOT, P., MARION, D. & PONCHET, M. 2002. From elicitins to lipid-transfer proteins: a new insight in cell signalling involved in plant defence mechanisms. *Trends in plant science,* 7**,** 293-296.

BLEVINS, T., RAJESWARAN, R., SHIVAPRASAD, P. V., BEKNAZARIANTS, D., SI-AMMOUR, A., PARK, H.-S., VAZQUEZ, F., ROBERTSON, D., MEINS, F., HOHN, T. & POOGGIN, M. M. 2006. Four plant Dicers mediate viral small RNA biogenesis and DNA virus induced silencing. *Nucleic acids research,* 34**,** 6233-6246.

BLOCK, A., LI, G., FU, Z. Q. & ALFANO, J. R. 2008. Phytopathogen type III effector weaponry and their plant targets. *Current Opinion in Plant Biology,* 11**,** 396-403.

BLOCK, A. & ALFANO, J. R. 2011. Plant targets for *Pseudomonas syringae* type III effectors: virulence targets or guarded decoys? *Current Opinion in Microbiology,* 14**,** 39-46.

BOISSY, G., O'DONOHUE, M., GAUDEMER, O., PEREZ, V., PERNOLLET, J. C. & BRUNIE, S. 1999. The 2.1 Å structure of an elicitin-ergosterol complex: A recent addition to the Sterol Carrier Protein family. *Protein science,* 8**,** 1191-1199.

BOLLER, T. & FELIX, G. 2009. A renaissance of elicitors: perception of microbe-associated molecular patterns and danger signals by pattern-recognition receptors. *Annual review of plant biology,* 60**,** 379-406.

BOLTON, M. D. 2009. Primary metabolism and plant defense-fuel for the fire. *Molecular Plant-Microbe Interactions,* 22**,** 487-497.

BOLWELL, G. P. 1999. Role of active oxygen species and NO in plant defence responses. *Current Opinion in Plant Biology,* 2**,** 287-294.

BOMBARELY, A., ROSLI, H. G., VREBALOV, J., MOFFETT, P., MUELLER, L. A. & MARTIN, G. B. 2012. A draft genome sequence of *Nicotiana benthamiana* to enhance molecular plant-microbe biology research. *Molecular Plant-Microbe Interactions,* 25**,** 1523-1530.

BONNET, P., BOURDON, E., PONCHET, M., BLEIN, J.-P. & RICCI, P. 1996. Acquired resistance triggered by elicitins in tobacco and other plants. *European Journal of Plant Pathology,* 102**,** 181-192.

BOOTHROYD, J. & DUBREMETZ, J. 2008. Kiss and spit: the dual roles of *Toxoplasma* rhoptries. *Nature Reviews Microbiology,* 6**,** 79-88.

BOS, J., KANNEGANTI, T., YOUNG, C., CAKIR, C., HUITEMA, E., WIN, J., ARMSTRONG, M., BIRCH, P. & KAMOUN, S. 2006. The C-terminal half of *Phytophthora infestans* RXLR effector AVR3a is sufficient to trigger R3a-mediated hypersensitivity and suppress INF1-induced cell death in *Nicotiana benthamiana*. *Plant Journal,* 48**,** 165.

BOS, J. I., CHAPARRO-GARCIA, A., QUESADA-OCAMPO, L. M., GARDENER, B. B. M. & KAMOUN, S. 2009. Distinct amino acids of the *Phytophthora infestans* effector AVR3a condition activation of R3a hypersensitivity and suppression of cell death. *Molecular Plant-Microbe Interactions,* 22**,** 269-281.

BOS, J. I. B., PRINCE, D., PITINO, M., MAFFEI, M. E., WIN, J. & HOGENHOUT, S. A. 2010a. A Functional Genomics Approach Identifies Candidate Effectors from the Aphid Species *Myzus persicae* (Green Peach Aphid). *PLoS Genet,* 6**,** e1001216.

BOS, J. I., ARMSTRONG, M. R., GILROY, E. M., BOEVINK, P. C., HEIN, I., TAYLOR, R. M., ZHENDONG, T., ENGELHARDT, S., VETUKURI, R. R. & HARROWER, B. 2010b. *Phytophthora infestans* effector AVR3a is essential for virulence and manipulates plant immunity by stabilizing host E3 ligase CMPG1. *Proceedings of the National Academy of Sciences,* 107**,** 9909-9914.

BOUTEMY, L. S., KING, S. R., WIN, J., HUGHES, R. K., CLARKE, T. A., BLUMENSCHEIN, T. M., KAMOUN, S. & BANFIELD, M. J. 2011. Structures of *Phytophthora* RXLR effector proteins. *Journal of Biological Chemistry,* 286**,** 35834-35842.

BOUWMEESTER, K., DE SAIN, M., WEIDE, R., GOUGET, A., KLAMER, S., CANUT, H. & GOVERS, F. 2011. The lectin receptor kinase LecRK-I. 9 is a novel *Phytophthora* resistance component and a potential host target for a RXLR effector. *PLoS pathogens,* 7**,** e1001327.

BOZKURT, T. O., SCHORNACK, S., WIN, J., SHINDO, T., ILYAS, M., OLIVA, R., CANO, L. M., JONES, A. M. E., HUITEMA, E., VAN DER HOORN, R. A. L. & KAMOUN, S. 2011. *Phytophthora infestans* effector AVRblb2 prevents secretion of a plant immune protease at the haustorial interface. *Proceedings of the National Academy of Sciences*.

BOZKURT, T. O., SCHORNACK, S., BANFIELD, M. J. & KAMOUN, S. 2012. Oomycetes, effectors, and all that jazz. *Current Opinion in Plant Biology*.

BRENNAN, S. & COWAN, P. 1992. A suite of programs for calculating x-ray absorption, reflection, and diffraction performance for a variety of materials at arbitrary wavelengths. *Review of scientific instruments,* 63**,** 850-853.

BRIGNETI, G., MARTÍN-HERNÁNDEZ, A. M., JIN, H., CHEN, J., BAULCOMBE, D. C., BAKER, B. & JONES, J. D. 2004. Virus-induced gene silencing in *Solanum* species. *The Plant Journal,* 39**,** 264-272.

BRUNNER, F., ROSAHL, S., LEE, J., RUDD, J. J., GEILER, C., KAUPPINEN, S., RASMUSSEN, G., SCHEEL, D. & NÜRNBERGER, T. 2002. Pep-13, a plant defense-inducing pathogen-associated pattern from *Phytophthora* transglutaminases. *The EMBO journal,* 21**,** 6681-6688.

BURCH-SMITH, T. M., ANDERSON, J. C., MARTIN, G. B. & DINESH-KUMAR, S. P. 2004. Applications and advantages of virus-induced gene silencing for gene function studies in plants. *The Plant Journal,* 39**,** 734-746.

BUTT, T. R., EDAVETTAL, S. C., HALL, J. P. & MATTERN, M. R. 2005. SUMO fusion technology for difficult-to-express proteins. *Protein expression and purification,* 43**,** 1-9.

CALLUS, B. A., VERHAGEN, A. M. & VAUX, D. L. 2006. Association of mammalian sterile twenty kinases, Mst1 and Mst2, with hSalvador via C-terminal coiled coil domains, leads to its stabilization and phosphorylation. *FEBS Journal,* 273**,** 4264-4276.

CARDARELLI, L., PELL, L. G., NEUDECKER, P., PIRANI, N., LIU, A., BAKER, L. A., RUBINSTEIN, J. L., MAXWELL, K. L. & DAVIDSON, A. R. 2010. Phages have adapted the same protein fold to fulfill multiple functions in virion assembly. *Proceedings of the National Academy of Sciences,* 107**,** 14384-14389.

CHAIWONGSAR, S., OTEGUI, M. S., JESTER, P. J., MONSON, S. S. & KRYSAN, P. J. 2006. The protein kinase genes MAP3Kε1 and MAP3Kε2 are required for pollen viability in *Arabidopsis thaliana*. *The Plant Journal,* 48**,** 193-205.

CHAIWONGSAR, S., STROHM, A. K., SU, S.-H. & KRYSAN, P. J. 2012. Genetic analysis of the *Arabidopsis* protein kinases MAP3Kε1 and MAP3Kε2 indicates roles in cell expansion and embryo development. *Frontiers in plant science,* 3, 228.

CHAMPION, A., JOUANNIC, S., GUILLON, S., MOCKAITIS, K., KRAPP, A., PICAUD, A., SIMANIS, V., KREIS, M. & HENRY, Y. 2004a. *At*SGP1, *At*SGP2 and MAP4Kα are nucleolar plant proteins that can complement fission yeast mutants lacking a functional SIN pathway. *Journal of Cell Science,* 117**,** 4265-4275.

CHAMPION, A., PICAUD, A. & HENRY, Y. 2004b. Reassessing the MAP3K and MAP4K relationships. *Trends in plant science,* 9**,** 123-129.

CHAPARRO-GARCIA, A., WILKINSON, R. C., GIMENEZ-IBANEZ, S., FINDLAY, K., COFFEY, M. D., ZIPFEL, C., RATHJEN, J. P., KAMOUN, S. & SCHORNACK, S. 2011. The receptor-like kinase SERK3/BAK1 is required for basal resistance against the late blight pathogen *Phytophthora infestans* in *Nicotiana benthamiana*. *PLoS ONE,* 6**,** e16608.

CHEN, V. B., ARENDALL, W. B., HEADD, J. J., KEEDY, D. A., IMMORMINO, R. M., KAPRAL, G. J., MURRAY, L. W., RICHARDSON, J. S. & RICHARDSON, D. C. 2009. MolProbity: all-atom structure validation for macromolecular crystallography. *Acta Crystallographica Section D: Biological Crystallography,* 66**,** 12-21.

CHENG, B., YU, X., MA, Z., DONG, S., DOU, D., WANG, Y. & ZHENG, X. 2012. *Phytophthora sojae* effector Avh331 suppresses the plant defence response by disturbing the MAPK signalling pathway. *Physiological and molecular plant pathology,* 77**,** 1-9.

CHOU, S., KRASILEVA, K. V., HOLTON, J. M., STEINBRENNER, A. D., ALBER, T. & STASKAWICZ, B. J. 2011. *Hyaloperonospora arabidopsidis* ATR1 effector is a repeat protein with distributed recognition surfaces. *Proceedings of the National Academy of Sciences,* 108**,** 13323-13328.

CLAY, K. & KOVER, P. X. 1996. The Red Queen hypothesis and plant/pathogen interactions. *Annual review of phytopathology,* 34**,** 29-50.

COLCOMBET, J. & HIRT, H. 2008. *Arabidopsis* MAPKs: a complex signalling network involved in multiple biological processes. *Biochem. J,* 413**,** 217-226.

COLLINGE, D. B., JØRGENSEN, H. J. L., LUND, O. S. & LYNGKJÆR, M. F. 2010. Engineering Pathogen Resistance in Crop Plants: Current Trends and Future Prospects. Annual review of phytopathology, 48, 269-291.

COSIO, E. G., FREY, T. & EBEL, J. 1992. Identification of a high-affinity binding protein for a hepta-β-glucoside phytoalexin elicitor in soybean. *European journal of biochemistry,* 204**,** 1115-1123.

COWTAN, K. 2006. The Buccaneer software for automated model building. 1. Tracing protein chains. *Acta Crystallographica Section D,* 62**,** 1002-1011.

COWTAN, K. 2010. Recent developments in classical density modification. *Acta Crystallographica Section D: Biological Crystallography,* 66**,** 470-478.

CUI, H., WANG, Y., XUE, L., CHU, J., YAN, C., FU, J., CHEN, M., INNES, R. W. & ZHOU, J.-M. 2010. *Pseudomonas syringae* Effector Protein AvrB Perturbs *Arabidopsis* Hormone Signaling by Activating MAP Kinase 4. *Cell Host & Microbe,* 7**,** 164-175.

CUNNAC, S., LINDEBERG, M. & COLLMER, A. 2009. *Pseudomonas syringae* type III secretion system effectors: repertoires in search of functions. *Current Opinion in Microbiology,* 12**,** 53-60.

DAMASCENO, C., BISHOP, J., RIPOLL, D., WIN, J., KAMOUN, S. & ROSE, J. 2008. Structure of the Glucanase Inhibitor Protein (GIP) Family from *Phytophthora* Species Suggests Coevolution with Plant Endo- -1, 3-Glucanases. *Molecular Plant-Microbe Interactions,* 21**,** 820-830.

DAN, I., WATANABE, N. M. & KUSUMI, A. 2001. The Ste20 group kinases as regulators of MAP kinase cascades. *Trends in cell biology,* 11**,** 220-230.

DANGL, J. L. & JONES, J. D. G. 2001. Plant pathogens and integrated defence responses to infection. *Nature,* 411**,** 826-833.

DAVIS, I. W., LEAVER-FAY, A., CHEN, V. B., BLOCK, J. N., KAPRAL, G. J., WANG, X., MURRAY, L. W., ARENDALL III, W. B., SNOEYINK, J. & RICHARDSON, J. S. 2007. MolProbity: all-atom contacts and structure validation for proteins and nucleic acids. *Nucleic acids research,* 35**,** W375-W383.

DAWKINS, R. 1982. *The extended phenotype,* Oxford University Press Oxford.

DE LORENZO, G., BRUTUS, A., SAVATIN, D. V., SICILIA, F. & CERVONE, F. 2011. Engineering plant resistance by constructing chimeric receptors that recognize damage-associated molecular patterns (DAMPs). *Febs Letters,* 585**,** 1521-1528.

DE MARCO, A. 2009. Strategies for successful recombinant expression of disulfide bond-dependent proteins in *Escherichia coli*. *Microbial cell factories,* 8**,** 26.

DEL POZO, O., PEDLEY, K. F. & MARTIN, G. B. 2004. MAPKKKα is a positive regulator of cell death associated with both plant immunity and disease. *The EMBO journal,* 23**,** 3072-3082.

DELAROSA, S., GUILLEMETTE, J., PAPILLON, J., HAN, Y.-S., KRISTOF, A. S. & CYBULSKY, A. V. 2011. Activity of the Ste20-like kinase, SLK, is enhanced by homodimerization. *American Journal of Physiology-Renal Physiology,* 301**,** F554-F564.

DELPIRE, E. & GAGNON, K. 2008. SPAK and OSR1: STE20 kinases involved in the regulation of ion homoeostasis and volume control in mammalian cells. *Biochem. J,* 409**,** 321-331.

DEMELER, B., SCOTT, D., HARDING, S. & ROWE, A. 2005. Modern Analytical Ultracentrifugation: Techniques and Methods. *Royal Society of Chemistry (UK)***,** 210-229.

DERMAN, A. I., PRINZ, W. A., BELIN, D. & BECKWITH, J. 1993. Mutations that allow disulfide bond formation in the cytoplasm of *Escherichia coli*. *Science,* 262**,** 1744-1747.

DESLANDES, L. & RIVAS, S. 2012. Catch me if you can: bacterial effectors and plant targets. *Trends in plant science,* 17**,** 644-655.

DESVEAUX, D., SINGER, A. U. & DANGL, J. L. 2006. Type III effector proteins: doppelgangers of bacterial virulence. *Current Opinion in Plant Biology,* 9**,** 376-382.

DESVEAUX, D., SINGER, A. U., WU, A.-J., MCNULTY, B. C., MUSSELWHITE, L., NIMCHUK, Z., SONDEK, J. & DANGL, J. L. 2007. Type III effector activation via nucleotide binding, phosphorylation, and host target interaction. *PLoS pathogens,* 3**,** e48.

DIXON, R. A. 1986. The phytoalexin response: elicitation, signalling and control of host gene expression. *Biological Reviews,* 61**,** 239-291.

DJAMEI, A., PITZSCHKE, A., NAKAGAMI, H., RAJH, I. & HIRT, H. 2007. Trojan horse strategy in *Agrobacterium* transformation: abusing MAPK defense signaling. *Science Signaling,* 318**,** 453.

DODDS, P. N., LAWRENCE, G. J., CATANZARITI, A.-M., TEH, T., WANG, C.-I., AYLIFFE, M. A., KOBE, B. & ELLIS, J. G. 2006. Direct protein interaction underlies gene-for-gene specificity and coevolution of the flax resistance genes and flax rust avirulence genes. *Proceedings of the National Academy of Sciences,* 103**,** 8888-8893.

DODDS, P. N. & RATHJEN, J. P. 2010. Plant immunity: towards an integrated view of plant–pathogen interactions. *Nature Reviews Genetics,* 11**,** 539-548.

DOEHLEMANN, G. & HEMETSBERGER, C. 2013. Apoplastic immunity and its suppression by filamentous plant pathogens. *New Phytologist,* 198**,** 1001-1016.

DONG, S., YIN, W., KONG, G., YANG, X., QUTOB, D., CHEN, Q., KALE, S. D., SUI, Y., ZHANG, Z. & DOU, D. 2011. *Phytophthora sojae* avirulence effector Avr3b is a secreted NADH and ADP-ribose pyrophosphorylase that modulates plant immunity. *PLoS pathogens,* 7**,** e1002353.

DOU, D., KALE, S. D., WANG, X., CHEN, Y., WANG, Q., WANG, X., JIANG, R. H., ARREDONDO, F. D., ANDERSON, R. G. & THAKUR, P. B. 2008a. Conserved C-terminal motifs required for avirulence and suppression of cell death by *Phytophthora sojae* effector Avr1b. *Plant Cell,* 20**,** 1118-1133.

DOU, D., KALE, S., WANG, X., JIANG, R., BRUCE, N., ARREDONDO, F., ZHANG, X. & TYLER, B. 2008b. RXLR-mediated entry of *Phytophthora sojae* effector Avr1b into soybean cells does not require pathogen-encoded machinery. *The Plant Cell Online,* 20**,** 1930.

DRENTH, A., JANSSEN, E. & GOVERS, F. 1995. Formation and survival of oospores of *Phytophthora infestans* under natural conditions. *Plant Pathology,* 44**,** 86-94.

DU, J., BIJSTERBOSCH, G., JACOBSEN, E., VISSER, R. G. & VLEESHOUWERS, V. G. A. A. 2012. PS04-180: Surface-mediated response to elicitins is providing a novel layer of resistance to *Phytophthora infestans* in potato. *In:* XV International Congress of MPMI, Kyoto, Japan.

DU, J., TIAN, Z., LIU, J., VLEESHOUWERS, V. G., SHI, X. & XIE, C. 2013. Functional analysis of potato genes involved in quantitative resistance to *Phytophthora infestans*. *Molecular biology reports,* 40**,** 957-967.

EBRAHIM, S., USHA, K. & SINGH, B. 2011. Pathogenesis-related (PR) proteins in plant defense mechanism. *Science against microbial pathogens: communicating current research and technological advances. Extremadura: Formatex Research Center,* 1**,** 1043-1054.

ELLIS, J. G. & DODDS, P. N. 2011. Showdown at the RXLR motif: Serious differences of opinion in how effector proteins from filamentous eukaryotic pathogens enter plant cells. *Proceedings of the National Academy of Sciences,* 108**,** 14381-14382.

ELLISDON, A. M., JANI, D., KÖHLER, A., HURT, E. & STEWART, M. 2010. Structural basis for the interaction between yeast Spt-Ada-Gcn5 acetyltransferase (SAGA) complex components Sgf11 and Sus1. *Journal of Biological Chemistry,* 285**,** 3850-3856.

EMSLEY, P. & COWTAN, K. 2004. Coot: model-building tools for molecular graphics. *Acta Crystallographica Section D: Biological Crystallography,* 60**,** 2126-2132.

ESPOSITO, D. & CHATTERJEE, D. K. 2006. Enhancement of soluble protein expression through the use of fusion tags. *Current Opinion in Biotechnology,* 17**,** 353-358.

EVANS, P. 2005. Scaling and assessment of data quality. *Acta Crystallographica Section D: Biological Crystallography,* 62**,** 72-82.

EVANS, P. R. 2011. An introduction to data reduction: space-group determination, scaling and intensity statistics. *Acta Crystallographica Section D: Biological Crystallography,* 67**,** 282-292.

FIELDS, S. & SONG, O.-K. 1989. A novel genetic system to detect protein protein interactions. *Nature* 340**,** 245 - 246.

FISHER, M. A., MCKINLEY, K. L., BRADLEY, L. H., VIOLA, S. R. & HECHT, M. H. 2011. *De Novo* Designed Proteins from a Library of Artificial Sequences Function in *Escherichia coli* and Enable Cell Growth. *PLoS ONE,* 6**,** e15364.

FISHER, M. C., HENK, D. A., BRIGGS, C. J., BROWNSTEIN, J. S., MADOFF, L. C., MCCRAW, S. L. & GURR, S. J. 2012. Emerging fungal threats to animal, plant and ecosystem health. *nature,* 484**,** 186-194.

FLIEGMANN, J., MITHÖFER, A., WANNER, G. & EBEL, J. 2004. An ancient enzyme domain hidden in the putative β-glucan elicitor receptor of soybean may play an active part in the perception of pathogen-associated molecular patterns during broad host resistance. *Journal of Biological Chemistry,* 279**,** 1132-1140.

FLIER, W., KESSEL, G., VAN DEN BOSCH, G. & TURKENSTEEN, L. 2002a. Impact of new populations of *Phytophthora infestans* on integrated late blight management. *PPO-Special Report no. 8***,** 193.

FLIER, W. G., KESSEL, G. J., SCHEPERS, H. & TURKENSTEEN, L. J. 2002b. The impact of oospores of *Phytophthora* infestans on late blight epidemics. *Late Blight: Managing the Global Threat***,** 18-22.

FLOR, H. 1971. Current status of the gene-for-gene concept. *Annual Review of Phytopathology,* 9**,** 275-296.

FRY, W. & GOODWIN, S. 1997. Re-emergence of potato and tomato late blight in the United States. *Plant Disease,* 81**,** 1349-1357.

FRY, W. 2008. *Phytophthora infestans*: the plant (and R gene) destroyer. *Mol. Plant Pathol.,* 9**,** 385-402.

GARMAN, E. F. & OWEN, R. L. 2005. Cryocooling and radiation damage in macromolecular crystallography. *Acta Crystallographica Section D: Biological Crystallography,* 62**,** 32-47.

GASTEIGER, E., HOOGLAND, C., GATTIKER, A., DUVAUD, S. E., WILKINS, M. R., APPEL, R. D. & BAIROCH, A. 2005. Protein identification and analysis tools on the ExPASy server. *The proteomics protocols handbook***,** 571-607.

. GAULIN, E., JAUNEAU, A., VILLALBA, F., RICKAUER, M., ESQUERRÉ-TUGAYÉ, M.-T. & BOTTIN, A. 2002. The CBEL glycoprotein of *Phytophthora parasitica* var-*nicotianae* is involved in cell wall deposition and adhesion to cellulosic substrates. *Journal of Cell Science,* 115**,** 4565-4575.

GAULIN, E., DRAMÉ, N., LAFITTE, C., TORTO-ALALIBO, T., MARTINEZ, Y., AMELINE-TORREGROSA, C., KHATIB, M., MAZARGUIL, H., VILLALBA-MATEOS, F. & KAMOUN, S. 2006. Cellulose binding domains of a *Phytophthora* cell wall protein are novel pathogen-associated molecular patterns. *The Plant Cell Online,* 18**,** 1766-1777.

GAULIN, E., BOTTIN, A. & DUMAS, B. 2010. Sterol biosynthesis in oomycete pathogens. *Plant signaling & behavior,* 5**,** 258-260

GEISSE, S., GRAM, H., KLEUSER, B. & KOCHER, H. P. 1996. Eukaryotic expression systems: a comparison. *Protein expression and purification,* 8**,** 271-282.

GHOSH, I., HAMILTON, A. D. & REGAN, L. 2000. Antiparallel leucine zipper-directed protein reassembly: application to the green fluorescent protein. *JOURNAL-AMERICAN CHEMICAL SOCIETY,* 122**,** 5658-5659.

GILROY, E. M., TAYLOR, R. M., HEIN, I., BOEVINK, P., SADANANDOM, A. & BIRCH, P. R. 2011. CMPG1-dependent cell death follows perception of diverse pathogen elicitors at the host plasma membrane and is suppressed by *Phytophthora infestans* RXLR effector AVR3a. *New Phytologist,* 190**,** 653-666.

GLAZEBROOK, J. 2005. Contrasting mechanisms of defense against biotrophic and necrotrophic pathogens. *Annu Rev Phytopathol,* 43**,** 205-27.

GONZÁLEZ-LAMOTHE, R., TSITSIGIANNIS, D. I., LUDWIG, A. A., PANICOT, M., SHIRASU, K. & JONES, J. D. 2006. The U-box protein CMPG1 is required for efficient activation of defense mechanisms triggered by multiple resistance genes in tobacco and tomato. *The Plant Cell Online,* 18**,** 1067-1083.

GOUGET, A., SENCHOU, V., GOVERS, F., SANSON, A., BARRE, A., ROUGÉ, P., PONT-LEZICA, R. & CANUT, H. 2006. Lectin receptor kinases participate in protein-protein interactions to mediate plasma membrane-cell wall adhesions in *Arabidopsis*. *Plant Physiology,* 140**,** 81-90.

GRANT, M. R., GODIARD, L., STRAUBE, E., ASHFIELD, T., LEWALD, J., SATTLER, A., INNES, R. W. & DANGL, J. L. 1995. Structure of the *Arabidopsis RPM1* gene enabling dual specificity disease resistance. *Science,* 269**,** 843-846.

GREENBERG, C. S., BIRCKBICHLER, P. J. & RICE, R. H. 1991. Transglutaminases: multifunctional cross-linking enzymes that stabilize tissues. *The FASEB journal,* 5**,** 3071-3077.

GROUFFAUD, S., VAN WEST, P., AVROVA, A. O., BIRCH, P. R. & WHISSON, S. C. 2008. Plasmodium falciparum and Hyaloperonospora parasitica effector translocation motifs are functional in Phytophthora infestans. *Microbiology,* 154**,** 3743-3751.

GUEST, D. & BROWN, J. 1997. Plant defences against pathogens. *Plant pathogens and plant diseases. Rockvale Publications, Armidale***,** 263-286.

GÜRLEBECK, D., JAHN, S., GÜRLEBECK, N., SZCZESNY, R., SZUREK, B., HAHN, S., HAUSE, G. & BONAS, U. 2009. Visualization of novel virulence activities of the *Xanthomonas* type III effectors AvrBs1, AvrBs3 and AvrBs4. *Molecular Plant Pathology,* 10**,** 175-188.

HAACKE, A., FENDRICH, G., RAMAGE, P. & GEISER, M. 2009. Chaperone over-expression in *Escherichia coli*: Apparent increased yields of soluble recombinant protein kinases are due mainly to soluble aggregates. *Protein Expression and Purification,* 64**,** 185-193.

HAAS, B. J., KAMOUN, S., ZODY, M. C., JIANG, R. H. Y., HANDSAKER, R. E., CANO, L. M., GRABHERR, M., KODIRA, C. D., RAFFAELE, S., TORTO-ALALIBO, T., BOZKURT, T. O., AH-FONG, A. M. V., ALVARADO, L., ANDERSON, V. L., ARMSTRONG, M. R., AVROVA, A., BAXTER, L., BEYNON, J., BOEVINK, P. C., BOLLMANN, S. R., BOS, J. I. B., BULONE, V., CAI, G., CAKIR, C., CARRINGTON, J. C., CHAWNER, M., CONTI, L., COSTANZO, S., EWAN, R., FAHLGREN, N., FISCHBACH, M. A., FUGELSTAD, J., GILROY, E. M., GNERRE, S., GREEN, P. J., GRENVILLE-BRIGGS, L. J., GRIFFITH, J., GRUNWALD, N. J., HORN, K., HORNER, N. R., HU, C.-H., HUITEMA, E., JEONG, D.-H., JONES, A. M. E., JONES, J. D. G., JONES, R. W., KARLSSON, E. K., KUNJETI, S. G., LAMOUR, K., LIU, Z., MA, L., MACLEAN, D., CHIBUCOS, M. C., MCDONALD, H., MCWALTERS, J., MEIJER, H. J. G., MORGAN, W., MORRIS, P. F., MUNRO, C. A., O'NEILL, K., OSPINA-GIRALDO, M., PINZON, A., PRITCHARD, L., RAMSAHOYE, B., REN, Q., RESTREPO, S., ROY, S., SADANANDOM, A., SAVIDOR, A., SCHORNACK, S., SCHWARTZ, D. C., SCHUMANN, U. D., SCHWESSINGER, B., SEYER, L., SHARPE, T., SILVAR, C., SONG, J., STUDHOLME, D. J., SYKES, S., THINES, M., VAN DE VONDERVOORT, P. J. I., PHUNTUMART, V., WAWRA, S., WEIDE, R., WIN, J., YOUNG, C., ZHOU, S., FRY, W., MEYERS, B. C., VAN WEST, P., RISTAINO, J., GOVERS, F., BIRCH, P. R. J., WHISSON, S. C., JUDELSON, H. S. & NUSBAUM, C. 2009. Genome sequence and analysis of the Irish potato famine pathogen *Phytophthora infestans*. *Nature,* 461**,** 393-398.

HAEGEMAN, A., MANTELIN, S., JONES, J. T. & GHEYSEN, G. 2012. Functional roles of effectors of plant-parasitic nematodes. *Gene,* 492**,** 19-31.

HALEY, B. & ZAMORE, P. D. 2004. Kinetic analysis of the RNAi enzyme complex. *Nature structural & molecular biology,* 11**,** 599-606.

HALIM, V. A., HUNGER, A., MACIOSZEK, V., LANDGRAF, P., NÜRNBERGER, T., SCHEEL, D. & ROSAHL, S. 2004. The oligopeptide elicitor Pep-13 induces salicylic acid-dependent and-independent defense reactions in potato. *Physiological and molecular plant pathology,* 64**,** 311-318.

HALIM, V. A., ALTMANN, S., ELLINGER, D., ESCHEN-LIPPOLD, L., MIERSCH, O., SCHEEL, D. & ROSAHL, S. 2009. PAMP-induced defense responses in potato require both salicylic acid and jasmonic acid. *The Plant Journal,* 57**,** 230-242.

HAMILTON, M. D., NUARA, A. A., GAMMON, D. B., BULLER, R. M. & EVANS, D. H. 2007. Duplex strand joining reactions catalyzed by vaccinia virus DNA polymerase. *Nucleic acids research,* 35**,** 143-151.

HAMMOND, J. B. W. & KRUGER, N. J. 1994. The Bradford method for protein quantitation. *In:* WALKER, J. M. (ed.) *New Protein Techniques.* Humana Press.

HAMMOND-KOSACK, K. E. & PARKER, J. E. 2003. Deciphering plant-pathogen communication: fresh perspectives for molecular resistance breeding. *Current Opinion in Biotechnology,* 14**,** 177-193.

HANAHAN, D. 1983. Studies on transformation of *Escherichia coli* with plasmids. *Journal of molecular biology,* 166**,** 557-580.

HARDHAM, A. R. & BLACKMAN, L. M. 2009. Molecular cytology of *Phytophthora*–plant interactions. *Australasian Plant Pathology,* 39**,** 29-35.

HARPER, J., WAANDERS, E. & KEELING, P. 2005. On the monophyly of chromalveolates using a six-protein phylogeny of eukaryotes. *International Journal of Systematic and Evolutionary Microbiology,* 55**,** 487.

HASHIMOTO, M., KOMATSU, K., MAEJIMA, K., OKANO, Y., SHIRAISHI, T., ISHIKAWA, K., TAKINAMI, Y., YAMAJI, Y. & NAMBA, S. 2012. Identification of three MAPKKKs forming a linear signaling pathway leading to programmed cell death in *Nicotiana benthamiana*. *BMC plant biology,* 12**,** 103.

HAVERKORT, A., BOONEKAMP, P., HUTTEN, R., JACOBSEN, E., LOTZ, L., KESSEL, G., VISSER, R. & VAN DER VOSSEN, E. 2008. Societal costs of late blight in potato and prospects of durable resistance through cisgenic modification. *Potato Research,* 51**,** 47-57.

HEESE, A., HANN, D. R., GIMENEZ-IBANEZ, S., JONES, A. M. E., HE, K., LI, J., SCHROEDER, J. I., PECK, S. C. & RATHJEN, J. P. 2007. The receptor-like kinase SERK3/BAK1 is a central regulator of innate immunity in plants. *PNAS,* 104**,** 12217-12222.

HEIL, M. & BOSTOCK, R. M. 2002. Induced systemic resistance (ISR) against pathogens in the context of induced plant defences. *Annals of Botany,* 89**,** 503-512.

HERRMANN, C., HORN, G., SPAARGAREN, M. & WITTINGHOFER, A. 1996. Differential interaction of the ras family GTP-binding proteins H-Ras, Rap1A, and R-Ras with the putative effector molecules Raf kinase and Ral-guanine nucleotide exchange factor. *Journal of Biological Chemistry,* 271**,** 6794-6800.

HO, S. N., HUNT, H. D., HORTON, R. M., PULLEN, J. K. & PEASE, L. R. 1989. Site-directed mutagenesis by overlap extension using the polymerase chain reaction. *Gene,* 77**,** 51-59.

HOGENHOUT, S. A., VAN DER HOORN, R. A. L., TERAUCHI, R. & KAMOUN, S. 2009. Emerging Concepts in Effector Biology of Plant-Associated Organisms. *Molecular Plant-Microbe Interactions,* 22**,** 115-122.

HOLM, L. & ROSENSTRÖM, P. 2010. Dali server: conservation mapping in 3D. *Nucleic acids research,* 38**,** W545-W549.

HU, C.-D., CHINENOV, Y. & KERPPOLA, T. K. 2002. Visualization of interactions among bZIP and Rel family proteins in living cells using bimolecular fluorescence complementation. *Molecular cell,* 9**,** 789.

HUBER, A. H., NELSON, W. J. & WEIS, W. I. 1997. Three-Dimensional Structure of the Armadillo Repeat Region of β-Catenin. *Cell,* 90**,** 871-882.

HUFFAKER, A. & RYAN, C. A. 2007. Endogenous peptide defense signals in *Arabidopsis* differentially amplify signaling for the innate immune response. *Proceedings of the National Academy of Sciences,* 104**,** 10732-10736.

HUITEMA, E., VLEESHOUWERS, V. G., CAKIR, C., KAMOUN, S. & GOVERS, F. 2005. Differences in intensity and specificity of hypersensitive response induction in Nicotiana spp. by INF1, INF2A, and INF2B of Phytophthora infestans. *Molecular Plant-Microbe Interactions,* 18**,** 183-193.

ICHIMURA, K., SHINOZAKI, K., TENA, G., SHEEN, J., HENRY, Y., CHAMPION, A., KREIS, M., ZHANG, S., HIRT, H., WILSON, C., HEBERLE-BORS, E., ELLIS, B. E., MORRIS, P. C., INNES, R. W., ECKER, J. R., SCHEEL, D., KLESSIG, D. F., MACHIDA, Y., MUNDY, J., OHASHI, Y. & WALKER, J. C. 2002. Mitogen-activated protein kinase cascades in plants: a new nomenclature. *Trends in plant science,* 7**,** 301-308.

ILLERGÅRD, K., ARDELL, D. H. & ELOFSSON, A. 2009. Structure is three to ten times more conserved than sequence—A study of structural response in protein cores. *Proteins: Structure, Function, and Bioinformatics,* 77**,** 499-508.

INGLE, R. A., CARSTENS, M. & DENBY, K. J. 2006. PAMP recognition and the plant–pathogen arms race. *Bioessays,* 28**,** 880-889.

JACKSON, A. L., BARTZ, S. R., SCHELTER, J., KOBAYASHI, S. V., BURCHARD, J., MAO, M., LI, B., CAVET, G. & LINSLEY, P. S. 2003. Expression profiling reveals off-target gene regulation by RNAi. *Nature biotechnology,* 21**,** 635-637.

JACKSON, A. L., BURCHARD, J., SCHELTER, J., CHAU, B. N., CLEARY, M., LIM, L. & LINSLEY, P. S. 2006. Widespread siRNA "off-target" transcript silencing mediated by seed region sequence complementarity. *RNA,* 12**,** 1179-1187.

JEFFERS, S. & ALDWINCKLE, H. 1987. Enhancing detection of *Phytophthora cactorum* in naturally infested soil. *Phytopathology,* 77**,** 1475-1482.

JIN, H., AXTELL, M. J., DAHLBECK, D., EKWENNA, O., ZHANG, S., STASKAWICZ, B. & BAKER, B. 2002. NPK1, an MEKK1-like mitogen-activated protein kinase kinase kinase, regulates innate immunity and development in plants. *Developmental cell,* 3**,** 291-297.

JIN, H., LIU, Y., YANG, K.-Y., KIM, C. Y., BAKER, B. & ZHANG, S. 2003. Function of a mitogen-activated protein kinase pathway in N gene-mediated resistance in tobacco. *The Plant Journal,* 33**,** 719-731.

JONES, D. A. & TAKEMOTO, D. 2004. Plant innate immunity - direct and indirect recognition of general and specific pathogen-associated molecules. *Current Opinion in Immunology,* 16**,** 48-62.

JONES, J. D. G. & DANGL, J. L. 2006. The plant immune system. *Nature,* 444**,** 323-329.

JOUANNIC, S., CHAMPION, A., SEGUI-SIMARRO, J.-M., SALIMOVA, E., PICAUD, A., TREGEAR, J., TESTILLANO, P., RISUEÑO, M.-C., SIMANIS, V., KREIS, M. & HENRY, Y. 2001. The protein kinases *At*MAP3Kε1 and *Bn*MAP3Kε1 are functional homologues of *S. pombe* cdc7p and may be involved in cell division. *The Plant Journal,* 26**,** 637-649.

JUDELSON, H. S., TYLER, B. M. & MICHELMORE, R. W. 1991. Transformation of the oomycete pathogen, Phytophthora infestans. *Mol. Plant-Microbe Interact,* 4**,** 602-607.

JUDELSON, H. S. & BLANCO, F. A. 2005. The spores of *Phytophthora*: Weapons of the plant destroyer. *Nature Reviews Microbiology,* 3**,** 47-58.

KALE, S. D., GU, B., CAPELLUTO, D. G. S., DOU, D., FELDMAN, E., RUMORE, A., ARREDONDO, F. D., HANLON, R., FUDAL, I., ROUXEL, T., LAWRENCE, C. B., SHAN, W. & TYLER, B. M. 2010. External Lipid PI3P Mediates Entry of Eukaryotic Pathogen Effectors into Plant and Animal Host Cells. *Cell,* 142**,** 284-295.

KAMOUN, S., YOUNG, M., GLASCOCK, C. B. & TYLER, B. M. 1993. Extracellular protein elicitors from *Phytophthora*: host-specificity and induction of resistance to bacterial and fungal phytopathogens. *Molecular Plant Microbe Interactions,* 6**,** 15-15.

KAMOUN, S., YOUNG, M., FORSTER, H., COFFEY, M. D. & TYLER, B. M. 1994. Potential Role of Elicitins in the Interaction between *Phytophthora* Species and Tobacco. *Appl. Environ. Microbiol.,* 60**,** 1593-1598.

KAMOUN, S., VAN WEST, P., DE JONG, A. J., DE GROOT, K. E., VLEESHOUWERS, V. G. A. A. & GOVERS, F. 1997. A Gene Encoding a Protein Elicitor of *Phytophthora infestans* Is Down-Regulated During Infection of Potato. *Molecular Plant-Microbe Interactions,* 10**,** 13-20.

KAMOUN, S., VAN WEST, P., VLEESHOUWERS, V., DE GROOT, K. & GOVERS, F. 1998. Resistance of *Nicotiana benthamiana* to *Phytophthora infestans* is mediated by the recognition of the elicitor protein INF1. *The Plant Cell Online,* 10**,** 1413.

KAMOUN, S., HAMADA, W. & HUITEMA, E. 2003. Agrosuppression: A bioassay for the hypersensitive response suited to high-throughput screening. *Molecular Plant-Microbe Interactions,* 16**,** 7-13.

KAMOUN, S. 2006. A catalogue of the effector secretome of plant pathogenic oomycetes. *Annu. Rev. Phytopathol.,* 44**,** 41-60.

KAMOUN, S. 2007. Groovy times: filamentous pathogen effectors revealed. *Current Opinion in Plant Biology,* 10**,** 358-365.

KAMOUN, S. B., SEGRETIN, M. E. & SCHORNACK, S. 2013. *LATE BLIGHT RESISTANCE GENES.* WO patent application C07K 14/415.

KANNEGANTI, T., HUITEMA, E. & KAMOUN, S. 2007. In planta expression of oomycete and fungal genes. *METHODS IN MOLECULAR BIOLOGY-CLIFTON THEN TOTOWA-,* 354**,** 35.

KANNEGANTI, T.-D., HUITEMA, E., CAKIR, C. & KAMOUN, S. 2006. Synergistic Interactions of the Plant Cell Death Pathways Induced by *Phytophthora infestans* Nep1-Like Protein *Pi*NPP1.1 and INF1 Elicitin. *Molecular Plant-Microbe Interactions,* 19**,** 854-863.

KANZAKI, H., SAITOH, H., ITO, A., FUJISAWA, S., KAMOUN, S., KATOU, S., YOSHIOKA, H. & TERAUCHI, R. 2003. Cytosolic HSP90 and HSP70 are essential components of INF1-mediated hypersensitive response and non-host resistance to *Pseudomonas cichorii* in *Nicotiana benthamiana*. *Molecular Plant Pathology,* 4**,** 383-391.

KANZAKI, H., SAITOH, H., TAKAHASHI, Y., BERBERICH, T., ITO, A., KAMOUN, S. & TERAUCHI, R. 2008. *Nb*LRK1, a lectin-like receptor kinase protein of *Nicotiana benthamiana,* interacts with *Phytophthora infestans* INF1 elicitin and mediates INF1-induced cell death. *Planta,* 228**,** 977-987.

KAPILA, J., DE RYCKE, R., VAN MONTAGU, M. & ANGENON, G. 1997. An *Agrobacterium*-mediated transient gene expression system for intact leaves. *Plant science,* 122**,** 101-108.

KARIMI, M., INZÉ, D. & DEPICKER, A. 2002. GATEWAY™ vectors for *Agrobacterium*-mediated plant transformation. *Trends in plant science,* 7**,** 193-195.

KASCHANI, F., SHABAB, M., BOZKURT, T., SHINDO, T., SCHORNACK, S., GU, C., ILYAS, M., WIN, J., KAMOUN, S. & VAN DER HOORN, R. A. 2010. An effector-targeted protease contributes to defense against *Phytophthora infestans* and is under diversifying selection in natural hosts. *Plant Physiology,* 154**,** 1794-1804.

KELLER, H., BLEIN, J.-P., BONNET, P. & RICCI, P. 1996. Physiological and molecular characteristics of elicitin-induced systemic acquired resistance in tobacco. *Plant Physiology,* 110**,** 365-376.

KHATIB, M., LAFITTE, C., ESQUERRÉ-TUGAYÉ, M.-T., BOTTIN, A. & RICKAUER, M. 2004. The CBEL elicitor of *Phytophthora parasitica* var. *nicotianae* activates defence in *Arabidopsis thaliana* via three different signalling pathways. *New Phytologist,* 162**,** 501-510.

KIM, T.-W., GUAN, S., SUN, Y., DENG, Z., TANG, W., SHANG, J.-X., SUN, Y., BURLINGAME, A. L. & WANG, Z.-Y. 2009. Brassinosteroid signal transduction from cell-surface receptor kinases to nuclear transcription factors. *Nature Cell Biology,* 11**,** 1254-1260.

KIRSCH, C., LOGEMANN, E., LIPPOK, B., SCHMELZER, E. & HAHLBROCK, K. 2001. A highly specific pathogen-responsive promoter element from the immediate-early activated CMPG1 gene in *Petroselinum crispum*. *The Plant Journal,* 26**,** 217-227.

KJEMTRUP, S., NIMCHUK, Z. & DANGL, J. 2000. Effector proteins of phytopathogenic bacteria: bifunctional signals in virulence and host recognition. *Current opinion in microbiology,* 3**,** 73-78.

KLEIN, D., SCHMEING, T., MOORE, P. & STEITZ, T. 2001. The kink-turn: a new RNA secondary structure motif. *The EMBO journal,* 20**,** 4214-4221.

KONCZ, C. & SCHELL, J. 1986. The promoter of TL-DNA gene 5 controls the tissue-specific expression of chimaeric genes carried by a novel type of *Agrobacterium* binary vector. *Molecular and General Genetics MGG,* 204**,** 383-396.

KONG, Q., QU, N., GAO, M., ZHANG, Z., DING, X., YANG, F., LI, Y., DONG, O. X., CHEN, S. & LI, X. 2012. The MEKK1-MKK1/MKK2-MPK4 kinase cascade negatively regulates immunity mediated by a mitogen-activated protein kinase kinase kinase in Arabidopsis. *The Plant Cell Online,* 24**,** 2225-2236.

KRISSINEL, E. & HENRICK, K. 2007. Inference of macromolecular assemblies from crystalline state. *Journal of molecular biology,* 372**,** 774-797.

KROJ, T., RUDD, J. J., NÜRNBERGER, T., GÄBLER, Y., LEE, J. & SCHEEL, D. 2003. Mitogen-activated Protein Kinases Play an Essential Role in Oxidative Burst-independent Expression of Pathogenesis-related Genes in Parsley. *Journal of Biological Chemistry,* 278**,** 2256-2264.

KVITKO, B. H., PARK, D. H., VELÁSQUEZ, A. C., WEI, C.-F., RUSSELL, A. B., MARTIN, G. B., SCHNEIDER, D. J. & COLLMER, A. 2009. Deletions in the Repertoire of *Pseudomonas syringae* pv. *tomato* DC3000 Type III Secretion Effector Genes Reveal Functional Overlap among Effectors. *PLoS Pathog,* 5**,** e1000388.

KYRIAKIS, J. M. 1999. Signaling by the germinal center kinase family of protein kinases. *Journal of Biological Chemistry,* 274**,** 5259-5262.

LAEMMLI, U. K. 1970. Cleavage of structural proteins during the assembly of the head of bacteriophage T4. *nature,* 227**,** 680-685.

LAMOUR, K., WIN, J. & KAMOUN, S. 2007. Oomycete genomics: new insights and future directions. *FEMS microbiology letters,* 274**,** 1-8.

LANGER, G., COHEN, S. X., LAMZIN, V. S. & PERRAKIS, A. 2008. Automated macromolecular model building for X-ray crystallography using ARP/wARP version 7. *Nature protocols,* 3**,** 1171-1179.

LASCOMBE, M.-B., RETAILLEAU, P., PONCHET, M., BLEIN, J.-P. & PRANGE, T. 2007. Structure of sylvaticin, a new-elicitin-like protein from *Pythium sylvaticum*. *Acta Crystallographica Section D: Biological Crystallography,* 63**,** 1102-1108.

LASKOWSKI JR, M. & KATO, I. 1980. Protein inhibitors of proteinases. *Annual review of biochemistry,* 49**,** 593-626.

LATIJNHOUWERS, M., DE WIT, P. & GOVERS, F. 2003. Oomycetes and fungi: similar weaponry to attack plants. *Trends in Microbiology,* 11**,** 462-469.

LEE, C. C., WOOD, M. D., NG, K., ANDERSEN, C. B., LIU, Y., LUGINBÜHL, P., SPRAGGON, G. & KATAGIRI, F. 2004. Crystal Structure of the Type III Effector AvrB from *Pseudomonas syringae*. *Structure,* 12**,** 487-494.

LEE, A. H.-Y., PETRE, B. & JOLY, D. L. 2013. Effector wisdom. *New Phytologist,* 197**,** 375-377.

LEONELLI, L., PELTON, J., SCHOEFFLER, A., DAHLBECK, D., BERGER, J., WEMMER, D. E. & STASKAWICZ, B. 2011. Structural elucidation and functional characterization of the *Hyaloperonospora arabidopsidis* effector protein ATR13. *PLoS pathogens,* 7**,** e1002428.

LESLIE, A. & POWELL, H. 2007. Evolving Methods for Macromolecular Crystallography, edited by RJ Read & JL Sussman. *Dordrecht: Springer. doi,* 10**,** 978-1.

LETUNIC, I., DOERKS, T. & BORK, P. 2012. SMART 7: recent updates to the protein domain annotation resource. *Nucleic acids research,* 40**,** D302-D305.

LINDBO, J. A. 2007. TRBO: a high-efficiency tobacco mosaic virus RNA-based overexpression vector. *Plant Physiology,* 145**,** 1232-1240.

LINDEBERG, M., MYERS, C., COLLMER, A. & SCHNEIDER, D. 2008. Roadmap to new virulence determinants in *Pseudomonas syringae*: Insights from comparative genomics and genome organization. *Molecular Plant-Microbe Interactions,* 21**,** 685-700.

LINDEBERG, M., CUNNAC, S. & COLLMER, A. 2012. *Pseudomonas syringae* type III effector repertoires: last words in endless arguments. *Trends in microbiology,* 20**,** 199-208.

LIU, Y., SCHIFF, M., MARATHE, R. & DINESH-KUMAR, S. 2002. Tobacco Rar1, EDS1 and NPR1/NIM1 like genes are required for N-mediated resistance to tobacco mosaic virus. *The Plant Journal,* 30**,** 415-429.

LIU, Y., SCHIFF, M. & DINESH-KUMAR, S. 2004. Involvement of MEK1 MAPKK, NTF6 MAPK, WRKY/MYB transcription factors, COI1 and CTR1 in N-mediated resistance to tobacco mosaic virus. *The Plant Journal,* 38**,** 800-809.

LIU, Y., REN, D., PIKE, S., PALLARDY, S., GASSMANN, W. & ZHANG, S. 2007. Chloroplast-generated reactive oxygen species are involved in hypersensitive response-like cell death mediated by a mitogen activated protein kinase cascade. *The Plant Journal,* 51**,** 941-954.

LU, R., MALCUIT, I., MOFFETT, P., RUIZ, M. T., PEART, J., WU, A.-J., RATHJEN, J. P., BENDAHMANE, A., DAY, L. & BAULCOMBE, D. C. 2003a. High throughput virus-induced gene silencing implicates heat shock protein 90 in plant disease resistance. *The EMBO journal,* 22**,** 5690-5699.

LU, R., MARTIN-HERNANDEZ, A. M., PEART, J. R., MALCUIT, I. & BAULCOMBE, D. C. 2003b. Virus-induced gene silencing in plants. *Methods,* 30**,** 296-303.

LU, Y. J., SCHORNACK, S., SPALLEK, T., GELDNER, N., CHORY, J., SCHELLMANN, S., SCHUMACHER, K., KAMOUN, S. & ROBATZEK, S. 2012. Patterns of plant subcellular responses to successful oomycete infections reveal differences in host cell reprogramming and endocytic trafficking. *Cellular microbiology,* 14**,** 682-697.

MAO, G., MENG, X., LIU, Y., ZHENG, Z., CHEN, Z. & ZHANG, S. 2011. Phosphorylation of a WRKY transcription factor by two pathogen-responsive MAPKs drives phytoalexin biosynthesis in *Arabidopsis*. *The Plant Cell Online,* 23**,** 1639-1653.

MARCHLER-BAUER, A., LU, S., ANDERSON, J. B., CHITSAZ, F., DERBYSHIRE, M. K., DEWEESE-SCOTT, C., FONG, J. H., GEER, L. Y., GEER, R. C., GONZALES, N. R., GWADZ, M., HURWITZ, D. I., JACKSON, J. D., KE, Z., LANCZYCKI, C. J., LU, F., MARCHLER, G. H., MULLOKANDOV, M., OMELCHENKO, M. V., ROBERTSON, C. L., SONG, J. S., THANKI, N., YAMASHITA, R. A., ZHANG, D., ZHANG, N., ZHENG, C. & BRYANT, S. H. 2011. CDD: a Conserved Domain Database for the functional annotation of proteins. *Nucleic acids research,* 39**,** D225-D229.

MARGULIS, L. & SCHWARTZ, K. 2000. *Five Kingdoms: An Illustrated Guide to the Phyla of Life on Earth,* New York, W.H. Freeman & Co.

MARTIN, G. B., BOGDANOVE, A. J. & SESSA, G. 2003. UNDERSTANDING THE FUNCTIONS OF PLANT DISEASE RESISTANCE PROTEINS. *Annual review of plant biology,* 54**,** 23-61.

MATEOS, F. V., RICKAUER, M. & ESQUERRÉ-TUGAYÉ, M.-T. 1997. Cloning and characterization of a cDNA encoding an elicitor of *Phytophthora parasitica* var. *nicotianae* that shows cellulose-binding and lectin-like activities. *Molecular Plant-Microbe Interactions,* 10**,** 1045-1053.

MCCOY, A. J., GROSSE-KUNSTLEVE, R. W., ADAMS, P. D., WINN, M. D., STORONI, L. C. & READ, R. J. 2007. Phaser crystallographic software. *Journal of applied crystallography,* 40**,** 658-674.

MCDOWELL, J. & DANGL, J. 2000. Signal transduction in the plant immune response. *Trends in Biochemical Sciences,* 25**,** 79-82.

MCHALE, L., TAN, X., KOEHL, P. & MICHELMORE, R. 2006. Plant NBS-LRR proteins: adaptable guards. *Genome Biology,* 7**,** 212.

MEHDY, M. C. 1994. Active oxygen species in plant defense against pathogens. *Plant Physiology,* 105**,** 467.

MELECH-BONFIL, S. & SESSA, G. 2010. Tomato MAPKKKε is a positive regulator of cell-death signaling networks associated with plant immunity. *The Plant Journal,* 64**,** 379-391.

MEYER, D. E. & CHILKOTI, A. 1999. Purification of recombinant proteins by fusion with thermally-responsive polypeptides. *Nature biotechnology,* 17**,** 1112-1115.

MIKES, V., MILAT, M.-L., PONCHET, M., PANABIÈRES, F., RICCI, P. & BLEIN, J.-P. 1998. Elicitins, Proteinaceous Elicitors of Plant Defense, Are a New Class of Sterol Carrier Proteins. *Biochemical and Biophysical Research Communications,* 245**,** 133-139.

MONDRAGÓN-PALOMINO, M., MEYERS, B. C., MICHELMORE, R. W. & GAUT, B. S. 2002. Patterns of Positive Selection in the Complete NBS-LRR Gene Family of *Arabidopsis thaliana*. *Genome Research,* 12**,** 1305-1315.

MORA-GARCÍA, S., VERT, G., YIN, Y., CAÑO-DELGADO, A., CHEONG, H. & CHORY, J. 2004. Nuclear protein phosphatases with Kelch-repeat domains modulate the response to brassinosteroids in *Arabidopsis*. *Genes & development,* 18**,** 448-460.

MORGAN, W. & KAMOUN, S. 2007. RXLR effectors of plant pathogenic oomycetes. *Curr. Opin. Microbiol.,* 10**,** 332-338.

MORIYOSHI, K. 2009. pBT, a novel vector for tetracycline-regulated yeast three-hybrid assay. *Nucleic acids research,* 37**,** e11-e11.

MUDGIL, Y., SHIU, S.-H., STONE, S. L., SALT, J. N. & GORING, D. R. 2004. A large complement of the predicted *Arabidopsis* ARM repeat proteins are members of the U-box E3 ubiquitin ligase family. *Plant Physiology,* 134**,** 59-66.

MUKHTAR, M. S., CARVUNIS, A.-R., DREZE, M., EPPLE, P., STEINBRENNER, J., MOORE, J., TASAN, M., GALLI, M., HAO, T. & NISHIMURA, M. T. 2011. Independently evolved virulence effectors converge onto hubs in a plant immune system network. *Science Signaling,* 333**,** 596.

MULLIS, K. B. 1990. The unusual origin of the polymerase chain reaction. *Scientific American,* 262**,** 56-61.

MURSHUDOV, G. N., VAGIN, A. A. & DODSON, E. J. 1997. Refinement of macromolecular structures by the maximum-likelihood method. *Acta Crystallographica Section D: Biological Crystallography,* 53**,** 240-255.

NAVAZA, J. 1994. Collaborative Computational Project, Number 4. The CCP4 Suite: Programs for protein crystallogaphy. *Acta Crystallogr. A,* 50**,** 760-763.

NICAISE, V., ROUX, M. & ZIPFEL, C. 2009. Recent advances in PAMP-triggered immunity against bacteria: pattern recognition receptors watch over and raise the alarm. *Plant Physiology,* 150**,** 1638-1647.

NICASTRO, G., ORSOMANDO, G., FERRARI, E., MANCONI, L., DESARIO, F., AMICI, A., NASO, A., CARPANETO, A., PERTINHEZ, T. A., RUGGIERI, S. & SPISNI, A. 2009. Solution structure of the phytotoxic protein PcF: The first characterized member of the *Phytophthora* PcF toxin family. *Protein science,* 18**,** 1786-1791.

NIELSEN, H., ENGELBRECHT, J., BRUNAK, S. & VON HEIJNE, G. 1997. Identification of prokaryotic and eukaryotic signal peptides and prediction of their cleavage sites. *Protein engineering,* 10**,** 1-6.

NÜRNBERGER, T., NENNSTIEL, D., JABS, T., SACKS, W. R., HAHLBROCK, K. & SCHEEL, D. 1994. High affinity binding of a fungal oligopeptide elicitor to parsley plasma membranes triggers multiple defense responses. *Cell,* 78**,** 449-460.

NÜRNBERGER, T. & BRUNNER, F. 2002. Innate immunity in plants and animals: emerging parallels between the recognition of general elicitors and pathogen-associated molecular patterns. *Current Opinion in Plant Biology,* 5**,** 318-324.

NÜRNBERGER, T., BRUNNER, F., KEMMERLING, B. & PIATER, L. 2004. Innate immunity in plants and animals: striking similarities and obvious differences. *Immunological Reviews,* 198**,** 249-266.

OH, S.-K., YOUNG, C., LEE, M., OLIVA, R., BOZKURT, T. O., CANO, L. M., WIN, J., BOS, J. I. B., LIU, H.-Y., VAN DAMME, M., MORGAN, W., CHOI, D., VAN DER VOSSEN, E. A. G., VLEESHOUWERS, V. G. A. A. & KAMOUN, S. 2009. *In Planta* Expression Screens of *Phytophthora infestans* RXLR Effectors Reveal Diverse Phenotypes, Including Activation of the *Solanum bulbocastanum* Disease Resistance Protein Rpi-blb2. *Plant Cell,* 21**,** 2928-2947.

OH, C.-S., PEDLEY, K. F. & MARTIN, G. B. 2010. Tomato 14-3-3 protein 7 positively regulates immunity-associated programmed cell death by enhancing protein abundance and signaling ability of MAPKKK α. *The Plant Cell Online,* 22**,** 260-272.

OH, C.-S. & MARTIN, G. B. 2011. Tomato 14-3-3 protein TFT7 interacts with a MAP kinase kinase to regulate immunity-associated programmed cell death mediated by diverse disease resistance proteins. *Journal of Biological Chemistry,* 286**,** 14129-14136.

OLIVA, R., WIN, J., RAFFAELE, S., BOUTEMY, L., BOZKURT, T. O., CHAPARRO-GARCIA, A., SEGRETIN, M. E., STAM, R., SCHORNACK, S. & CANO, L. M. 2010. Recent developments in effector biology of filamentous plant pathogens. *Cellular microbiology,* 12**,** 705-715.

OSMAN, H., MIKES, V., MILAT, M. L., PONCHET, M., MARION, D., PRANGÉ, T., MAUME, B. F., VAUTHRIN, S. & BLEIN, J. P. 2001a. Fatty acids bind to the fungal elicitor cryptogein and compete with sterols. *Febs Letters,* 489**,** 55-58.

OSMAN, H., VAUTHRIN, S., MIKES, V., MILAT, M.-L., PANABIÈRES, F., MARAIS, A., BRUNIE, S., MAUME, B., PONCHET, M. & BLEIN, J.-P. 2001b. Mediation of elicitin activity on tobacco is assumed by elicitin-sterol complexes. *Molecular biology of the cell,* 12**,** 2825-2834.

OTTMANN, C., LUBERACKI, B., KÜFNER, I., KOCH, W., BRUNNER, F., WEYAND, M., MATTINEN, L., PIRHONEN, M., ANDERLUH, G. & SEITZ, H. U. 2009. A common toxin fold mediates microbial attack and plant defense. *Proceedings of the National Academy of Sciences,* 106**,** 10359-10364.

PANAVAS, T., SANDERS, C. & BUTT, T. R. 2009. SUMO fusion technology for enhanced protein production in prokaryotic and eukaryotic expression systems. *In:* ULRICH, H. D. (ed.) *SUMO Protocols.* Humana Press.

PANDEY, S. P. & SOMSSICH, I. E. 2009. The role of WRKY transcription factors in plant immunity. *Plant Physiology,* 150**,** 1648-1655.

PANSTRUGA, R. & DODDS, P. N. 2009. Terrific protein traffic: the mystery of effector protein delivery by filamentous plant pathogens. *Science (New York, NY),* 324**,** 748.

PANTALEO, V., SZITTYA, G. & BURGYÁN, J. 2007. Molecular Bases of Viral RNA Targeting by Viral Small Interfering RNA-Programmed RISC. *Journal of Virology,* 81**,** 3797-3806.

PAPADOPOULOS, J. S. & AGARWALA, R. 2007. COBALT: constraint-based alignment tool for multiple protein sequences. *Bioinformatics,* 23**,** 1073-1079.

PAPP, E. & CSERMELY, P. 2006. Chemical chaperones: mechanisms of action and potential use. *In:* STARKE, B. K. & GAESTEL, M. (eds.) *Molecular Chaperones in Health and Disease.* Springer Berlin Heidelberg.

PASSARDI, F., PENEL, C. & DUNAND, C. 2004. Performing the paradoxical: how plant peroxidases modify the cell wall. *Trends in plant science,* 9**,** 534-540.

PEART, J. R., LU, R., SADANANDOM, A., MALCUIT, I., MOFFETT, P., BRICE, D. C., SCHAUSER, L., JAGGARD, D. A. W., XIAO, S., COLEMAN, M. J., DOW, M., JONES, J. D. G., SHIRASU, K. & BAULCOMBE, D. C. 2002. Ubiquitin ligase-associated protein SGT1 is required for host and nonhost disease resistance in plants. *Proceedings of the National Academy of Sciences of the United States of America,* 99**,** 10865-10869.

PEMBERTON, C. L. & SALMOND, G. P. C. 2004. The Nep1-like proteins—a growing family of microbial elicitors of plant necrosis. *Molecular Plant Pathology,* 5**,** 353-359.

PIECHOTTA, K., GARBARINI, N., ENGLAND, R. & DELPIRE, E. 2003. Characterization of the Interaction of the Stress Kinase SPAK with the Na+-K+-2Cl–Cotransporter in the Nervous System EVIDENCE FOR A SCAFFOLDING ROLE OF THE KINASE. *Journal of Biological Chemistry,* 278**,** 52848-52856.

PITZSCHKE, A., SCHIKORA, A. & HIRT, H. 2009. MAPK cascade signalling networks in plant defence. *Current Opinion in Plant Biology,* 12**,** 421.

POTATO GENOME SEQUENCING CONSORTIUM, XU, X., PAN, S., CHENG, S., ZHANG, B., MU, D., NI, P., ZHANG, G., YANG, S., LI, R., WANG, J., ORJEDA, G., GUZMAN, F., TORRES, M., LOZANO, R., PONCE, O., MARTINEZ, D., DE LA CRUZ, G., CHAKRABARTI, S. K., PATIL, V. U., SKRYABIN, K. G., KUZNETSOV, B. B., RAVIN, N. V., KOLGANOVA, T. V., BELETSKY, A. V., MARDANOV, A. V., DI GENOVA, A., BOLSER, D. M., MARTIN, D. M., LI, G., YANG, Y., KUANG, H., HU, Q., XIONG, X., BISHOP, G. J., SAGREDO, B., MEJÍA, N., ZAGORSKI, W., GROMADKA, R., GAWOR, J., SZCZESNY, P., HUANG, S., ZHANG, Z., LIANG, C., HE, J., LI, Y., HE, Y., XU, J., ZHANG, Y., XIE, B., DU, Y., QU, D., BONIERBALE, M., GHISLAIN, M., HERRERA, M. R., GIULIANO, G., PIETRELLA, M., PERROTTA, G., FACELLA, P., O'BRIEN, K., FEINGOLD, S. E., BARREIRO, L. E., MASSA, G. A., DIAMBRA, L., WHITTY, B. R., VAILLANCOURT, B., LIN, H., MASSA, A. N., GEOFFROY, M., LUNDBACK, S., DELLAPENNA, D., BUELL, C. R., SHARMA, S. K., MARSHALL, D. F., WAUGH, R., BRYAN, G. J., DESTEFANIS, M., NAGY, I., MILBOURNE, D., THOMSON, S. J., FIERS, M., JACOBS, J. M., NIELSEN, K. L., SØNDERKÆR, M., IOVENE, M., TORRES, G. A., JIANG, J., VEILLEUX, R. E., BACHEM, C. W., DE BOER, J., BORM, T., KLOOSTERMAN, B., VAN ECK, H., DATEMA, E., HEKKERT, B., GOVERSE, A., VAN HAM, R. C. & VISSER, R. G. 2011. Genome sequence and analysis of the tuber crop potato. *Nature,* 475**,** 189-195.

PRINCE, C. & JIA, Z. 2012. Measurement of detergent concentration using 2,6-dimethylphenol in membrane-protein crystallization. *Acta Crystallographica Section D,* 68**,** 1694-1696.

PRINGA, E., MARTINEZ-NOEL, G., MÜLLER, U. & HARBERS, K. 2001. Interaction of the ring finger-related U-box motif of a nuclear dot protein with ubiquitin-conjugating enzymes. *Journal of Biological Chemistry,* 276**,** 19617-19623.

QI, M. & ELION, E. A. 2005. MAP kinase pathways. *Journal of Cell Science,* 118**,** 3569-3572.

QUTOB, D., KAMOUN, S. & GIJZEN, M. 2002. Expression of a *Phytophthora sojae* necrosis-inducing protein occurs during transition from biotrophy to necrotrophy. *Plant Journal,* 32**,** 361-374.

RAFFAELE, S., FARRER, R. A., CANO, L. M., STUDHOLME, D. J., MACLEAN, D., THINES, M., JIANG, R. H. Y., ZODY, M. C., KUNJETI, S. G., DONOFRIO, N. M., MEYERS, B. C., NUSBAUM, C. & KAMOUN, S. 2010a. Genome Evolution Following Host Jumps in the Irish Potato Famine Pathogen Lineage. *Science,* 330**,** 1540-1543.

RAFFAELE, S., WIN, J., CANO, L. & KAMOUN, S. 2010b. Analyses of genome architecture and gene expression reveal novel candidate virulence factors in the secretome of Phytophthora infestans. *BMC genomics,* 11**,** 637.

RAFIQI, M., ELLIS, J. G., LUDOWICI, V. A., HARDHAM, A. R. & DODDS, P. N. 2012. Challenges and progress towards understanding the role of effectors in plant–fungal interactions. *Current Opinion in Plant Biology,* 15**,** 477-482.

RATCLIFF, F. G., MACFARLANE, S. A. & BAULCOMBE, D. C. 1999. Gene silencing without DNA: RNA-mediated cross-protection between viruses. *The Plant Cell Online,* 11**,** 1207-1215.

RATCLIFF, F., MARTIN-HERNANDEZ, A. M. & BAULCOMBE, D. C. 2001. Technical advance: tobacco rattle virus as a vector for analysis of gene function by silencing. *The Plant Journal,* 25**,** 237-245.

RATHJEN, J. P., CHANG, J. H., STASKAWICZ, B. J. & MICHELMORE, R. W. 1999. Constitutively active Pto induces a Prf-dependent hypersensitive response in the absence of avrPto. *The EMBO journal,* 18**,** 3232-3240.

READER, J. 2009. Potato: A History of the Propitious Esculent. Yale University Press.

REISS, K., KIRCHNER, E., GIJZEN, M., ZOCHER, G., LÖFFELHARDT, B., NÜRNBERGER, T., STEHLE, T. & BRUNNER, F. 2011. Structural and Phylogenetic Analyses of the GP42 Transglutaminase from *Phytophthora sojae* Reveal an Evolutionary Relationship between Oomycetes and Marine Vibrio Bacteria. *Journal of Biological Chemistry,* 286**,** 42585-42593.

RIBOLDI-TUNNICLIFFE, A. & HILGENFELD, R. 1999. Cryocrystallography with oil-an old idea revived. *Journal of applied crystallography,* 32**,** 1003-1005.

RIDOUT, C., SKAMNIOTI, P., PORRITT, O., SACRISTAN, S., JONES, J. & BROWN, J. 2006. Multiple avirulence paralogues in cereal powdery mildew fungi may contribute to parasite fitness and defeat of plant resistance. *The Plant Cell Online,* 18**,** 2402.

RIZZO, D., GARBELOTTO, M. & HANSEN, E. 2005. *Phytophthora ramorum*: integrative research and management of an emerging pathogen in California and Oregon forests. *Annu. Rev. Phytopathol.,* 43**,** 309-335.

ROBERTSON, D. 2004. VIGS vectors for gene silencing: many targets, many tools. *Annu. Rev. Plant Biol.,* 55**,** 495-519.

ROCHE, D. B., BUENAVISTA, M. T., TETCHNER, S. J. & MCGUFFIN, L. J. 2011. The IntFOLD server: an integrated web resource for protein fold recognition, 3D model quality assessment, intrinsic disorder prediction, domain prediction and ligand binding site prediction. *Nucleic acids research,* 39**,** W171-W176.

RODEWALD, J. & TROGNITZ, B. 2013. *Solanum* resistance genes against *Phytophthora infestans* and their corresponding avirulence genes. *Molecular Plant Pathology*.

RODRIGUES, M. L., ARCHER, M., MARTEL, P., MIRANDA, S., THOMAZ, M., ENGUITA, F. J., BAPTISTA, R. P., PINHO E MELO, E., SOUSA, N. & CRAVADOR, A. 2006. Crystal structures of the free and sterol-bound forms of β-cinnamomin. *Biochimica et Biophysica Acta (BBA)-Proteins and Proteomics,* 1764**,** 110-121.

ROSE, J., HAM, K., DARVILL, A. & ALBERSHEIM, P. 2002. Molecular cloning and characterization of glucanase inhibitor proteins: coevolution of a counterdefense mechanism by plant pathogens. *The Plant Cell Online,* 14**,** 1329.

ROSSMANN, M. 1990. The molecular replacement method. *Acta Crystallographica Section A,* 46**,** 73-82.

ROTENBERG, D., THOMPSON, T. S., GERMAN, T. L. & WILLIS, D. K. 2006. Methods for effective real-time RT-PCR analysis of virus-induced gene silencing. *Journal of Virological Methods,* 138**,** 49-59.

RUSTÉRUCCI, C., STALLAERT, V., MILAT, M.-L., PUGIN, A., RICCI, P. & BLEIN, J.-P. 1996. Relationship between active oxygen species, lipid peroxidation, necrosis, and phytoalexin production induced by elicitins in *Nicotiana*. *Plant Physiology,* 111**,** 885-891.

SAINSBURY, F. & LOMONOSSOFF, G. P. 2008. Extremely High-Level and Rapid Transient Protein Production in Plants without the Use of Viral Replication. *Plant Physiology,* 148**,** 1212-1218.

SAINSBURY, F., THUENEMANN, E. C. & LOMONOSSOFF, G. P. 2009. pEAQ: versatile expression vectors for easy and quick transient expression of heterologous proteins in plants. *Plant Biotechnology Journal,* 7**,** 682-693.

SAMUEL, M. A., MUDGIL, Y., SALT, J. N., DELMAS, F., RAMACHANDRAN, S., CHILELLI, A. & GORING, D. R. 2008. Interactions between the S-domain receptor kinases and *At*PUB-ARM E3 ubiquitin ligases suggest a conserved signaling pathway in *Arabidopsis*. *Plant Physiology,* 147**,** 2084-2095.

SAUNDERS, D. G., BREEN, S., WIN, J., SCHORNACK, S., HEIN, I., BOZKURT, T. O., CHAMPOURET, N., VLEESHOUWERS, V. G., BIRCH, P. R. & GILROY, E. M. 2012. Host Protein BSL1 associates with *Phytophthora infestans* RXLR effector AVR2 and the *Solanum demissum* immune receptor R2 to mediate disease resistance. *The Plant Cell Online,* 24**,** 3420-3434.

SCHEEFF, E. D. & BOURNE, P. E. 2005. Structural Evolution of the Protein Kinase–Like Superfamily. *PLoS computational biology,* 1**,** e49.

SCHILMILLER, A. L. & HOWE, G. A. 2005. Systemic signaling in the wound response. *Current Opinion in Plant Biology,* 8**,** 369-377.

SCHLEGEL, M. 2003. Phylogeny of eukaryotes recovered with molecular data: highlights and pitfalls. *European Journal of Protistology,* 39**,** 113-122.

SCHORNACK, S., HUITEMA, E., CANO, L. M., BOZKURT, T. O., OLIVA, R., DAMME, M. V., SCHWIZER, S., RAFFAELE, S., CHAPARRO-GARCIA, A., FARRER, R., SEGRETIN, M. E., BOS, J., HAAS, B. J., ZODY, M. C., NUSBAUM, C., WIN, J., THINES, M. & KAMOUN, S. 2009. Ten things to know about oomycete effectors. *Molecular Plant Pathology,* 10**,** 795-803.

SCHORNACK, S., VAN DAMME, M., BOZKURT, T. O., CANO, L. M., SMOKER, M., THINES, M., GAULIN, E., KAMOUN, S. & HUITEMA, E. 2010. Ancient class of translocated oomycete effectors targets the host nucleus. *Proceedings of the National Academy of Sciences,* 107**,** 17421-17426.

SCHULTZ, J., MILPETZ, F., BORK, P. & PONTING, C. P. 1998. SMART, a simple modular architecture research tool: Identification of signaling domains. *Proceedings of the National Academy of Sciences,* 95**,** 5857-5864.

SCHWARZ, D. S., DING, H., KENNINGTON, L., MOORE, J. T., SCHELTER, J., BURCHARD, J., LINSLEY, P. S., ARONIN, N., XU, Z. & ZAMORE, P. D. 2006. Designing siRNA That Distinguish between Genes That Differ by a Single Nucleotide. *PLoS Genet,* 2**,** e140.

SCOFIELD, S. R., TOBIAS, C. M., RATHJEN, J. P., CHANG, J. H., LAVELLE, D. T., MICHELMORE, R. W. & STASKAWICZ, B. J. 1996. Molecular basis of gene-for-gene specificity in bacterial speck disease of tomato. *Science,* 274**,** 2063-2065.

SEGONZAC, C., FEIKE, D., GIMENEZ-IBANEZ, S., HANN, D. R., ZIPFEL, C. & RATHJEN, J. P. 2011. Hierarchy and Roles of Pathogen-Associated Molecular Pattern-Induced Responses in *Nicotiana benthamiana*. *Plant Physiology,* 156**,** 687-699.

SELLS, M. A. & CHERNOFF, J. 1997. Emerging from the Pak: the p21-activated protein kinase family. *Trends in cell biology,* 7**,** 162-167.

SENCHOU, V., WEIDE, R., CARRASCO, A., BOUYSSOU, H., PONT-LEZICA, R., GOVERS, F. & CANUT, H. 2004. High affinity recognition of a *Phytophthora* protein by *Arabidopsis* via an RGD motif. *Cellular and Molecular Life Sciences CMLS,* 61**,** 502-509.

SEREBRIISKII, I. G. ESTOJAK, J., BERMAN, M., & GOLEMIS, E. 2000. Approaches to detecting false positives in yeast two-hybrid systems. *Biotechniques,* 282, 328-336.

SEREBRIISKII, I. G. & KOTOVA, E. 2004. Analysis of protein-protein interactions utilizing dual bait yeast two-hybrid system. *Methods Mol Biol.,* 261, 263-296.

SHELDRICK, G. M. 2010. Experimental phasing with SHELXC/D/E: combining chain tracing with density modification. *Acta Crystallographica Section D: Biological Crystallography,* 66**,** 479-485.

SIERRA, R., RODRÍGUEZ-R, L. M., CHAVES, D., PINZÓN, A., GRAJALES, A., ROJAS, A., MUTIS, G., CÁRDENAS, M., BURBANO, D. & JIMÉNEZ, P. 2010. Discovery of *Phytophthora infestans* genes expressed in planta through mining of cDNA libraries. *PLoS ONE,* 5**,** e9847.

SOGIN, M. L. & SILBERMAN, J. D. 1998. Evolution of the protists and protistan parasites from the perspective of molecular systematics. *International Journal for Parasitology,* 28**,** 11-20.

SOHN, K. H., LEI, R., NEMRI, A. & JONES, J. D. G. 2007. The downy mildew effector proteins ATR1 and ATR13 promote disease susceptibility in *Arabidopsis thaliana*. *Plant Cell,* 19**,** 4077-4090.

SOHN, K. H., HUGHES, R. K., PIQUEREZ, S. J., JONES, J. D. G. & BANFIELD, M. J. 2012. Distinct regions of the *Pseudomonas syringae* coiled-coil effector AvrRps4 are required for activation of immunity. *Proceedings of the National Academy of Sciences,* 109**,** 16371-16376.

SOYANO, T., NISHIHAMA, R., MORIKIYO, K., ISHIKAWA, M. & MACHIDA, Y. 2003. NQK1/NtMEK1 is a MAPKK that acts in the NPK1 MAPKKK-mediated MAPK cascade and is required for plant cytokinesis. *Genes & development,* 17**,** 1055-1067.

STAVRINIDES, J., MA, W. & GUTTMAN, D. 2006. Terminal reassortment drives the quantum evolution of type III effectors in bacterial pathogens. *PLoS Pathog* 2**,** e104.

STEWART, E. J., ÅSLUND, F. & BECKWITH, J. 1998. Disulfide bond formation in the *Escherichia coli* cytoplasm: an in vivo role reversal for the thioredoxins. *The EMBO journal,* 17**,** 5543-5550.

SUAREZ-RODRIGUEZ, M. C., ADAMS-PHILLIPS, L., LIU, Y., WANG, H., SU, S.-H., JESTER, P. J., ZHANG, S., BENT, A. F. & KRYSAN, P. J. 2007. MEKK1 is required for flg22-induced MPK4 activation in *Arabidopsis* plants. *Plant Physiology,* 143**,** 661-669.

TAKEMOTO, D., HARDHAM, A. R. & JONES, D. A. 2005. Differences in cell death induction by *Phytophthora* elicitins are determined by signal components downstream of MAP kinase kinase in different species of *Nicotiana* and cultivars of *Brassica rapa* and *Raphanus sativus*. *Plant Physiology,* 138**,** 1491-1504.

TAMURA, K., PETERSON, D., PETERSON, N., STECHER, G., NEI, M. & KUMAR, S. 2011. MEGA5: molecular evolutionary genetics analysis using maximum likelihood, evolutionary distance, and maximum parsimony methods. *Molecular biology and evolution,* 28**,** 2731-2739.

TANI, S., YATZKAN, E. & JUDELSON, H. S. 2004. Multiple pathways regulate the induction of genes during zoosporogenesis in *Phytophthora infestans*. *Molecular Plant-Microbe Interactions,* 17**,** 330-337.

THOMMA, B. P., NÜRNBERGER, T. & JOOSTEN, M. H. 2011. Of PAMPs and effectors: the blurred PTI-ETI dichotomy. *The Plant Cell Online,* 23**,** 4-15.

TIAN, M., HUITEMA, E., DA CUNHA, L., TORTO-ALALIBO, T. & KAMOUN, S. 2004. A Kazal-like Extracellular Serine Protease Inhibitor from *Phytophthora infestans* Targets the Tomato Pathogenesis-related Protease P69B. *Journal of Biological Chemistry,* 279**,** 26370-26377.

TIAN, M., BENEDETTI, B. & KAMOUN, S. 2005. A Second Kazal-Like Protease Inhibitor from *Phytophthora infestans* Inhibits and Interacts with the Apoplastic Pathogenesis-Related Protease P69B of Tomato. *Plant Physiol.,* 138**,** 1785-1793.

TIAN, M., WIN, J., SONG, J., VAN DER HOORN, R., VAN DER KNAAP, E. & KAMOUN, S. 2007. A *Phytophthora infestans* Cystatin-Like Protein Targets a Novel Tomato Papain-Like Apoplastic Protease. *Plant Physiol.,* 143**,** 364-377.

TICKLE, I. J., LASKOWSKI, R. A. & MOSS, D. S. 1998. Rfree and the Rfree ratio. I. Derivation of expected values of cross-validation residuals used in macromolecular least-squares refinement. *Acta Crystallographica Section D: Biological Crystallography,* 54**,** 547-557.

TORTO, T. A., LI, S., STYER, A., HUITEMA, E., TESTA, A., GOW, N. A. R., VAN WEST, P. & KAMOUN, S. 2003. EST mining and functional expression assays identify extracellular effector proteins from the plant pathogen *Phytophthora*. *Genome Res.,* 13**,** 1675-1685.

TORTO-ALALIBO, T., TRIPATHY, S., SMITH, B., ARREDONDO, F., ZHOU, L., LI, H., CHIBUCOS, M., QUTOB, D., GIJZEN, M. & MAO, C. 2007. Expressed sequence tags from *Phytophthora sojae* reveal genes specific to development and infection. *Molecular Plant-Microbe Interactions,* 20**,** 781-793.

TURNER, R. 2005. After the famine: Plant pathology, *Phytophthora infestans*, and the late blight of potatoes, 1845-1960. *Historical Studies in the Physical and Biological Sciences,* 35**,** 341-370.

TYLER, B. 2002. Molecular basis of recognition between *Phytophthora* species and their hosts. *Annu. Rev. Phytopathol,* 40**,** 137-167.

TYLER, B. M., KALE, S. D., WANG, Q., TAO, K., CLARK, H. R., DREWS, K., ANTIGNANI, V., RUMORE, A., HAYES, T., PLETT, J. M., FUDAL, I., GU, B., CHEN, Q., AFFELDT, K. J., BERTHIER, E., FISCHER, G. J., DOU, D., SHAN, W., KELLER, N. P., MARTIN, F., ROUXEL, T. & LAWRENCE, C. B. 2013. Microbe-Independent Entry of Oomycete RxLR Effectors and Fungal RxLR-Like Effectors Into Plant and Animal Cells Is Specific and Reproducible. *Molecular Plant-Microbe Interactions,* 26**,** 611-616.

UI-TEI, K., NAITO, Y., TAKAHASHI, F., HARAGUCHI, T., OHKI-HAMAZAKI, H., JUNI, A., UEDA, R. & SAIGO, K. 2004. Guidelines for the selection of highly effective siRNA sequences for mammalian and chick RNA interference. *Nucleic acids research,* 32**,** 936-948.

VALENTINE, T., SHAW, J., BLOK, V. C., PHILLIPS, M. S., OPARKA, K. J. & LACOMME, C. 2004. Efficient Virus-Induced Gene Silencing in Roots Using a Modified Tobacco Rattle Virus Vector. *Plant Physiology,* 136**,** 3999-4009.

VAN DAMME, M., BOZKURT, T. O., CAKIR, C., SCHORNACK, S., SKLENAR, J., JONES, A. M. E. & KAMOUN, S. 2012. The Irish Potato Famine Pathogen *Phytophthora infestans* Translocates the CRN8 Kinase into Host Plant Cells. *PLoS Pathog,* 8**,** e1002875.

VAN DER BIEZEN, E. A. & JONES, J. D. G. 1998. Plant disease-resistance proteins and the gene-for-gene concept. *Trends in Biochemical Sciences,* 23**,** 454-456.

VAN DER HOORN, R. A. L., LAURENT, F., ROTH, R. & DE WIT, P. J. G. M. 2000. Agroinfiltration is a versatile tool that facilitates comparative analyses of Avr 9/Cf-9-induced and Avr 4/Cf-4-induced necrosis. *Molecular Plant-Microbe Interactions,* 13**,** 439-446.

VAN DER HOORN, R. A. L. & KAMOUN, S. 2008. From Guard to Decoy: A New Model for Perception of Plant Pathogen Effectors. *Plant Cell,* 20**,** 2009-2017.

VAN DROGEN, F., O'ROURKE, S. M., STUCKE, V. M., JAQUENOUD, M., NEIMAN, A. M. & PETER, M. 2000. Phosphorylation of the MEKK Ste11p by the PAK-like kinase Ste20p is required for MAP kinase signaling *in vivo*. *Current Biology,* 10**,** 630-639.

VAN LAREBEKE, N., ENGLER, G., HOLSTERS, M., VAN DEN ELSACKER, S., ZAENEN, I., SCHILPEROORT, R. & SCHELL, J. 1974. Large plasmid in *Agrobacterium tumefaciens* essential for crown gall-inducing ability.

VAN VALEN, L. 1973. A new evolutionary law. *Evolutionary Theory,* 1**,** 1-30.

VLEESHOUWERS, V. G. A. A., RIETMAN, H., KRENEK, P., CHAMPOURET, N., YOUNG, C., OH, S.-K., WANG, M., BOUWMEESTER, K., VOSMAN, B., VISSER, R. G. F., JACOBSEN, E., GOVERS, F., KAMOUN, S. & VAN DER VOSSEN, E. A. G. 2008. Effector Genomics Accelerates Discovery and Functional Profiling of Potato Disease Resistance and *Phytophthora infestans* Avirulence Genes. *PLoS ONE,* 3**,** e2875.

VOINNET, O. 2001. RNA silencing as a plant immune system against viruses. *TRENDS in Genetics,* 17**,** 449-459.

VOINNET, O., RIVAS, S., MESTRE, P. & BAULCOMBE, D. 2003. An enhanced transient expression system in plants based on suppression of gene silencing by the p19 protein of tomato bushy stunt virus. *The Plant Journal,* 33**,** 949-956.

VON HEIJNE, G. 1990. The signal peptide. *Journal of Membrane Biology,* 115**,** 195-201.

WANG, C.-I. A., GUNČAR, G., FORWOOD, J. K., TEH, T., CATANZARITI, A.-M., LAWRENCE, G. J., LOUGHLIN, F. E., MACKAY, J. P., SCHIRRA, H. J. & ANDERSON, P. A. 2007. Crystal structures of flax rust avirulence proteins AvrL567-A and-D reveal details of the structural basis for flax disease resistance specificity. *The Plant Cell Online,* 19**,** 2898-2912.

WANG, Y., LI, J., HOU, S., WANG, X., LI, Y., REN, D., CHEN, S., TANG, X. & ZHOU, J.-M. 2010. A *Pseudomonas syringae* ADP-Ribosyltransferase Inhibits *Arabidopsis* Mitogen-Activated Protein Kinase Kinases. *The Plant Cell Online,* 22**,** 2033-2044.

WANG, Q., HAN, C., FERREIRA, A. O., YU, X., YE, W., TRIPATHY, S., KALE, S. D., GU, B., SHENG, Y., SUI, Y., WANG, X., ZHANG, Z., CHENG, B., DONG, S., SHAN, W., ZHENG, X., DOU, D., TYLER, B. M. & WANG, Y. 2011. Transcriptional Programming and Functional Interactions within the *Phytophthora sojae* RXLR Effector Repertoire. *The Plant Cell Online,* 23**,** 2064-2086.

WATSON, J. M., FUSARO, A. F., WANG, M. & WATERHOUSE, P. M. 2005. RNA silencing platforms in plants. *Febs Letters,* 579**,** 5982-5987.

WAWRA, S., AGACAN, M., BODDEY, J. A., DAVIDSON, I., GACHON, C. M. M., ZANDA, M., GROUFFAUD, S., WHISSON, S. C., BIRCH, P. R. J., PORTER, A. J. & VAN WEST, P. 2012. Avirulence Protein 3a (AVR3a) from the Potato Pathogen *Phytophthora infestans* Forms Homodimers through Its Predicted Translocation Region and Does Not Specifically Bind Phospholipids. *Journal of Biological Chemistry,* 287**,** 38101-38109.

WERNER, E. D., LEE, J., HANSEN, L., YUAN, M. & SHOELSON, S. E. 2004. Insulin Resistance Due to Phosphorylation of Insulin Receptor Substrate-1 at Serine 302. *Journal of Biological Chemistry,* 279**,** 35298-35305.

WHISSON, S. C., BOEVINK, P., LUCY MOLELEKI, ANNA O. AVROVA, JUAN G. MORALES, ELEANOR M. GILROY, MILES R. ARMSTRONG, SEVERINE GROUFFAUD, PIETER VAN WEST, SEAN CHAPMAN, INGO HEIN, IAN K. TOTH, PRITCHARD, L. & BIRCH, P. R. J. 2007. A translocation signal for delivery of oomycete effector proteins into host plant cells. *Nature,* 450**,** 115-118.

WIN, J., KANNEGANTI, T.-D., TORTO-ALALIBO, T. & KAMOUN, S. 2006. Computational and comparative analyses of 150 full-length cDNA sequences from the oomycete plant pathogen *Phytophthora infestans*. *Fungal Genetics and Biology,* 43**,** 20-33.

WIN, J., MORGAN, W., BOS, J., KRASILEVA, K., CANO, L., CHAPARRO-GARCIA, A., AMMAR, R., STASKAWICZ, B. & KAMOUN, S. 2007. Adaptive evolution has targeted the C-terminal domain of the RXLR effectors of plant pathogenic oomycetes. *The Plant Cell Online,* 19**,** 2349.

WIN, J., CHAPARRO-GARCIA, A., BELHAJ, K., SAUNDERS, D., YOSHIDA, K., DONG, S., SCHORNACK, S., ZIPFEL, C., ROBATZEK, S. & HOGENHOUT, S. Year. Effector biology of plant-associated organisms: concepts and perspectives. *In:* Cold Spring Harbor symposia on quantitative biology, 2012a. Cold Spring Harbor Laboratory Press.

WIN, J., KRASILEVA, K. V., KAMOUN, S., SHIRASU, K., STASKAWICZ, B. J. & BANFIELD, M. J. 2012b. Sequence Divergent RXLR Effectors Share a Structural Fold Conserved across Plant Pathogenic Oomycete Species. *PLoS Pathog,* 8**,** e1002400.

WINN, M. D., BALLARD, C. C., COWTAN, K. D., DODSON, E. J., EMSLEY, P., EVANS, P. R., KEEGAN, R. M., KRISSINEL, E. B., LESLIE, A. G. & MCCOY, A. 2011. Overview of the CCP4 suite and current developments. *Acta Crystallographica Section D: Biological Crystallography,* 67**,** 235-242.

WINTER, J., NEUBAUER, P., GLOCKSHUBER, R. & RUDOLPH, R. 2000. Increased production of human proinsulin in the periplasmic space of *Escherichia coli* by fusion to DsbA. *Journal of Biotechnology,* 84**,** 175-185.

WRATHER, J. & KOENNING, S. 2006. Estimates of disease effects on soybean yields in the United States 2003 to 2005. *Journal of nematology,* 38**,** 173.

WU, C., WHITEWAY, M., THOMAS, D. Y. & LEBERER, E. 1995. Molecular Characterization of Ste20p, a Potential Mitogen-activated Protein or Extracellular Signal-regulated Kinase Kinase (MEK) Kinase Kinase from *Saccharomyces cerevisiae*. *Journal of Biological Chemistry,* 270**,** 15984-15992.

WULF, J., PASCUZZI, P. E., FAHMY, A., MARTIN, G. B. & NICHOLSON, L. K. 2004. The solution structure of type III effector protein AvrPto reveals conformational and dynamic features important for plant pathogenesis. *Structure,* 12**,** 1257-1268.

XU, P., ZHANG, Y., KANG, L., ROOSSINCK, M. J. & MYSORE, K. S. 2006. Computational Estimation and Experimental Verification of Off-Target Silencing during Posttranscriptional Gene Silencing in Plants. *Plant Physiology,* 142**,** 429-440.

YAENO, T. & SHIRASU, K. 2013. The RXLR motif of oomycete effectors is not a sufficient element for binding to phosphatidylinositol monophosphates. *Plant signaling & behavior,* 8**,** e23865.

YAENO, T., LI, H., CHAPARRO-GARCIA, A., SCHORNACK, S., KOSHIBA, S., WATANABE, S., KIGAWA, T., KAMOUN, S. & SHIRASU, K. 2011. Phosphatidylinositol monophosphate-binding interface in the oomycete RXLR effector AVR3a is required for its stability in host cells to modulate plant immunity. *Proceedings of the National Academy of Sciences,* 108**,** 14682–14687.

YAMAMIZO, C., KUCHIMURA, K., KOBAYASHI, A., KATOU, S., KAWAKITA, K., JONES, J. D., DOKE, N. & YOSHIOKA, H. 2006. Rewiring mitogen-activated protein kinase cascade by positive feedback confers potato blight resistance. *Plant Physiology,* 140**,** 681-692.

YAN, X., HU, S., GUAN, Y.-X. & YAO, S.-J. 2012. Coexpression of chaperonin GroEL/GroES markedly enhanced soluble and functional expression of recombinant human interferon-gamma in Escherichia coli. *Applied microbiology and biotechnology,* 93**,** 1065-1074.

YANG, K.-Y., LIU, Y. & ZHANG, S. 2001. Activation of a mitogen-activated protein kinase pathway is involved in disease resistance in tobacco. *Proceedings of the National Academy of Sciences,* 98**,** 741-746.

YANG, Z. R., THOMSON, R., MCNEIL, P. & ESNOUF, R. M. 2005. RONN: the bio-basis function neural network technique applied to the detection of natively disordered regions in proteins. *Bioinformatics,* 21**,** 3369-3376.

YOSHIDA, K., SCHUENEMANN, V. J., CANO, L. M., PAIS, M., MISHRA, B., SHARMA, R., LANZ, C., MARTIN, F. N., KAMOUN, S., KRAUSE, J., THINES, M., WEIGEL, D. & BURBANO, H. A. 2013. The rise and fall of the *Phytophthora infestans* lineage that triggered the Irish potato famine. *eLife,* 2**,** e00731.

YOSHIOKA, H., NUMATA, N., NAKAJIMA, K., KATOU, S., KAWAKITA, K., ROWLAND, O., JONES, J. D. & DOKE, N. 2003. *Nicotiana benthamiana* gp91phox homologs NbrbohA and NbrbohB participate in H2O2 accumulation and resistance to *Phytophthora infestans*. *The Plant Cell Online,* 15**,** 706-718.

YUSTEIN, J. T., XIA, L., KAHLENBURG, J. M., ROBINSON, D., TEMPLETON, D. & KUNG, H.-J. 2003. Comparative studies of a new subfamily of human Ste20-like kinases: homodimerization, subcellular localization, and selective activation of MKK3 and p38. *Oncogene,* 22**,** 6129-6141.

ZHANG, J. & LAUTAR, S. 1996. A Yeast Three-Hybrid Method to Clone Ternary Protein Complex Components. *Analytical Biochemistry,* 242**,** 68-72.

ZHANG, S., DU, H. & KLESSIG, D. F. 1998. Activation of the tobacco SIP kinase by both a cell wall–derived carbohydrate elicitor and purified proteinaceous elicitins from *Phytophthora* spp. *The Plant Cell Online,* 10**,** 435-449.

ZHANG, J., SHAO, F., LI, Y., CUI, H., CHEN, L., LI, H., ZOU, Y., LONG, C., LAN, L., CHAI, J., CHEN, S., TANG, X. & ZHOU, J.-M. 2007. A *Pseudomonas syringae* Effector Inactivates MAPKs to Suppress PAMP-Induced Immunity in Plants. *Cell Host & Microbe,* 1**,** 175-185.

ZIPFEL, C. & FELIX, G. 2005. Plants and animals: a different taste for microbes? *Current Opinion in Plant Biology,* 8**,** 353-360.

ZIPFEL, C., KUNZE, G., CHINCHILLA, D., CANIARD, A., JONES, J. D. G., BOLLER, T. & FELIX, G. 2006. Perception of the Bacterial PAMP EF-Tu by the Receptor EFR Restricts *Agrobacterium*-Mediated Transformation. *Cell,* 125**,** 749-760.

ZIPFEL, C. 2008. Pattern-recognition receptors in plant innate immunity. *Current opinion in immunology,* 20**,** 10-16.

ZIPFEL, C. 2009. Early molecular events in PAMP-triggered immunity. *Current Opinion in Plant Biology,* 12**,** 414-420.

ZUO, J., NIU, Q. W., & CHUA, N. H. 2000. An estrogen receptor-based transactivator XVE mediates highly inducible gene expression in transgenic plants. *The Plant Journal,* 24, 265-273.